A UNITED STATES DEPARTMENT OF COMMERCE PUBLICATION

SECTION A

JOURNAL OF RESEARCH

of the NATIONAL BUREAU OF STANDARDS

JNBAAR 76A (6) 547-689, Nov.-Dec. 1972

Physics and Chemistry

U.S. DEPARTMENT OF COMMERCE
National Bureau of Standards

Journal of Research

of the

National Bureau of Standards

A. Physics and Chemistry

Nov.–Dec. • 1972

VOLUME • 76A

NUMBER • 6

Editor: C. W. Beckett

Associate Editor: D. D. Wagman

Publication dates:
Feb. 1, Apr. 1, June 1, Aug. 1, Oct. 1, Dec. 1, 1972

J. Res. Nat. Bur. Stand. (U.S.), A

JOURNAL OF RESEARCH

The National Bureau of Standards Journal of Research reports research and development in the fields of activity shown at right. Also included from time to time are survey articles on topics closely related to the Bureau's scientific and technical program.

The Journal is published in two separate sections as follows:

A. Physics and Chemistry

Contains papers of interest primarily to scientists working in these fields. Issued six times a year. Annual subscription: domestic, $17.00; foreign $21.25. Single copy, varies.

B. Mathematical Sciences

Presents studies and compilations designed mainly for the mathematician and the theoretical physicist. Issued quarterly. Annual subscription: domestic, $9.00; foreign, $11.25. Single copy, $2.25.

The National Bureau of Standards[1] was established by an act of Congress March 3, 1901. The Bureau's overall goal is to strengthen and advance the Nation's science and technology and facilitate their effective application for public benefit. To this end, the Bureau conducts research and provides: (1) a basis for the Nation's physical measurement system, (2) scientific and technological services for industry and government, (3) a technical basis for equity in trade, and (4) technical services to promote public safety. The Bureau consists of the Institute for Basic Standards, the Institute for Materials Research, the Institute for Applied Technology, the Center for Computer Sciences and Technology, and the Office for Information Programs.

THE INSTITUTE FOR BASIC STANDARDS provides the central basis within the United States of a complete and consistent system of physical measurement; coordinates that system with measurement systems of other nations; and furnishes essential services leading to accurate and uniform physical measurements throughout the Nation's scientific community, industry, and commerce. The Institute consists of a Center for Radiation Research, an Office of Measurement Services and the following divisions:

Applied Mathematics—Electricity—Heat—Mechanics—Optical Physics—Linac Radiation[2]—Nuclear Radiation[2]—Applied Radiation[2]—Quantum Electronics[3]—Electromagnetics[3]—Time and Frequency[3]—Laboratory Astrophysics[3]—Cryogenics[3].

THE INSTITUTE FOR MATERIALS RESEARCH conducts materials research leading to improved methods of measurement, standards, and data on the properties of well-characterized materials needed by industry, commerce, educational institutions, and Government; provides advisory and research services to other Government agencies; and develops, produces, and distributes standard reference materials. The Institute consists of the Office of Standard Reference Materials and the following divisions:

Analytical Chemistry—Polymers—Metallurgy—Inorganic Materials—Reactor Radiation—Physical Chemistry.

THE INSTITUTE FOR APPLIED TECHNOLOGY provides technical services to promote the use of available technology and to facilitate technological innovation in industry and Government; cooperates with public and private organizations leading to the development of technological standards (including mandatory safety standards), codes and methods of test; and provides technical advice and services to Government agencies upon request. The Institute also monitors NBS engineering standards activities and provides liaison between NBS and national and international engineering standards bodies. The Institute consists of the following technical divisions and offices:

Engineering Standards Services—Weights and Measures—Flammable Fabrics—Invention and Innovation—Vehicle Systems Research—Product Evaluation Technology—Building Research—Electronic Technology—Technical Analysis—Measurement Engineering.

THE CENTER FOR COMPUTER SCIENCES AND TECHNOLOGY conducts research and provides technical services designed to aid Government agencies in improving cost effectiveness in the conduct of their programs through the selection, acquisition, and effective utilization of automatic data processing equipment; and serves as the principal focus within the executive branch for the development of Federal standards for automatic data processing equipment, techniques, and computer languages. The Center consists of the following offices and divisions:

Information Processing Standards—Computer Information—Computer Services—Systems Development—Information Processing Technology.

THE OFFICE FOR INFORMATION PROGRAMS promotes optimum dissemination and accessibility of scientific information generated within NBS and other agencies of the Federal Government; promotes the development of the National Standard Reference Data System and a system of information analysis centers dealing with the broader aspects of the National Measurement System; provides appropriate services to ensure that the NBS staff has optimum accessibility to the scientific information of the world, and directs the public information activities of the Bureau. The Office consists of the following organizational units:

Office of Standard Reference Data—Office of Technical Information and Publications—Library—Office of International Relations.

[1] Headquarters and Laboratories at Gaithersburg, Maryland, unless otherwise noted; mailing address Washington, D.C. 20234.
[2] Part of the Center for Radiation Research.
[3] Located at Boulder, Colorado 80302.

U.S. DEPARTMENT OF COMMERCE
Peter G. Peterson, Secretary
National Bureau of Standards,
Lawrence M. Kushner, Acting Director

Order all publications from the Superintendent of Documents
U.S. Government Printing Office, Washington, D.C. 20402

The Secretary of Commerce has determined that the publication of this periodical is necessary in the transaction of the public business required by law of this Department. Use of funds for printing this periodical has been approved by the Director of the Office of Management and Budget through June 30, 1976.

JOURNAL OF RESEARCH of the National Bureau of Standards—A. Physics and Chemistry
Vol. 76A, No. 6, November–December 1972

Absolute Spectrofluorometry

W. H. Melhuish

**The Institute of Nuclear Sciences, Department of Scientific and Industrial Research
Private Bag, Lower Hutt, New Zealand**

(July 11, 1972)

The last 10 years has seen the increasing publication of the emission spectra of organic, inorganic and metal-chelate compounds, but there is no agreed method of presentation of such spectra. In the few cases where corrected emission spectra have been published, there is often no mention of the units used for the intensity coordinate or the method used for correcting spectra. A method of reporting absolute fluorescence spectra originally put forward in 1962 will be reexamined and improved. The two best known methods for calibrating spectrometers for absolute spectrofluorometry: (a) standard tungsten lamp, (b) quantum counter method, will be critically examined, and the limitations and possible improvements in accuracy will be proposed. The criteria for an emission standard will be examined and the use of emission standards for calibrating spectrofluorometers discussed. It is suggested that the distribution of emission standards to laboratories measuring corrected fluorescence spectra and the analysis and publication of the results should be done in the near future.

Key words: Actinometers; calibration of spectrofluorometers; detectors, absolute; fluorescence spectra, corrected; quantum counters; spectrofluorometers, design; spectrofluorometry, absolute; standard lamps; standards, fluorescence; thermopiles.

I. Introduction

Although fluorescence from organic molecules or molecular complexes has been used for many years as a method of trace analysis especially in biochemical and medical work, it was not until the introduction of commercial spectrofluorometers in the 1950's that fluorescence spectra began to appear in the literature in any great numbers. The selectivity and accuracy of analysis was greatly improved by measuring fluorescence spectra and also it became possible to recognize organic molecules in very dilute solution from their fluorescence spectra. The use of fluorescence spectra in many photophysical investigations such as determination of quantum efficiencies of fluorescence, studies on the configuration of ground and excited states, electronic energy transfer and so on, has become increasingly important in the last 10 or 15 years [1, 2].[1]

The emission spectrum recorded by a spectrofluorometer, unlike an absorption spectrum, is greatly distorted by the response function of the instrument (sensitivity as a function of wavelength), and by artefacts such as scattered light in the analyzing monochromator. The response function of the spectrofluorometer is determined by the transmission of the monochromator as a function of wavelength, the spectral sensitivity of the detector (usually a photomultiplier tube) and the variation in transmission and focusing properties of lenses (if used) with wavelength. The response function can only be reliably measured by using a source of known spectral energy distribution. Absolute spectrofluorometry, therefore, is mainly concerned with the problem of obtaining sources with accurately known spectral distributions.

Despite increasing publication of fluorescence spectra, especially in the last 10 years, it is disappointing to find that most spectra have not been corrected in any way and are thus of limited use to other workers. In the few cases where corrected spectra have been published, it seems customary to give the intensity "in arbitrary units" and provide no information on the dimensions of the units or the method used for correction. Those who publish fluorescence spectra should take note of a joint statement made by a number of investigators in 1962 [3] which stresses the importance of reporting the method of correction, subtracting "background fluorescence" and using appropriate units (e.g. quanta s^{-1} per unit wave number interval). This list has been extended by Demas and Crosby [4] to include those factors which are important when measuring quantum efficiencies of fluorescence from emission spectra.

In view of the fact that absolute calibration of spectrofluorometers is an exacting task requiring equipment not available in many laboratories, it would seem important to encourage the use of fluorescence emission standards. These can be used in three ways: (a) for presentation alongside the spectrum being investi-

[1] Figures in brackets indicate the literature references at the end of this paper.

gated so that the reader can correct the spectrum from the most recently known figures for the standard, (b) for calibrating spectrofluorometers, (c) for use in a ratio spectrofluorometer to give the ratio of the unknown to standard at each wavelength. Some standards have already been proposed [5, 6, 7], but new ones need to be found, especially in the ultraviolet and near infrared regions.

In this account of absolute spectrofluorometry, no attempt has been made to completely review the literature. The reader will find further references in the recent review article on photoluminescence quantum yields by Demas and Crosby [4]. Rather the emphasis will be on the experimental methods in absolute spectrofluorometry with a critical examination of methods of calibration, suggestions for improving accuracy and recommendations on nomenclature.

II. Definitions

A. Units

The recommended radiometric and photometric units as defined by the Système International d'Unitès (SI), are the joule (J), the watt (W) and the lumen (lm). The symbols and defining equations for quantities used in emission studies are:

radiant energy	$= Q$ (J)
radiant flux, φ	$= dQ/dt$ (W)
irradiance, E	$= d\varphi/dA$ (W m^{-2})
spectral irradiance, $E(\lambda)$	$= dE/d\lambda$ (W m^{-2} nm^{-1})

The spectral irradiance, $E(\lambda)$, is commonly used to record the output of black bodies and tungsten lamps. Unfortunately, there are no SI units for photon quantities and in this review we will use the nomenclature recently recommended by Muray, Nicodemus, and Wunderman [8]. The authors propose placing a "q" as a subscript on radiometric quantity to denote a photon quantity. Thus the photon units for some of the emission quantities would be:

photon energy	$= Q_q$ ($h\nu$)
photon flux, φ_q	$= dQ_q/dt$ ($h\nu$ s^{-1})
photon irradiance, E_q	$= d\varphi_q/dA$ ($h\nu$ s^{-1} m^{-2})
photon spectral irradiance, $E_q(\lambda)$	$= dE_q/d\lambda$ ($h\nu$ s^{-1} m^{-2} nm^{-1})
or $E_q(\tilde{\nu})$	$= dE_q/d\tilde{\nu}$ ($h\nu$ s^{-1} m^{-2} (cm^{-1})$^{-1}$)

In the past, the quantity $E_q(\tilde{\nu})$ has been variously labelled I, q, B, $Q(\tilde{\nu})$, etc., but the new symbol would appear to be less confusing and we recommend its adoption.

B. Presentation of Emission Spectra

The integrated corrected emission spectrum is proportional to the fluorescence efficiency. The most useful quantity for photochemists is the quantum fluorescence efficiency which is proportional to $\int_0^\infty E_q(\lambda)d\lambda$ or $\int_0^\infty E_q(\tilde{\nu})d\tilde{\nu}$. Thus the most useful spectra for publication are $E_q(\lambda)$ or $E_q(\tilde{\nu})$ spectra in which the maximum of the curve is given as $E_q(\tilde{\nu}) = 1.00$. Many workers report fluorescence spectra on a wavelength scale, but a wave number scale is to be preferred especially when vibrational structure is present. It is important to remember that the shapes and positions of the peaks of fluorescence spectra depend on the units used. This is illustrated in figure 1. Here $E(\lambda)$ and $E_q(\tilde{\nu})$ for quinine in 1 N H_2SO_4 are plotted on the same graph. The relation between the various units for emission spectra can be shown from the work of Ejder [9] to be:

$$\lambda^3 E(\lambda) = \lambda^2 E_q(\lambda) = \lambda E(\tilde{\nu}) = E_q(\tilde{\nu}).$$

Thus emission spectra can be readily transformed by multiplying by the appropriate power of λ; e.g. an $E_q(\tilde{\nu})$ spectrum can be converted to an $E_q(\lambda)$ spectrum by multiplying by λ^{-2}.

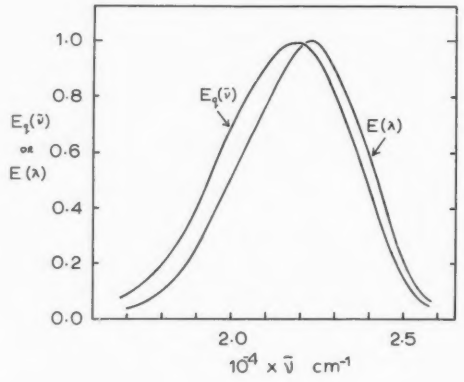

FIGURE 1. $E_q(\tilde{\nu})$ and $E(\lambda)$ spectra of quinine (10^{-4} M) in N H_2SO_4.

C. Glossary

The following abbreviations will be used in the following text, diagrams and tables:

FS = front surface
SV = side view
φ_f = quantum efficiency of fluorescence
OD = optical density or absorbance
PM = photomultiplier
M = monochromator
QC = quantum counter
TP = thermopile
$S(\tilde{\nu})$ = spectrofluorometer response function required to give $E_q(\tilde{\nu})$ emission spectra
λ = wavelength (nm)
$\tilde{\nu} = 1/\lambda$ = wave number (cm^{-1}).

III. Equipment

A. Excitation Sources

Undoubtedly the most popular exciting source for fluorescence is the high pressure xenon lamp in combination with a wide aperture grating monochromator. In order to get sufficient light at wavelengths shorter than 300 nm, it is common to use lamps of 450 watts or larger and these have the advantage of being somewhat more stable than the lower wattage lamps. If a very intense exciting source is needed, a medium or high pressure mercury lamp can be used with appropriate filters. When measuring the fluorescence spectra of concentrated solutions, powder or single crystals where front surface illumination is necessary (Sec. V), stray light from the exciting monochromator can be a problem, especially if the fluorescence emission from the sample is weak. Stray light can either be light appearing in the second or higher orders, or instrumental scatter of many wavelengths. This second type of instrumental scatter is easily demonstrated by placing the eye at the exit slit of the excitation monochromator when its wavelength is set in the UV region. Interference from second order stray light can be greatly reduced by using suitable nonfluorescent cutoff filters or bandpass filters [10]. Unfortunately few commercial spectrofluorometers have filter holders and it is necessary to have them fitted. Double grating monochromators will reduce instrumental scattered light to a large extent, but the throughput is also reduced. Good practical discussions on the use of filters and monochromators is given by Kortüm [11] and Parker [2].

The amount of stray light from a Gillieson type monochromator (as modified by Schroder [12]) when a mercury lamp is placed at the entrance slit is shown in figure 2, dashed line. The wavelength setting was 365 nm, the bandwidth was 20 nm and the 390 lines/mm grating was blazed at 350 nm. The light output was scanned with a Jarrell-Ash[2] 1/4 meter grating monochromator. The units are φ_q for the mercury lines and $E_q(\tilde{\nu})$ for the continuum. A Wratten 2 C filter (λ cutoff at 390 nm) was placed at the entrance slit of the 1/4 meter monochromator to eliminate errors due to scattering and multiple diffraction of the intense line in the analyzing monochromator (see Sec. III, B). The stray mercury lines may be further reduced by choosing a suitable bandpass filter for the exciting line.

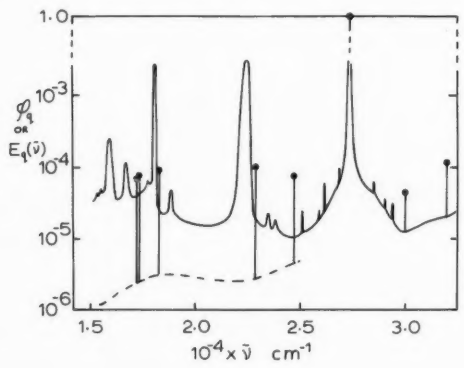

FIGURE 2. Stray light in excitation and analyzing monochromators. ● = mercury lines.

Dashed line: stray light from excitation monochromator set as 365 nm with a mercury lamp at entrance slit, and a 2c filter at exit slit.

Solid line: spurious peaks due to stray light in analyzing monochromator set at 365 nm, with a mercury lamp at the entrance slit.

B. Analyzing Monochromators

The most readily available and least expensive monochromator is the single grating instrument based on the Ebert-Fastie or Czerny-Turner mountings (fig. 3, b and c).

The Gillieson mounting (fig. 3a) is sometimes used in monochromators intended for excitation purposes. Most commercial instruments use single grating monochromators and provided one is aware of their limitations, they are adequate for measuring the rather broad fluorescence spectra given by organic molecules in solution. The advantages of grating monochromators over prism ones are: (a) linear wavelength dispersion, (b) high aperture and (c) easy interchange of gratings for different spectral regions. However, the grating monochromator generally has higher scattered light and the overlapping of orders can be a problem.

The most important source of stray light in a grating monochromator, particularly one of large aperture, is

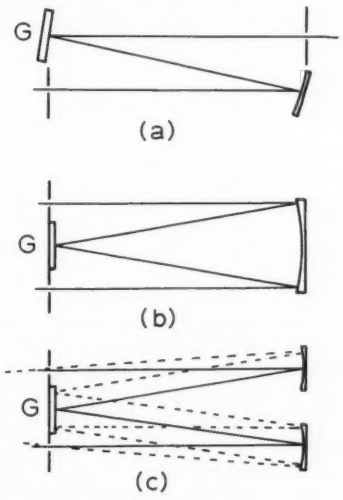

FIGURE 3. Types of grating monochromators: (a) Gillieson, (b) Ebert-Fastie, (c) Czerny-Turner. (G = plane grating).

[2] In order to adequately describe materials and experimental procedures, it was occasionally necessary to identify commercial products by manufacturer's name or label. In no instances does such identification imply endorsement by the National Bureau of Standards, nor does it imply that the particular product or equipment is necessarily the best available for that purpose.

multiple diffraction. One possible pathway for double diffraction is shown by the dashed lines in Figure 3c. This well known problem has not been quantitatively investigated until recently [12, 13]. Multiple-diffracted light can be reduced with a mask, but this reduces the transmission of the monochromator. An experimental determination of stray light in the Jarrell-Ash 1/4 meter grating monochromator with a grating blazed at 600 nm is shown in figure 2, solid line. The exciting wavelength was 365 nm and the baffle inside the monochromator was removed for these measurements. Many of the spurious peaks shown are due to multiple diffraction as may be proved by removing the exciting light with a Wratten 2 C filter; the peaks disappear, but the stray mercury lines from the excitation monochromator are not affected. This spurious light is particularly troublesome when scattered exciting light cannot be avoided as when measuring multicrystalline material from the FS or measuring solutions with a very low fluorescent intensity. In these cases it is advisable to remove the exciting light with a sharp cutoff filter and make corrections for any fluorescence absorbed by the filter. The minimizing and correction of stray light in spectrofluorometry will be further discussed in Section V, A.

C. Detectors and Amplifiers

The detector used in spectrofluorometry is the photomultiplier. End-window photomultipliers are to be preferred, since there is no grid in front of the photosurface to obstruct the narrow light beam from the exit slit of the analyzing monochromator. A quartz window photomultiplier with an S–20 photosurface has been found to have good sensitivity over the range 220 to 800 nm. A modern tube such as the EMI type 9698 QB has a very low dark current ($\sim 10^{-10}$A) and does not need cooling.

For fluorescence spectral measurements in the range 800 to 1100 nm, a cooled photomultiplier with and S–1 sensitivity curve is commonly used. It is possible that an uncooled P–I–N silicon diode may prove to be a more useful detector in this wavelength region [14], but unfortunately the surface areas of silicon photodiodes presently available are too small to be useful in spectrofluorometry.

For amplification of photocurrents of $\geq 10^{-12}$ A, solid state electrometers of the type described by Weinberger [15] are quite adequate and inexpensive. Selectable time constants ranging from 0.1–2 s. should be included in the amplifier to improve the signal-to-noise ratio. Photocurrents less than 10^{-12} A are best measured by photon counting. Not only is it possible to use simple amplifiers and discriminators [16, 17] but greater accuracy with shorter sampling times is achieved [18]. It should be noted that the photocathode should be at ground potential when the photomultiplier is used for photon counting to minimize noise due to current leakage from the photocathode.

D. Design of Spectrofluorometers

Parker [2] has discussed the design of spectrofluorometers and several instruments have been described in the literature [19, 22]. Few instruments, however, are completely satisfactory if they are required to perform a number of different functions, and we believe the following criteria should be examined before building a spectrofluorometer:

(a) There should be space around the sample so that heating and cooling baths, flow cells, liquid helium Dewars, etc., may be fitted.
(b) The instrument should be double beam in order to eliminate light source fluctuation and have the ability to measure excitation spectra.
(c) The sample should be capable of being observed from the front face and from the side.
(d) Excitation light source should be easily exchangeable.
(e) There should be space for fitting filters at the exit beam of the excitation monochromator and at the entrance slit of the analyzing monochromator.
(f) Space should be available for fitting chopping discs, e.g., for measuring phosphorescence spectra.
(g) The scanning speed should be accurately adjustable over a wide range.
(h) Amplifiers should have adjustable time constants to improve the signal-to-noise ratio.

A design used in this laboratory which meets all of these requirements is shown in figure 4. Three con-

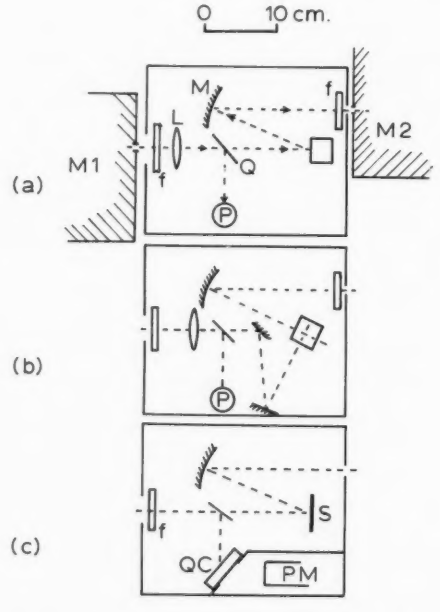

FIGURE 4. Spectrofluorometer design. M1, M2 = monochromators, Q = quartz beam splitter, f = filters, M = spherical aluminized mirror, P = photocell, PM = photomultiplier, QC = quantum counter, S = scatterer, L = quartz lens.

figurations are shown: (a) for measuring fluorescence spectra using FS excitation, (b) for measuring fluorescence spectra with SV and (c) configuration for calibrating the analyzing monochromator and photomultiplier, using the quantum counter method (Sec. IV, C). Light shields have not been shown on the diagram. Excitation spectra can be measured by replacing P in figure 4a with a quantum counter. The two signals from the monitoring photocell (or quantum counter photomultiplier) and the analyzing photomultiplier are amplified by electrometers and led to a ratio recorder of the type described by Haugen and Marcus [19]. Components are held rigidly on a series of optical benches contained in a hinged box between the two monochromators.

The spectrum recorded by spectrofluorometers is usually an uncorrected one plotted on a wavelength scale. The correction of the spectrum and replotting on a wave number scale is very laborious and instruments for the direct correction of spectra, as they are recorded, have been described [22, 23]. However these corrected curves must still be replotted if a wave number scale is required. The use of small, inexpensive on-line computers is becoming increasingly common and in the future it is likely that these will be used to correct both ordinates and plot the spectrum directly. The only additional equipment needed for the spectrofluorometer is a digital voltmeter with binary coded decimal (BCD) output and several stepping motors. Interfacing to a small computer such as the PDP–8 presents no problems.

IV. Calibration Methods

A. Introduction

The emission spectrum recorded by a simple spectrofluorometer, i.e., one without built-in automatic correction devices, is distorted not only by the scattering artefacts described in Section III, B, but also by the wavelength dependence of the detector and monochromator transmission. Only two calibration procedures for determining this response function have so far been developed. The first method depends on the assumption that a tungsten lamp operated at a color temperature, T_c, has a spectral distribution of a black body at T_c K multiplied by the emissivity ($\epsilon(\lambda)$) of tungsten:

$$E(\lambda) = \frac{8\pi hc\,\lambda^{-5}\,\epsilon(\lambda)}{[\exp(0.01438/\lambda T_c)]-1} \qquad (1)$$

where λ is in meters.

This emission standard is then used to calibrate the system as described in Section IV, B.

The second method makes use of an intense source of light and a monochromator. A detector of known response measures the watts (or quanta s^{-1}) emerging from the exit slit at various wavelengths. This calibrated source is then used to determine the response function of the spectrofluorometer. These two methods will be critically examined in Sections B and C, following.

It is important to note that the spectrofluorometer is not being calibrated under precisely the same conditions that pertain to the measuring of fluorescence spectra. Errors may arise if: (a) different areas of the grating or prism are illuminated; (b) different areas of the photomultiplier photocathode are illuminated; or (c) if the calibration curve depends on the plane of polarization of the light.

B. Tungsten Lamp Calibration

Vavilov [33], one of the first to measure a corrected fluorescense spectrum, made visual spectrometric comparisons between the output of a tungsten lamp of known color temperature and the radiant flux from a fluorescent solution. The greatest source of error in the use of tungsten lamps appears to be the uncertainty in the spectral emissivity ($\epsilon(\lambda)$) of tungsten. To overcome this error, Stair et al. [24] at the National Bureau of Standards, Washington, D.C., individually calibrate tungsten strip lamps against a high temperature black body, and it is probable that these lamps (type U90) are the most accurate spectral radiant sources presently available. The uncertainty in output ranges from a maximum of 8 percent at short wavelengths to 3 percent at long wavelengths [24]. A description of the use of a standard tungsten lamp is given by Christiansen and Ames [25]. Certain precautions must be taken in the use of standard tungsten lamps. The lamp housing dimensions, the position and the current used must be precisely as specified and the radiance must be taken normal to the tungsten strip from a small area in the middle.

The output of tungsten lamps is very low in the near UV region and care must be taken to correct for stray light by the filter subtraction method [25]. We have found in practice that it is not possible to use the NBS standard lamp below about 340 nm when calibrating a single grating monochromator and photomultiplier, owing to excessive stray light.

A good standard lamp, such as the NBS type U90 is expensive, difficult to use and has a limited lifetime. The usual practice is to compare the standard lamp against an inexpensive lamp which is used as a secondary standard. Such lamps are commercially available. Care must be taken with secondary standards that errors are not introduced by reflections from the glass envelope. Lippert et al. [5] made a secondary standard lamp which was filled with argon and backed by a horn-shaped absorber of the sort used in Raman spectroscopy.

C. Calibrated Emission Monochromator

The idea of taking a xenon lamp and monochromator and measuring the radiant flux from the exit slit in order to calibrate a monochromator and photomultiplier appears to have first been advanced by White et al. [26]. They used fluorescein in NaOH to detect the number of quanta s^{-1} emerging from the mono-

chromator over the wavelength range 250 to 300 nm. Melhuish [27] and Parker [28] describe the method in more detail. Since the accuracy of the method depends primarily on the detector used to measure the radiant flux, we will discuss detectors in more detail below (Sec. IV, D). A fixed fraction of the flux from the exit beam of the exciting monochromator is reflected [27] or scattered [28] into the analyzing monochromator and the photomultiplier current measured at each wavelength. Eastman [29] scatters the light into the analyzing monochromator with colloidal silica (Ludox) in order to have a geometry close to what will be used when measuring fluorescence spectra. In calculating the correction factor, $S(\tilde{\nu})$, it is important to allow for the wavelength dependence of the scatterer and the transmission characteristics of the quantum counter window and any beam splitters used in the optical system. For the apparatus used in this laboratory (fig. 4c),

$$S(\tilde{\nu}) = \frac{\varphi_q(\tilde{\nu})M(\tilde{\nu})W_1(\tilde{\nu})}{W_2(\tilde{\nu})\int_0^\infty R(\tilde{\nu})d\tilde{\nu}}$$

where $\varphi_q(\tilde{\nu})$ = relative number quanta s^{-1} observed by the detector
$M(\tilde{\nu})$ = reflectivity of scatterer
$W_1(\tilde{\nu})$ = transmittance of the quartz beam splitter
$W_2(\tilde{\nu})$ = transmittance of the quantum counter window
$R(\tilde{\nu})$ = recorder deflection

Equation (2) is strictly valid only if $S(\tilde{\nu})$ is constant over the bandwidth of slit used in the analyzing monochromator, typically 4 to 6 nm. A preliminary calibration is made using equation (2) to determine $S(\tilde{\nu})$. The correct calibration factor is then calculated from

$$S_{\text{corr.}}(\tilde{\nu}) = \frac{\varphi_q(\tilde{\nu})M(\tilde{\nu})W_1(\tilde{\nu})}{W_2(\tilde{\nu})\int_0^\infty [S(\tilde{\nu}_0)/S(\tilde{\nu})]R(\tilde{\nu})d\tilde{\nu}} \quad (3)$$

where $S(\tilde{\nu}_0)$ is the correction factor at the center of the scanned band. $S_{\text{corr.}}(\tilde{\nu})$ will usually differ from $S(\tilde{\nu})$ by not more than 2 or 3 percent, except in the region of 700 to 800 nm where the photomultiplier sensitivity changes very rapidly with wavelength. This procedure allows one to choose any slit width for the excitation and analyzing monochromator and is the most reliable method to use. Very little error is introduced if peak heights instead of $\int_0^\infty R(\tilde{\nu})d\tilde{\nu}$ are measured provided, (a) the bandwidth of the light leaving the excitation monochromator is 4 or 5 times less than the bandwidth of the analyzing monochromator and, (b) $S(\tilde{\nu})$ does not change rapidly over the bandwidth defined by the slit of the analyzing monochromator. Calibration by measuring peak height was used by Melhuish [27] and Parker [28], a procedure which was justified because $S(\tilde{\nu})$ did not change rapidly with wavelength over the wavelength range investigated.

It has been pointed out by Børresen and Parker [30] that any silica focusing lenses in the excitation monochromator system can cause calibration errors because a constant area of the scatterer receives varying amounts of the exciting flux depending on the wavelength, while the quantum counter measures the total photon flux in the beam.

The accuracy of this method of calibration rests on the accuracy of the response of the detector measuring $\varphi_q(\tilde{\nu})$ (Sec. IV, D) and on the accuracy to which the spectral reflectivity factor $M(\tilde{\nu})$ is known. Aluminum films were used in the calibration technique described previously [27] because if these are prepared by rapid evaporation at low pressure, the reflectivity is constant over a wide wavelength range [31]. The reflectivity of magnesium oxide seems to be less well known. Values published by Benford, Schwartz and Lloyd [32] were obtained using an integrating sphere. Multiple scattering in the sphere could result in a lower reflectivity at some wavelengths, than for a single scattering. We have recently found that the spectral reflectivity of fresh MgO (1 mm thick) to be the same as a freshly deposited aluminum film to within ±1.5 percent from 340 to 800 nm (fig. 5). There was a slight decrease (~3 percent) at 300 nm, the shortest wavelength investigated. Good values of $M(\tilde{\nu})$ for single scattering from MgO are clearly needed, especially since the MgO scatterer is used in the determination of absolute quantum efficiencies of fluorescence [43].

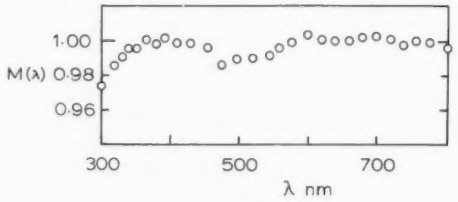

FIGURE 5. Reflectivity ($M(\lambda)$) of freshly deposited MgO versus a fresh rapidly deposited aluminum surface.

D. Detectors

The calibration of the emission monochromator by measuring the energy of quanta s^{-1} from the exit beam requires a detector with an accurately known spectral response. Three detectors have been used for this and each of these will be critically examined.

(1) Thermopiles: These detectors are coated with a layer which absorbs the radiation, causing the heating of a number of thermopiles. The thermoelectric current must be amplified with a high gain, low drift current amplifier. Thermopiles are generally compensated for changes in ambient temperature, but warm objects, such as the human body or a hot lamp housing, can cause changes in output. The absorbing coating on

thermopiles (lamp black or blackened gold) is often assumed to absorb all UV, visible and infrared light, but this is not true. The reflectivity of lamp black is known to increase in the UV region and so for a properly calibrated thermopile, the reflectivity of the actual coating on the junctions ought to be measured. The response curves of three thermopiles measured by Christiansen and Ames [25] differ considerably from each other (40–80 percent at 250 nm) so that it cannot be assumed that all thermopiles have a constant sensitivity over a wide wavelength range. The chief disadvantage of the thermopile is its low sensitivity. The measurement of the output of the emission monochromator becomes very difficult as a result of the narrow bandwidth required (1 to 3 nm) for calibration of the analyzing monochromator and photomultiplier. The wide wavelength response of a thermopile might actually be a disadvantage since stray infrared energy in the beam would also be detected. White et al. [26] and Rosen and Edelman [21] have used thermopiles for calibration purposes on the assumption of the flat energy response.

(2) Quantum Counters: Early investigations by Vavilov [33] showed that the energy efficiency of many dyes in solution was approximately proportional to the exciting wavelength (i.e. φ_f independent of λ) except near the absorption maximum. Further work by Anderson and Bird [34], Harrison and Leighton [35] and Bowen [36] showed that for many dyes, φ_f was independent of wavelength over a wide range and that such solutions could, therefore, be used to determine quanta s^{-1} in the UV and visible region by measuring the fluorescent flux from a fairly concentrated solution of the dye. Rhodamine B (4 g/l in ethylene glycol) was first tested and used as a wide range quantum counter by Melhuish [37]. An important innovation of this new quantum counter was to move the photomultiplier so that no directly transmitted light could be detected. It was now possible to reliably measure the quanta s^{-1} in a broad fluorescence band even if the tail of the band extended beyond 600 nm. The preferred geometry for a quantum counter is that of Parker [38] which not only avoids errors from directly transmitted light, but uses the full thickness of the quantum counter as a filter (fig. 4c). By comparing the rhodamine B quantum counter with a thermopile [27, 39] it has been shown that the response of the quantum counter is constant to within about ± 5 percent from 220 to 600 nm. Deviations which are observed may in fact be due to the thermopile and not the quantum counter [27]. Another method of testing a quantum counter is to use one for measuring excitation spectra. For an ideal quantum counter, the excitation spectrum should agree with the absorption spectrum, provided that φ_f is independent of λ and the OD of the fluorescent solution being measured does not exceed 0.05. A series of substances may be selected to cover a wide wavelength range and by limiting the excitation range to only one electronic band, the probability that φ_f changes with wavelength is reduced. Figure 6a shows the percent deviation of the excitation spectrum from the absorption spectrum for solutions of 2 amino-pyridine, quinine, 3 amino-phthalimide, proflavine, fluorescein, rhodamine B and methylene blue using a rhodamine B quantum counter in the apparatus shown in figure 6b. Solutions were freshly prepared since deterioration occurred when the solutions were exposed to light. The φ_f of quinine in 1 N H_2SO_4, for example, was 25 percent too low at 310 nm if left for three days in the light. The dashed line in figure 6a shows the comparison of a thermopile with the rhodamine B quantum counter [27].

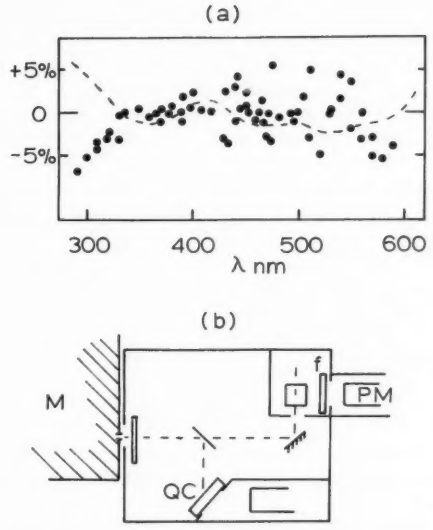

FIGURE 6. (a) Deviation of excitation spectra from absorption spectra (±3%).
(b) Apparatus for measuring excitation spectra.

Methylene blue has been used as a quantum counter by Seely [40]. A 1.5 g/l solution of methylene blue in ethylene glycol can be used from 520 to 700 nm, but it is about 50 times less sensitive than the rhodamine B quantum counter when both are used with an S–20 photomultiplier.

The advantage of the quantum counter over the thermopile is its high sensitivity. Moreover, if several different fluorescent compounds are used as quantum counters, all of which give the same response, we can be reasonably assured that we are actually measuring the quanta s^{-1} in the beam. The apparatus needed for calibrating an analyzing monochromator and photomultiplier using a quantum counter is illustrated in figure 4c. The excitation monochromator has a bandwidth of 1 to 2 nm and the analyzing monochromator a bandwidth of 4 to 8 nm. A filter cutting off at 350 nm is inserted at f (fig. 4c) when calibrating between 400 and 700 nm. The outputs from the amplifier connected to the quantum counter and the photomultiplier amplifier are fed to a ratio recorder. It is important to refer back to a particular wavelength from time to time, to correct for drift in the system.

(3) Actinometers: At least one author [26] has calibrated the output of an emission monochromator using the uranyl oxalate actinometer. The quantum yield of the more sensitive ferrioxalate actinometer has been measured as a function of wavelength by Parker and Hatchard [42] and could probably be used for calibration, although long exposure times would still be required. The wavelength response of the actinometer is not constant and its yield at different wavelengths must be measured against a detector such as the thermopile. Thus, the accuracy of the yield versus wavelength of the actinometer can be no better than the thermopile, which, as we have seen above, may not be very well known especially in the UV region.

E. Polarization Effects

The transmission of a grating monochromator depends on the direction of polarization of light incident on the entrance slit. Thus the correction factor, $S(\bar{\nu})$, which has been measured for completely unpolarized light will not apply to plane polarized light. Figure 7 shows the correction curves for a Jarrell-Ash ¼ meter monochromator (blaze = 600 nm) and a 9698–QB (S–20) photomultiplier. If the fluorescence spectrum being measured is not completely depolarized the correction factor $S(\bar{\nu})$ obtained for unpolarized light cannot be used for correcting the spectrum. The true spectrum might be obtained using a polarizer at the entrance slit of the analyzing monochromator and recording ∥ and ⊥ spectra, correcting each by the appropriate $S(\bar{\nu})$ curve and adding. It is also important to recognise that the $S(\bar{\nu})$ depends on the plane of polarization when investigating polarization of emission spectra using a grating monochromator.

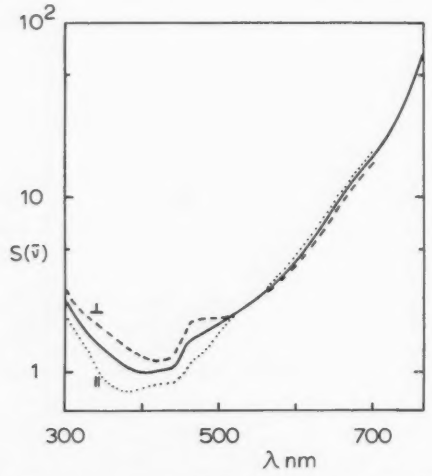

FIGURE 7. Correction curves $[S(\bar{\nu})]$ for a grating monochromator and photomultiplier ——— = unpolarized light, ····· = polarization ∥ to grating rulings, - - - - - = polarization ⊥ to grating rulings.

The light from the exit slit of a grating monochromator is also polarized to some extent, the degree of polarization varying with the wavelength setting. Hence, in using this light to calibrate an analyzing monochromator as described in Section IV, C, it is important to depolarize the light by scattering off a magnesium oxide scatterer. The use of an aluminum reflector can sometimes give errors of 10 percent or more and, therefore, should not be used.

V. Methods of Measuring Spectra

A. Dilute Solutions

When the absorption spectrum overlaps the fluorescence spectrum, a true fluorescence spectrum, free from reabsorption effects, can only be obtained in dilute solution. It is important that the cell be blackened with matt black paint on three sides, if observation is from the front surface, or two sides, if viewed from the side. The use of side viewing reduces stray exciting light which is particularly important if the exciting wavelength is within the emission band. Stray light is due to the following causes:

(a) fluorescence of the solvent and cell material
(b) Raman and Rayleigh scattering by the solvent molecules
(c) scattering of light at interfaces or from dust in the solution.

Stray exciting light can often be reduced by filtering the solution to remove solid particles and this should be done as normal practice. Sometimes it is possible to choose a light filter which prevents stray exciting light from reaching the inlet slit of the analyzing monochromator, but does not absorb any of the fluorescence. Stray background light should always be checked after the measurement of the fluorescence spectrum by filling the cell with clean solvent and rescanning. Any stray light is then subtracted from the observed fluorescence spectrum.

Most spectrofluorometers measure fluorescence emitted at right angles to the exciting beam (SV mode). The decrease of fluorescence in these instruments as the concentration of the fluorescence is increased, sometimes attributed to concentration quenching, is actually a geometric effect caused by a shift in the region of absorption in the cell towards the front surface where it cannot be seen. Thus, at high concentrations of solute, the fluorescence must be observed from the same side as the exciting light enters (FS mode). FS viewing may also be used for dilute solutions; in fact, more fluorescence can be collected by the analyzing monochromator than in the SV mode. However, stray exciting light scattered from the front face of the cell will be much larger than in the SV mode. We have found that a $5 \times 10^{-6}\,M$ (3 parts per million) solution of quinine in H_2SO_4 excited at 365 nm to be the lowest concentration that can be used in the FS mode before stray light becomes excessive.

Before correcting the fluorescence spectrum it is important to see if the refractive index of the solvent varies over the emission band scanned since the amount of light entering the slit of the analyzing monochromator from the fluorescent solution is proportional to n^2. For a fluorescent solute in benzene, for example, the photon irradiance increases by 3 percent from 434 to 588 nm as a result of dispersion in liquid benzene.

B. Concentrated Solutions and Crystals

When the absorption coefficient of the sample for the exciting light is so high that absorption is virtually complete in the first millimeter or less of the sample, fluorescence must be observed from the front surface. The scattering of exciting light into the analyzing monochromator now becomes a problem, especially if the sample is multicrystalline. Furthermore, it is not usually possible to measure a blank for crystalline samples. Although the use of a double monochromator for analyzing the fluorescence helps, the only real solution is to use a sharp cutoff filter to remove the exciting light. If the fluorescence emission falls within the region where the filter absorbs, the transmission of the filter must be measured and the observed fluorescence spectrum corrected for absorption by the filter.

A more serious error arises from reabsorption of fluorescence if the absorption and fluorescence spectra overlap. This error can be corrected by making use of the equation for reabsorption of fluorescence for the special case of front surface viewing [43]. For highly absorbing solutions where shifts in the region of absorption can be neglected, this equation becomes

$$dB(\lambda') = A f(\lambda') d\lambda' \alpha_\lambda (1 + \varphi K' + \varphi^2 K'' + \ldots) \int_0^l \exp\left[-(\alpha_\lambda + \alpha_{\lambda'} x) z\right] dz \qquad (4)$$

where a prime refers to fluorescence, unprimed to the exciting light,

A = constant
$f(\lambda')$ = true (corrected) fluorescence spectrum
$dB(\lambda')$ = observed (corrected) fluorescence spectrum
$\alpha = 2.303\,\epsilon C$ where ϵ = molar extinction coefficient and C = molar concentration
x = sec $[\sin^{-1}(\sin\theta/n)]$ where θ = angle between the exciting beam ($\perp$ to the cell face) and the observing beam and n = refractive index of the solvent
l = thickness of the cell
z = distance from the front face
$K', K'', \ldots$ = reabsorption-emission factor [43]
φ = absolute quantum efficiency of fluorescence.

Equation (4) can be simplified further if absorption of the exciting light is sufficiently high that

$$\exp -(\alpha_\lambda + \alpha_{\lambda'} x) \ll 1$$

and it is assumed that all the K factors are equal. Then

$$dB(\lambda') = [A/(1-\varphi K)]\,[\alpha_\lambda/(\alpha_\lambda + \alpha_{\lambda'} x)] f(\lambda')\, d\lambda'. \qquad (5)$$

Since the first term in square brackets is independent of λ, the observed spectrum $dB(\lambda')$ may be corrected by multiplying by $(\alpha_\lambda + \alpha_{\lambda'} x)/\alpha_\lambda$ at each wavelength.

Perylene in ethanol has a large overlap between absorption and fluorescence spectra and this compound has been used to test eq (5). The fluorescence spectra of 5×10^{-4} M and 10^{-6} M solutions of perylene in a 10 mm cell is shown in figure 8. The solution was excited and observed from the front surface. The spectrum was corrected using the rhodamine B quantum counter method (Sec. IV, C and D) using an MgO scatterer. The cell was blackened on 3 sides and corrections were made for stray light with solvent in the cell. The bandwidth of the analyzing monochromator was 1.5 nm. The spectrum of the 5×10^{-4} M solution, when corrected by eq (5) (Open circles, fig. 8) agrees well with the 10^{-6} M spectrum.

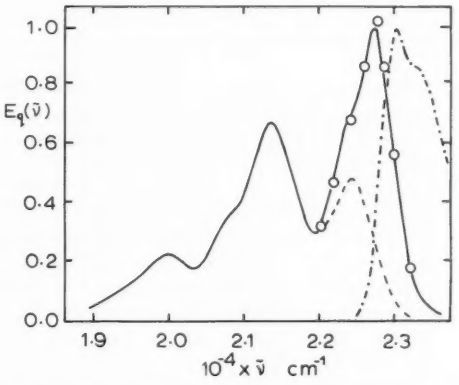

FIGURE 8. Fluorescence spectra of perylene in ethanol, $\lambda_e = 365$ nm, FS. ——— $= 10^{-6}$ M, - - - - - $= 5 \times 10^{-4}$ M, - · - · - · = absorption spectrum.

By using a very thin cell and choosing an excitation wavelength where α_λ is as large as possible, the reabsorption effect can be minimised. Thus, 5×10^{-4} M perylene in a 0.2 mm-cell when excited at 404 nm gives a fluorescence spectrum almost identical ($\pm 3\%$) with the 10^{-6} M spectrum in the 1-cm cell.

C. Narrow Bands

The measurement of a fluorescence spectrum with narrow bands require narrow slits and a slow scanning speed. As a rough guide to the settings needed to record a spectrum without significant error, we may use

the equation of Petrash [44] which states that the error in a recorded band of Gaussian or dispersion shape is approximately proportional to

$$(\gamma^{-5} d\lambda/dt)^{4/9} \qquad (6)$$

where $d\lambda/dt$ = scan rate and γ = half-line width. Thus, if the time constant of the spectrofluorometer is adjusted so that the error in the recording is no greater than 1 percent, the scanning rate would have to be reduced nearly 100 times to record a band of one-tenth the width with the same accuracy. An incorrect setting of scanning rate or time constant is easily observed by stopping the scan on the steeply rising part of the band and observing any subsequent movement of the pen to a higher reading.

D. Reporting Corrected Fluorescence Spectra

The most useful fluorescence spectrum for publication is one measured in very dilute solution where errors due to reabsorption of fluorescence are negligible. However, there are several other factors which could influence the shape of the spectrum and, therefore, the author should give a complete description of the measuring conditions. These are listed below (see Ref. 3). Conditions (a) to (d) are the most important, but the complete list should be given if the spectrum is suggested as a standard.

(a) If a standard tungsten lamp is used for calibration, describe the origin and the accuracy of its spectral distribution. Were corrections made for scatter in the monochromator? (See Sec. IV, B.)
(b) If a standard fluorescent substance is used, give the author and list the factors (d) to (m) below.
(c) If a quantum counter, thermopile or actinometer is used for calibration, give full details of the detector. Describe the system used with particular reference to the spectral reflectance of the scatterer used.
(d) Clearly state the units used for the fluorescence flux; $E_q(\tilde{\nu})$ = quanta s^{-1} per unit wave number interval is preferred.
(e) Were corrections made for stray background light using the pure solvent? (See Sec. V, A.)
(f) State the geometry of the apparatus, whether front surface or side viewing and the dimensions of the cell.
(g) Give the bandwidth of the analyzing monochromator.
(h) The source, purity and concentration of solute should be stated.
(i) The solvent used and method of purification should be noted.
(j) The temperature should be given.
(k) Was the cell blackened on any of its faces?
(l) State the excitation wavelength and its spectral purity.
(m) Give φ_f, if known.

Some commercial spectrofluorometers record absolute fluorescence spectra. It is important to know what units are used for the fluorescence flux and convert to quanta s^{-1} per unit wave number interval, if necessary. These instruments use thermopiles or correction cams in order to automatically correct the emission spectrum and their accuracy is, therefore, uncertain. In reporting fluorescence spectra obtained with these instruments, it would seem desirable to include the spectrum of one or more standards.

E. Future Developments

If the time comes when there are a sufficient number of precisely known standards covering a wide wavelength range, a double beam spectrofluorometer, which takes the ratio of the fluorescence fluxes of the unknown and standard at such wavelength, would overcome the necessity of calibrating the analyzing monochromator and detector. If the observed ratio of unknown to the standard at the frequency is $R(\tilde{\nu})$, then

$$Eq\ (\tilde{\nu})_x = Eq\ (\tilde{\nu})_s \times R(\tilde{\nu})$$

where subscript x = unknown, and s = standard.

Lippert et al. [5] describe a double beam spectrofluorometer of this design using a 13 Hz chopping frequency. The advantage of a double beam system is that fluctuation in the exciting light or in the gain of the photomultiplier does not influence the recorded spectrum.

VI. Standards

A. Introduction

An absolute emission standard is ideally one which satisfies the following criteria:

(a) Broad wavelength range with no fine structure
(b) Small overlap between absorption and fluorescence spectra
(c) Easily obtained and purified
(d) Stable
(e) High φ_f
(f) Spectrum independent of exciting wavelength
(g) Clear, free from scattering centers
(h) Completely depolarized emission.

A standard with a broad emission band with no peaks is important so that the spectrum does not depend on the resolution of the analyzing monochromator. A high φ_f and a reasonably high OD at the exciting wavelength are both important to reduce errors due to stray light (Sec. V, A). A number of absolute standards have been proposed, notably by Lippert et al. [5], but the quinine spectrum is the only one measured by a number of authors. The new standard 2-amino pyridine proposed by Rusakowicz and Testa [45] covers approximately the same wavelength range as 2-naphthol and is to be preferred since it does not have the temperature effects shown by the latter.

The effect of reabsorption of fluorescence on the emission spectrum has been discussed in Section V, B. Although standards should be measured in very dilute solution where reabsorption has no effect, sometimes spectra are determined at high concentrations. It is important, therefore, to have some idea of what region of the standard spectrum might be affected by reabsorption. The upper limit of the error due to reabsorption is given by eq (5). The term $A=\alpha_\lambda/(\alpha_\lambda+\alpha_{\lambda'}x)$ has been included in tables 1 to 5 to show the wave number region where reabsorption errors can be expected.

B. Individual Standards

1. Quinine in sulfuric acid (fig. 9). Table 1 lists the determination since 1941 of the absolute fluorescence spectrum of quinine. Many of these figures have been taken from rather small diagrams and are therefore not accurate to better than ± 3 percent. All spectra have been converted to $E_q(\tilde{\nu})$ spectra using the appropriate conversion factors.

We have found that for a 10^{-4} *M* solution of quinine viewed from the FS, the spectrum is unaffected by: (a) varying the sulfuric acid concentration from 0.1 to 2 *N*, (b) varying the exciting wavelength from 260 to 390 nm, (c) measuring three different brands of quinine. Thus the differences between the published quinine spectra are almost certainly due to calibration errors. The largest deviations are found for those spectra determined from a tungsten lamp calibration.

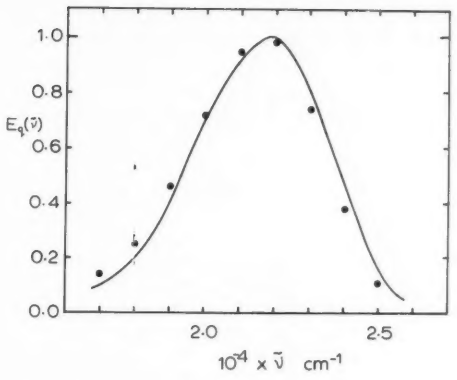

FIGURE 9. Quinine, 10^{-4} *M* in *N* H_2SO_4 (25 °C, $\lambda_e = 365$ nm). ● = Lippert [5].

TABLE 1. Absolute fluorescence spectrum of quinine in H_2SO_4 ($\lambda_e = 365$ nm)

$10^{-3}\times\tilde{\nu}$ cm^{-1}	A[a]	$E_q(\tilde{\nu})$										
25	0.95	0.07	0.105	0.105	0.135	0.105	0.15	0.10	0.16	0.14	0.15	0.152
24	.98	.36	.43	.375	.37	.375	.46	.37	.47	.46	.49	.480
23	1.00	.78	.80	.740	.79	.74	.80	.78	.80	.78	.83	.810
22		.99	.99	.980	.99	.98	1.00	.99	.99	.99	.99	1.00
21		.92	.91	.950	.92	.97	0.92	.97	.92	.97	.93	0.915
20		.56	.67	.715	.68	.75	.70	.74	.70	.77	.70	.710
19		.35	.40	.460	.40	.47	.42	.41	.42	.51	.42	.405
18		.20	.215	.240	.20	.26	.21	.21	.24	.26	.21	.200
17		.....	.104	.140	.09	.16	.10	.....	.11	.11	.08	.095
Ref.		47	6	5	48	7	27	21	46	29	22	41
Solvent		2*N*	2*N*	0.1*N*	0.1*N*	1*N*	1*N*	1*N*	0.5*N*	0.1*N*	.....	1*N*
Mode		*FS*	*FS*	*FS*	*SV*	*FS*	*SV*	*SV*	*SV*	*SV*	*SV*	*FS*
Conc(*M*)		10^{-5}	10^{-5}	10^{-3}	2×10^{-6}	5×10^{-3}	2×10^{-6}	10^{-5}	2×10^{-5}	.....	.....	10^{-4}
Calibration[b]		*L*	*L*	*L*	*L*	*L*	*L*+*Q*	*T*	*Q*	*Q*	*Q*	*Q*

[a] $A=\alpha_\lambda/(\alpha_\lambda+\alpha_{\lambda'}x)$

[b] *L* = tungsten lamp calibration, *Q* = quantum counter calibration
T = thermopile calibration

2. 2-Naphthol (fig. 10). Lippert et al. [5] have published the absolute fluorescence spectrum of 2×10^{-4} *M* 2-naphthol in a 0.02 *N*, pH 4.62 acetate buffer at various temperatures. In using this standard, the temperature and the composition must be known, and the concentration and pH of the buffer must be exactly as specified by Lippert. Børresen [46] has published the absolute emission spectrum of a 10^{-4} *M*

solution of 2-naphthol using an instrument calibrated with the rhodamine B quantum counter. The results are given in table 2.

We have also checked the spectrum using the quantum counter method of calibration and found good agreement with Børresen's results, but rather poor agreement with Lippert.

3. 3-Amino phthalimide (fig. 11). A comparison of Lippert's spectrum with the absolute spectrum recently measured in this laboratory is given in table 3.

TABLE 2. Absolute fluorescence spectrum of 2-naphthol in 0.02 *N* acetate (pH 4.62 − 4.68) ($\lambda_e = 313$ nm)

$10^{-3}\times\tilde{\nu}$ cm^{-1}	A[a]	$E_q(\tilde{\nu})$						
30	0.51	0.220	0.380	0.220	0.36	0.370	0.220	0.345
29	.93	.860	.900	.860	.90	.900	.860	.930
28.5	.99	.980	.995	.980	.97	.980	.980	1.00
28	1.00	.980	.955	.980	.97	.970	.985	.950
27		.745	.680	.740	.71	.745	.750	.715
26		.625	.590	.620	.62	.628	.630	.620
25		.780	.800	.770	.72	.750	.790	.825
24		.915	.930	.900	.80	.842	.930	.895
23		.810	.785	.795	.65	.630	.825	.670
22		.550	.515	.535	.41	.390	.565	.405
21		.300	.245	.295	.22	.224	.305	.235
20		.140	.092	.135	.095	.125	.145	.135
Ref.		5	49	5	46	41	5	41
Temp. (°C)		24	24	23	22.7	22.7	25	25
Conc. (M)		2×10^{-4}	10^{-5}	2×10^{-4}	10^{-4}	5×10^{-5}	2×10^{-4}	5×10^{-5}
Mode		FS	SV	FS	SV	FS	FS	FS
Calibration[b]		*L*	*Q*+*L*	*L*	*Q*	*Q*	*L*	*Q*

[a] $A = \alpha_\lambda/(\alpha_\lambda + \alpha_{\lambda'}x)$

[b] L = tungsten lamp calibration. Q = quantum counter calibration

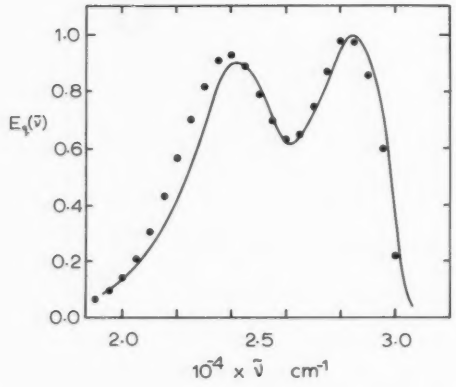

FIGURE 10. 2-Naphthol, 5×10^{-5} *M* in 0.02 *N* acetate, pH 4.65 (25 °C, $\lambda_e = 313$ nm). ● = Lippert [5].

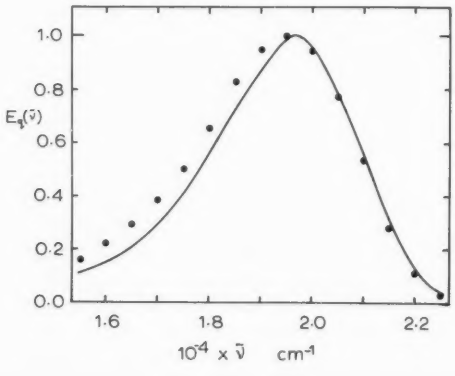

FIGURE 11. 3-Aminophthalimide, 2×10^{-4} *M* in *N* H_2SO_4 (25 °C, $\lambda_e = 365$ nm). ● = Lippert [5].

TABLE 3. Absolute fluorescence spectrum of 3-amino phthalimide in H_2SO_4 at 25 °C $\lambda_e = 365$ nm

$10^{-3} \times \tilde{\nu}$ cm^{-1}	A[a]	$E_q(\tilde{\nu})$	
23	0.97	0.01	—
22.5	.99	.03	0.04
22	1.00	.110	.125
21.5		.280	.308
21		.530	.560
20.5		.775	.790
20		.945	.955
19.5		1.000	.990
19		0.950	.875
18.5		.825	.725
18		.650	.565
17.5		.500	.402
17		.385	.290
16.5		.295	.207
16		.220	.151
15.5		.160	—
Ref.		5	41
Conc. (M)		5×10^{-4}	2×10^{-4}
Mode		FS	FS
Solvent		0.1 N	1 N
Calibration[b]		L	Q

[a] $A = \alpha_\lambda/(\alpha_\lambda + \alpha_{\lambda'} x)$

[b] L = tungsten lamp calibration, Q = quantum counter calibration

4. *m*-Dimethylamino nitrobenzene (DNB) (fig. 12). Lippert et al. [5] measured the absolute emission spectrum of DNB in 30 percent benzene and 70 percent hexane. Table 4 compares this spectrum with the one measured in this laboratory. The spectrofluorometer was calibrated with rhodamine B and methylene blue quantum counters. A disadvantage of this standard is its low φ_f and this, coupled with the fact that the instrumental sensitivity is decreasing in the region of the emission spectrum, results in a poor signal-to-noise ratio.

TABLE 4. Absolute fluorescence spectrum of *m*-dimethylamino nitrobenzene at 25 °C in 30 percent benzene, 70 percent hexane (λ_e = 365 nm)

$10^{-3} \times \tilde{\nu}$ cm^{-1}	A[a]	$E_q(\tilde{\nu})$	
22	0.93	0.03	0.10
21	.98	.235	.41
20	1.00	.610	.80
19		.935	1.00
18		.975	0.86
17		.825	.68
16		.615	.48
15		.405	.31
14		.235	.17
13		.110	—
Ref.		5	41
Conc. (M)		10^{-4}	5×10^{-4}
Mode		FS	FS
Calibration[b]		L	Q

[a] $A = \alpha_\lambda/(\alpha_\lambda + \alpha_{\lambda'} x)$

[b] L = tungsten lamp calibration, Q = quantum counter calibration

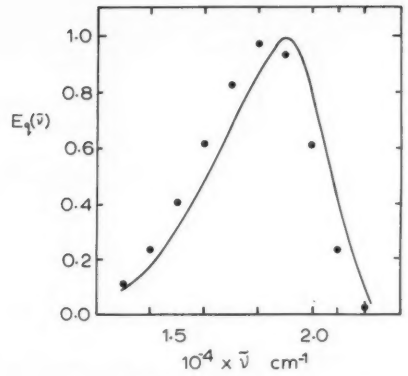

FIGURE 12. *m*-Dimethylamino-nitrobenzene, 5×10^{-4} M in 30 percent benzene, 70 percent hexane (25 °C, $\lambda_e = 365$ nm). ● = Lippert [5].

5. 2-Aminopyridine (fig. 13). The corrected fluorescence spectrum of 2-amino pyridine determined by Rusakowicz and Testa [45] using a tungsten lamp for calibration is given in table 5. The spectrum measured

TABLE 5. Absolute fluorescence spectrum of 2-amino-pyridine in H_2SO_4 at 25 °C

$10^{-3} \times \tilde{\nu}$ cm^{-1}	A[a]	$E_q(\tilde{\nu})$	
31	0.64	0.03	0.05
30.5	.82		.145
30	.94	.17	.325
29.5	.97		.540
29	1.00	.575	.686
28.5			.840
28		.93	.960
27.5			1.000
27		.99	0.980
26.5			.920
26		.805	.790
25.5			.660
25		.52	.530
24.5			.405
24		.26	.310
23.5			.222
23		.138	.148
22.5			.102
22		.068	.075
Ref.		45	41
Solvent		0.1 N	1 N
Conc.		10^{-5}	10^{-5}
Mode		SV	FS
Calibration[b]		L	Q
λ_e nm		285	313

[a] $A = \alpha_\lambda/(\alpha_\lambda + \alpha_{\lambda'} x)$

[b] L = tungsten lamp calibration, Q = quantum counter calibration

in this laboratory using the quantum counter method of calibration is in good agreement with their spectrum.

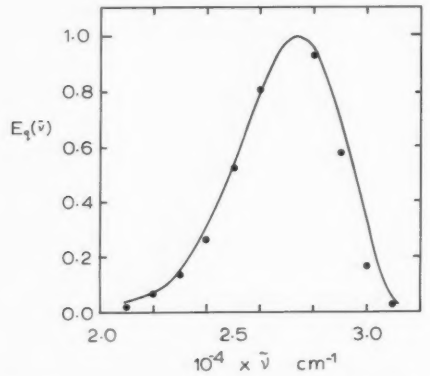

FIGURE 13. 2-Aminopyridine, 10^{-5} *M* in *N* H_2SO_4 (25 °C, $\lambda_e = 313$ nm). ● = Rusakowicz and Testa [45].

C. New Standards

The greatest lack, at present, is for standards in the ultraviolet and near infrared regions of the spectrum. Reisfeld et al. [50] recommend thallium activated potassium chloride as an emission standard in the UV region. For the red and near infrared regions, rhodamine *B* and methylene blue might be used since these substances have a high φ_f. Preliminary measurements in this laboratory (fig. 14) indicate that these two would cover the range 18,000 to 12,000 cm^{-1}.

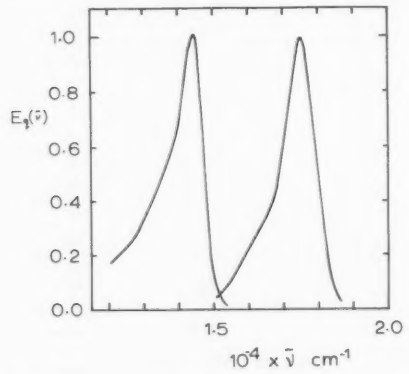

FIGURE 14. Rhodamine B, 5×10^{-6} *M* and methylene blue, 5×10^{-5} *M* in ethanol (25 °C, $\lambda_e = 436$ nm).

VII. References

[1] Birks, J. B., Photophysics' (John Wiley and Sons, Inc., New York, N.Y., 1970).

[2] Parker, C. A., Photoluminescence of Solutions (Elsevier, New York, N.Y., 1968).

[3] Chapman, J. H., Förster, Th., Kortüm, G., Lippert, E., Melhuish, W. H., Nebbia, G., Parker, C. A., Phot. Soc. Group Bull. No. 14, 378 (1962), Appl. Spectroscopy **17,** 171 (1963); Z. Anal. Chem. **197,** 431 (1963).

[4] Demas, J. N., and Crosby, G. A., J. Phys. Chem. **75,** 991 (1971).

[5] Lippert, E., Nagele, W., Seibold-Blankenstein, I., Staiger, W., Voss, W., Z. Anal. Chem. **170,** 1 (1959).

[6] Kortüm, G., and Hess, W., Z. Phys. Chem. NF **19,** 9 (1959).

[7] Melhuish, W. H., J. Phys. Chem. **64,** 762 (1960).

[8] Muray, J. J., Nicodemus, F. E., Wunderman, I., Appl. Opt. **10,** 1465 (1971).

[9] Ejder, E., J. Opt. Soc. Amer., **59,** 223 (1969).

[10] Bennett, H. F., and McBride, W. R., Appl. Opt. **3,** 919 (1964).

[11] Kortüm, G., Kolorimetrie, Photometrie u. Spektrometrie 4th ed. (1962) (Springer-Verlag, Berlin, 1955).

[12] Mitteldorf, J. J., and Landon, D. O., Appl. Opt. **7,** 1431 (1968).

[13] Pribram, J. K., and Penchina, C. M., Appl. Opt. **7,** 2005 (1968).

[14] Fisher, R., Appl. Opt. **7,** 1079 (1968).

[15] Weinberger, R. G., Elect. Aug. 30, 58 (1971).

[16] Akins, D. L., Schwartz, S. E., Bradley-Moore, C., Rev. Sci. Instrum. **39,** 715 (1968).

[17] Lampton, M., and Primbsch, J. H., Rev. Scient. Instr. **42,** 731, (1971).

[18] Jones, R., Oliver, C. J., and Pike, E. R., Appl. Opt. **10,** 1673 (1971).

[19] Haugen, C. R., and Marcus, R. J., Appl. Opt. **3,** 1049 (1964).

[20] Turner, G. K., Science **146,** 183 (1964).

[21] Rosen, P., and Edelman, G. M., Rev. Sci. Instrum. **36,** 809, (1968).

[22] Cundall, R. B., and Evans, G. B., J. Sci. Instr. (J. Phys. E.) **1,** 305 (1968).

[23] Lipsett, F. R., J. Opt. Soc. Amer. **49,** 673 (1959).

[24] Stair, R., Johnston, R. G., Hallbach, E. W., J. Res. Nat. Bur. Stand. (U.S.), **64A,** 291 (1960).

[25] Christiansen, R. L., and Ames, I., J. Opt. Soc. Amer. **51,** 224 (1961).

[26] White, C. E., Ho, M., Weimer, E., Anal. Chem. **32,** 438 (1960).

[27] Melhuish, W. H., J. Opt. Soc. Amer. **52,** 1256 (1962).

[28] Parker, C. A., Anal. Chem. **34,** 502 (1962).

[29] Eastman, J. W., Photochem. and Photobiol. **6,** 55 (1967).

[30] Børresen, H. C., and Parker, C. A., Anal. Chem. **38,** 1073 (1968).

[31] Hass, G., and Waylonis, J. E., J. Opt. Soc. Amer. **51,** 719 (1961).

[32] Benford, F., Schwartz, S., Lloyd, G. P., J. Opt. Soc. Amer. **38,** 964 (1948).

[33] Vavilov, S. I., Phil. Mag. **43,** 307 (1922); Z. Phys. **42,** 311 (1927).

[34] Anderson, W. T., Bird, L. F., Phys. Rev. **32,** 293 (1928).

[35] Harrison, G. R., Laighton, P. A., Phys. Rev. **38,** 899 (1931).

[36] Bowen, E. J., Proc. Roy. Soc. **154A,** 749 (1936).

[37] Melhuish, W. H., N.Z. J. Sci. and Tech. **37B,** 142 (1955).

[38] Parker, C. A., Nature **182,** 1002 (1958).

[39] Yguerabide, J., Rev. Scient. Instr. **39,** 1048 (1968).

[40] Seely, G. R., J. Phys. Chem. **73,** 125 (1969).

[41] Melhiush, W. H., unpublished. Apparatus used shown in figure 4a.

[42] Hatchard, G. G., Parker, C. A., Proc. Roy. Soc. **235A,** 518 (1956).

[43] Melhuish, W. H., J. Phys. Chem. **65,** 229 (1961).

[44] Petrash, C. G., Opt. and Spect. **6,** 516 (1959).

[45] Rusakowicz, R., and Testa, A. C., J. Phys. Chem. **72,** 2680 (1968).

[46] Borresen, H. C., Act. Chem. Scand. **19,** 2089 (1965).

[47] Kortüm, G., and Finckh, B., Spect. Act. **2,** 137 (1941).

[48] Parker, C. A., and Rees, W. T., Analyst **85,** 587 (1960).

[49] Unpublished (1962) using the apparatus in Ref. 27.

[50] Reisfeld, R., Honigbaum, A., and Velapoldi, R. A., J. Opt. Soc. Amer. **61,** 1422 (1971).

(Paper 76A6–741)

JOURNAL OF RESEARCH of the National Bureau of Standards—A. Physics and Chemistry
Vol. 76A, No. 6, November–December 1972

Absolute Quantum Efficiencies

G. A. Crosby*

Department of Chemistry, Washington State University, Pullman, Washington 99163

J. N. Demas

Department of Chemistry, University of Virginia, Charlottesville, Virginia 22901

and

J. B. Callis

Department of Chemistry, University of Washington, Seattle, Washington 98105

(July 11, 1972)

Recent developments in several areas of chemistry, laser technology, photodetector instrumentation, and calorimetry are surveyed, and their probable impact on the measurement of quantum yields is assessed. Chemical developments include: (a) synthesis and design of new luminescent molecules that could possibly serve as standards, (b) application of improved separation techniques to provide samples of extreme purity, and (c) advances in photochemistry that portend the development of wide-range chemical actinometers. The potential use of lasers in quantum-yield measurements and their advantages over conventional sources for application in both optical and calorimetric techniques are pointed out. New methods of quantum-yield measurements, based on the novel characteristics of laser pump sources, are suggested, including the feasibility of measuring yields under time-resolved conditions and of employing internal standards. The possible lifting of wavelength restrictions on both laser sources and detector devices and the implications of these developments for extending the spectral range of quantum-yield measurements are discussed. The current status of calorimetry for determining yields is surveyed, and the impact of recent technology on the feasibility of developing calorimetric methods competitive with optical methods is assessed.

Key words: Calorimetry in quantum yields; laser, use in quantum yields; photodetectors in quantum yields; quantum efficiencies.

I. Introduction

The explosive developments of science and technology in the last quarter century have been mirrored in the steady rise of optical methods in chemistry, physics, and biology. Today the use of fluorescence and phosphorescence in fundamental and applied investigations is routine. Initially focussed on frequency and relative intensity measurements, the effort during the last few years has begun to encompass determinations of efficiencies of large classes of luminescent materials. Such a measurement, the quantum-yield determination, is one step removed in difficulty from recording energy, measuring relative luminescence intensity, or monitoring rate of decay (at least for times beyond a microsecond) of excited species. The result is that developments in quantum-yield technology have lagged behind those in the other areas. Recently, however, the technological advances relevant to quantum-yield measurements and the increased interest in obtaining efficiencies signal that a comprehensive analysis should be carried out on the present needs for accurate quantum efficiencies and an assessment be made of the current developments in the methods of determining them.

The present article is not an attempt to review the field of quantum-yield measurements. Although considerable space is devoted to optical and calorimetric methods for determining yields, no attempt has been made to review these techniques adequately either. (For a comprehensive review of optical methods, see ref. [1].[1]) Rather the thrust of the present article is to point out a few of the obvious needs for accurate yield information, to note some of the current progress in

*Prepared during the tenure of AFOSR (NC)-OAR, USAF, Grant No. AFOSR-72-2207.

[1] Figures in brackets indicate the literature references at the end of this paper.

instrumentation technology and chemistry that may lead to better yield determinations, and to suggest a few avenues of investigation that appear ready for development. Our remarks are restricted mainly to solutions and rigid glasses. For readers interested in yields from solid materials, we direct them to the review article by Lipsett and to the original literature [2–10]. Gas phase determinations are also not discussed, although recent publications show that the field is expanding [11–13].

II. The Importance of the Quantum Efficiency

The luminescence quantum efficiency of a compound (Φ) is defined as the fraction of molecules that emit a photon after direct excitation by the source. The terms absolute yield, quantum yield, yield, and efficiency are all used interchangeably throughout this article.

Recent research developments in many areas of physical, chemical, and biological research have reached a stage where the lack of absolute quantum efficiencies is seriously hampering further progress. We enumerate here a few areas where such information could be decisive. In theoretical chemistry, studies of radiative and especially radiationless processes have been proliferating [14–18]. The role of various terms within the Hamiltonian (vibronic, spin-orbit) [19–22] and the effect of substituents on both radiative and radiationless rate constants of isolated molecules are under scrutiny [23–25]. The interactions of excited species with the host molecules in condensed phases are not well understood, but some information is beginning to accumulate [26, 27]. Reliable efficiencies are needed on many classes of molecules to test the predictions implicit in the formalisms and to unearth new problems.

An especially important fundamental problem concerns the limits of applicability of the Strickler-Berg equation [28] for obtaining radiative lifetimes of excited states from the inverse absorption processes [29]. Serious discrepancies exist between the measured natural radiative lives (τ_{0_m}), as obtained from the equation $\tau_{0_m} = \tau_f/\phi_f$ where τ_f is the fluorescence decay time and ϕ_f is the fluorescence quantum yield, and those calculated by the Strickler-Berg relation. These discrepancies exist for simple molecules (e.g., SO_2) [30] and for larger systems such as diphenylpolyenes [31]. The lifetimes can be anomalously long [32, 33] or anomalously short [34]. Large intermolecular [33] or intramolecular configurational changes [34] have been invoked to rationalize the results. More quantum efficiencies are required to quantify the experimental situation.

A second problem in the application of the Strickler-Berg equation involves the selection of degeneracy factors for upper (g_u) and lower (g_l) states involved in the transitions when application is made to formally forbidden transitions ($S \rightarrow T$). For hydrocarbons at the usual refrigerant temperatures ($\geq$ 50 K) a value of $g_u = 3$ is reasonable, since the level splitting is much smaller than kT and thermal equilibrium is established among the nearly isoenergetic levels. For systems where spin-orbit coupling is large, such as encountered in d–d [35] and charge-transfer [36, 37] excited states, the splittings may be comparable to or even greater than kT. Then measured quantum yields and lifetimes are expected to be temperature dependent, and the Strickler-Berg relation can only really be applied and tested after careful studies of temperature-dependent decay times [38] and quantum yields [39] have been carried out. Reliable quantum efficiencies for many model systems are needed.

Another area where reliable quantum efficiencies are lacking, and one where the role of experimental yields can be decisive, is in determining the effects of deuteration on the radiationless rate constants for degrading excitation energy. Theoretical classifications of radiationless processes according to "strong" and "weak" coupling limits have been made. In the first case, no important deuterium effects on radiationless rates are predicted; in the latter, large changes due to deuteration are expected [40]. Few systems have been studied experimentally to distinguish these coupling limits. It is manifest that major decisions about the relative importance of various mechanisms for fundamental radiationless processes could be made from quantum-yield comparisons of deuterated and nondeuterated molecules [41–43].

The present status of organic photochemical research also warrants the effort of measuring accurate luminescence yields. Particularly important is a knowledge of efficiencies for organic molecules that can be used as energy donors or acceptors in photosensitization experiments. Reliable yields on series of closely related molecules whose singlet or triplet states span important energy regions would aid substantially in the design of experiments to test mechanisms of energy transfer and to control photochemical products. The need for yields of organic systems is compounded by the fact that mixed solvents and unconventional pure solvents are sometimes necessary. Thus, the known efficiencies of compounds must be extrapolated into systems where conditions differ radically from those prevailing during the original determinations.

Not only total quantum yields, as defined initially, but yields from particular levels in molecules exhibiting multiple level luminescence are needed. Such quantities are of paramount importance for assessing relative quenching rates of excited singlet and triplet levels, for obtaining efficiencies of intersystem crossing, and for relating measured quantities to theoretically defined parameters. The processes associated with a typical organic system are illustrated in figure 1. In terms of the rate constants displayed on the figure, we can define: $\phi_f = k_f/(k_f + k_{q_f} + k_{is})$, $\phi_p = k_p/(k_p + k_{q_p})$, and $\phi_{is} = k_{is}/(k_{is} + k_f + k_{q_f})$. It is obvious that Φ, the total measured quantum yield as defined earlier, equals $\phi_f + \phi_p$ provided the only processes occurring after excitation are those depicted in the figure. It is also clear that the sum of ϕ_f and ϕ_{is} may or may not be unity depending upon the existence of singlet quench-

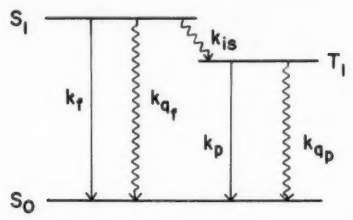

FIGURE 1. Principal pathways of degradation of an excited organic molecule. ⟶, radiative decay; ⇝, radiationless decay. k_f= radiative rate constant for depopulating S_1; k_{q_f}= radiationless rate constant for depopulating S_1; k_{is}= radiationless rate constant for converting from S_1 to T_1; k_p= radiative rate constant for depopulating T_1; k_{q_p}= radiationless rate constant for depopulating T_1. $k_f/(k_f+k_{q_f}+k_{is})=\phi_f$ (quantum yield of fluorescence from S_1). $k_p/(k_p+k_{q_p})=\phi_p$ (quantum yield of phosphorescence from T_1). $k_{is}/(k_{is}+k_f+k_{q_f})=\phi_{is}$ (quantum yield of intersystem crossing).

ing (k_{q_f}). A particularly important quantity is ϕ_{is}. It measures the efficiency of populating the triplet state, thus producing a reactive species responsible for many photochemical reactions and frequently serving as an efficient energy donor.

Several methods have been proposed to determine ϕ_{is} [44–51]. Different photophysical properties and processes have been utilized and ingenious techniques have been devised to extract ϕ_{is} from the data. Nonetheless, the methods rely eventually on the measurement of a photoluminescence quantum yield. A fundamental question raised by these measurements of intersystem crossing yields is whether the sum of $\phi_f+\phi_{is}$ is indeed unity. The equality has been shown to hold for a number of aromatics [52–57] and for porphin and its derivatives [58]. Exceptions abound, however, [59] and the experimental situation is still unclear [60]. Accurate and extensive quantum-yield measurements are necessary in order to establish or refute the stated equality as a fundamental (or rarely violated) law of luminescence. For pyrene, k_{f_q} is reported to be negligible at 77 K but competitive with k_f at room temperature [61].

The role of quantum-yield measurements in providing information on biologically important systems is expanding rapidly. Reports of quantum yields of naturally occurring bases [62] as functions of pH are providing insight into the possible fundamental physiological functions of these materials. Useful information on conformations and the nature of the excited states of biopolymers [63–65] has been provided from fluorescence measurements on oligonucleotides and polynucleotides containing fluorescent purine analogs. Some of the reported quantum yields are extremely low dictating new demands for accurate quantitative measurements at low light levels.

The real power and usefulness of fluorescent probes in biological systems are becoming appreciated. A typical example is 2-*p*-toluidinyl-6-naphthalenesulfonate (TNS), one of a series of compounds that are practically nonfluorescent in water but strongly fluorescent in organic solvents or when bound to protein molecules. This substance can be used as an extrinsic fluorescent chromophore for the study of protein conformations [66, 67], in the study of nitrogen antibody interactions [68], in following protein conformational changes produced by metal ion binding [69], and in elucidating enzyme activation processes [70]. In spite of its obvious importance it is significant that the mechanism by which the fluorescence of this molecule is changed by the medium is still not well understood. Spectroscopic studies, including detailed and accurate quantum-yield determinations, are of fundamental importance for molecules of this type and should be actively sought.

The need for quantum yields of inorganic molecules is also manifest and growing. Especially those materials classed as inorganic coordination compounds, usually containing some organic moieties, deserve considerable attention. This class of molecules, long utilized empirically in fluorescence metal analysis, has only relatively recently been recognized as providing candidates for electro-optical devices [71], for fundamental studies of radiative and radiationless transitions [35, 36], and for energy donors in inorganic photochemical studies [72]. The real possibility of engineering these molecules to have predetermined frequency ranges, high yields, and appropriate chemical properties [73] opens up a whole range of new experiments that were not possible just a few years ago. Needed, however, is detailed information on their spectroscopic properties, especially their absolute efficiencies, and the temperature dependences thereof. The near infrared region, virtually inaccessible at present to quantum-efficiency measurements can possibly be made accessible by the use of complexes possessing low-lying emitting levels, particularly those molecules displaying charge-transfer luminescence. Yet, few yields of these compounds have been measured, and none, to our knowledge, of compounds emitting beyond 800 nm.

We digress here to present some information on a few representative transition-metal complexes whose unique luminescence properties are not yet well recognized. Complexes of ruthenium(II), osmium(II), and iridium(III) with π-conjugated ligands display visible and near-UV absorption spectra dominated by strong charge-transfer absorption bands of high intensity ($2000 \leq \epsilon \leq 20{,}000$, where ϵ is the molar absorptivity) (figs. 2, 3, 4). In the case of osmium(II) complexes, the absorption bands extend well into the red region of the spectrum. Upon irradiation these molecules emit light with good efficiencies at low temperature ($>10\%$), and some are still reasonably efficient at room temperature in fluid solution. In figures 2 and 3 it is seen that the quantum yields are independent of wavelength, a property of fundamental and applied importance.

Other spectroscopic properties of interest of these molecules are evident in figure 4. One sees that each emission spectrum consists of a unique electronic band. This is a feature characteristic of all these systems at

474-414 O - 73 - 2

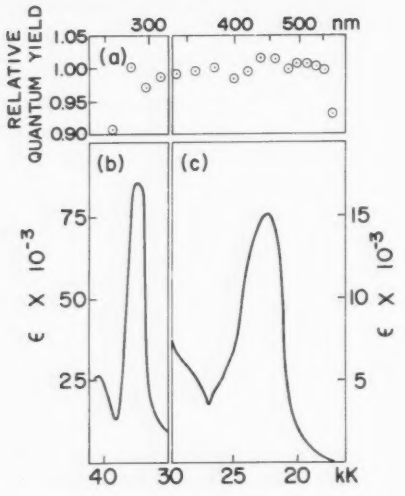

FIGURE 2. Relative quantum yield (a) and absorption spectrum (b, c) of tris(2,2′-bipyridine)ruthenium(II) chloride in methanol at room temperature: (a) 0.2 g/5 ml in a 1-cm cell, (b, c) 6.7×10^{-5} *M* in a 1-cm cell. The first and last yield points are less accurate than the others. [Ref: J. N. Demas and G. A. Crosby, J. Amer. Chem. Soc. **93**, 2841 (1971).]

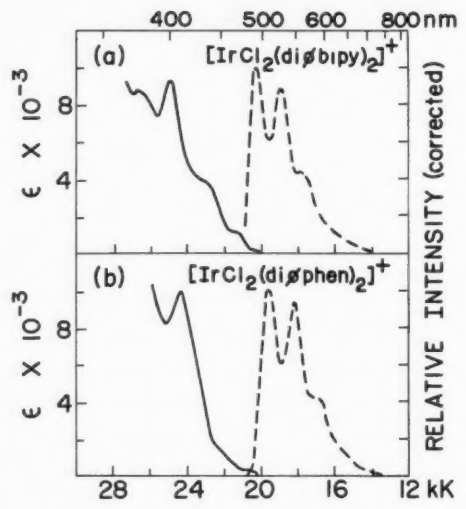

FIGURE 4. Absorption (———) and luminescence (- - -) spectra of phenyl-substituted iridium(III) complexes in ethanol-methanol glass (4 : 1, *v/v*) at 77 K. (a) *cis*-dichlorobis(4,4′-diphenyl-2,2′-bipyridine)-iridium(III) chloride, (b) *cis*-dichlorobis(4,7-diphenyl-1,10-phenanthroline)iridium(III) chloride. [Ref: R. J. Watts and G. A. Crosby, J. Amer. Chem. Soc. **94**, 2606 (1972).]

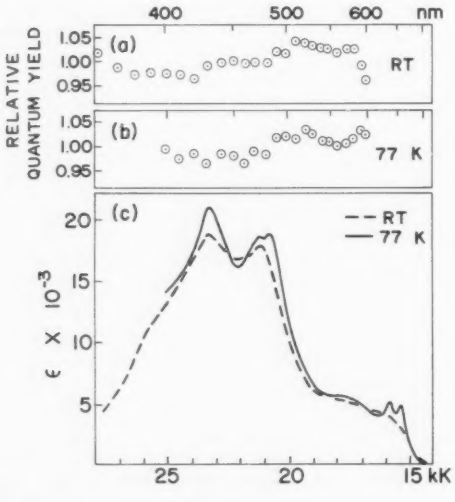

FIGURE 3. Relative quantum yields (a, b) and absorption spectra (c) or tris(1,10-phenanthroline)osmium(II) iodide in ethanol-methanol (4:1, *v/v*): (a) 4.5×10^{-7} *M* in a 1.76-cm cell at room temperature; (b) 4.5×10^{-7} *M* in a 1.76-cm cell at 77 K (glass); (c) - - -, 9.0×10^{-6} *M* in a 10-cm cell at room temperature; ———, 7.12×10^{-5} *M* and 1.42×10^{-5} *M* in 1.76-cm cells at 77 K (glass). [Ref: J. N. Demas and G. A. Crosby, J. Amer. Chem. Soc. **93**, 2841 (1971).]

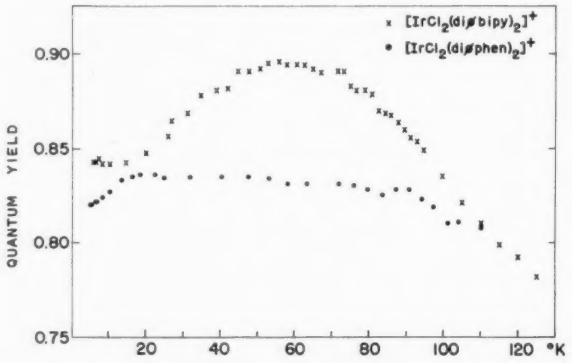

FIGURE 5. Temperature dependence of quantum yields. ×, *cis*-dichlorobis(4,4′-diphenyl-2,2′-bipyridine)iridium(III) chloride. ○, *cis*-dichlorobis(4,7-diphenyl-1,10-phenanthroline)iridium(III) chloride. Both molecules were dissolved in poly(methylmethacrylate) and irradiated with ~ 365 nm radiation.

temperatures above 77 K [35–37]. Furthermore, the measured decay times are on the order of microseconds, thus falling between those limits normally encountered for established fluorescences and phosphoresences. Finally, the capability of tuning the frequency by ligand change is apparent.

Additional spectroscopic features of importance are evident in figure 5. Not only are the yields of some of the molecules extremely high but, also, for some of them, the efficiencies are virtually temperature independent over large ranges. Because of the favorable chemical properties of these substances and their unique luminescence behavior, considerable fundamental information concerning the excited state properties of transition-metal complexes can be gleaned

from studies of their photoluminescences. Particularly important are accurate determinations of quantum yields as a function of temperature [38, 39]. Their possible value as fluorescence standards and as components in chemical actinometers is discussed below.

III. Standards

The absolute determination of quantum yields is a measurement fraught with difficulties. Understandably, workers have resorted to the much more convenient and rapid technique of measuring yields relatively, i.e., by comparison with known standards. Perforce, this procedure shifts a major burden of the accuracy of the final figure to the standard. Thus, the real need for more and better standards. Compounding the problem is the necessity to have standards for various solvents, for various temperature ranges, for wide ranges of wavelengths, and for different states of matter (solid, plastic, glasses, solutions). This is a stiff order. When one considers the importance of standards, the small number of well-studied ones, and the disconcerting disagreement of reliable workers on the actual reported efficiencies, the magnitude of the problem of obtaining good standards is revealed. [Relative yield measurements are so much easier to perform than absolute ones, however, that the demand for absolute standards will continue to increase.] An account of commonly used standards and an assessment of the reliability of their yield values are available [1]. Additional information on common standards and some interesting suggestions for new ones are contained in the article by Testa [74]. Many workers choose standards possessing favorable chemical properties for relative measurements even though the accuracy of some of the "standard" yields is not well substantiated.

The incidence on the market of commercial instruments that can measure yields routinely also increases the need for standards. In fact, institution of a program to remeasure old standards and search for new ones has considerable merit, in our opinion. If a bank of reliable standards could be built and marketed, which would provide checks on both research results and instrumentation throughout the country, a mass of misinformation would be clarified, and future additions of shoddy yield data to the literature would be measurably reduced. Such a program seems appropriate for the National Bureau of Standards.

At this juncture we wish to point out again the unusual optical properties of inorganic complexes, especially those of ruthenium, osmium, and iridium described above. It is our contention that they deserve serious study as candidates for standards, as well as for numerous other applications in spectroscopy and photochemistry. Because their properties can be modified by ligand substitution, ligand modification, and change of counter ion, it is possible to design them to have specified frequencies, high yields, and desirable solubilities. Thus, molecules can be engineered to dissolve in most common solvents. Their potential as quantum-yield standards should be studied, especially if internal standards (see below) were employed.

Finally, we wish to call attention to recent developments in purification procedures that bear on the accuracy of quantum-yield measurements. Chemical purity of any fluorescent compound is always desired; for quantum-yield standards it is a stringent requirement. This aspect of quantum-yield work has been repeatedly emphasized [1, 29, 75], not only for quantum-yield measurements but for emission spectroscopy in general. Intense light sources commonly employed to measure low yields exacerbate the impurity problems. The use of lasers dictates adherence to criteria for chemical purity far stricter than those normally applied [76]. Increases in detector sensitivity and the employment of high aperature equipment to monitor weak emitters place still greater demand for high standards of chemical purity. The availability of image intensifier tubes adds a new dimension to the impurity problem [77].

The virtues of thin-layer chromatography, column chromatography, and zone refining as supplements to the classical chemical techniques for obtaining high purity are relatively well known. Not commonly appreciated, however, are the remarkable chemical separations obtainable with the use of dextran molecular sieves in column chromatography. Although usually employed for biochemical separations, the effectiveness of molecular sieves for purifying inorganic materials is not common knowledge [78]. Indeed, the usual conception of the primary mechanism responsible for such separations (dominant role of molecular size) leads one to predict that molecules of similar size and shape should not be separable with such procedures. Yet, separations of isomeric, six-coordinated complexes of transition metals have been accomplished [73]. In fact, the discriminatory ability of the Sephadex gels to separate the components of reaction mixtures is so acute that surface adsorption activity must be at work in addition to steric effects [79].

Because of the many desirable features of gel filtration chromatography as a purification technique we strongly recommend its use both for purifying fluorescence standards and for preparing samples in general. For transition-metal complexes where reaction mixtures can produce a host of chemically and spectroscopically similar molecules, efficient separations are mandatory. In many cases gel filtration provides a superb answer to the problem.

IV. Quantum Efficiencies by Optical Methods

The first reliable method for measuring quantum yields by an optical technique was introduced by Vavilov in 1924 [80]. The method is a substitution technique employing a solid scatterer as a standard. The experiment requires two basic measurements. First, the detector monitors the sample luminescence that is generated by total absorption of the excitation light focussed to a point in the cell. Then the detector

records the light diffusely scattered by a magnesium oxide surface substituted for the original cuvette. From these data and some ancillary measurements, the absolute quantum yield can be computed. A detailed description of the technique including the derivation of equations is given in reference 1. Basic improvements on the method were the introduction of a quantum counter by Bowen in 1937 [81] and the incorporation of the refractive index correction by Förster in 1950 [82]. Refinements by McClure et al. [83] in the early 50's and the introduction of the rhodamine B quantum counter in 1955 by Melhuish [84] resulted in a method of measurement that has produced some of the most accurate quantum yields available.

In 1957 Weber and Teale [49] made a step forward by the introduction of solution scatterers for standards. This technique introduces its own special problems and limitations but is easier to carry out than the basic Vavilov method [1]. Numerous workers have devised improvements and modifications of both the Vavilov and the Weber-Teale methods for determining quantum yields, yet the measurements are still relatively tedious to perform and have many associated problems.

The difficulties inherent in absolute procedures and the demand for yield measurements on hosts of compounds have led workers to devise simple relative methods for performing the measurement. In these methods the yield of an unknown is compared with the "known" quantum yield of a standard material. Relative methods fall into two categories, optically dense and optically dilute. In the former, concentrated solutions are employed to absorb all the incident flux; in the latter, dilute solutions insure negligible diminution of the excitation beam across that part of the sample viewed by the detector. Optically dense quantum-yield measurements relative to a standard can be made extremely rapidly and are subject to moderate errors provided the substances satisfy somewhat rigid requirements. The accuracy can be low due to effects associated primarily with high concentrations. Optically dilute methods generally avoid problems created by solute-solute interactions and, due to the availability of high quality spectrofluorometers and their components, have become the preferred techniques for obtaining yields.

An analysis of optically dilute methods, the useful equations and their limits of validity, and the problems associated with this kind of measurement are contained in reference 1. We refer the interested reader to this review and the references therein. We wish to point out here, however, two problems associated specifically with yields obtained by optically dilute procedures that modern laser technology should admirably solve, (a) inaccurate (high) yields caused by strong light from a broad band source leaking through the filter system and (b) inaccurate yields produced by uncertainties in the effective absorbances of samples over the finite bandpass of the filters or monochromator excitation system (see *Lasers*, below).

For routine determinations of quantum yields by optical methods, the use of optically thin solutions versus optically thin standards is probably the best method available. The reported reproducibility is quite good (1–2%), and the agreement between laboratories is excellent (<5%) for some molecules. Considerable improvement in accuracy is to be expected from substituting lasers for conventional sources and from incorporating modern electronics and detectors into the systems. Although frequently reported with high precision [35–37], the accuracy of quantum yields obtained from substances dissolved in rigid glasses may not be high in spite of the good reproducibility. The relative importance of polarization errors is especially vexing to assess for rigid systems, and more work on this aspect of the optically dilute methods is badly needed [85].

Finally, we reiterate that both the optically dense and optically dilute techniques are still relative ones. Whatever systematic errors are built into the standards will be reflected in the results. Accurately measured standards are urgently needed.

A. Recent Developments in Instrumentation

We turn now to highlight some recent instrumentation advances that bear on optical methods of determining quantum yields. Lasers are by far the most important development, but the significance of available high sensitivity Raman instrumentation and recent improvements in photodetectors deserve attention.

1. Lasers

Lasers are now available in a wealth of types, powers, and configurations. The salient features of the most common varieties are reviewed in table 1. This list is by no means complete. In many cases, commercially available items are listed, and data have been drawn frequently from the manufacturer's literature. It should be further noted that specialized design frequently can improve many of the listed characteristics. In addition, because of the rapid advances in laser technology, this table will surely be obsolete by the time it is printed. The interested reader should consult the latest issues of the laser trade journals (e.g., *Laser Focus* and *Laser Sphere*) and other technical journals for up-to-date information. An especially valuable source is reports on advanced seminars in laser technology [86].

Most significant for luminescence and quantum-yield work is the high continuous wave (cw) powers available in the near UV and visible from argon lasers. The continuous tunability of the cw pumped dye lasers and their remarkably narrow line widths are also particularly noteworthy. Pulsed nitrogen lasers with their extremely short duration pulses and UV frequencies are ideally suited for most lifetime measurements and even for nanosecond photolysis. By driving a dye laser with a nitrogen laser and selecting the wavelength with an intracavity grating, one can preserve the extremely short durations and relatively high powers (one to two orders of magnitude in power are sometimes lost), but the added feature of continuous tunability from the

TABLE 1. Characteristics of selected lasers

Continuous Wave Lasers

TYPE **Discrete Line Lasers**	λ, nm	POWERS	MONOCHROMATICITY
Ar [a]	351.1 + 363.8; 457.9; 472.7; 476.5; 488.0; 496.5; 501.7; 514.5; 528.7	20 mW to 2 W	< 0.001 Å
Kr [a]	350.7 + 356.4; 476.2; 482.5; 520.8; 530.9; 568.2; 647.1; 676.4; 752.5; 799.3	20–500 mW	< 0.001 Å
Tunable Lasers			
cw pumped dyes with intracavity λ selection [a]	520–690	10–160 mW	0.1 Å normal to 0.001 Å

Pulsed Lasers

TYPE **Discrete Line Lasers**	λ, nm	POWERS	MONOCHROMATICITY	DURATION, nsec
N_2 [b]	337.1	1–10 1–100 kW peak 0.5 W average	~1 Å	5–10
Nd^{3+}-YAG	266 (frequency quadrupled), 13 lines from 473 to 679 (frequency doubled), 13 lines from 946 to 1358	1–5 kW peak 10–100 m W average	< 1 Å	100–400
Ruby	694 (Q-switched)	100 MW peak 1 J per pulse	0.1 Å	20 [d]
	347 (frequency doubled)	10 MW peak	0.1 Å	20 [d]
Tunable Lasers				
Flashlamp pumped dyes [c]	340–>650	0.25 J/pulse 600 kW peak 25 mW average	< 1–10 Å	100–500 [d]
N_2-laser pumped dyes [b]	360–>650	2–150 μJ/pulse 1–10 kW peak 1–50 m W average	< 1–20 Å	2–10 [d]
Nd^{3+}-YAG pumped dyes [e]	540–670 and 270–340	20–700 W peak 0.2–25 mW average	< 1 Å	
Parametric oscillator [e]	650–3000	50–700 W peak 1–10 mW average	≤ 1 Å to 0.001 Å	70–150

[a] Data for lasers from Spectra-Physics and Coherent Radiation.
[b] Data for AVCO Everett Research Lab. lasers.
[c] Data for Synergetics Research, Inc. lasers and from references [88, 89, 90, 91].
[d] Mode locking can yield picosecond pulses (< 0.1 nsec), although spectra bandwidth will usually be increased. See references [90, 91].
[e] Data for Chromatix laser.

near UV through the visible is obtained. These characteristics are ideal for carrying out time-resolved spectroscopy, a powerful fundamental and analytical tool. The large pulse energies available from the flashlamp-pumped dye lasers are also attractive for some studies, and systems can be built for minimal cost [87–89].

From table 1 the benefits accrued from replacing conventional light sources with a laser source are manifest. The powers available far exceed those normally obtained from even wide bandpass conventional sources. This power gain, however, can be obtained at no loss in spectral purity, and for most molecular systems one can treat the sample absorbance as constant over the excitation line. Thus, one of the significant sources of error mentioned above in quantum-yield and excitation-spectra determinations is eliminated. The higher powers available from the lasers also permit the use of more dilute solutions; this reduces the trivial errors of self absorption and secondary emission.

In addition to the high powers and narrow line widths, lasers have other advantages. Typically, the laser beam is of very small size. A cw argon laser, for example, has a beam diameter of 1 to 2 mm. It is highly coherent and can be focussed to an essentially diffraction limited spot. This high degree of focusability is commonly exploited in Raman work where the laser is directed down the long axis of a microcapillary. The use of a microcapillary cell would also yield significant advantages in luminescence spectroscopy. There would be negligible reabsorption, and the source composed of the emitting volume would be a near line. Thus the emissions could be focussed extremely efficiently onto the entrance slit of an emission monochromator, even for very narrow emission bandpasses. Such a system could not be used with even moderately photosensitive materials, however, unless a flow system were employed. Microcapillary cells have a further disadvantage for comparative work due to the higher precision required for reproducible alignment.

There seems little doubt that the wavelength range, the pulse duration, and the available powers of most of the types of lasers will be greatly improved. With progress in mode-locking [90–92] it seems reasonable to anticipate that the dye lasers will yield repetitive, stable, and continuously tunable subnanosecond pulses extending from the UV to near-IR regions. Such a tunable, short duration source would represent truly a delta function excitation flash for luminescence lifetime measurements and time-resolved spectroscopy, with little sacrifice in power or spectral purity. For dye lasers especially, considerable improvements in peak and average power are anticipated as the pulsed nitrogen lasers become more efficient. Wavelength range limitations of tunable dye lasers will almost certainly become relaxed as the dyes are frequency doubled into the UV, and new dyes will surely extend the available range well into the infrared. Already the entire range between 7000 and 11,700 Å has been covered by pumping photographic film sensitizer dyes with Q-switched ruby lasers [93]. A number of parametric oscillators has been constructed that exhibit continuous tunability from 7000 to 20,000 Å, and efficiencies of 45 percent have been reported [94].

Referring to the optical quantum-yield methods sketched above, we cannot think of a technique that would not benefit substantially from the replacement of the conventional light source with the laser. We have no doubt that where low cost is not a prime factor, but accuracy is of paramount importance, lasers will eventually become the excitation source of choice. This statement applies to calorimetric methods also.

2. *Raman Instrumentation*

The developments of laser Raman spectroscopy have yielded a whole new line of optical components that are admirably suited for luminescence and quantum-yield measurements as well. One of the principal areas of progress is monochromator technology. Quite fast, extremely-low stray-light, double monochromators have been produced. Stray light in these devices is so low that one can scan to within a few wave numbers of the laser line pump. Such superb stray light rejection makes them a natural choice for luminescence and quantum-yield measurements, especially when laser excitation is employed. It is noteworthy that much of the impetus for the development of very high power krypton and argon lasers also stemmed from the needs of the Raman spectroscopist.

Photomultipliers have also undergone enormous improvements. By reducing the effective photocathode size and cooling the tubes to reduce the dark current, the dark backgrounds have been reduced to a few counts per second (e.g., tubes of the IT&T[2] type). All this has been accomplished with an extended red response S–20 photocathode, which may exhibit a quantum efficiency of several percent beyond 800 nm.

Thus the modern unmodified Raman instrument using an argon laser source represents a nearly ideal excitation-detection system for luminescence, at least when the molecules absorb in the region of the laser lines. The ready availability of these Raman spectrometers within many laboratories also adds to their attractiveness for such work. Almost any further advances in Raman technology are certain to be adaptable with benefit for making luminescence measurements and for determining quantum efficiencies.

3. *Photodetectors*

In addition to the restricted area tubes used in Raman spectroscopy, there have been other significant advances in detector technology. RCA, for example, has introduced a line of gallium arsenide and indium-doped gallium arsenide extended red-response

[2] In order to adequately describe materials and experimental procedures, it was occasionally necessary to identify commercial products by manufacturer's name or label. In no instances does such identification imply endorsement by the National Bureau of Standards, nor does it imply that the particular product or equipment is necessarily the best available for that purpose.

photomultipliers. The gallium arsenide tubes typically have quantum efficiencies of 1.4 percent at 860 nm. With indium doping, the red response is further extended, and RCA will supply tubes having efficiencies of 1 percent at 950 nm, 0.2 percent at 1000 nm, and 0.1 percent at 1060 nm. In addition to having remarkably deep infrared penetration, these tubes have quite low dark currents even at room temperature; in most cases they can be regarded essentially as a quantum jump better than the old infrared tubes with S–1 response. Further improvements seem likely since gallium arsenide photosensitive surfaces have been prepared having maximum quantum efficiencies of 80 percent [95].

Semiconductor diodes are also improving. Germanium diodes of the type used in nuclear instrumentation make superb optical detectors [96]. They can have large areas (> 1 cm $\times > 1$ cm) and sensitivities comparable to photomultipliers. Their noise equivalent power (NEP) is $\sim 10^{-15}$ W/Hz$^{1/2}$ from the visible to beyond 1600 nm. Their stability and near quantum flat response of ~ 0.6 has led to the suggestion that they be used as replacements for thermopile radiation detectors [96].

When operated in the avalanche mode, these photodiodes have many of the characteristics of photomultipliers. They still have the high quantum efficiencies of the solid state photodiodes but also exhibit a limited gain multiplication. Typically, their sensitivities stretch well into the near infrared. Texas Instruments, for example, has introduced a series of silicon and germanium photodiodes packaged with amplifiers (TIXL 74–76). For the silicon system, the NEP at 900 nm is less than 5×10^{-13} W/Hz$^{1/2}$. For the germanium ones, the NEP is $\sim 2 \times 10^{-12}$ W/Hz$^{1/2}$ at 1060 nm or $\sim 6 \times 10^{-12}$ W/Hz$^{1/2}$ at 1540 nm. With properly biased photodiodes, single photon counting is even possible. With germanium photodiodes, NEP's of $\sim 10^{-13}$ W/Hz$^{1/2}$ at 1500 nm have been realized. Germanium devices are usable to beyond 1700 nm [97]. It seems reasonable that further improvement in these avalanche devices will yield even higher sensitivity in the near-IR region. It is even possible that they will become competitive with photomultipliers in the visible-UV regions. In a spectrophotometry application weak transient absorption during flash photolysis has been detected in the 0.6–1.1 μ region with the aid of an inexpensive silicon photodiode [98].

If the major source of noise in an optical experiment is due to the photon statistics, then the signal-to-noise ratio depends upon the square root of the quantum efficiency of the detector. Thus for high light level experiments the high quantum efficiency of photodiodes is a distinct advantage for noise discrimination, especially in the near infrared.

B. New Experimental Techniques

1. Internal Standardization

Internal standardization is frequently used in analytical chemistry. To date, however, we are aware of no use of an internal standard for quantum-yield measurements. This failure has been a result of the experimental difficulties involved rather than because of any undesirable fundamental features of the technique itself. In fact, internal standardization is probably one of the more elegant and useful techniques for accurate relative quantum-yield determinations. The method appears especially feasible in view of modern instrumental developments.

In the internal standardization procedure both the unknown and standard would be contained in the same solution. The emission spectra of the two compounds would then be run in a single scan of the emission instrument. From the relative emission intensities of the standard and the unknown and their absorbances one would then calculate the efficiency of the unknown relative to the standard by normal procedures. The advantages of such a procedure are numerous. Since the standard and unknown are in the same solvent and cell, refractive index corrections are all but nonexistent, and radiation trapping is essentially identical between both samples. Errors introduced by cell mismatch are eliminated. There are, of course, serious restrictions on the method. The standard and the unknown must emit in well-resolved spectral regions (by means of time-resolved spectroscopy, even this restriction may be lifted). They must also absorb at the same wavelength.

Several experimental difficulties must be considered closely if satisfactory results are to be obtained using an internal standard. Because the standard and unknown are present in the same solution, great care must be taken to prevent any bimolecular quenching or energy-transfer processes, since their occurrence would modify the yields of the species present [99]. As long as one is using optically dilute solutions, there is no problem with long-range energy transfer of the Förster-type. This would not, however, always be true if optically dense solutions were employed.

Diffusion-controlled processes must also be considered. One can readily show that even if a sample has a component with a lifetime as long as 1 μs that is quenched by the other one at the diffusion controlled limit (10^{10} M^{-1} s^{-1}) then the concentration of the second species must exceed 10^{-6} M to cause 1 percent quenching of the first. Since optically dilute measurements are usually carried out at optical densities less than 0.01, then any second component with $\epsilon \geq 10^4$ at the exciting wavelength would introduce a negligible error. Of course, if the first compound has a lifetime of less than 1 μs or the quenching proceeded with a rate less than the diffusion-controlled limit, then this already weak restriction would be relaxed still further. For example, if the standard's lifetime were 10^{-8} s (a typical fluorescence lifetime), then the maximum permissible concentration of the second species would be 10^{-4} M; this would permit molecules with $\epsilon \geq 10^2$ to be measured. The same arguments apply to the second component. Most materials and standards would have coefficients satisfying this condition in some region. Thus, because of bimolecular

quenching it appears that the internal standardization technique is largely limited to optically dilute measurements. Consequently, all of the restrictions and limitations on any optically dilute method are present [1].

The remaining serious difficulty or source of error envisioned in a procedure employing an internal standard is that inherent in accurately calibrating any spectrometer over a wide wavelength range. Also, some compounds have extremely wide emission bandwidths; then difficulty will be encountered in obtaining satisfactory standards. Transition-metal complexes, as discussed above, may possibly be designed for appropriate standards. Sensitivity, even when working with low yield substances under optically dilute conditions, does not appear to present a severe limitation for the method.

In summary, we believe that the use of an internal standard in relative quantum-yield determinations deserves serious consideration for investigation and development. If well-defined standards become readily available, the method could eventually become one of the preferred ways of running high-accuracy yield determinations.

V. Quantum Efficiencies by Actinometric Methods

The principle of the actinometric method for measuring quantum yields is conceptually simple. One merely surrounds the sample completely with an actinometer solution, measures the apparent intensity of the emitted radiation, and then, using the same type of actinometer solution, monitors the intensity of the excitation beam. If the irradiated solution is totally absorbing, the ratio of the two intensities is the absolute quantum yield. Whereas actinometers are capable of measuring absolute intensities, this technique is, in fact, a relative method since the absolute yield of the actinometer need not be known. To our knowledge, this method has not been used for measuring optically excited luminescence efficiencies. It has, however, been utilized in a suitably modified form for measuring chemiluminescence yields [100].

The principal reason for the nonadoption of an actinometric method is experimental. Most actinometers have quantum yields that are strongly wavelength dependent, and their absorption characteristics make it difficult to arrange to have all of the emitted light absorbed over the very wide wavelength ranges encountered in molecular luminescences. Because of these factors it is difficult to obtain an accurate measurement of the intensities of both the excitation beam and the broad molecular emission with the same actinometer. With the advent of new sources and actinometers, however, actinometric methods may achieve a useful place in absolute quantum-yield measurements.

Before launching into speculative discussion we point out that the potassium salt of *trans*-$[Cr(NH_3)_2(NCS)_4]$ (Reinecke) is an excellent wide-range actinometer covering the 300 to 600-nm region [101]. Its yield has been measured over an extended wavelength range, and it is reasonably sensitive. Unfortunately, it is not without its shortcomings. To absorb most of the emitted light in the 300 to 600-nm range, rather concentrated and/or thick solutions are required (about 1.5 cm at a concentration of 5×10^{-2} *M*). The compound also exhibits a slow but bothersome thermal decomposition. Finally, there is a slight, although perhaps not real, variation of the quantum yield with wavelength, a variation that is, however, small enough that reliable corrections could be made. No one has confirmed the original yields, and the initial data were taken at somewhat greater wavelength intervals than would be desirable for precise corrections. Notwithstanding these objections, Reinecke's salt is even now usable as a wide-range actinometer for yield determinations.

Recent photochemical investigations portend the development of additional wide-range actinometers. Demas and Adamson [102] have found that tris(2,2′-bipyridine)ruthenium(II) sensitizes, by a diffusion-controlled process, the redox decomposition of tris(oxalato)cobaltate(III). Since the donor has a broad, intense absorption, it is quite easy to obtain, with thin solutions, total absorption of incident light from the UV to beyond 500 nm. The decomposition of the $[Co(C_2O_4)_3]^{3-}$ may be readily monitored spectrophotometrically (unfortunately not with quite the high sensitivity of the ferrioxalate). Furthermore, since the efficiency of population of the donor level is believed to be unity and to occur virtually instantaneously following excitation, the system has a decomposition yield that is inherently wavelength independent and that has a broader range than most other actinometers. In its present form, their system is not, however, a useful actinometer. With modifications it, or a related system, may become practical.

Lasers make the actinometric method for measuring yields appear even more attractive. The excellent focusability of lasers permits an extremely small entrance aperture to be used and thus minimizes the error due to loss of radiation through the excitation port. Also, because the laser beam is inherently well collimated, one could use relatively dilute solutions in very long cells and irradiate down the cylindrical axis. In this way trivial reabsorption effects would be minimized. A device built along these lines might look much like a condenser with the outer cooling jacket filled with the actinometer solution. Of course, any measurement based on an optically dilute method would be subject to the normal corrections, and the optically dense method would be prone to its usual inherent errors. In spite of these objections, common to all optical quantum-yield measurements, it seems that the actinometric method has distinct possibilities even now with potassium Reinecke, and it will probably become more attractive with time, especially as the developments in modern inorganic photochemistry gain momentum and uncover new photochemical reactions and sensitizers.

VI. Quantum Efficiencies by Calorimetric Methods

Although measurement of quantum efficiencies optically involves generally familiar instrumentation, this statement cannot be made about calorimetric procedures. Recently, however, developments in technology point toward a gaining importance of calorimetry in the field of quantum yields, and we wish to discuss some of them. Because of their relative unfamiliarity, we present here a more detailed account of the various methods employed in calorimetry than was included above for the optical methods.

Calorimetric methods of measuring quantum yields are based on the assumption that energy absorbed from a beam of light incident upon a solution of fluorescent molecules is either lost through reemitted photons or degraded to heat by radiationless processes. The objective of calorimetric techniques is to measure the energy yield of these radiationless processes, Y_h, which is defined as the ratio of heat energy produced to incident photon energy absorbed. Y_h is obtained by measuring the ratio of the heating produced by irradiation of the fluorescent sample to the heating produced by irradiation of a nonfluorescent sample that absorbs the same fraction of the excitation energy.

In the absence of photochemistry, the fluorescence [103] energy yield is the complement of Y_h and the quantum yield of fluorescence is related to it by the formula

$$\Phi = (\bar{\nu}_a/\bar{\nu}_f)(1 - Y_h) \tag{1}$$

where $\bar{\nu}_a$ and $\bar{\nu}_f$ are the average frequencies (cm^{-1}) of absorbed and fluorescence photons, respectively, defined by the formulas

$$\bar{\nu}_a = [\int I_a(\lambda) A(\lambda) d\lambda/\lambda]/[\int I_a(\lambda) A(\lambda) d\lambda] \tag{2}$$

$$\bar{\nu}_f = [\int I_f(\lambda) d\lambda/\lambda]/[\int I_f(\lambda) d\lambda] \tag{3}$$

$I_f(\lambda)$ and $I_a(\lambda)$ are the fluorescence and excitation intensities at wavelength λ, $A(\lambda)$ is the percent absorbance of the sample with a pathlength equal to the cell dimension, and the integrals are over the fluorescence and excitation bands, respectively. Since $\bar{\nu}_f$ and $\bar{\nu}_a$ are easily measured with high precision by standard photometric techniques, they will not be discussed further here [1, 29].

Several important factors favor calorimetric methods for the determination of absolute quantum yields: (a) The method serves as a valuable independent check of the assumptions used in photometric techniques for measuring Φ_f; in particular, corrections for experimental geometry, index of refraction changes, and polarization effects are largely eliminated. (b) Using relatively crude apparatus, some workers have obtained values of Y_h with a precision comparable to those obtained by other methods [29]. (c) The calorimetric method works well with samples that emit in the near infrared where the sensitivity of optical techniques is relatively low. Recent developments in photodetectors are alleviating this problem, however (see above).

With the usual procedures and components, the principal disadvantages and limitations of the method have been the following: (a) The insensitivities of the calorimeters used thus far have forced workers to use highly absorbing samples; consequently, large corrections for reabsorption of the fluorescence [29, 104] are required. (b) The method has been limited to substances possessing high quantum yields. (c) Measurements have been confined to liquid samples at room temperature. (d) Methods devised thus far have been tedious and time consuming to perform.

Recent advances in calorimetry, especially in the technology of light sources and transducers, and improvements in methods of data acquisition portend wider acceptance of the technique for obtaining quantum efficiencies. The generality, sensitivity, and ease of performance of calorimetric methods will undoubtedly improve. Our purpose here is to review some of the advances in methods and components and to indicate possibilities for still greater improvements.

A. Calorimeters

The calorimetric apparatus consists of an excitation source, a means for selecting a bandwidth of the incident radiation, and a calorimeter to measure the heat energy produced during irradiation. The science of calorimetry is a mature field of endeavor, and the reader desirous of a general background in the subject is referred to the several books and recent reviews now available [105–108]. Let us begin our discussion of calorimetric apparatus by considering the constraints on the calorimeter imposed by the requirements for measuring quantum yields. First, provision must be made for admitting the exciting light. Second, the calorimeter must be designed so that all fluorescence escapes the cell. Third, since the sample will not be uniformly irradiated, the average or total heating must be detected. Fourth, the calorimeter must be very sensitive. In general, the sensitivity requirements will depend on the energy of the incident radiation, the absorbance of the sample, and the value of the quantum yield to be measured. A straightforward analysis of the propagation of errors in the calorimetric method shows that in order to measure a value of $\Phi_f = 0.5$ with a precision of 1 percent, the heating of the nonfluorescent sample must be measured with a precision of 0.1 percent.

It is shown later that most calorimeters detect the heating power produced by steady state irradiation. If the incident radiation power is 100 mW, and we are using samples that absorb 10 percent of the beam or less to avoid reabsorption effects, then our calorimeter must be capable of measuring a heating power of 10 μW with a signal-to-noise ratio of unity.

It is now obvious that the method for detecting heat flow in the calorimeter must be very sensitive. Most

calorimeters use temperature transducers to measure heat flow. One figure of merit, useful for evaluating temperature transducers, is their noise equivalent temperature (*NET*) given by the following expression

$$NET = [N/S(\Delta f)^{1/2}] \text{ deg/Hz}^{1/2} \quad (4)$$

where N is the noise voltage developed by the transducer, S is the voltage sensitivity of the transducer, and Δf is the noise bandwidth. The *NET* is defined as the temperature change required to generate a signal-to-noise ratio of unity when the detector noise is referred to a one cycle bandwidth.

One common method for measuring temperature changes in calorimetry is by means of a thermopile. Generally, the limiting noise in this device is due to the Johnson noise of its resistance. For a 100-junction copper-constantan thermopile of 100 Ω resistance, the *NET* is calculated to be 0.2 μdeg/Hz$^{1/2}$. The tiny voltages associated with these devices can be conveniently measured by means of a commercially available nV amplifier such as the Keithley Model 148. The construction of thermopiles is an art and is discussed by Hill [109], Howarth [110], and Evans [111].

Resistance thermometers have also been used for calorimetric work. Larsen [112] has shown that the sensitivity of platinum resistance thermometers operated by an ac bridge approaches the theoretical limit imposed by the Johnson noise of the device. He gives a *NET* of 20.5 μdeg/Hz$^{1/2}$ for a commercially available 500 Ω platinum resistance thermometer. These tranducers are very stable with time, are smaller in size than thermopiles, and do not require reference junctions.

The use of thermistors in calorimetry has been discussed by Meites et al. [113]. Previously, these temperature transducers have been criticized for calorimetric work because of long term instabilities [112]. Meites et al. found, however, that operation of selected and aged 100 K thermistors at low power levels (18 μW) allowed reliable detection of temperature changes of 10 μdeg by means of a dc bridge and recording potentiometer. The *NET* as predicted by consideration of the Johnson noise is even lower, 0.7 μdeg/Hz$^{1/2}$. Attainment of this resolution will probably require use of an ac bridge and phase sensitive detection. Thermistors also offer advantages due to their small sizes and fast response times.

In addition to temperature transducers, one can also employ volume transducers to measure heat flow. The volume change, ΔV, produced at constant pressure in response to a heat change, ΔQ, is given by the formula

$$\Delta V = \alpha \Delta Q / C_p \rho \quad (5)$$

where α is the thermal expansion coefficient of the sample, ρ is its density, and C_p is its heat capacity per gram. A simple dilatometer for measuring volume changes in calorimetric experiments has been used by Seybold, Gouterman, and Callis [29]. In their apparatus, the sample is contained in a cell open to the atmosphere only through a capillary tube. The volume of the solution is visually monitored as it expands up the capillary. Volume changes as small as 7×10^{-5} cm^3 can be measured; for a 10-cm^3 ethanol sample this corresponds to a temperature rise of 7×10^{-3} °C. Further increases in sensitivity in capillary dilatometers can be obtained by using a travelling microscope [114] or a photocell to measure changes in the height of the liquid in the capillary.

A greatly improved technique for measuring volume changes has been developed by Callis, Gouterman, and Danielson [44]. These workers use a capacitor microphone to detect volume changes. They claim a noise equivalent volume (*NEV*) change of 4×10^{-10} cm^3 referred to a 1-Hz bandwidth, which corresponds to a *NET* of 0.04 μdeg/Hz$^{1/2}$ for heating 10 cm^3 of ethanol. In addition to its sensitivity, this technique has other advantages: (a) The volume change is independent of the size of sample irradiated, whereas the magnitude of the temperature change depends on the size of the sample. (b) Equation (5) is valid even though a uniform temperature is not established if, at all points, ΔT is small enough so that the equation holds locally. Thus, the sample need not be stirred. (c) The response time of this apparatus is limited only by the transit time for sound in the cell. Disadvantages of the volumetric technique are: (a) The electronics, as originally devised by Callis et al. are ac coupled. Use of a capacitance bridge can overcome this disadvantage, however. (b) The apparatus is sensitive to vibration and acoustical noise and therefore must be isolated from both. (c) For water, an important solvent, $\alpha/\rho C_p$ is ~10 times lower than for organic solvents.

All of the calorimeters we shall discuss in this paper are surrounded by an isothermal shield, and thus all can be characterized by the same energy flow equation

$$dH/dt = FY_h P(t) - KH(t). \quad (6)$$

$H(t)$ is the heat energy retained in the sample, F is the fraction of incident power absorbed by the solute, $P(t)$ is the incident radiation power, and K is the first-order heat loss constant under the assumption that all heat losses are newtonian. We have neglected heating due to absorption by the solvent and reabsorption of fluorescence photons. These effects are discussed elsewhere [1].

Two cases of eq (6) may be distinguished: (a) When the heat loss term is negligible, the calorimeter is an adiabatic one. (b) When the heat loss term is large, the calorimeter is a conduction calorimeter. When the heating input is exactly balanced by an equal cooling, then the calorimeter is known as a compensation calorimeter.

Let us first consider the use of the conduction type calorimeter as employed by Alentsev [104] for measuring Y_h. The calorimeter consists of a thin cell suspended in a chamber whose walls are maintained at a constant temperature. Temperature changes are measured by means of a thermopile. The measuring

junctions are arranged symmetrically around the lateral wall of the cell, and the reference junctions are buried in the isothermal wall. The major source of heat loss is through the thermopile itself. A schematic of the apparatus is shown in figure 6. Since temperature changes are measured, we can use the relationship $H(t)=C_p[T(t)-T_0]$ to convert eq (6) to a form involving the instantaneous temperature.

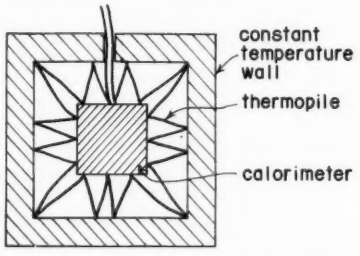

FIGURE 6. Conduction calorimeter.

$$dT(t)/dt=[FY_hP(t)/C_p]-K[T(t)-T_0] \quad (7)$$

where T_0 is the temperature of the wall. For steady state irradiation (P constant), the solution to eq (7) is

$$T(t)-T_0=FY_hP(KC_p)^{-1}[1-\exp(-Kt)]. \quad (8)$$

After a time $t \gg 1/K$ the maximum temperature rise, ΔT_m, is reached.

$$\Delta T_m=FY_hP(KC_p)^{-1}. \quad (9)$$

The ratio of ΔT_m for the fluorescent sample to ΔT_m for a nonfluorescent sample that absorbs the same fraction of incident light gives Y_h, provided K and C_p are the same. For a given energy input, ΔT_m can be maximized by using the lowest value of K and C_p. As used for determination of Y_h, the conduction calorimeter may be thought of as a power measuring device, and thus a factor of merit is its noise equivalent power (*NEP*), which is defined as the power input required to generate a signal-to-noise ratio of unity when the detector noise is referred to a 1-Hz bandwidth. For the conduction calorimeter

$$NEP=NET(K)C_p \quad (10)$$

where the *NET* is that of the temperature transducer used. For a *NET* of 1 μdeg, a heat capacity of 10 cal/°C and a K^{-1} of 10 min, one obtains a *NEP* of 0.07 μW. In practice, the best conduction calorimeters [115] exhibit a *NEP* of 0.2 μW; but even this value is far better than that obtained by Alentsev. The limit of sensitivity of this apparatus is apparently determined by the temperature stability of the environment of the calorimeter [115]. Design and construction of conduction type microcalorimeters is discussed extensively by Evans [111] and by Calvet and Prat [115, 116]. In the most advanced designs [111, 115, 116], the experiment is conducted differentially, i.e., the temperature difference between the irradiated sample in one cell and an identical unirradiated sample in a twin cell is measured. This technique greatly increases the long term stability of the apparatus and is to be recommended for any type of dc calorimetry.

As employed for conventional calorimetric measurements, conduction calorimeters are not stirred. This is possible if a large number of thermocouples is distributed evenly over the surface of the calorimeter so that the average surface temperature is measured. For fluorescence measurements, however, it is ideal to have all of the fluorescence escape the cell. Thus, the thermopiles should occupy only a tiny fraction of the cell surface. The cell must be stirred. Unfortunately, stirring produces its own heating, which gives rise to additional noise in the system [111].

Perhaps the major disadvantage of using conduction calorimeters is that long times are required for measurement. For a K^{-1} equal to 10 min, one must wait at least 1 h for the sample to come into equilibrium, and additional time will be taken waiting for the temperature to stabilize.

Some recent work by Chastel and Tachoire [117] suggests that the commercially available and highly perfected Tian-Calvet conduction microcalorimeter may be used in a virtually unmodified form in conjunction with a pulsed light source. The calorimeter is shown schematically in figure 7. The cell is made of glass or quartz, which is surrounded by a metallic "can" whose inside is coated with a totally absorbing black substance. The thermocouples are

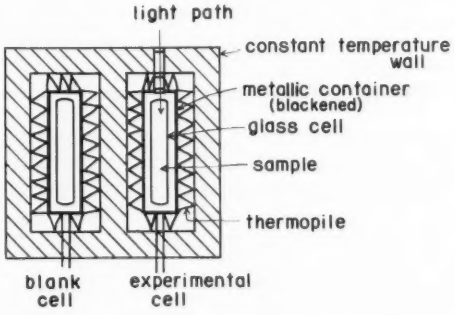

FIGURE 7. Tian-Calvet conduction microcalorimeter modified for quantum-yield determination.

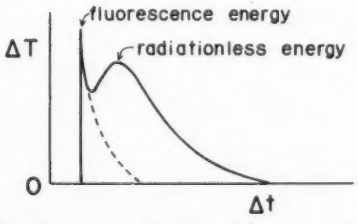

FIGURE 8. Thermogram from Tian-Calvet microcalorimeter.

affixed to the metallic cell. Irradiation of the sample produces a double flux of light and heat. The light is converted to heat through absorption by the metallic cylinder. A recording of the temperature as registered by the thermocouples versus time in the form of a thermogram would be expected to yield the results shown in figure 8. The first peak is due to light absorbed at the cylinder; the second is due to heat diffusing from the sample produced by radiationless processes. If the response times of the apparatus to heat and light are determined, then it is easy to separate the two responses and obtain the energy yields. Chastel and Tachoire have obtained excellent results on energy yields of flash sources for photography in this manner.

A second type of calorimeter, which can be used for measurements of Y_h, is a heat flow compensation calorimeter. The design of such calorimeters has been discussed by Sturtevant [118]. In these devices, heating produced by irradiation is balanced by an equal amount of cooling power supplied by a thermoelectric module. The null heating point is sensed by a temperature transducer. Thus, the cooling power supplied is a direct measure of the energy input power. An apparatus is shown schematically in figure 9. This device

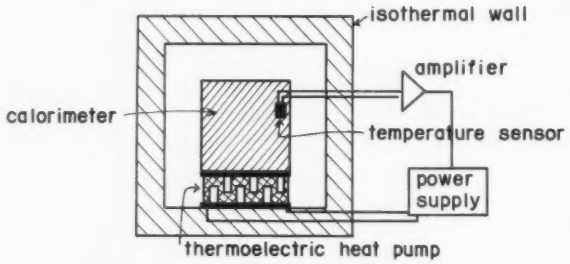

FIGURE 9. Heat flow compensation calorimeter.

is also essentially a power measuring apparatus, and its factor of merit is given by the *NEP*, which is related to the *NET* of the temperature sensor, as follows:

$$NEP = NET(C_p)\tau^{-1} \tag{11}$$

where τ is the time constant of the temperature detection. To minimize the *NEP*, one desires the lowest values of heat capacity and *NET* and the longest time constant. For a $NET = 1$ μdeg, $C_p = 10$ cal/°C, and $\tau = 10$ the *NEP* is 4.2 μW. This type of calorimeter may also be used in a differential mode where the difference between an irradiated and unirradiated cell is measured.

Adiabatic calorimeters are a third possibility for Y_h measurements. They have been employed in this manner by Seybold, Gouterman, and Callis [29] and by Gudmundson et al. [119]. In these devices one attempts to eliminate heat transfer between the calorimeter and its surroundings. Because of the tiny temperature changes involved, this ideal is best approached by conducting experiments in a constant temperature jacket calorimeter for short time periods so that heat losses are negligible. As with conduction calorimeters, adiabatic calorimeters can be used with steady or pulsed sources. If the sample is irradiated by a steady light source, the temperature rise can be measured as a function of time. In this case, the calorimeter may be thought of as a power measuring device, and the minimum detectable power level will be related to the *NET* of the temperature sensor by the formula

$$NEP = NET(C_p)\Delta t^{-1} \tag{12}$$

where Δt is the maximum time after the start of irradiation at which a measurement can be made. For the isothermal jacket calorimeter this condition will be $K\Delta t \ll 1$ where K is the rate of newtonian heat loss. For a *NET* of 1 μdeg, a C_p of 10 cal/°C, and a Δt of 100 s, a *NEP* of 0.42 μW is obtained. If a pulsed light source is used, the net temperature rise is measured. In this case, the calorimeter determines the integral of the incident power, and thus a figure of merit is the noise equivalent energy change, *NEE*, which is just the *NET* of the temperature sensor times the heat capacity of sample and calorimeter. Thus, for a *NET* of 1 μdeg and a 10 cal/°C heat capacity, we obtain a *NEE* of 10 μcal. This method is attractive because pulsed light sources of high energy are readily available (e.g., pulsed lasers), and heating due to absorption of fluorescence by the calorimeter can be separated by its time dependence.

Thus far, all of the types of calorimeters we have discussed are, in principle, capable of measuring very low power levels and will allow elimination of reabsorption corrections. They all have a common single disadvantage, however. The measurements are performed near zero frequency and are tedious and time consuming. Further, the temperature of the calorimeter and surroundings must be controlled to the *NET* of the temperature sensing device if the lowest possible *NEP* of the calorimeter is to be realized.

Currently, a new technique for calorimetric measurements of Y_h, which can overcome some of the disadvantages of conventional calorimetry, is under development. Essentially the apparatus is the flash calorimeter of Callis, Gouterman, and Danielson [44] shown in figure 10. It consists of a glass cuvette, one wall of which is the compliant diaphragm of a capacitor microphone. The valve attached to one side of the cell serves as a capillary leak so that the liquid can slowly enter or leave the cell. This prevents slow pressure changes that would occur in a completely closed cell subject to temperature drifts and the dc component of repetitive excitation.

Because of the fast response time of this apparatus, the exciting light is modulated, and the resultant heating is detected at the frequency of the modulation by phase sensitive techniques. The advantages of ac methods of doing experiments is well known [120]. Briefly, all experiments are contaminated with noise, some of which has a $1/f^n$ frequency dependence. This latter noise is dominant in calorimetric measure-

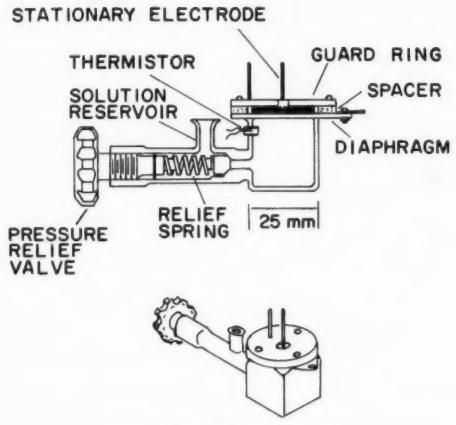

FIGURE 10. Flash calorimeter.

ments, which are performed at low frequencies where thermal drifts are important. By modulation one can shift the frequency domain of the experiment to a point where noise due to thermal drifts is no longer important and thermostating can be eliminated. By means of phase sensitive detection, very narrow bandwidths can also be obtained, further discriminating against noise.

Due to these advantages, it is worthwhile to consider in more detail this new method for determining Y_h. Assume that the light intensity has the time dependent form

$$P(t) = P_0(1 + \cos \omega t). \tag{13}$$

P_0 is the steady state power in cal/s and ω is the modulation frequency. The heating in the cell in response to the excitation is given by eq (6). We may combine eqs (5) and (6) to obtain a differential equation for the time dependence of the volume change

$$dV(t)/dt = [\alpha F Y_h/\rho C_p] P(t) - K'V(t) \tag{14}$$

where K' is the first-order rate constant for removal of the excess volume change and is given by

$$K' = \alpha K/C_p + K''. \tag{15}$$

In this expression, K'' is the rate constant for the capillary leak. Integration of eq (14) gives for the steady state solution

$$V(t) = Y_h P_0(\cos \omega t)/\rho C_p \omega \tag{16}$$

where we have assumed that $\omega \gg K'$.

The amplitude of the signal will, therefore, be inversely dependent upon the frequency of modulation. In practice, the experiment should be done at the lowest frequency commensurate with unimportant $1/f$ noise. This apparatus, like the other calorimeters discussed, is also a power detector, and its *NEP* will be given by

$$NEP = NEV(C_p)\rho\omega/\alpha. \tag{17}$$

For a *NEV* of 10^{-10} cm^3, $\rho C_p/\alpha = 4 \times 10^2$ cal/cm^3, and $\omega = 1$ s^{-1}, we obtain a *NEP* of 0.2 μW. In addition to its great sensitivity, the advantages of this technique over others we have thus far discussed are the elimination of elaborate thermostating and the execution of measurements rapidly.

An alternative method for using the flash calorimeter is to employ a pulsed exciting source. If a fairly high repetition rate is achieved, the volume change can be stored in a computer and averaged over many repetitions. If the noise is random, then the improvement in signal-to-noise ratio will increase as the square root of the number of experiments averaged.

B. Light Sources

The ideal light source for calorimetric measurements must be of high intensity, stable with time, and of high spectral purity. Thus far, only conventional noncoherent light sources have been used. Tungsten lamps are very stable with time but give useful output only in the visible region of the spectrum; further, their high infrared output is difficult to remove. High pressure mercury and mercury-xenon arc lamps appear to be the most useful of the noncoherent light sources. They generate high-intensity pressure-broadened lines in the visible and ultraviolet, produce a tolerable infrared output, and can be easily stabilized. Monochromatization of light from noncoherent sources has been achieved through use of solution filters, but complete removal of infrared light is not possible. In contrast, interference filters can be fabricated to specification and will remove most unwanted infrared radiation.

Potentially the most useful light sources for calorimetric yield measurements are lasers, just as they are for optical quantum-yield measurements. As discussed above, there are now commercially available several different types of cw gas lasers that lase at a variety of frequencies in the spectral region 320 to 650 nm. The 2-W argon ion laser is a good example (see table 1). Other gas phase lasers commercially available and of possible use in calorimetry are Kr, He-Ne, He-Cd, Se, and Xe. The amplitude stability of these lasers can be made as high as 0.1 percent. Generally, there is some noncoherent plasma radiation in the beam, but this may be removed by interference filters and the use of long pathlengths. The principal drawback to these devices is that their outputs are limited to specific lines, and it is always desirable to excite a molecule at the maximum of its absorption. The availability of the laser-pumped dye lasers should remedy this problem. The narrow line widths, stable outputs, and tuning capabilities over wide spectral regions make them prime candidates for sources in calorimetric quantum-yield determinations.

If a pulsed light source can be used, then the flash-lamp-pumped dye laser is an ideal choice. As discussed previously, these sources can be tuned continuously in the region 340–600 nm using several different dyes, and their extension farther into the infrared is already at hand. Good short term amplitude stability and high energies per pulse are commercially available in coaxially pumped systems.

C. Conclusions

Calorimetric methods for measuring quantum yields have been little used in the past because of the difficulty of making the measurements and, to some extent, because of the average photochemist's unfamiliarity with the techniques. Recent advances in the technology of calorimetry, the progress in transducer design, and the availability of laser excitation sources promise considerable improvements in the rapidity and accuracy of calorimetric methods. These improvements should lead to wider appreciation of this powerful technique for attacking the fundamental problem of measuring radiative and radiationless efficiencies of excited molecular systems.

VII. References

[1] Demas, J. N., and Crosby, G. A., J. Phys. Chem., **75,** 991 (1971).
[2] Lipsett, F. R., Progr. Dielectrics, **7,** 217 (1967).
[3] Saxena, V. N., Ind. J. Pure Appl. Phys., **9,** 407 (1971).
[4] Saxena, V. N., Rense, W. A., and Bruner, E. C., Jr., J. Opt. Soc. Amer., **60,** 865 (1970).
[5] Thornton, W. A., J. Electrochem. Soc., **116,** 286 (1969).
[6] Bruner, E. C., Jr., J. Opt. Soc. Amer., **59,** 204 (1969).
[7] Hammer, A., and Wolf, H. C., Phys. Status Solidi, **33,** K25 (1969).
[8] Nygaard, K. J., Brit. J. Appl. Phys., **15,** 597 (1964).
[9] Kristianpoller, N., J. Opt. Soc. Amer., **54,** 1285 (1964).
[10] Allison, R., Burns, J., and Tuzzolino, A. J., ibid., **54,** 747 (1964).
[11] Al-Ani, Kh., and Phillips, D., J. Phys. Chem., **75,** 3662 (1971).
[12] Borisevich, N. A., and Tolstorozhev, G. B., Bull. Acad. Sci., USSR, Phys. Ser., **34,** 574 (1970).
[13] Nakamura, K., J. Chem. Phys., **53,** 998 (1970).
[14] Robinson, G. W., and Frosch, R. P., ibid., **37,** 1962 (1962).
[15] Robinson, G. W., and Frosch, R. P., ibid., **38,** 1187 (1963).
[16] Siebrand, W., in The Triplet State, A. B. Zahlan, Ed. (Cambridge University Press, London, 1967), p. 31.
[17] Siebrand, W., J. Chem. Phys., **47,** 2411 (1967).
[18] Siebrand, W., ibid., **46,** 440 (1967).
[19] Lin, S. H., ibid., **44,** 3759 (1966).
[20] Bixon, M., and Jortner, J., ibid., **48,** 715 (1968).
[21] Henry, B. R., and Siebrand, W., ibid., **54,** 1072 (1971).
[22] Burland, D. M., and Robinson, G. W., ibid., **51,** 4548 (1969).
[23] Rusakowicz, R., and Testa, A. C., Spectrochim. Acta, **27A,** 787 (1971).
[24] Klueger, J., Fischer, G., Fischer, E., Goedicke, Ch., and Stegemeyer, H., Chem. Phys. Lett., **8,** 279 (1971).
[25] Lentz, P., Blume, H., and Schulte-Frohlinde, D., Ber. Bunsenges. Phys. Chem., **74,** 484 (1970).
[26] Sharafy, S., and Muszkat, K. A., J. Amer. Chem. Soc., **93,** 4119 (1971).
[27] Eastman, J. W., Spectrochim. Acta., **26A,** 1545 (1970).
[28] Strickler, S. J., and Berg, R. A., J. Chem. Phys., **37,** 814 (1962).
[29] Seybold, P. G., Gouterman, M., and Callis, J., Photochem. Photobiol., **9,** 229 (1969).
[30] Douglas, A. E., J. Chem. Phys., **45,** 1007 (1966).
[31] Birks, J. B., and Dyson, D. J., Proc. Roy. Soc., Ser. A, **275,** 135 (1963).
[32] Briegleb, G., Trencseni, J., and Herre, W., Chem. Phys. Lett., **3,** 146 (1969).
[33] Kobayashi, T., Yoshihara, K., and Nagakura, S., Bull. Chem. Soc. Japan, **44,** 2603 (1971).
[34] El-Bayoumi, M. A., Dalle, J. D., and O'Dwyer, M. F., J. Amer. Chem. Soc., **92,** 3494 (1970).
[35] Demas, J. N., and Crosby, G. A., ibid., **92,** 7262 (1970).
[36] Demas, J. N., and Crosby, G. A., ibid., **93,** 2841 (1971).
[37] Watts, R. J., and Crosby, G. A., ibid., **94,** 2606 (1972).
[38] Harrigan, R. W., and Crosby, G. A., Abstracts, 163rd National Meeting of the American Chemical Society, Boston, Mass., April 1972, Phys. 105.
[39] Hager, G. D., and Crosby, G. A., 1972, unpublished results.
[40] Englman, R., and Jortner, J., Mol. Phys., **18,** 145 (1970).
[41] Lim, E. C., and Bhattacharjee, H. R., Chem. Phys. Lett., **9,** 249, (1971).
[42] Ricci, R. W., Photochem. Photobiol., **12,** 67 (1970).
[43] Thomas, T. R., Watts, R. J., and Crosby, G. A., J. Chem. Phys. (in press).
[44] Callis, J. B., Gouterman, M., and Danielson, J. D. S., Rev. Sci. Instrum., **40,** 1599 (1969).
[45] Bonnier, J. M., and Jardon, P., J. Chim. Phys. Physicochim. Biol., **67,** 577 (1970); **66,** 1506 (1969).
[46] Bonnier, J. M., Jardon, P., and Blanchi, J. P., Bull. Soc. Chim. Fr., **12,** 4787 (1968).
[47] Wilkinson, F., and Dubois, J. T., J. Chem. Phys., **39,** 377 (1963).
[48] Förster, Th., Ann. Physik, **2,** 55 (1948).
[49] Weber, G., and Teale, F. W. J., Trans. Faraday Soc., **53,** 646 (1957).
[50] Pringsheim, P., Fluorescence and Phosphorescence (Interscience Publishers, Inc., New York, N.Y., 1949).
[51] Bowers, P. G., and Porter, G., Proc. Roy. Soc., Ser. A, **299,** 348 (1967).
[52] Medinger, T., and Wilkinson, F., Trans. Faraday Soc., **61,** 620 (1965).
[53] Horrocks, A. R., Medinger, T., and Wilkinson, F., Chem. Commun., 452 (1965).
[54] Medinger, T., and Wilkinson, F., Trans. Faraday Soc., **62,** 1785 (1966).
[55] Horrocks, A. R., Kearvell, A., Tickle, K., and Wilkinson, F., ibid., **62,** 3393 (1966).
[56] Horrocks, A. R., Medinger, T., and Wilkinson, F., Photochem. Photobiol., **6,** 21, (1967).
[57] Horrocks, A. R., and Wilkinson, F., Proc. Roy, Soc., Ser. A, **306,** 257 (1968).
[58] Gradyushko, A. T., Sevchenko, A. N., Solovyov, K. N., and Tsvirko, M. P., Photochem. Photobiol., **11,** 387 (1970).
[59] Ermolaev, V. L., and Sveshnikova, E. B., Acta Phys. Polon., **34,** 771 (1968).
[60] Seybold, P. G., and Gouterman, M., J. Mol. Spectrosc., **31,** 1 (1969).
[61] Kropp, J. L., Dawson, W. R., and Windsor, M. W., J. Phys. Chem., **73,** 1747 (1969).
[62] Gill, J. E., Photochem. Photobiol., **11,** 259 (1970).
[63] Leng, M., Pochon, F., and Michelson, A. M., Biochim. Biophys. Acta, **169,** 338 (1968).
[64] Pochon, F., Leng, M., and Michelson, A. M., ibid., **169,** 350 (1968).
[65] Ward, D. C., Reich, E., and Stryer, L., J. Biol. Chem., **244,** 1228 (1969).
[66] Edelman, G. M., and McClure, W. O., Accounts Chem. Res., **1,** 65 (1968).
[67] Stryer, L., Science, **162,** 526 (1968).
[68] Winkler, M., J. Mol. Biol., **4,** 118 (1962).
[69] Kingdon, H., Fed. Proc., **26,** 842 (1967).
[70] McClure, W. O., and Edelman, G. M., Biochemistry, **6,** 567 (1967).
[71] Crosby, G. A., Harrigan, R. W., and Watts, R. J., patent applied for.
[72] Demas, J. N., and Adamson, A. W., J. Amer. Chem. Soc., **93,** 1800 (1971).
[73] Watts, R. J., and Crosby, G. A., ibid., **93,** 3184 (1971).
[74] Testa, A. C., Fluorescence News, **4,** No. 4, 1 (1969).
[75] Gill, J. E., Photochem. Photobiol., **9,** 313 (1969).
[76] Spencer, R. D., Vaughan, W. M., and Weber, G., in Molecular Luminescence, E. C. Lim, Ed. (W. A. Benjamin, New York, N.Y., 1969), p. 607.

[77] Ness, S., and Hercules, D. M., Anal. Chem., **41**, 1467 (1969).
[78] Druding, L. F., and Kauffman, G. B., Coordin. Chem. Rev., **3**, 409 (1968).
[79] Clifford, H. J., Ph. D. dissertation, University of New Mexico, 1971.
[80] Vaviloy, S. I., Z. Phys., **22**, 266 (1924).
[81] Bowen, E. J., and Sawtell, J. W., Trans. Faraday Soc., **33**, 1425 (1937).
[82] Förster, Th., Fluoreszenz Organischer Verbindungen (Vandenhoeck-Ruprecht, Göttingen, Germany, 1951).
[83] Gilmore, E. H., Gibson, G. E., and McClure, D. S., J. Chem. Phys., **20**, 829 (1952); **23**, 399 (1955).
[84] Melhuish, W. H., New Zealand J. Sci. Tech., **37**, 142 (1955).
[85] Almgren, M., Photochem. Photobiol., **8**, 231 (1968).
[86] S.P.I.E. Seminar Proceedings, Developments in Laser Technology, Vol. 20, University of Rochester, 1969.
[87] Hanna, D. C., and Smith, R. C., Sci. J., **5**, 53 (1969).
[88] Goldstein, A., and Dacol, F. H., Rev. Sci. Instrum., **40**, 1597 (1969).
[89] Furumoto, H. W., and Ceccon, H. L., IEEE, J. Quant. Electron., **6**, 262 (1970).
[90] Soffer, B. H., and Linn, J. W., J. Appl. Phys., **39**, 5859 (1968).
[91] Snavely, B. B., Proc. IEEE, **57**, 1374 (1969).
[92] DeMaria, A. J., Glenn, W. H., and Mack, M. E., Phys. Today, **24**, 19 (1971).
[93] Sorokin, P., Sci. Amer., **220**, 30 (1969).
[94] Smith, R. G., Anal. Chem., **41**, 75A (1969).
[95] Tansley, T. L., and Ralph, J. E., J. Phys. D, **3**, 807 (1970).
[96] Mathur, D. P., McIntyre, R. J., and Webb, P. P., Appl. Opt., **9**, 1842 (1970).
[97] Haecker, W., Groezinger, O., and Pilkuhn, M. H., Appl. Phys. Lett., **19**, 113 (1971).
[98] Melhuish, W. H., J. Phys. E, **4**, 60 (1971).
[99] Bojarski, C., Kusba, J., and Obermüller, G., Z. Naturforsch., **A26**, 255 (1971).
[100] Weller, A., and Zachariasse, K., Chem. Phys. Lett., **10**, 424 (1971).
[101] Wegner, E. E., and Adamson, A. W., J. Amer. Chem. Soc., **88**, 394 (1966).
[102] Demas, J. N., and Adamson, A. W., Manuscript in preparation.
[103] The term fluorescence is used here in the general sense, i.e., to include all radiative processes whether spin allowed or spin forbidden.
[104] Alentsev, M. A., National Research Council of Canada Technical Translation TT-433, Zh. Eksp. Teor. Fiz., **21**, 133 (1951).
[105] Brown, H. D., Ed., Biochemical Microcalorimetry (Academic Press, Inc., New York, N.Y., 1969).
[106] Wadsö, I., Quart. Rev. Biophys., **3**, 383 (1970).
[107] McCullough, J. P., and Scott, D. W., Ed., Experimental Thermodynamics, Vol. 1 (Plenum Press, Inc., New York, N. Y., 1968).
[108] Weissberger, A., Ed., Techniques of Organic Chemistry, 3d ed, Vol. 1 (Interscience Publishers, Inc., New York, N.Y., 1959), Ch. 10.
[109] Hill, A. V., Trails and Trials in Physiology (Edward Arnold, London, 1965).
[110] Howarth, J. V., Quart. Rev. Biophys., **3**, 429 (1970).
[111] Evans, W. J., in Biochemical Microcalorimetry, H. D. Brown, Ed. (Academic Press, Inc., New York, N.Y., 1969), Ch. 14.
[112] Larsen, N. T., Rev. Sci. Instrum., **39**, 1 (1968).
[113] Meites, T., Meites, L., and Jaitly, J. N., J. Phys. Chem., **73**, 3801 (1969).
[114] Zamyatnin, A. A., Russ. J. Phys. Chem., **45**, 567 (1971).
[115] Calvet, E., and Prat, H., Recent Progress in Microcalorimetry (translated by H. A. Skinner)(The Macmillan Co., New York, N.Y., 1963).
[116] Calvet, E., and Prat, H., Microcalorimetrie (Masson, Paris, 1956).
[117] Chastel, R., and Tachoire, H., Rev. Gen. Elec., **77**, 871 (1968).
[118] Buzzell, A., and Sturtevant, J. M., J. Amer. Chem. Soc., **73**, 2454 (1951).
[119] Cudmundsen, R. A., Marsh, O. J., and Matovich, E., J. Chem. Phys., **39**, 272 (1963).
[120] Wilson, E. B., Introduction to Scientific Research (McGraw-Hill Book Co., Inc., New York, N.Y., 1952).

(Paper 76A6-742)

JOURNAL OF RESEARCH of the National Bureau of Standards—A. Physics and Chemistry
Vol. 76A, No. 6, November–December 1972

Phosphorimetry*

J. D. Winefordner

Department of Chemistry, University of Florida, Gainesville, Florida 32601

(July 26, 1972)

Phosphorimetry in the past has received limited use because the precision of reproducibility was inadequate, there were solvent limitations, and preparation of test specimens was difficult and time consuming. Detection limits have now been lowered by more than two orders of magnitude by using a rotating capillary sample cell, a more stable excitation-source power supply, and aqueous solvents. These steps have also increased precision by more than an order of magnitude. Considerable reduction in time and effort of sampling and measurement has been effected compared to phosphorimetric measurements made with standard procedures and commercial equipment. Twenty microliters of aqueous solution is all that is required to fill a quartz capillary cell by capillary action. Capillary cells filled with aqueous solutions do not crack when cooled to 77 K or when returned to room temperature. Rotation of the sample cell minimizes effects due to cell orientation and thus improves precision. Reduction of background phosphorescence results in improved accuracy of analysis. A study was made of the influence of methanol-water mixtures and of sodium-halide aqueous solutions on the magnitude of phosphorescence signals from several substances and of the effect on signal-to-noise ratios. The optimum solvent system for many phosphorimetric measurements is discussed. Analytical results are given for several organic substances measured by phosphorimetry at 77 K. These results are compared with those from previous studies by older methods.

Key words: Aqueous solvents in phosphorimetry; phosphorimetry; rotating capillary cell; solvents for phosphorimetry.

I. Introduction

Phosphoresence is a type of photoluminescence in which radiation is emitted by a molecule following radiational excitation of the molecule by means of radiation of higher energy than the emitted radiation. Phosphorescence involves two singlet-triplet transitions and as a result has a longer lifetime than fluorescence which involves two singlet-singlet transitions. Because the first triplet level of a molecule with an even number of electrons has lower energy than the first excited singlet level of the same molecule, phosphorescence also involves lower energy transitions than fluorescence, and so the phosphorescence spectrum of a given molecule occurs at longer wavelengths than the fluorescence spectrum of the same molecule. The mechanism of the production of phosphorescence is well known [1–3][1] and so will not be discussed. This manuscript is concerned with the analytical uses of phosphorescence for quantitative analyses of organic molecules—called phosphorimetry. Zander [4], Winefordner, McCarthy, and St. John [5], Winefordner, St. John, and McCarthy [6], McCarthy [7], and Winefordner, Schulman, and O'Haver [8] have reviewed and described the instrumentation, the methodology, and the uses of phosphorimetry.

Phosphorimetry has been used during the past decade for a limited number of quantitative analyses, e.g., the analysis of impurities in polycyclic aromatic hydrocarbons [9–11], in coal tar fractions [12], in air [13–15], and in petroleum fractions [16–18], the analysis of inhibitors in petroleum products [19], the analysis of pesticides, fungicides, oils, etc., in foods [20–25], and the analysis of amino acids and pharmaceuticals in biological fluids [27–35]. It is evident that up to now, phosphorimetry has been utilized only sparingly as an analytical tool for quantitative analysis and has been confined primarily to those cases where other analytical methods, such as fluorimetry and absorption spectrophotometry, either cannot be used due to lack of sensitivity or presence of interferences or give ambiguous results, and so additional analytical information is desirable. In fact, fluorimetry and absorption spectrophotometry have often been used for quantitative analyses which could quite well have been performed with greater precision, accuracy, and speed by means of phosphorimetry. The lack of use of phosphorimetry (with commercial spectrofluorimeters with phosphoroscope attachments) for quantitative analysis has been a result of the following factors: (i) the greater complexity and time to carry out an analysis due to the use of small sample cells which are difficult

*Research was carried out as part of a study on the phosphorimetric analysis of drugs in blood and urine, supported by a U.S. Public Health Service Grant (GM–11373–09).

[1] Figures in brackets indicate the literature references at the end of this paper.

474-414 O - 73 - 3

to clean, fill, align, and empty, the need for solvents which form clear, rigid glasses at liquid nitrogen temperatures, and the use of liquid nitrogen for sample cell cooling; (ii) the poor precision and accuracy of measurements due to the difficulty of alignment of the sample cell in the Dewar flask containing the coolant, due to the poor source stability—particularly long term drift, and due to the ease of contamination of glassware, cells, and solvents; and (iii) the marginal sensitivity (limits of detection) for many molecules due to light losses resulting from the excessive number of optical surfaces, the small sample cells, and the use of the phosphoroscope (mechanical chopper) which cuts out more than 75 percent of the measured signal as compared to continuous excitation-measurement. In this manuscript, the instrumental methods utilized in the author's laboratory to eliminate or minimize the above limitations will be described and typical analytical data indicating the improvement in results will be given.

II. Typical Commercial Phosphorimeter

In order to compare the improvements made in phosphorimetric instrumentation, it is necessary to describe the typical commercial phosphorimeter. A block diagram of a typical commercial spectrophotofluorimeter with rotating can phosphoroscope which has been used by the author (e.g., AMINCO SPF[2] with phosphoroscope assembly) is shown in figure 1. The source of excitation energy is generally a continuously-operated xenon arc lamp driven from a well-regulated dc power supply so as to minimize long-term drift. A portion of the source radiation is introduced into the excitation monochromator to produce a small spectral band of excitation radiation which is focused upon the sample cell, usually a quartz tube (containing sample) which is placed in a quartz Dewar flask which contains a coolant (usually liquid nitrogen) for freezing the sample (see fig. 2). A fraction of the phosphorescence emission is observed by the emission monochromator, and the wavelength region of interest is thus presented to the transducer, usually a multiplier phototube with an S–4 or S–5 response. In the averaging dc measurement systems, frequently employed in commercial spectrophotofluorimeters, the current (usually 10^{-6} to 10^{-9} A) is amplified and either read out directly from a meter face or on a time base or x–y recorder (the x–y recorder is most frequently employed when utilizing one of the monochromators in the scanning mode for recording of spectra, and the time-base recorder is often used for quantitative measurements at one set of excitation and emission wavelengths).

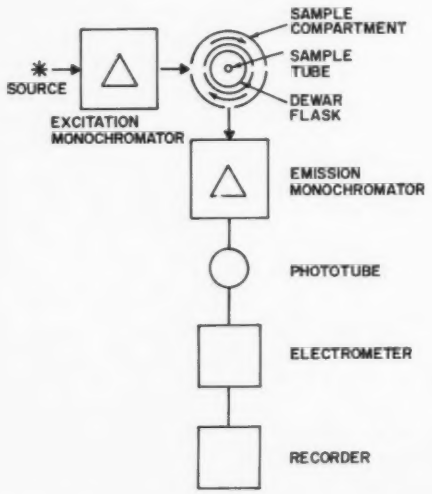

FIGURE 1. Block diagram of typical commercial analytical spectrophotofluorimeter with phosphoroscope attachment.

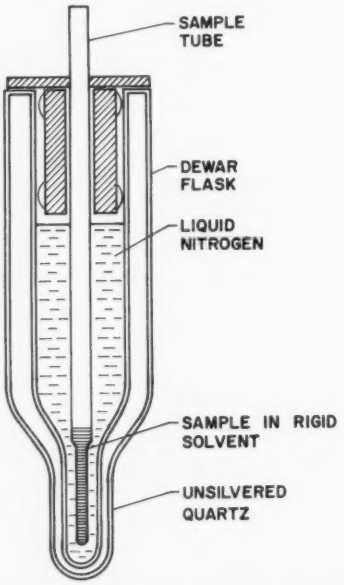

FIGURE 2. Schematic diagram of typical commercial sampling system for phosphorimetry.

A means for terminating exciting light and allowing measurement of a portion of the phosphorescence radiation without interference from the intense, scattered, incident radiation and the faster decaying fluorescence radiation must be included in the phosphorimeter design. The instrument diagrammed in figure 1 utilizes a typical rotating-can phosphoroscope, shown in greater detail in figure 3. In operation, the sample is excited for a short time through a window in the can; the can rotates to terminate excitation, after

[2] In order to adequately describe materials and experimental procedures, it was occasionally necessary to identify commercial products by manufacturer's name or label. In no instances does such identification imply endorsement by the National Bureau of Standards, nor does it imply that the particular product or equipment is necessarily the best available for that purpose.

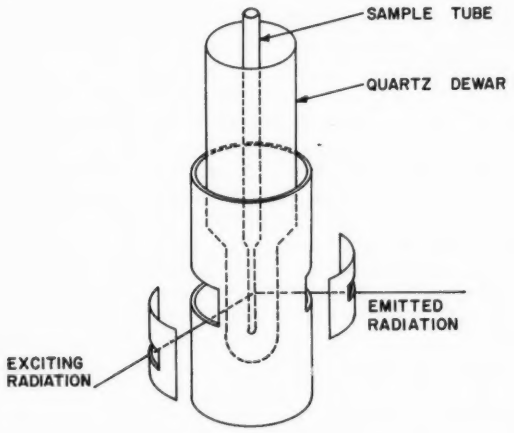

FIGURE 3. Schematic diagram of a typical rotating can phosphoroscope.

which another window is presented to the detection axis. The phosphorescence signal is observed through this window until the window moves off-axis, then the process is repeated. The instrumental response time constant employed in the dc measurement systems used with such phosphorimeters is usually made sufficiently large so as to provide a steady phosphorescence signal at all but the slowest phosphoroscope speeds.

Other means of modulation, such as the Becquerel disc phosphoroscope and pulsed source-gated detector systems, are not used in commercially available phosphorimeters. The pulsed source-gated detector system is by far the most versatile and potentially the most useful analytical system for phosphorimetry. All improvements discussed in this manuscript will be with respect to the system described above and shown in figure 1.

III. Instrumental Improvements in Phosphorimetry

A. Solvent Selection and Sampling Technique Improvements

Phosphorescence is generally not observed in liquid solutions at room temperature because radiationless deactivation due to collisions which occur within the lifetime of the excited molecule result in low phosphorescence quantum yields [36] producing phosphorescence signals buried within the phosphorescence background noise [37]. Therefore, all analytical phosphorimetric studies have been carried out in rigid media [4–8]. The criteria previously used to select a solvent for phosphorimetry have been: solubility of the analyte; low phosphorescence background (easy to purify); and formation of a clear, rigid glass at 77 K (boiling point of liquid nitrogen which is a safe, inexpensive, optically transparent coolant).

Unfortunately few solvents, particularly very polar ones, form transparent glasses at 77 K [38–40]. Ethanol is an excellent polar solvent for phosphorimetry. Small volume percents of water, mineral acids, and strong bases can also be combined with ethanol to produce clear rigid media at 77 K. The most popular mixed solvent has been EPA (a 5:5:2 volume ratio of diethyl ether, isopentane, and ethanol). Unfortunately, these solvents either do not have good solubility characteristics or result in irreversible changes of many organic species, particularly those of biological importance. Solvents, which are crystalline or severely-cracked at 77 K, have been used for some qualitative studies [41–44] but have generally been ignored or discounted as solvents for quantitative measurements. Scattering [45] and surface reflections [46] have been cited as reasons for not using snowed media [4–8] in analytical studies. The cracks or crystals create optical inhomogeneities in the medium which result in nonreproducible phosphorescence signals. Freed and Vise [29], as well as Parker and Hatchard [47], have suggested the use of an internal standard (spectrally removed from the molecule of interest) to be used as a reference to compensate for variations in sample positioning and cracking of the medium. The use of an internal standard offers a reasonable solution to the problem of sample positioning and occasional cracking; however, the choice of an internal standard satisfying the above criteria and not undergoing chemical or physical interaction with the compound being studied is extremely difficult and time consuming. In addition, the use of an internal standard is not applicable to the case of snowed or cracked media because the phosphorescence signal may be influenced by the extent of scattering, which can be wavelength dependent as long as the effective particle size is small [48, 49].

An alternative to the internal standard technique was suggested first by Hollifield and Winefordner [50] and later improved upon by Zweidinger and Winefordner [51] and still later by Lukasiewicz, Rozynes, Sanders, and Winefordner [52], and by Lukasiewicz, Mousa, and Winefordner [53, 54] all of whom used a rotating sample cell assembly to average all orientations of the sample cell, thus resulting in greater precision and accuracy of phosphorometric measurements in clear, rigid glasses [50], in rigid organic snows [51], and in rigid, aqueous snows [52–54]. In addition, there are no difficulties encountered with sample positioning and alignment.

Lukasiewicz, et al. [52–54] have added another great improvement to allow the measurement of aqueous or predominately aqueous solutions at 77 K by means of phosphorimetry. These workers used an open quartz capillary cell as the sample cell. Sample solutions ($\sim 20\ \mu l$) fill the cell by capillary action, and the sample cell is then rotated as described above. As a result of the open capillary cell, these cells with predominately, or pure, aqueous solutions do not crack when rapidly cooled to liquid N_2 temperatures or when warmed back to room temperature by use of a heat gun. Of course, the major advantage of using aqueous or aqueous-organic solutions in phos-

phorimetry are: most biochemical species are more soluble in aqueous solutions than in the solvents needed to produce clear, rigid glasses at liquid nitrogen temperatures; the solution conditions, e.g., pH, ionic strength, etc., can be varied for optimal analytical results; water is easier to obtain in higher phosphorimetric purity than most organic solvents; and contamination problems are less when water can be used to clean glassware, cells, and equipment.

The rotating sample cell assembly currently being used is a modification of the one described by Hollofield and Winefordner [50]; the present system, described in detail by Zweidinger and Winefordner [51] and modified by Lukasiewicz, et al. [52–54], is shown in figure 4. The rotating assembly consists primarily of a Varian A60–A high resolution NMR spinner assembly (Varian Associates, Palo Alto, Calif.) mounted on an AMINCO phosphoroscope sample compartment in place of the usual lid. The pressure cap of the spinner assembly is covered with black tape to ensure a completely light-tight sample compartment. The rotating sample cell is driven by a flow of nitrogen gas or air taken from a compressed gas cylinder. The sample cell must have a 6 mm o.d. and be about 25 cm long. The sample rotation is maintained at some constant speed between 450 and 1400 rpm; the actual speed is unimportant as long as it is constant during a series of measurements and can be assured by means of a normal two-stage regulator and a rotameter flow meter to monitor the gas flow rate. The normal quartz sample cells used by Zweidinger and Winefordner [51] were 5 mm o.d. and 3 mm i.d., whereas the quartz capillary cells used by Lukasiewicz, et al. [52–54] were 5.0 mm o.d. and 0.90 mm i.d. The cells were made of synthetic, high-purity, optical-grade quartz (Quartz Scientific Co., Eastlake, Ohio for the capillary tubing and Amersil, Inc., Hillside, New Jersey for the normal tubing).

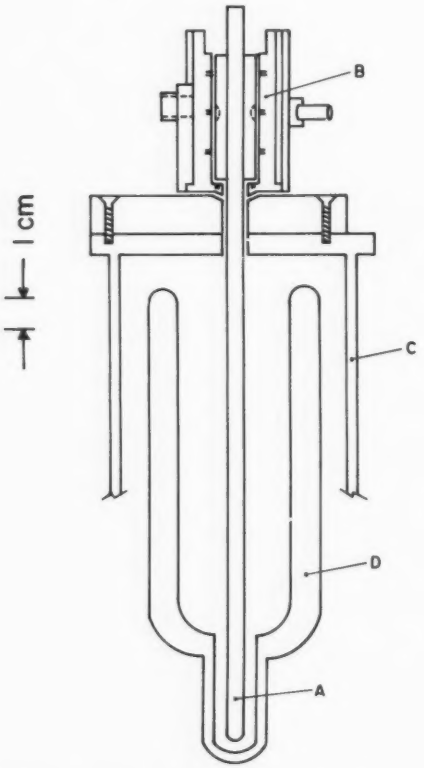

FIGURE 4. Schematic diagram of rotating sample cell assembly [51].
A. Quartz sample cell
B. Varian (909614–04) spinner assembly for NMR
C. Aminco light cover mount
D. Aminco quartz Dewar flask

Reprinted from Anal. Chem. **42**, 643 (1970). Copyright (1970) by the American Chemical Society. Reprinted by permission of the copyright owner.

The inherent photoluminescence of the quartz resulted in an appreciable "phosphorescence" background, especially with the capillary cells. However, the long-lived luminescence of the quartz cells could be minimized by mounting an excitation polarizer oriented perpendicular to the sample cell length between the sample cell housing and excitation monochromator entrance slit. Luminescence excitation spectra of the long-lived component of the quartz capillary sample cells are shown in figures 5 and 6. It can be seen from the results in figure 6 that the lowest background was obtained when both polarizers were used. For quantitative work, however, use of both polarizers is undesirable because each polarizer has a low transmittance and the loss of sensitivity is compounded. The background resulting when only one polarizer was used in the excitation beam was slightly higher than that obtained with two polarizers but still approximately 100 times lower than the background obtained without the use of the excitation polarizer.

The improvement in precision of measurement when the normal sample cell was rotated as opposed to not rotated is given in table 1. It should be stressed that the rotating sample cell holder, even when used in the stationary aligned mode (no rotation), can provide and increase in precision of as much as tenfold over the same cell in random orientation. When the normal sample cell is rotated, a further improvement in precision of about twofold is obtained (see table 1). It is interesting to note that the precision for snowed and cracked matrices is not significantly different from that for an ethanolic, clear matrix. The stationary, randomly oriented sample cell measurements were considerably more precise than those obtained by Hollifield and Winefordner [50] because of the close tolerances of the present rotating sample cell system. One great advantage of using the rotating sample cell is the simplicity of positioning the cell. After the normal sample cell is cleaned and filled (requires about five minutes), the cell with the Teflon (du Pont) turbine is simply dropped into place and spun by flow

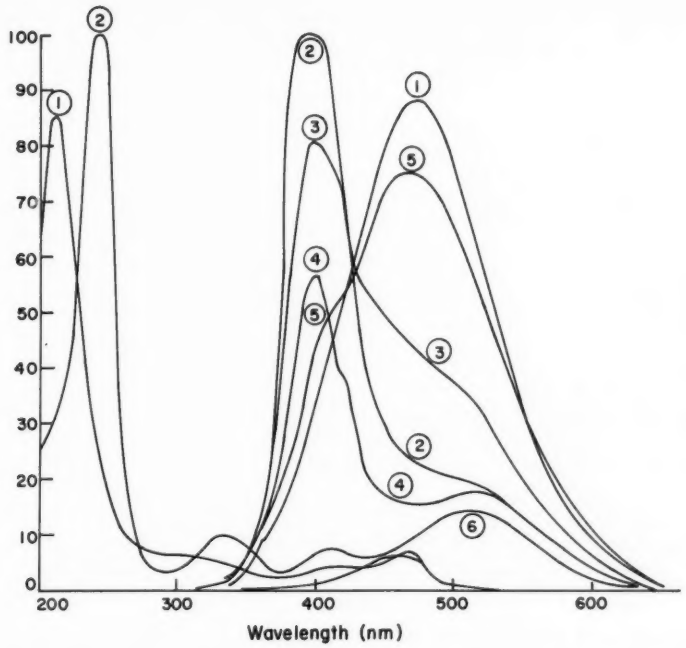

FIGURE 5. Excitation and emission spectra of long-lived component of quartz capillary sample tube (no polarizer used) spectra 1, 2, 3, 4, 5, and 6 corresponding to excitation at wavelengths 210, 240, 230, 250, 220, and 280 nm respectively.

Reprinted from Anal. Chem. **44**, 238 (1972). Copyright (1972) by the American Chemical Society. Reprinted by permission of the copyright owner.

TABLE 1. Precision of phosphorescence measurements [a] for clear glasses and snows using rotating sample cell assembly [51]

Number of determinations	Nature of matrix	Relative percent standard deviation: Stationary [a,d] random orientation	Stationary [a,e] aligned	Rotating [a,f]
4	Clear [b]	8.7	1.3	0.8
6	Clear [b]	6.0	0.5	0.8
5	Cracked [b]	13.7	3.4	1.4
11	Clear [b]	3.1	0.9	0.3
10	Clear [b]	2.9	2.8	1.0
5	Snow [c]	3.6	1.6	0.9
10	Snow [c]	2.8	0.8	0.6
10	Snow [c]	2.7	2.4	0.7

[a] Phosphorescence measurements were made on 1.6×10^{-5} *M* sulfanilamide solutions which give a signal five orders of magnitude above phototube dark current. The normal rotating sample cell was used.

[b] Ethanol solvent.

[c] Isooctane : ethanol, 4 : 1, *v/v* mixture as solvent.

[d] This column is indicative of the reproducibility obtainable with the commercial sampling system.

[e] This column gives results for the rotating normal sample cell assembly but with the normal cell stationary in the assembly.

[f] This column gives results for the rotating normal sample cell assembly but with the normal cell rotating in the assembly.

of compressed air. As a result of spinning the cell, the inner filter effect is also minimized.

A series of 10 replicate determinations of 1 μg/ml 2-thiouracil in 10 percent *v/v* methanol-water were measured to determine the precision obtainable with the rotating quartz capillary cell. The relative standard deviation obtained was 1.5 percent. This is an improvement of nearly an order of magnitude over the stationary quartz capillary tube system used by Lukasiewicz, Rozynes, Sanders, and Winefordner [52], and compares favorably with the standard deviations of results obtained with normal rotating sample cells (see table 1). The major noise contribution in the system with the rotating capillary cell arises from wobble of the cell caused by the loose fit of the turbine sleeve in the spinner assembly. If the capillary cell were held rigidly by the turbine sleeve so that no wobble occurs on rotation the precision would probably be comparable to the best data reported in table 1 for the larger, normal quartz, sample cell.

B. Improvements in Precision and Accuracy of Phosphorimetry

The relative percent standard deviations obtainable with the typical commercial system shown sche-

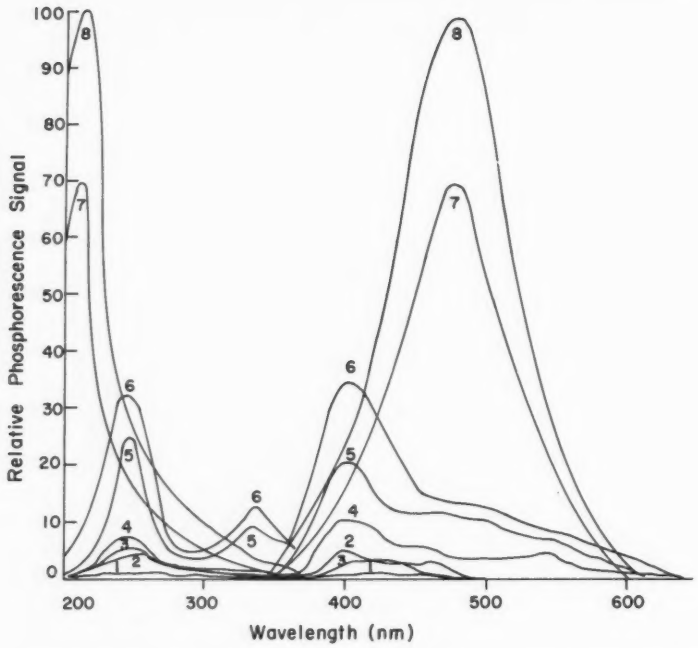

FIGURE 6. Excitation and emission spectra of long-lived component of quartz capillary sample tube, using polarized radiation; orientation of polarizers with respect to vertical axis of cell as follows [52]:

	Excitation	Emission
1.	⊥	∥
2.	∥	∥
3.	⊥	⊥
4.	∥	⊥
5.	∥	no polarizer
6.	⊥	no polarizer
7.	no polarizer	⊥
8.	no polarizer	∥

Spectra 1 thru 6 were obtained with a gain of 5-fold; full-scale approximately equal to twice level of dark current of multiplier phototube. Spectra 7 and 8 were obtained with a gain of unity.

Reprinted from Anal. Chem. **44,** 239 (1972). Copyright (1972) by the American Chemical Society. Reprinted by permission of the copyright owner.

matically in figure 1 are given in table 1. By using the rotating sample cell system as well as a more stable xenon lamp power supply, the precision of phosphorimetric measurements can be increased by as much as tenfold (see data in table 1). In addition, the contamination of glassware, solvents, and sample cells with phosphorescent impurities seriously limits precision of measurements, particularly at low concentrations of analyte. Zweidinger, Sanders, and Winefordner [55] have described techniques for cleanup of sample cells and glassware. These authors recommend cleaning the sample cells and glassware used in solution preparation in an ultrasonic cleaner for about 30 seconds or in concentrated nitric acid if there is serious contamination; when contamination is extremely serious the item can be heated in an oven or placed directly in a flame. Of course, solvents used in phosphorimetry should be purified by distillation, zone freezing, or some other separation method. It should be stressed that distillation of demineralized

water results in a solvent of extremely low phosphorescence background compared to ethanol, EPA, or any other commonly used organic solvent.

By use of an elliptical source condensing system and a more stable xenon lamp power supply, it was possible to reduce drift and noise by about tenfold as compared to those obtained with the standard power supply in the commercial phosphorimeter. The elliptical source condensing system is commercially available (in our case, from American Instrument Co., Inc., Silver Spring, Maryland). The xenon lamp power supply system was assembled using a highly regulated power supply (Harrison Lab Model 6268 A, Hewlett-Packard, Palo Alto, Calif.) operating in the constant current mode at 7.5 A (150 W lamp) with the addition of the starter circuit shown in figure 7.

A comparison of phosphorescence signals and signal-to-noise ratios obtained with the rotating normal sample cell and the Zweidinger, Sanders, and Winefordner [55] sample cell cleanup procedure with the earlier cleanup procedure of Tin and Winefordner [56] is given in table 2.

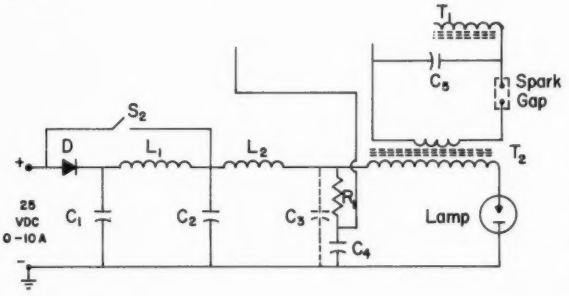

FIGURE 7. Starter circuit for xenon arc lamp (51).

C_1, C_2, C_3—0.5 μF (300 VDC)
C_4 —1300 μF (300 VDC)
C_5 —0.01 μF (30,000 VDC)
C_6 —100 μF (300 VDC)
R_1 —1 Ω
R_2 —1 k Ω
R_3 —1.8 k Ω
S_1 —Momentary contact switch
S_2 —15 Ampere switch—to be closed only after lamp ignites
L_1 —300 mH (10 A, hand wound on ferrite core)
L_2 —30 mH (15 A, hand wound on ferrite core)
D —Diode (15 A, 300 PIV)
T_1 —Autotransformer
T_2 —10 : 1 Ratio transformer

Reprinted from Anal. Chem. **42**, page 643 (1970). Copyright (1970) by the American Chemical Society. Reprinted by permission of the copyright owner.

C. Decrease in Limits of Detection in Phosphorimetry

Limits of detection in phosphorimetry are reduced if either the signal level can be increased and/or the noise level can be reduced. By use of the more stable xenon lamp power supply, the elliptical source condensing system, the rotating sample cell assembly, and the improved cleanup procedure as well as the use of aqueous solutions for some molecules, the noise level is reduced and thus detection limits are also reduced. By use of more intense continuously operated or pulsed with gated detector, light sources phosphorescence signals can also be increased and detection limits are decreased even more.

TABLE 2. Comparision of signals and signal-to-noise ratios with rotating normal sample cell and with or without new cleanup procedure [55]

	Signal (nA)[a,b]	Signal-to-background fluctuation[b,c]	Signal-to-noise[b,d]
Conventional cleanup procedure	1.5(0.05)[e,f]	2.5	100[15][e]
New cleanup procedure	0.3[f]	25	45

[a] Signal is due to impurities in ethanol (solvent) background.
[b] All signals, signal-to-background fluctuations, and signal-to-noise ratios are approximate. Excitation is at 262 nm and emission is measured at 380 nm.
[c] Background fluctuation is percent standard deviation of five background readings.
[d] Time constant for all measurements was 0.3 s.
[e] Values in parentheses were obtained without the Aminco elliptical condensing system (American Instrument Co., Inc., Silver Spring, Maryland).
[f] Dark current is approximately 0.02 nA.

The improvement in detection limits, resulting primarily from noise reduction due to the processes described in the above paragraph, is given in table 3 for the measurement of several organic molecules using normal sample cells in the rotating sample cell assembly. Similarily, detection limits obtained for several organic molecules measured using the quartz capillary cells in the rotating sample cell assembly are given in table 4. The range of linearity and limits of detection reported in table 4 compare favorably with those previously obtained in clear, rigid glasses in the normal sample cell (see table 3), even though the sample volume is an order of magnitude smaller with the capillary cell. Because of the small volume of sample solution retained in the capillary tube, the total number of grams of analyte necessary for a determination is in the picogram region, and thus phosphorimetry can be considered both a trace and micro method of analysis. This should be of particular importance in biological and clinical applications where sample size is often limited. The average slopes of the analytical curves (logarithm of phosphorescence signal versus logarithm of analyte concentration) for the molecules in tables 3 and 4 are 0.94 which approaches the ideal slope of unity for phosphorescence signals in snowed matrices [51]. Both positive and negative deviations

TABLE 3. Phosphorescence characteristics of several organic studied molecules [51]

Compound	Solvent	Concentration range (M) of near linearity	Slope of linear portion	Relative percent standard deviation [a]	Linear correlation coefficient	Limit of detection (μg/ml [g])	Limit of detection (μg/ml [h])
Toluene	Ethanol [b]	10^{3}	0.94	1.5	0.9999	0.03	.....
Toluene	Propylene glycol: [c] water/ (9 : 1, *v/v*)	10^{3}	.76	[d] 2.5	.9999	.03	.....
Toluene	Isooctane [c]	10^{3}	.89	[e] 0.9 [f] (6.1)	.9998	.02	.....
Sulfanilamide	Isooctane: [c] Ethanol/ (4 : 1, *v/v*)	10^{5}	.96	[e] .8 [a] (1.1)	.9998	.0004	[i] .012
Oxythiamine HCl	Isooctane: [c] Ethanol/ (4 : 1, *v/v*)	10^{2}	1.01	1.9	1.0000	.34	.....
3-Acetylpyridine	Isooctane [c]	10^{5}	1.03	1.9	1.0000	.012	[i] 3.6

[a] For samples giving signals 5 times the limit of detection.
[b] Formed clear glasses.
[c] Formed snowed samples.
[d] Harrison power supply not used.
[e] Linear portion of the analytical curve.
[f] Nonlinear portion of the analytical curve.
[g] Limits of detection in this study [51].
[h] Best previous limits of detection using standard commercial phosphorimetric equipment.
[i] From Reference 57.

TABLE 4. Phosphorescence characteristics of molecules studied [54]

Compound	Slope of linear portion	Limit of detection (μg/ml)	Number of grams [b] at limit of detection	Concentration range of near linearity
p-Nitrophenol [c]	0.88	7×10^{-3}	1.24×10^{-10}	10^{4}
Sulfamethazine [a]	1.01	6×10^{-3}	1.07×10^{-10}	10^{4}
2-Thiouracil [a]	0.81	7×10^{-4}	1.24×10^{-11}	10^{4}

[a] Solvent 10 percent (*v/v*) methanol water, all solutions formed snowed samples.
[b] Volume of sample retained in capillary tube calculated as 17.8 μl.
[c] Solvent 10 percent (*v/v*) methanol water with 1 percent by volume saturated NaOH added.

from a slope of unity have been observed; however, much more data is necessary before a conclusion can be drawn as to whether an individual molecule perturbs the crystalline matrix and alters the slope or whether the deviations can be attributed to instrumental parameters influencing the precision and accuracy of signal measurements. Present theory assumes the scattering coefficient of the sample is not a function of solute molecule or concentration [51, 53].

D. Pulsed-Source Gated-Detector Phosphorimetric System

Fisher and Winefordner [58] have described a pulsed-source gated-detector system for phosphorimetry; such a system was shown to allow an increase in selectivity of analysis due to the use of time resolution [59], which will not be discussed here, and an increase in sensitivity of analysis due to the increased signal-to-noise ratio. The latter increase is a result of an increased signal and a decreased noise. The basis of pulsed-source systems and the system of Fisher and Winefordner [58] will be briefly described in the following paragraphs.

A pulsed-source gated-detector phosphorimetric system consists of much of the same equipment found in the commercial continuously operated source mechanically modulated phosphorimeters; the exception being that no mechanical phosphoroscope is required in the pulsed system. Also, the source of excitation energy is a short-arc high-pressure xenon flashtube rather than a continuously operated xenon arc lamp (usually 150 W); pulsed sources are operated from rather simple electronic circuits and power supplies and have operating characteristics suitable for the excitation of (fast) phosphors, e.g., a blackbody temperature of around 7000 K, a pulse rate as high as several thousand hertz, and most important, a pulse duration on the order of several microseconds (a duty cycle of about 10^{-3}). With too short a pulse, not enough molecules will be excited per excitation-emission cycle to permit the observation of analytically useful phosphorescence signals. With too long a pulse, the early portions of the emission decay curves of fast phosphors will be buried in source scatter noise. Also, with long pulses, the phosphorescence background signal, often a result of slow phosphor species in the sample mixture, may become increasingly significant.

Readout devices for pulsed-source systems are more complex than dc systems employed in commercial phosphorimeters; three principal readout methods have been used. The method proposed by O'Haver and Winefordner [60], involved phototube pulsing (gating) as well as source pulsing and is schematically illustrated in figure 8; it is seen that the first event in the excitation-observation-of-emission cycle for a pulsed-source system is the intense burst of energy from the source with a flash duration half-width, t_f. During this time, the phosphorescence intensity climbs to a value I_0 and begins to decay exponentially. At a delay time, t_d, preferably after the source flash has decayed significantly, the multiplier phototube is turned on (a high-voltage negative pulse is applied to the dynode chain), and the luminescence signal is monitored. The phototube is then turned off by termination of the negative "on" pulse: if an integrating dc measurement system is used to monitor its output, the integrated luminescence intensity I is measured during the on-time t_p of the phototube. If desired, t_d may be varied in such a manner that the gate t_p is scanned along the decay curve, providing the readout device with a display of the phosphorescence decay. This method was more difficult to achieve instrumentally than the other two methods discussed in the following paragraph.

Two other readout methods for observation of fast phosphor emissions were used by Fisher and Winefordner [58]. In the *first* method, the phototube was operated continuously in the conventional manner, but an electronic gate examined the integrated phosphorescence intensity after a time delay of t_d over the time period t_p; this gate may also be scanned to display the decay curve. This method is termed the *box-car integrator method.* In the *second* method, the phototube was also continuously operated, but the signal for the entire decay curve was presented to a fast multichannel readout device. This method is called the *signal averager method.* The latter method is the simplest one of the three to use for pulsed source studies although the problems of measurement of fast electronic signals accompanied by noise are more important with this method.

The integrated luminescence intensity I (cross-hatched area in fig. 8) achieved with a pulsed-source gated-detector system is given [6] by

$$I = \frac{I_0 f t_f [\exp(-t_d/\tau)]\,[1-\exp(t_p/\tau)]}{[1-\exp(-1/f\tau)]}$$

assuming a dc type readout is used to measure I within the phototube "on" time t_p (terms are defined in fig. 8). If an ac system is used, I will not be directly proportional to f, the source pulse repetition frequency. Figure 9 gives the variation of relative re-

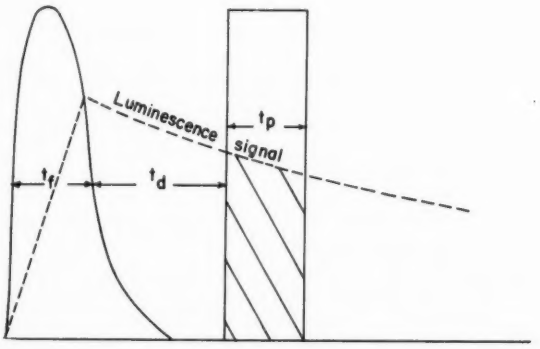

FIGURE 8. Schematic diagram of events occurring during one cycle of sample excitation and observation in a pulsed source phosphorimeter system [60].

Key to Symbols and Lines in Diagram

t_f = half-intensity width of the source flash

t_d = delay time after the end of the excitation pulse (assuming excitation pulse to be a rectangular) to the beginning of observation of the phosphorescence signal ("on" time of the detector or the readout system)

t_p = "on" time of detector or readout system

Dashed line represents buildup and decay of phosphorescence

Solid line tailing peak represents flash intensity temporal distribution

Solid line rectangular peak represents "on" time of detector or readout system

Cross-Hatched area represents measured integrated luminescence signal per source pulse

Reprinted from Anal. Chem. **38**, page 1259 (1966). Copyright (1966) by the American Chemical Society. Reprinted by permission of the copyright owner.

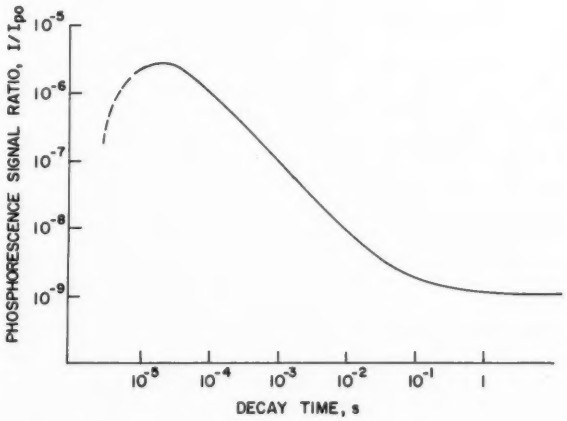

FIGURE 9. Plot of phosphorescence signal ratio (ratio of integrated intensity I to the steady state integrated intensity I_{po}) *versus* sample phosphorescence decay time τ[60] for case of pulsed source gated detector (see text for values of t_f, t_p, and t_d).

Reprinted from Anal. Chem. **38**, 1259 (1966). Copyright (1966) by the American Chemical Society. Reprinted by permission of the copyright owner.

sponse (ratio of integrated luminescence intensity I to the steady state integrated intensity I_0) with phosphor decay time τ for parameters typical of an analytically useful pulsed-source gated-detector system ($t_f = 10^{-6}$ s, $t_p = 10^{-5}$ s, $t_d = 10^{-5}$ s). It is evident by the existence of the maxima in figure 9, that the pulsed-source system is capable of providing selective response to short-lived phosphors over long-lived phosphors. This is of considerable importance, because the background phosphorescence signal, which often defines the limits of detection and precision for fast phosphors in alcoholic/hydrocarbon/ether solutions, is usually due to a long-lifetime phosphor impurity. For example, the pulsed system (represented in fig. 9) for a typical fast ($\tau = 1$ ms) sample phosphor in the presence of a slow ($\tau = 1$ s) background phosphor interferent should have a 200-fold greater rejection of background than the commercial mechanical phosphoroscope phosphorimeter.

Therefore, the principle advantages of pulsed-source phosphorimetry over conventional continuous operating sources with mechanical modulation are: the possibility of achieving higher peak source intensities during the measurement period and thus lower detection limits and the possibility of achieving greater selectivity for a given short-τ phosphor over a long-lived interferent. Lesser advantages also exist. For example, since a flashtube pulse may terminate in several microseconds, whereas a typical phosphoroscopic mechanical disk chopper has a termination time (transit time) t_t of 3×10^{-5} and a typical phosphoroscopic mechanical can chopper has a t_t of 1×10^{-4} s, shorter-lived phosphors (τ's as short as 10 μs) can be measured. In addition, since the temporal parameters t_f, t_d, and t_p may be more readily varied with a pulsed-source gated-detector system, larger signals can be measured and greater selectivity achieved. Gating the detector so that it is on for only a predetermined time results in an improvement of the signal-to-noise ratio and a reduction in detection limits, an increase in precision, and an improvement in the accuracy of measurement. Finally, because it is easy to determine the linearity of a log I versus t_d plot, a rapid check on the purity of the phosphor under study can be obtained as well as an estimate of the phosphor decay time, which may be useful for structural (qualitative) studies.

A block diagram of the pulsed-source gated-detector phosphorimeter used by Fisher and Winefordner [58] is given in figure 10; a schematic diagram of the flashtube trigger circuit is shown in figure 11. To compare the standard commercial (AMINCO in our case) spectrophotofluorimeter with rotating can phosphoroscope with the pulsed-source gated-detector system, it was decided to measure the limit of detection of a fast phosphor (4-bromoacetophenone, $\tau = 6.8$ ms) in purified ethanol which was known to contain a phosphorescence background due to a slow phosphor (unknown material, $\tau = 0.8$ s) having phosphorescence excitation and emission spectra which overlapped considerably the corresponding spectra of the fast phosphor. The limit of detection of 4-bromoacetophenone was 10^{-6} M when measured using the standard commercial spectrophotofluorimeter with rotating can phosphoroscope. However, with the pulsed-source gated-detector system of Fisher and Winefordner [58], the detection limit was found to be 10^{-8} M, even though

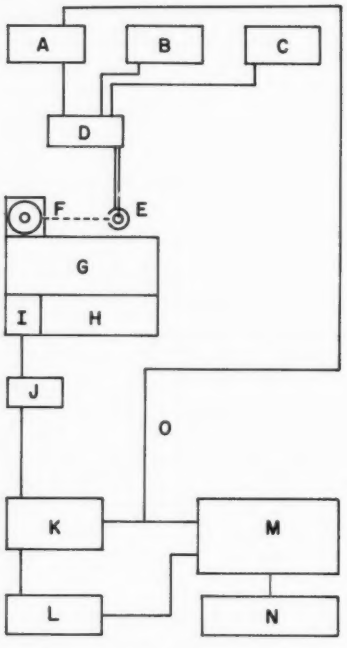

FIGURE 10. Block Diagram of Pulsed Source Phosphorimeter [58].

Key to Symbols

A. Pulse generator (Model 100, Datapulse Inc., Culver City, Calif.)
B. 300 V power supply (Model C-281, Lambda Electronics, Melville, N.Y.)
C. 1400 V power supply (Model 403 M, John Fluke Mfg., Co., Seattle, Washington)
D. Trigger circuit (see fig. 11)
E. Xenon flashtube compartment (Laboratory Constructed)
F. Sample cell compartment (identical to Aminco phosphoroscope accessory minus rotating phosphoroscope can)
G. Emission monochromator (Model EU-700, Heath Co., Benton Harbor, Michigan)
H. Phototube power supply (Model EU-701-30, Heath Co., Benton Harbor, Michigan)
I. RCA 1P28 photomultiplier tube
J. Load resistors (500 Ω to 3M Ω) and fast switching diodes
K. Oscilloscope (Model 545,Tektronix Inc., Orlando, Florida)
L. Preamplifier (Model 465A, Hewlett-Packard, Orlando, Florida)
M. Signal averager (Biomac Model 1000, Data Laboratories, Ltd., London, England), or Boxcar Integrator (Model 160, Princeton Applied Research, Princeton, New Jersey)
N. x-y Recorder

Reprinted from Anal. Chem., in press. Copyright (1972) by the American Chemical Society. Reprinted by permission of the copyright owner.

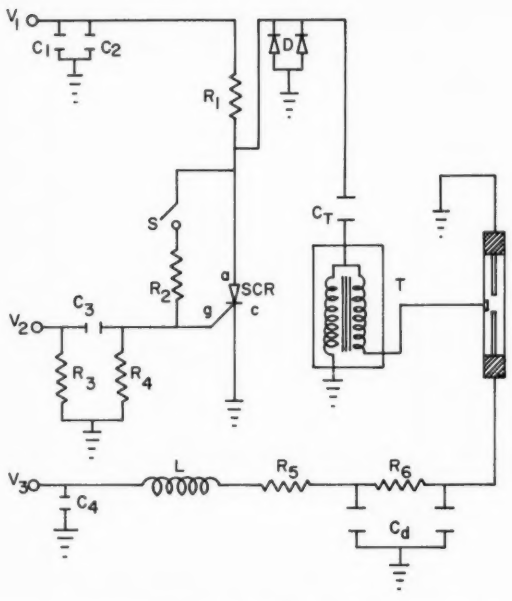

FIGURE 11. Schematic diagram of flashtube trigger circuit [58].

Value of Components

C_1 0.001 μF	R_1 100 kΩ	L ~ 100 μh
C_2 0.1 μF	R_2 33 kΩ	S SPST switch
C_3 0.022 μF	R_3 56 Ω	T EG & G TR 132 Trigger Transformer
C_4 0.002 μF	R_4 1.1 kΩ	V_1 300 V dc power supply
C_t 1.0 μF (600 V)	R_5 6.8 kΩ	V_2 15 V dc power supply
C_d 0.1 μF (5000 V)	R_6 190 kΩ	V_3 1400 V pulse power supply

Reprinted from Anal. Chem. 44, 953 (1972). Copyright (1972) by the American Chemical Society. Reprinted by permission of the copyright owner.

the average power of the continuously operated xenon source in the commercial system (150 W) was 75 times as great as the average power of the pulsed xenon flashlamp (2 W). The main reason for the 100-fold reduction in the limit of detection with the pulsed system is the reduction in noise, i.e., essentially no phosphorescence signal due to the long-lived background component was observed with the pulsed system, and so the noise level was only about twice the dark current shot noise level.

One other factor which contributes to phosphorescence background should be mentioned. The diethyl ether used in the Fisher and Winefordner [58] studies was Baker and Adamson anhydrous reagent grade. Listed as impurities in this solvent are "0.001 percent carbonyl (as $>C=0$)." As expected, this also produced a fast decaying phosphorescence background to which the pulsed instrumentation was responsive. Fortunately, the ether background was *very* short-lived, and this interferent decayed before introducing error into the phosphorescence signal of the analyte with the pulsed-source system.

IV. Noninstrumental Improvements in Phosphorimetry

Lukasiewicz, Rozynes, Sanders, and Winefordner [52] showed that phosphorescence signals remain nearly constant for a variety of analytes in snowed matrices of mixtures of ethanol/water (methanol/water) at 77 K over the range of 10 to 50 percent *v/v*; as the volume percent of ethanol (or methanol) increased from 0 percent to about 10 percent, the phosphorescence signals of 2-thiouracil, *p*-nitrophenol, or sulfamethazine increased by about 3 orders of magnitude and simultaneously the physical appearance of the frozen matrix changed from a translucent severly cracked medium to an opaque completely snowed matrix. The phosphorescence signal levels were nearly the same in either methanol/water or ethanol/water (10–50) percent *v/v* of alcohol/water), but the phosphorescence background level was considerably lower in the former than the latter solvent mixture (spectrograde methanol versus 95 percent ethanol). The increased phosphorescence signals of analytes in 10 to 50 percent *v/v* of alcohol/water mixtures at 77 K as compared to those in pure aqueous solutions was correlated with the physical nature (snow versus cracked glass) rather than with chemical properties of the analyte and/or the solvent as has been further verified by Lukasiewicz, Mousa, and Winefordner [53] (see below).

Lukasiewicz, Mousa, and Winefordner [53], in a more recent study, have made careful phosphorescence measurements of the influence of solvent (methanol/water and alkali-halide salt solutions) composition upon the phosphorescence of 3-indole acetic acid, hippuric acid, and sulfacetamide at 77 K. Typical results for the methanol/water mixtures at 77 K are shown in figure 12. The three analytes all show the same solvent dependency, i.e., a region where there is an abrupt increase in phosphorescence signal between 0 and 3 percent *v/v* methanol/water, followed by a plateau region between about 5–30 percent *v/v*, and a region where the phosphorescence signal decreases slightly for solutions with more than 30 percent methanol. Little or no spectral shift was observed for the phosphorescence excitation and emission spectra as a function of solvent composition. Perhaps the most significant observation was that each region corresponded to a visible change in the nature of the matrix. Pure water solutions were severely cracked, but nearly transparent. Addition of small amounts of methanol to water produced an opaque matrix which corresponded to the region of greatest slope in the solvent dependency curves. Between approximately 5 and 30 percent *v/v* methanol/water, the frozen matrix became completely snowed, and the signal remained nearly constant. Increasing the percentage of methanol even more resulted in a signal decrease which corresponded to the reappearance of a cracked, translucent,

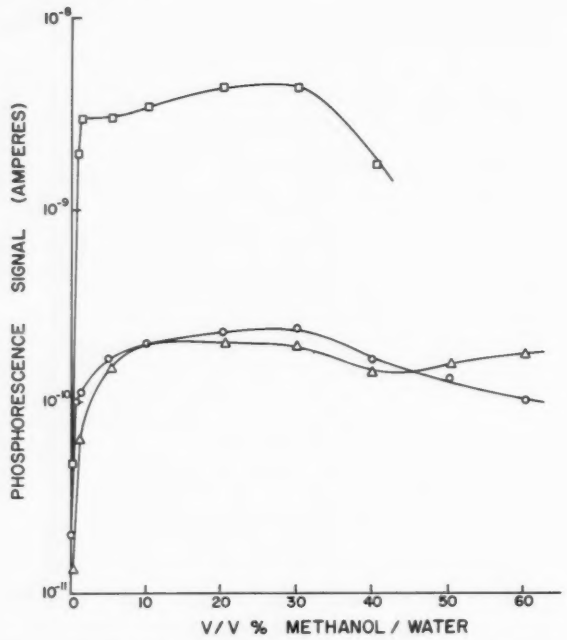

FIGURE 12. Phosphorescence Signal as Function of Solvent Composition (methanol-water) [53].

○ $2.0 \times 10^{-6}M$ 3-indole acetic acid
△ $4.7 \times 10^{-6}M$ hippuric acid
□ $1.7 \times 10^{-6}M$ sulfacetamide

Reprinted from Anal. Chem. **44**, 965 (1972). Copyright (1972) by the American Chemical Society. Reprinted by permission of the copyright owner.

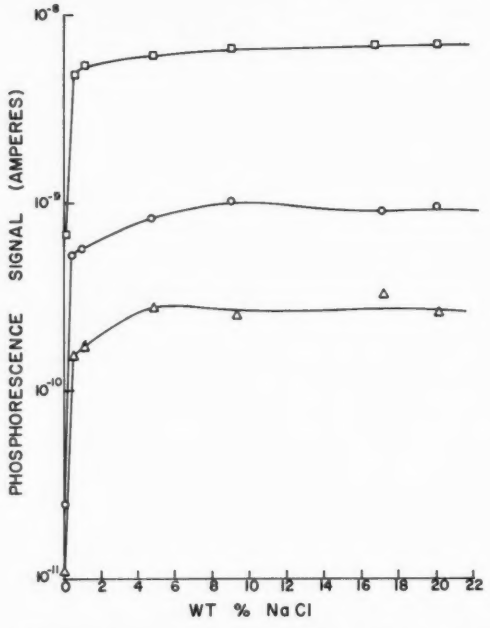

FIGURE 13. Phosphorescence Signal as Function of Solvent Composition (sodium chloride-water) [53].

○ $3.7 \times 10^{-6}M$ 3-indole acetic acid
△ $1.8 \times 10^{-6}M$ hippuric acid
□ $3.9 \times 10^{-6}M$ sulfacetamide

Reprinted from Anal. Chem. **44**, 965 (1972). Copyright (1972) by the American Chemical Society. Reprinted by permission of the copyright owner.

rigid matrix; the precision of measurement of phosphorescence signals for methanol/water solutions with 40 percent *v/v* or more methanol is poor because of the nonrandom cracking of the frozen solvent.

The shapes of the phosphorescence signal versus solvent composition curves when sodium chloride is added to water rather than methanol (or ethanol) are identical to those for the alcoholic solutions (fig. 13), and the previous conclusions regarding the physical nature of the matrix seem to be justified. It should be stressed, however, that the maximum phosphorescence signal for the NaCl solutions is about 3 times greater than the methanol/water solutions (the salt solutions at 77 K result in a rigid, snowed matrix with more finely divided particles than the snowed matrix for the methanolic solutions).

The use of the external heavy-atom effect to increase the transition probability from the first excited-singlet to the first excited-triplet state and therefore, to increase the sensitivity of phosphorescence, has also been reported [62, 63]. However, in the *past*, results obtained using the external heavy-atom effect have been of limited analytical value because of the following restrictions. First of all, the heavy-atom perturbant had to be appreciably soluble in the solvents used for phosphorimetry and also had to form clear, rigid glasses with the solvent. Second, the perturbant should not absorb in the same spectral regions as the compounds being studied. Third, the perturbant had to be available in extremely pure form, since impurities could cause a large background signal. Ethyl iodide has been most commonly used as an external perturbant; however, results obtained were limited because ethyl iodide did not fulfill all the requirements stated above, especially the last two. In aqueous solutions, however, the use of simple perturbants, such as alkali halide salts is possible. Solubility and purity of these salts make them desirable for phosphorimetric studies of aqueous solutions.

The effect of adding the alkali halide salts, NaI, NaBr, and NaCl to pure water solutions of 3-indole acetic acid, is shown in figure 14. The combined physical matrix and heavy-atom effect result in the greatest phosphorescence signals with added NaI. All three salts (see background spectra in fig. 14) result in significant phosphorescence background—NaBr giving the largest. Also, both NaBr and NaI solutions result in the same general shaped composition curve as for NaCl and alcohol with water, except that the NaI-water curve in figure 14 is somewhat sharper than the others. An increase in phosophorescence

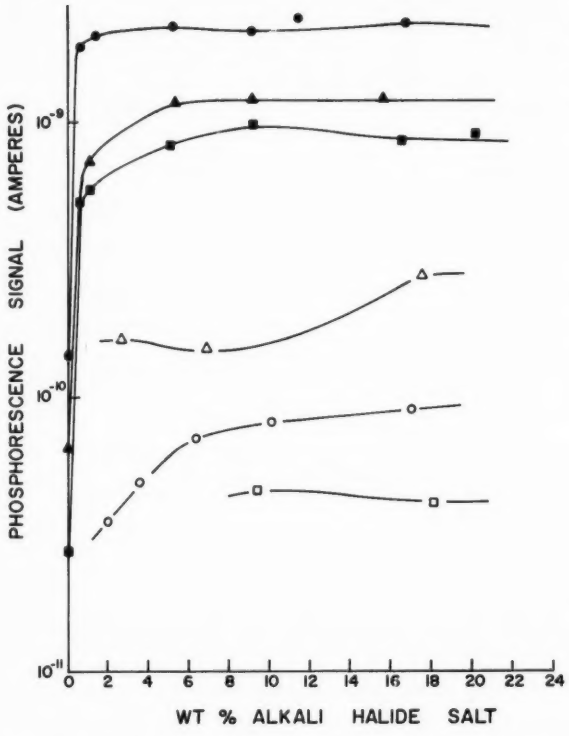

FIGURE 14. Phosphorescence Signal of $3.7 \times 10^{-6} M$, 3-indole Acetic Acid in Alkali Halide Salt Solution:

● aqueous NaI solution as solvent
▲ aqueous NaBr solution as solvent
■ aqueous NaCl solution as solvent

Phosphorescence background of alkali halide salt crystals:

○ NaI crystals
△ NaBr crystals
□ NaCl crystals

Excitation Wavelength 285 nm, emission wavelength 435 nm [53]. Reprinted from Anal. Chem. **44**, 965 (1972). Copyright (1972) by the American Chemical Society. Reprinted by permission of the copyright owner.

signal occurred for concentrations of NaI up to 1 *M*.

Therefore, the use of alkali-halide/water solutions as solvents for phosphorimetric analysis of polar organic molecules is advantageous for a number of reasons: alkali-halide salts may be obtained in ultrapure form, and thus phosphorescence background may be reduced to extremely low levels; salt solutions have the same matrix effect as alcohol/water solutions, while producing a much lower background signal; and, in the case of sodium iodide, an additional factor, namely the heavy-atom effect, enhances the phosphorescence signal. In some cases, however, use of aqueous sodium iodide solvents may be less desirable than other alkali halide salts. Phosphorescence decay time measurements for the compounds studied in this study by Lukasiewicz, Mousa, and Winefordner [53] indicated that decay times in aqueous sodium iodide solutions were considerably shorter than in methanol/water solutions. The changes in decay times for the compounds studied in aqueous sodium iodide and alcohol/water solutions are summarized in table 5. These observations are consistent with the heavy-atom perturbation theory [61]. Phosphorescence signals, however, did not increase for all three compounds listed in figure 13. A sixfold increase in phosphorescence signal was observed for 3-indole acetic acid, and a threefold increase for hippuric acid in 1 *M* sodium iodide. Sulfacetamide, on the other hand, showed a threefold decrease in signal even though the phosphorescence decay time was lower.

TABLE 5. Phosphorescence decay times in aqueous sodium iodide and aqueous alcohol solutions

Compound	Lifetime(s)	
	Solvent 10 percent *v/v* methanol-water	Solvent 1 *M* aqueous sodium iodide
3-Indole Acetic Acid.....	7.0	0.90
Sulfacetamide.....	1.7	0.83
Hippuric Acid.....	3.0	0.97

It is therefore quite evident that proper selection of the solvent for phosphorimetry can lead to an appreciable increase in phosphorescence signals of some species and in some cases an increase in selectivity of analysis. The advantages of using alkali-halide salt solutions over alcohol/water solutions as phosphorimetric solvents include: the availability and low cost of high purity salts; increased signal levels; and the high solubility of many biochemically related species.

V. References

[1] Hercules, D. M., Fluorescence and Phosphorescence Analysis, D. M. Hercules, Ed. (Wiley, Interscience, New York, 1966).
[2] Parker, C. A., Photoluminscence of Solutions (Elsevier, New York, 1968).
[3] Becker, R. S., Theory and Interpretation of Fluorescence and Phosphorescence (Wiley, Interscience, New York, 1969).
[4] Zander, M., The Application of Phosphorescence to the Analysis of Organic Compounds (Academic Press, New York, 1968).
[5] Winefordner, J. D., McCarthy, W. J., and St. John, P. A., Methods of Biochemical Analysis, D. Glick, Ed., Vol. **15** (Interscience, New York, 1967).
[6] Winefordner, J. D., St. John, P. A., and McCarthy, W. J., Chapter on Phosphorimetry, in Fluorescence Assay in Biology and Medicine, Vol. **II**, S. Udenfriend, Ed. (Academic Press, New York, 1969).
[7] McCarthy, W. J., Phosphorimetry, Chapter in Spectrochemical Methods of Analysis, J. D. Winefordner, Ed. (Wiley, New York, 1970).
[8] Winefordner, J. D., Schulman, S. G., and O'Haver, T. C., Luminescence Analysis in Analytical Chemistry (Wiley, New York, 1972).
[9] Zander, M., Angew. Chem. Intern. Ed. Engl. **4**, 930 (1965).
[10] Zander, M., Z. Anal. Chem. **226**, 251 (1967).
[11] Clar, E., and Zander, M., Chem. Ber. **89**, 749 (1956).
[12] Zander, M., Erdoel Kohle **19**, 279 (1966).
[13] Sawicki, E., Chemist-Analyst **53**, 88 (1964).
[14] Sawicki, E., and Johnson, H., Microchem. J. **8**, 85 (1964).

[15] Sawicki, E., Stanley, T. W., Pfaff, J. D., and Elbert, W. C., Anal. Chim. Acta **31,** 359 (1964).
[16] Sidorov, N. K., and Rodomakina, G. M., Uch. Zap. Saratovsk Gos. Univ. **69,** 161, (1960).
[17] Drushel, H. V., and Sommers, A. L., Anal. Chem. **38,** 101 (1966).
[18] Drushel, H. V., and Sommers, A. L., Anal. Chem. **38,** 19 (1966).
[19] Drushel, H. V., and Sommers, A. L., Anal. Chem. **36,** 836 (1964).
[20] McCarthy, W. J., and Winefordner, J. D., J. Assoc. Offic. Agr. Chemists. **48,** 915 (1965).
[21] Winefordner, J. D., and Moye, H. A., Anal. Chim. Acta **32,** 278 (1965).
[22] Moye, H. A., and Winefordner, J. D., J. Agr. Food Chem. **13,** 516 (1965).
[23] Moye, H. A., Winefordner, J. D., J. Agr. Food Chem. **13,** 533 (1965).
[24] Moye, H. A., J. Assoc. Off. Anal. Chem. **51,** 1260 (1968).
[25] Latz, H. W., and Hurtabise, R. J., J. Agr. Food Chem. **17,** 352 (1969).
[26] Latz, H. W., Madsen, B. C., Anal. Chem. **41,** 1180 (1969).
[27] Freed, S., and Salmre, W., Science **128,** 1341 (1958).
[28] Freed, S., Turnbull, J. H., and Salmre, W., Nature. **181,** 1831 (1958).
[29] Freed, S., and Vise, M. H., Anal. Biochem. **5,** 338 (1963).
[30] Hollifield, H. C., and Winefordner, J. D., Anal. Chim. Acta **36,** 362 (1966).
[31] Hollifield, H. C., and Winefordner, J. D., Talanta **14,** 103 (1967).
[32] Winefordner, J. D., and Tin, M., Anal. Chim. Acta **32,** 64 (1964).
[33] Hollifield, H. C., and Winefordner, J. D., Talanta **12,** 860 (1965).
[34] Hood, L. V. S., and Winefordner, J. D., Anal. Biochem. **27,** 523 (1969).
[35] Hood, L. V. S., and Winefordner, J. D., Anal. Chim. Acta **42,** 199 (1968).
[36] McCarthy, W. J., Parsons, M. L., and Winefordner, J. D., J. Chem. Educ. **44,** 136 (1967).
[37] St. John, P. A., McCarthy, W. J., and Winefordner, J. D., Anal. Chem. **38,** 1828 (1966).
[38] Winefordner, J. D., and St. John, P. A., Anal. Chem. **35,** 2211 (1963).
[39] Scott, D. R., and Allison, J. B., J. Phys. Chem. **66,** 561 (1962).
[40] Smith, F. J., Smith, J. K., and McGlynn, S. P., Rev. Sci. Instr. **33,** 1367 (1962).
[41] Kanda, Y., and Shimada, R., Spectrochim. Acta. **17,** 279 (1961).
[42] Sponer, H., Kanda, Y., and Blackwell, L., ibid. **16,** 1135 (1960).
[43] Kanda, Y., Shimada, R., and Saka, Y., ibid. **17,** 1 (1961).
[44] Kanda, Y., Shimada, R., Honada, K., and Kajigaeshi, S., ibid. **17,** 1268 (1961).
[45] Von Foerster, G., Z. Naturforsch. **18a,** 6201 (1963).
[46] Kubelka, D., and Munk, F., Z. Techn. Physik **12,** 593 (1931).
[47] Parker, C. A., and Hatchard, G., Trans. Faraday Soc. **57,** 1894 (1961).
[48] Klasen, H. A., Philips Res. Rep. **2,** 68 (1947).
[49] Kortüm, G., Braun, W., and Herzog, G., Angew. Chem. Intern. Ed. **2,** 333 (1963).
[50] Hollifield, H. C., and Winefordner, J. D., Anal. Chem. **40,** 1759 (1968).
[51] Zweidinger, R. W., and Winefordner, J. D., Anal. Chem. **42,** 639 (1970).
[52] Lukasiewicz, R. J., Rozynes, P. A., Sanders, L. B., Winefordner, J. D., Anal. Chem. **44,** 237 (1972).
[53] Lukasiewicz, R. J., Mousa, J. J., and Winefordner, J. D., Anal. Chem. **44,** 963 (1972).
[54] Lukasiewicz, R. J., Mousa, J. J., and Winefordner, J. D., Anal. Chem. **44,** 1339 (1972).
[55] Zweidinger, R. W., Sanders, L. B., and Winefordner, J. D., Anal. Chim. Acta **47,** 558 (1969).
[56] Tin, M., and Winefordner, J. D., Anal. Chim. Acta **31,** 239 (1964).
[57] Sanders, L. B., Cetorelli, J. J., and Winefordner, J. D., Talanta **16,** 407 (1969).
[58] Fisher, R. P., and Winefordner, J. D. Anal. Chem. **44,** 948 (1972).
[59] Winefordner, J. D., Accnts, Chem. Res. **2,** 361 (1969).
[60] O'Haver, T. C., and Winefordner, J. D., Anal. Chem. **38,** 1258 (1966).
[61] McGlynn, S. P., Azumi, T., Kinoshita, M., Molecular Spectroscopy of the Triplet State (Prentice-Hall, Englewood Cliffs, New Jersey, 1969).
[62] Fresenius, M. Zander, Z. Anal. Chem. **226,** 251 (1967).
[63] Hood, L. V. S., and Winefordner, J. D., Anal. Chem. **38,** 1922 (1966).

(Paper 76A6–743)

JOURNAL OF RESEARCH of the National Bureau of Standards—A. Physics and Chemistry
Vol. 76A, No. 6, November–December 1972

Measurements of Absolute Values in Biochemical Fluorescence Spectroscopy

Raymond F. Chen

National Heart Institute, National Institutes of Health, Bethesda, Maryland 20014

(July 19, 1972)

Fluorescence spectroscopy is an important tool of the biochemist studying the structure and interactions of proteins and nucleic acids. The four basic quantities to measure accurately are: 1. spectra (corrected excitation and emission). 2. quantum yields (Q), 3. fluorescence decay characteristics, and 4. polarization. Commercially available instruments, with little modification, can be used to obtain these measurements, but the biochemist in this field is very dependent on the accuracy of measurements of substances he uses as standards. Confusion arises from disagreement between reported values for standards which may be used to calibrate a detector system to obtain quantum yields, or to set up lifetime and polarization photometers. For instance, the protein chemist is fond of using tryptophan and quinine as quantum yield standards, but Q for tryptophan has been variously reported as 0.13 and 0.20, and Q values for quinine bisulfate range from 0.4 to 0.7. The biochemist should also be aware of the problems inherent in the use of commerically available instruments in absolute measurements, as well as the special complications arising in complex biochemical systems where the fluorescence is heterogeneous.

Key words: Absolute fluorometry; absolute fluorometry in biochemistry; standard reference materials in fluorometry.

I. Introduction

A. Applications of Fluorescence Spectroscopy in Biochemistry

Within the last dozen years, biochemists have generally become aware of the value of fluorescence spectroscopy as a tool for the study of macromolecules such as proteins and nucleic acids. The marked increase in the use of fluorescence during recent years has also been due to improvements in instrumentation and techniques. Before discussing the types of measurements which are needed, let us consider some of the applications of fluorescence spectroscopy in physical biochemistry:

1. Obtaining Information on the Size and Shape of Macromolecules.

In 1952, Weber [1, 2][1] pointed out that the polarization of fluorescence of dyes attached to proteins could be used to give information on rotational relaxation times. These times were an estimate of the Brownian motion occurring during the lifetime of the excited state; hence, information was obtained concerning the size and shape of the proteins. The equation derived by Weber [1] to correlate the degree of polarization, P, with the fluorescence decay time τ, and the relaxation time ρ_h, was based on similar equations originally formulated by Perrin [3] and Levshin [4] for simple organic fluorophors:

$$\frac{1}{P}-\frac{1}{3}=\left(\frac{1}{P_0}-\frac{1}{3}\right)\left(1+\frac{3\tau}{\rho_h}\right) \tag{1}$$

where P_0 is the limiting polarization. Because the quantity τ/ρ_h is proportional to the ratio T/η (T, absolute temperature; η viscosity), a "Perrin plot" of $1/\mathrm{P}-1/3$ versus T/η obtained from polarization data with protein-dye conjugates at different temperatures and/or viscosities, contains all the information needed to calculate the rotational relaxation time of the molecule, provided the lifetime can be measured. Polarization data are also useful for following conformational changes such as unfolding or dissociation of a protein. Such events can frequently be monitored by no other known techniques [5]. Note that utilization of eq (1) requires both polarization and lifetime determinations.

2. Study of Binding Equilibria

The interaction of proteins with small ligands is a key function of proteins comprising certain physiological systems. This is especially true in the case of

[1] Figures in brackets indicate the literature references at the end of this paper.

enzymes, proteins with catalytic properties. Some of these ligands, such as coenzymes like reduced nicotinamide adenine dinucleotide (NADH) are naturally fluorescent, and the binding of the ligands is accompanied by a large (typically, 2- to 5-fold) enhancement of the quantum yield, alteration of the emission spectrum, and an increase in the polarization of fluorescence. Other ligands such as flavin coenzymes are quenched on binding to proteins. Also, Velick [6] showed that the ultraviolet fluorescence of proteins is often quenched on binding of certain ligands. Any or all of these changes in fluorescence parameters are useful in obtaining the stoichiometry and association constants of the binding.

3. Elucidation of the Nature of Binding Sites

The dielectric properties of different areas on proteins differ markedly; such differences can be signalled by the fluorescence behavior of fluorescent ligands bound to these areas. Dyes which have been useful in this regard have been dubbed "fluorescent probes". The Stokes shift and quantum yield of bound fluorescent probes have been used to estimate the microscopic dielectric constant of binding sites in proteins. An example of how the nature of the binding site affects fluorescence is given in figure 1. The 1-dimethylaminonapthalene-5-sulfonyl (DNS) group has emission properties which make it useful for a variety of fluorescence studies, including polarization. When DNS is used as a probe, a high quantum yield and a small Stokes shift is indicative of a nonpolar environment. Absorbed onto the active site of the enzyme, carbonic anhydrase, DNS in the form of the sulfonamide has a smaller Stokes shift than it does when adsorbed to BSA (bovine serum albumin) or attached covalently to the enzyme (fig. 1).

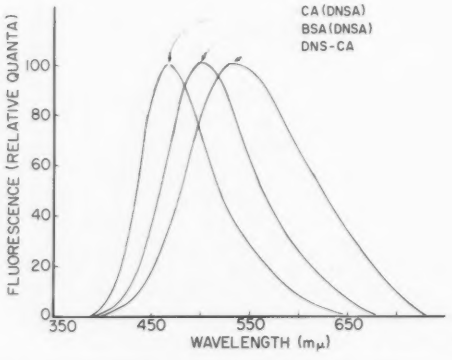

FIGURE 1. Corrected emission spectra of proteins containing the 1-dimethylamino-naphthalene-5-sulfonyl (DNS) group. CA(DNSA) and BSA(DNSA) are adsorbates of carbonic anhydrase and bovine serum albumin containing 1-dimethylamino-naphthalene-5-sulfonamide, and DNS–CA is a conjugate prepared by reacting carbonic anhydrase with DNS chloride. The curves are normalized to the same height. From Chen and Kernohan [7].

4. Study of the Environment Near Tryptophan and Tyrosine Residues in Proteins

Since it was discovered in the late 1950's that proteins have an ultraviolet fluorescence due to aromatic amino acids, much has been learned about the types of molecules or groups on a protein which can influence such fluorescence. The spectrum of tryptophanyl fluorescence is an indicator of the polarity of the environment near the emitting group. Changes in intrinsic fluorescence can be used to follow conformational changes or binding. Intrinsic fluorescence is a useful optical parameter for kinetic studies, including rapid reactions followed by stopped-flow or perturbation methods.

5. Determination of Intermolecular Distances by Energy Transfer

The radiationless transfer of energy from an excited chromophore to an acceptor molecule via a dipole-dipole resonance mechanism has been shown to occur in many intances. The theory of such energy transfer was studied by Förster [8] who developed a method for estimating the distance between donor and acceptor moieties based on their spectroscopic properties and the degree of energy transfer. Fluorometry is the best method for studying energy transfer, because this process is manifested by a quenching of the fluorescence of the donor and/or a sensitized fluorescence of the acceptor. A common example is that of a dye attached to a protein: the distance between the dye and the tryptophan residues may be estimated by the energy transfer from tryptophan to dye.

6. Study of the Orientation of Molecules Attached to Asymmetrical Macromolecules

By the use of polarized excitation, it is possible to obtain information on the orientation of ligands on a larger molecule. Using polarized photoselection, Lerman [9] determined that certain mutagenic dyes were attached with their planes perpendicular to the axis of deoxyribonucleic acid (DNA) molecules; this was the basis for his theory that mutagens intracalate between DNA base pairs. The orientation of dyes attached to proteins can similarly be studied by polarization measurements [10, 11]. The lack of a unique orientation of a dye fixed on a protein can also be detected. Such would be the case if dyes were attached in a random manner, or if a dye were attached to a flexible segment of the macromolecule.

7. Study of Changes in Conformation of Macromolecules

This is perhaps the most important use of fluorescence spectroscopy in biochemistry at present, and is accomplished by following changes in intrinsic fluorescence parameters as well as the fluorescence of attached groups. Such changes sometimes cannot be followed by other optical methods, and fluorescence

becomes the method of choice, especially for kinetic studies.

B. The Parallel Development of Fluorescence Spectroscopy and Instrumentation

From the preceding section, one can see that biochemical fluorescence spectroscopy requires the measurement of a variety of parameters: excitation and emission spectra, quantum yields, lifetimes, and polarization. The needs of biochemists often exceed those of individual physicists or physical chemists, although in biological fields investigators frequently are considerably less knowledgeable concerning instrumentation than physical scientists and are not qualified to construct their own instruments. However, commercially available instrumentation has improved and often has incorporated the best features of laboratory-built devices described in the literature. It is now possible to measure all of the above fluorescence parameters with available instrumentation. The development of such instrumentation has played an important role in the evolution of fluorescence techniques.

Following the description by Bowman et al. [12] in 1955 of the first spectrofluorometer, several instruments based on their design were produced commercially. Such instruments contain, basically, a xenon arc lamp, a sample compartment, two monochromators, and a photodetector system. The principal innovations by Bowman et al. were the introduction of the xenon arc as a source of energy continuum for fluorescence excitation, and the incorporation of two monochromators for excitation and emission. In this country, at least half a dozen spectrofluorometers of this type are marketed. There are probably thousands of these spectrofluorometers in use. They may serve as a basic tool for fluorescence spectroscopy and are of modest cost.

More sophisticated instruments are now available for determining spectra which have been designed to compensate for variations of exciting energy and photodetector response. These instruments generally cost 3 or 4 times as much as an uncompensated spectrofluorometer.

Polarization measurements have been made on light scattering photometers, filter fluorometers, and spectroflurometers [12]. Although specific instruments for fluorescence polarimetry do not seem to be generally used, the modification of other available instrumentation for such purposes poses no great problem. Even in the field of lifetime measurements there are commercial instruments available for the purpose. The TRW Instruments 75A (El Segundo, California)[2] fluorescence decay apparatus and the ORTEC Model 9200 fluorescence spectrometer are the first instruments for determining lifetimes, which were previously accessible only to those with considerable engineering skill.

II. Measurement of Fluorescence Parameters

A. Definition of the Term "Absolute"

The term "absolute" as used here refers to a property of a substance rather than its measurement. For example, the *absolute* quantum yield of a substance is the ratio of the photons emitted to the number of photons absorbed, in contrast to the *relative* quantum yield, the number of photons emitted by one substance as compared with another under specified conditions. Confusion may arise, because the phrase "absolute quantum yield" has been used by some workers to denote the quantum yield which has been measured by an "absolute" method; i.e., a method not requiring the use of a reference standard of known quantum yield. Absolute measurements are frequently required in certain bilogical fields like bioluminescence, but will not be treated here.

1. Excitation and Emission Spectra.

a. Definition.—The true, or absolute, fluorescence emission spectrum of a substance is a plot showing the relative number of photons emitted at different wavelengths; i.e., $dq/d\lambda$ versus λ, where q represents the total number of photons emitted and λ is the wavelength. Alternatively, the same information can be plotted on a frequency scale, $dq/d\nu$ versus ν in cm^{-1}. For simple organic compounds the emission spectrum is generally independent of the excitation wavelength, but for complex systems there is no single absolute emission spectrum since the emission may vary continuously with exciting light energy.

The excitation spectrum is a plot of the relative number of photons emitted at a given wavelength as a function of the exciting wavelength. The true, or corrected, excitation spectrum is compensated for any variations of excitation energy with wavelength. The corrected excitation spectrum is expected to coincide with the absorption spectrum in simple compounds, but this relationship may not hold in large biochemical systems.

b. Need for Corrected Spectra.—Absolute fluorescence spectra would be useful for comparing results from different laboratories and have long been advocated [14] as being the most suitable form of data presentation. Expensive spectrofluorometers are available for automatic recording of absolute fluorescence spectra. However, many uncorrected spectra are published even today, and some case can be made for continued use of uncorrected data. Thus, when the main point of a study is simply to show changes in fluorescence characteristics, there is little reason to take trouble to correct the spectra. The thousands of spectrofluorometers in use are equipped with similar

[2] In order to adequately describe materials and experimental procedures, it was occasionally necessary to identify commercial products by manufacturer's name or label. In no instances does such identification imply endorsement by the National Bureau of Standards, nor does it imply that the particular product or equipment is necessarily the best available for that purpose.

474-414 O - 73 - 4

gratings and photomultiplier tubes, so that uncorrected spectra from one laboratory can, in fact, be used for comparison with results from another laboratory.

Absolute spectra are more informative, are required for quantum yield determinations, and are necessary for calculations of natural lifetimes or energy transfer distances. Nonetheless, one can confidently predict continued use of uncorrected spectra in the literature.

c. Calibration of Lamp Output and Detector Response.—Since most biochemists utilize uncompensated spectrofluorometers, it should be pointed out that procedures for calibrating these instruments have been published, e.g. [5, 15, 16]. The main steps involve (a) Calibration and alignment of the monochromators with a line source such as a mercury pen lamp, (b) Calibration of the exciting source with a fluorescent screen solution, such as Rhodamine B or some other dye, and (c) Calibration of the detector response by comparing the recorded signal from a standard lamp with its known output.

An example of a detector response calibration curve is given in figure 2. The response of an RCA 1P28

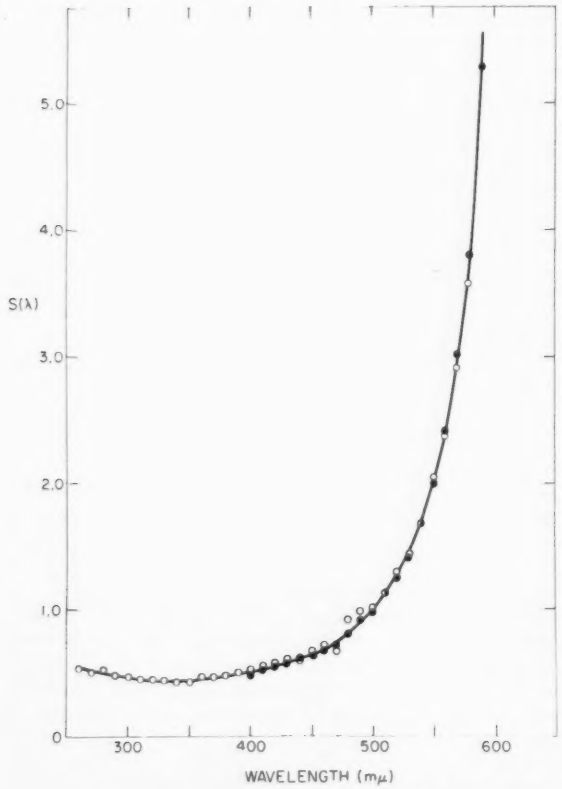

FIGURE 2. Detector calibration curve for Aminco-Bowman Spectrofluorometer fitted with 1P28 phototube and a grating blazed at 300 nm. Filled circles: data obtained with a National Bureau of Standards tungsten filament lamp. Open circles: data obtained with calibrated xenon arc lamp. $S(\lambda)$ is a function of the reciprocal of the sensitivity. From Chen [16]

Photomultiplier in an Aminco-Bowman spectrofluorometer fitted with a grating blazed for maximum response at 300 nm seems to be quite linear in the region from 290 nm to 400 nm. The detector system thus delivers "absolute" emission spectra for substances like proteins which emit in this range. By choosing suitable gratings and phototubes, it is sometimes possible to obtain linear response in regions of visible fluorescence as well, thus avoiding the need for point-by point correction of spectra.

The accuracy of detector calibration depends on such factors as the photometric accuracy of the system and the accuracy of the standard lamp calibration. Lee and Seliger [17] have considered at length all the possible errors involved in *absolute* calibrations of detector systems. Their interest was principally the determination of chemiluminescent quantum yields, and it was necessary to know the relation between the number of photons and the detector response. In contrast, the determination of true emission spectra require that the relative detector response at different wavelengths be specified. Hence, the uncertainty in Lee and Seliger's absolute calibrations, ± 4.5 percent, is an upper limit in the more usual calibrations.

Calibration of spectrofluorometers by the use of "standard spectra" of well-known substances has been advocated [18]. In theory this would be a very convenient method. Comparison of the apparent excitation spectrum of a simple compound could be made with its absorption spectrum to yield the correction factors for lamp output. The method eliminates the need for a front-surface illumination attachment [15], which is needed for calibrations using the fluorescent screen method. Comparing absorption and emission spectra has the disadvantage that the same dispersion generally cannot be used in the absorption and fluorescence spectrometers. Other disadvantages make the comparison-of-spectra method less desirable than the fluorescent screen method. The latter results in a continuous plot of photon output versus wavelength compared with the discontinuous plot obtained by spectral comparison. Also, several absorption spectra are required to achieve a desired optical density at regions of maxima and minima, and several fluorescence excitation spectra at different gain settings will be needed as well.

The use of "standard spectra" to calibrate the detector response is becoming common practice as more corrected spectra are published. Unfortunately, the reliability of any given published spectrum is unknown, and it would perhaps be helpful if some spectra were certified by a committee of experts. In the past, there have been many discrepancies in published emission spectra of quinine [19], although more recent spectra seem to agree closely [20–23] and could be used for detector calibration. One complication which we pointed out several years ago is that the emission spectrum of quinine shows a red shift when excited in the long wavelength edge of the absorption band [21]. This effect is shown in figure 3. The emission shift has been postulated by Fletcher [22] to be related

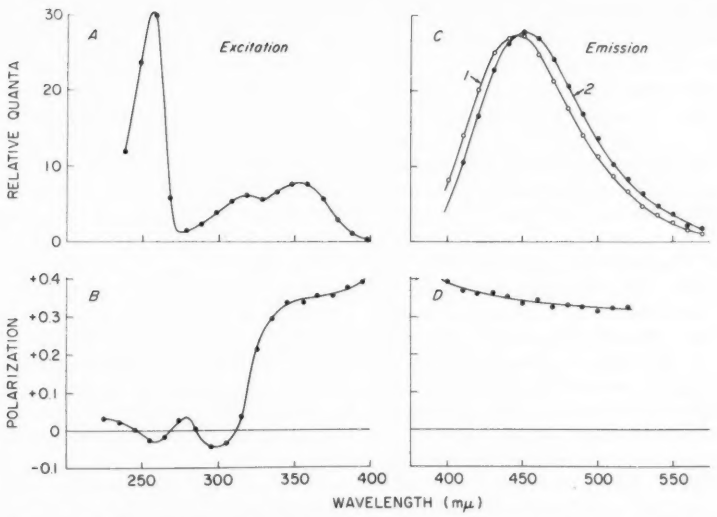

FIGURE 3. Fluorescence and polarization spectra of quinine in glycerol containing 0.1 N H_2SO_4 at 8 °C A. Excitation spectrum. B. Fluorescence polarization spectrum obtained with varied exciting wavelength and emission monochromator set at 450 nm. C. Corrected emission spectra obtained with excitation at 340 nm (curve 1) and 390 nm (curve 2). D. Variation of polarization in the emission band with constant excitation at 340 nm. From Chen [21].

to photoselection of quinine molecules with slightly different conformations. Other compounds also show this effect [21, 22, 24], which may involve what Fletcher calls rotatable auxochromes such as the methoxy group at the 6-position of the quinoline nucleus in quinine. At low temperatures, emission spectral shifts also occur due to the presence of different solvation states [25]. However, the spectrum of quinine under usual conditions of excitation should be suitable for a standard.

2. *Quantum Yield Measurements*

a. The Comparative Method of Determination.—In biochemistry, the quantum yield is most often obtained by comparison with a quantum yield standard. A spectrofluorometer is required, and the yield is calculated from the relation

$$\frac{Q_x}{Q_{st}} = \frac{F_x}{F_{st}} \times \frac{A_{st}}{A_x} \times \frac{\phi_{st}}{\phi_x} \times \frac{n_{st}^2}{n_x^2} \qquad (2)$$

where Q is the quantum yield, F is the area under the corrected emission spectrum, A is the optical absorbance at the exciting wavelength, ϕ is the relative photon output of the light source at that wavelength, and n is the refractive index. The subscripts x and st refer to the unknown and standard.

b. Factors Affecting the Accuracy.—

1. Accuracy of the emission detector response calibration. Any errors present may have little effect on the quantum yield calculations if the spectra of the standard and unknown are similar. One should not use fluorescein as a standard to determine quantum yields of ultraviolet fluorescence, for example.

2. "Bookkeeping" errors. Anyone who has attempted to perform quantum yield determinations must surely be impressed by the large number of factors which have to be inserted into the final calculations. Aside from the terms in eq (2), one must also remember that the photometer sensitivity may have been set at different values for standard and unknown, and the sensitivity scale may need recalibration. The absorbance, A, is usually read for concentrated solutions which then are diluted by some factor which renders self absorption unlikely in the fluorescence measurement; the dilution factor must be inserted. One can suspect that some of the large errors which have appeared in the literature are due to deficiencies in bookkeeping.

3. Determination of the absorbance. Although it would seem a simple matter to determine the absorbance of the test substances, errors arise because the wavelength calibrations of the spectrofluorometer and the spectrophotometer may be slightly incorrect. Excitation then may occur at a wavelength different from that at which the absorbance was measured. The bandwidth of the monochromators also are usually different, and the amount of error from this discrepancy depends on the spectral characteristics of the compounds. We have found that our average deviations for quantum yield determinations have been smaller when the unknown and standard are each excited at the peak of their long wavelength absorption bands. With

this method, one never need worry about slight monochromator alignment errors which would produce large errors in regions of sharply changing absorption.

4. Source output calibration. If sample and unknown are excited at the same wavelength, the term ϕ_{st}/ϕ_x of eq (2) reduces to one. However, since different wavelengths are usually used, some error may intrude. The lamp calibration curve for the xenon arc [16] is fairly smooth from 230–400 nm. In this region, if the exciting wavelengths for *x* and *st* are not too wide, one would not expect much error to be introduced if there is slight inaccuracy in the knowledge of the exciting wavelengths. Between 400 nm and 520 nm, however, there are some strong peaks in the xenon arc output. In this region, perhaps it would be best to use the same wavelength to excite both standard and unknown. The calibration curve itself might be erroneous due to factors such as impurities in the fluorescent screen substance. This may be checked by using several different screens, or by determining if the calibration curve allows for corrected excitation spectra which match the absorption spectra.

5. Polarization effects. In protein and nucleic acid fluorescence studies, the emission is frequently polarized due to the large size of the molecules. The resulting emission anisotropy can introduce an error into the quantum yield calculations even when unpolarized excitation is used, since even here, in instruments utilizing right-angle viewing geometry, the fluorescence is polarized. A number of papers have considered this problem [26–29]. Taking the worst possible case, Paoletti and Le Pecq [29] have estimated that a 15 percent error could occur in relative quantum yield measurements. However, an error this large could only occur with a sample showing maximum polarization in an instrument having large polarization artifacts, and where the fluorescence of standard and unknown were compared at individual emission wavelengths. Since the actual conditions for quantum yield assays are normally quite different, the errors are usually neglected, and indeed have never emerged as a great problem.

6. Accuracy of the value of the fluorescence standard.

a. Characteristics of quinine fluorescence. Recent reviews [30, 31] have pointed out the surprising discrepancies in reported quantum yields which exist in the literature and the controversy over the values of several well-known quantum yield standards. The most common standard is quinine in aqueous sulfuric acid solutions. An absolute yield of 0.55 for quinine in 1.0 *N* H_2SO_4 was reported by Melhuish [32, 33] as well as by Windsor and Dawson [30]. These workers employed absolute methods for the determination. A value of 0.58 for quinine in 0.1 *N* H_2SO_4 was reported by Eastman [34] using a technique which was probably less accurate. The report by Drobnik and Yearghers [35] that quinine probably had a yield of less than 0.4 must be dismissed, since Fletcher [36] was unable to duplicate their experiment and found a discrepancy of a factor of 6 in their reported *Q* for 2-aminopurine. Windsor and Dawson [30] pointed out that there were already literature reports that quinine yield was dependent on the concentration of sulfuric acid. Many investigators, including ourselves, were guilty of using 0.546 for the yield of quinine in 0.1 *N* H_2SO_4 rather than 1.0 *N* acid. We find that the quantum yield actually is 6 percent lower in the more dilute acid, so a yield of 0.51 should be used. The reason for the dependence of yield on acid concentration is not clear, but it must be an excited state phenomenon since we have been unable to demonstrate any significant change in absorption spectrum for quinine dissolved in 10 *N* H_2SO_4 compared with 0.1 *N* H_2SO_4.

Figure 4 shows the titration of quinine which has a midpoint at about pH 4.3 by absorption measurements. The optical density-pH titration curve shows the normal flattening at both ends, but the titration by fluorescence shows a slight continuing rise in the acid region, although the midpoint of the titration curve is the same. Figure 5 shows the variation of quinine fluorescence yield with sulfuric acid concentration. Several features may provide a clue as to the processes involved here. The fluorescence increases almost linearly from 0.1 *N* to 10 *N* H_2SO_4, although there is no change in absorption. However, we have also noted that $SO_4^=$ is a quencher of quinine fluorescence, although Stern-Volmer kinetics were not obtained. Thus the rise in quinine yield at high acid concentrations would be even larger except for the presence

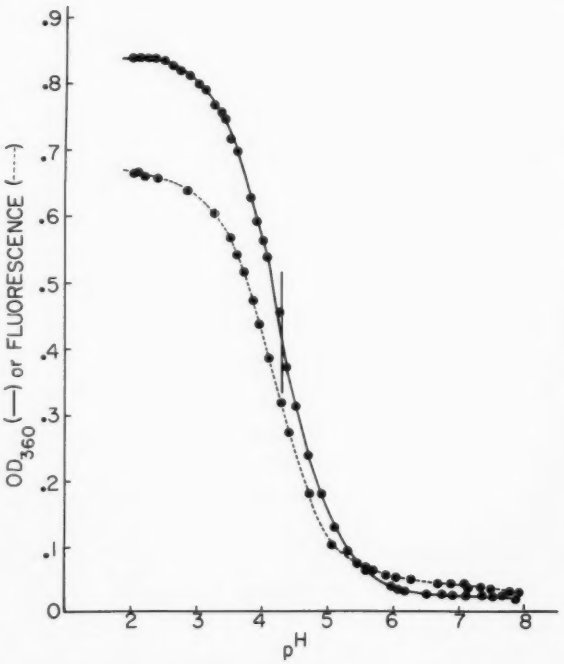

FIGURE 4. Titration of quinine monitored by fluorescence at 450 nm (---) or by optical density at 360 nm (—).

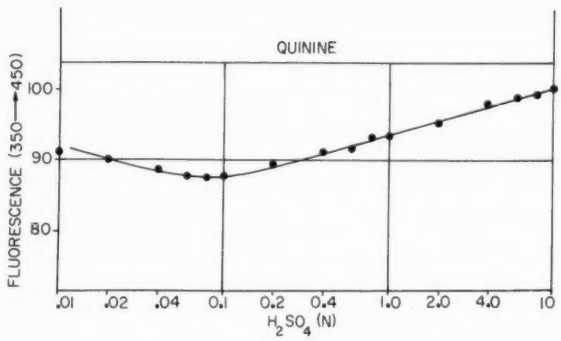

FIGURE 5. Effect of H_2SO_4 concentration on the fluorescence of quinine excited at 350 nm and monitored at 450 nm.

of sulfate ion. The slight increase in quinine yield at low acid concentration is reproducible and may be due to the lower concentration of sulfate ion.

Quinine is a good quantum yield standard for biochemical studies for several reasons. It is used in aqueous solutions. There is little overlap of absorption and emission spectra. The quantum yield is high. The material is obtained in pure form readily and is stable in acid solutions for months. There is little structure in the absorption spectrum and none in the emission spectrum, so high resolution equipment is not needed. The temperature dependence of the yield is relatively small. Figure 6 shows the temperature dependence of the yields of some compounds which might be useful as standards.

It is interesting that Rusakowicz and Testa [37] obtained a quantum yield of 0.46 for quinine in 0.1 *N* H_2SO_4 when comparing it with 9,10-diphenylanthracene, assumed to have a yield of 1.0 in cyclohexane. This value approaches Windsor and Dawson's value of 0.50 [30] and a value of 0.51 which we now favor. The value of 0.46 is fairly good since a very large refractive index correction (17%) was needed for comparing cyclohexane and water solutions. Nevertheless, there is no compelling reason to favor use of 0.46 rather than 0.51 as the yield for quinine in 0.1 *N* H_2SO_4.

The commonly accepted value for the quantum yield of quinine has also been challenged recently by Scott et al. [23], who claim that the yield in 0.1 *N* sulfuric acid is 0.70 ± 0.02. This value was determined from a comparison of measured lifetime with calculated natural lifetime, assuming the relation $Q = \tau/\tau_{nat.}$ This approach must be questioned, since the calculated natural lifetimes based on equations such as those of Förster [38] or Strickler and Berg [39] are quite approximate. Both Ware and Baldwin [40] and Birks and Dyson [41] noted the discrepancy between the measured and calculated lifetimes of quinine and have proposed explanations for this. The value of 0.70 must be too high, because many studies have used 0.55 as the value for quinine and have obtained values near unity for other compounds by comparison with quinine. Substitution of 0.70 for 0.55 would result in many quantum yields of greater than unity.

b. Controversy over the quantum yield of tryptophan. The most common quantum yield standard used in biochemistry for the ultraviolet region is tryptophan, because it has an emission which matches closely the tryptophanyl fluorescence of proteins. Here, too, there has been controversy over the quantum yield. Shore and Pardee [42] estimated Q to be 0.09, but used a rather crude method involving a spectrophotometer modified for fluorometry with filters. Teale and Weber [43] subsequently reported a value of 0.20, which has since been widely used. We reported that the value should be 0.13 [44] based on comparison with quinine in 0.1 *N* H_2SO_4 assumed (incorrectly) to have a yield of 0.55. Our value for tryptophan Q should be revised downward to 0.12 in view of the lower yield of quinine, 0.51. Also using quinine as a standard, Børresen [45] and Bridges and Williams [46] obtained tryptophan yields of 0.11 and 0.15. Eisinger [47] determined the tryptophan quantum yield to be 0.14 based on comparison with *p*-terphenyl, whose yield was 0.87. If Eisinger's data are correct, there can be no doubt that the value of 0.20 is much too high, for then the quantum yield of *p*-terphenyl would greatly exceed unity. We have convinced ourselves that 0.20 is, in fact, too high by similar comparisons with 9,10-diphenylanthracene and 2-aminopyridine (2AMP) which have very high quantum yields and have been recommended as standards [37, 48]. This simple experiment is recommended to anyone still in doubt concerning the quantum yield of tryptophan. While absolute measurements of quantum yield are difficult, relative quantum yields can easily be carried out with a precision of 5 percent. Therefore, if a standard with a supposed quantum yield of 1.0 is used, it is easy to determine an *upper limit* for the yield of any given unknown. Q determined in this way may be the real quantum yield, or, if the standard's Q turns out to be less than 1.0, some smaller value.

c. Other useful standards. Some quantum yields which have been measured in the author's laboratory are listed in table 1. Several values are at variance with those reported recently from Testa's laboratory [37, 48, 49]: 1. The yield of 2AMP is found to be 0.73 rather than 0.60. 2. The yield of 2AMP is found to be 6, rather than 13, times that of tryptophan. 3. A value of 0.55 for quinine in 1 *N* H_2SO_4 is consistent with our relative measurements, and is slightly higher than would be expected from the value of 0.46 reported for quinine in 0.1 *N* H_2SO_4.

Tryptophan with a quantum yield of 0.12 seems to be the best standard for protein quantum yields. The idea of using a protein as a quantum yield standard has occurred to us. However, when testing different commercial preparations of serum albumin, the most widely available protein in pure form, we have found wide variations in yield. Fresh tryptophan solutions are more suitable; solutions are not stable for more than one day.

There are, of course, many other compounds which might be suitable for standards, but the problem is to find compounds which have been examined in many

Table 1. Quantum yields of some possible standards

Compound	Q	Standard, Q_{st}
2-Aminopyridine, 0.1 N H_2SO_4	*0.74	9,10-diphenylanthracene, 1.0
Do.	.73	tryptophan, 0.12
Do.	.74	quinine, 1 N H_2SO_4, 0.55
Trytophan, water	*.12	9,10-diphenylanthracene, 1.0
Do.	.12	quinine, 1 N H_2SO_4, 0.55
1-dimethylaminonaphthalene-5-sulfonate, 0.1 M $NaHCO_3$	.34	Do.
4-Methylumbelliferone, 0.01 M NaOH	.64	Do.
4-Methylumbelliferone, 0.01 M HCl	.65	Do.
5-Hydroxyindole (serotonin), pH 7.4	.23	Do.
Tyrosine, water	.13	Do.
Phenylalanine, water	.022	Do.
Phenol, water	.13	Do.
1-dimethylaminonaphthalene-5-sulfonamide, pH 7.4	.051	Do.

All values were obtained by the author with the Aminco-Bowman spectrofluorometer and a Cary Model 11S spectrophotometer, except for those marked (*). The latter were determined with a Turner Model 210 spectrofluorometer. The author is indebted to Dr. H. Edelhoch for the use of this instrument.

different laboratories which agree on the quantum yield values. Fluorescein in aqueous base has frequently been used with a yield of 0.85 [cf. 50], and this is an excellent standard if the unknown has similar spectra. Biochemists will most often require aqueous standard solutions, since their samples are usually in water. The correction factor for refractive index differences between a given solvent and water may be quite large (+17% for cyclohexane solutions, for example). The correction factor is only approximate for the actual geometry existing in a given spectrofluorometer, and should be avoided wherever possible.

d. On the "certification" of quantum yield standards. In spite of our own confidence in the quantum yield data in table 1, we recognize that acceptance of compounds as standards comes only after agreement is reached between a number of reliable laboratories. Several studies have supported the values listed for tryptophan, 1-dimethylaminonaphthalene-5-sulfonate, quinine, 9,10-diphenylanthracene, and other compounds. Although a caveat has been issued [31] against the use of tryptophan as a standard, because of the controversy over its yield, a careful review of the data show that tryptophan Q is as well known as that of quinine. The use of quantum yield values for compounds over which controversy has not yet developed, because they have not been adequately investigated, seems irrational. The dearth of accepted quantum yield values is well brought out by the review of Demas and Crosby [31]. Perhaps one solution would be to carry out a cooperative study between several laboratories on a number of standards. This might speed the "certification" of standards.

3. Polarization Measurements

a. Definitions.—The degree of fluorescence polarization, P, is defined by

$$P=\frac{I_V-I_H}{I_V+I_H}.$$

If a fluorometer utilizes right-angle geometry, I_V and I_H refer to the intensities measured with the analyzer oriented normal and parallel to the direction of excitation. Fluorescence polarization is observed when the excitation is either polarized or unpolarized, provided that observation of the fluorescence is normal to the direction of excitation. If polarization observed with excitation polarized vertically (i.e., parallel to the orientation of the analyzer when measuring I_V) is p_p, the polarization observed with unpolarized, or natural, excitation, p_n, is given by

$$p_p=\frac{2p_n}{1+p_n}.$$

Most studies are carried out with polarized excitation because the absolute values of the polarization are higher ($-1/3 \leq p_p \leq +1/2$) than with natural light ($-1/7 \leq p_n \leq +1/3$). Perhaps the main reason for utilizing natural light is to obtain greater excitation intensities.

b. Measurement of polarization.—If a light-scattering photometer is adapted for polarization of fluorescence measurements, one is generally limited to excitation with certain mercury lines, and both excitation and emission are selected by filters. The use of a spectrofluorometer results in greater flexibility. There seem to be no commercially available instruments designed primarily for fluorescence polarimetry, but polarizing attachments are offered by makers of light-scattering photometers and spectrofluorometers.

c. Artifacts in polarization measurements.—1. Defective collimation. The definition of P given above is based on the assumption that the exciting and emitted rays are perfectly collimated. In long path-length instruments, such a condition is nearly achieved. However, we have found that some simple filter fluorometers are quite unsuited for polarization measurements because the lamp is large and placed close to the sample, and the photodetector is also adjacent to the sample chamber. Large lenses which collect the fluorescence emitted at large angles to the axis connecting the sample and the photodetector may also invalidate the polarization data.

2. Polarizer defects. These can be several types. Azumi and McGlynn [51] found that improperly fabricated Glan prisms rotated the beam of light as the prisms were turned from one orientation to the other. Errors in mounting can cause the ordinary (unpolarized) ray to pass to the sample, or the polarizers may be set at some angle to the desired orientation. Some film polarizers may have incomplete polarization, especially at short wavelengths. Most polaroid film polarizers do not seem to be light-fast and will rapidly bleach when exposed to a high intensity source. However, some light-fast film polarizers of large aperture are available [13]. A convenient arrangement for spectrofluorometers is to use such filters in the exciting beam, and polaroid analyzers before the photodetector, as shown in figure 7. This arrangement has been used by many workers with good results.

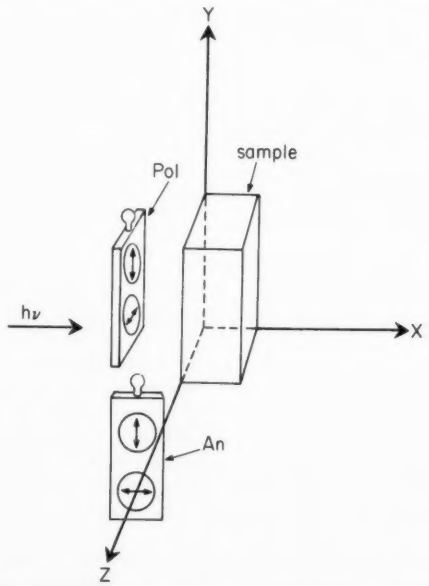

FIGURE 6. Recommended arrangement of polarizers in the Aminco-Bowman spectrofluorometer. The polarizers (Pol) and analyzers (An) are in sliding filter holders. From Chen and Bowman [13].

3. Spurious polarization introduced by the instrument. Light reflected from surfaces in a grating monochromator instrument becomes partly polarized, and such polarization must be corrected. In the exciting beam, this partial polarization is best rendered completely polarized; i.e., p_p rather than p_n is measured, especially in spectrofluorometers. The polarization introduced by the emission monochromator is wavelength dependent and related to variations in efficiency of the grating ("grating anomalies"). This artifact may be corrected by first determining the relative response of the detector system at any wavelength to horizontally and vertically polarized light. The grating correction factor, G, is obtained by observing a source of unpolarized light with the analyzer in the vertical and horizontal positions. A fluorescent sample can act as such a source if excited with horizontally polarized light. Polarization is then determined from

$$P=\frac{I_{VV}-GI_{VH}}{I_{VV}+GI_{VH}}$$

where $G=I_{HV}/I_{HH}$, and the subscripts refer to the orientations of the polarizer and analyzer.

G should depend only on the wavelength setting of the emission monochromator. For this reason, a calibration curve may be obtained with one or two highly fluorescent solutions and may be applied to measurements on other substances. The monochromator bandwidth should affect the G factor, but in our tests, the available bandwidths made very little difference in G [52]. Figure 8 shows the G factor

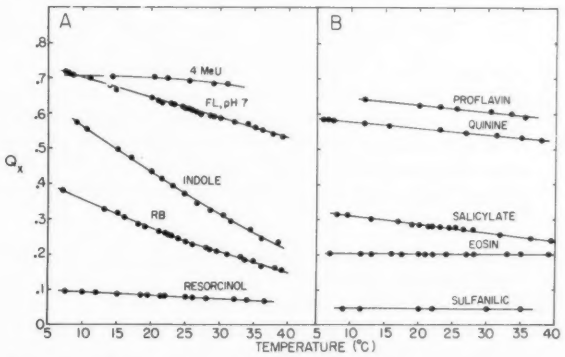

FIGURE 7. Variation of the quantum yield, Q_x, of some compounds with temperature. Abbreviations: 4 MeU, 4-methylumbelliferone; FL, fluorescein; RB, Rhodamine B.

calibration obtained with a spectrofluorometer. Although G could be measured for each sample, some solutions have very low fluorescence yield, and there may be large blank corrections required in determining I_{HV} and I_{HH}. A calibration curve obtained under better conditions is preferable. One of the interesting features of figure 8 is that G varies sharply with wavelength. Some authors [51] have suggested that G declines monotonically with wavelength, but this is clearly not the case.

4. Contributions from blanks. Like other measurements involving fluorescence intensity, polarization measurements should be rigorously corrected for blank contributions. If the G factor is known from prior calibration, polarization measurements still require four measured values: I_{VV} and I_{VH} for sample and blank. The magnitude of the blank relative to the sample signal can be large, as shown in figure 9 for the example involving bilirubin. Q for bilirubin bound to albumin is less than 0.01, and there is a background fluorescence due to impurities on albumin. There are relatively few instances where the blank can be neglected completely. Such might be the case of high quantum yield dyes dissolved in glycerol. A number of "automatic" fluorescence polarimeters have been described [53–55] in which I_{VH} and I_{VV} are measured simultaneously and ratioed electronically to give a function proportional to P. However, the common failing of these instruments is an inability to correct for the blank.

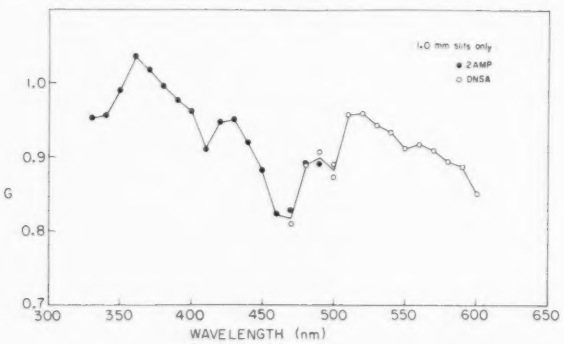

FIGURE 8. Dependence of the grating factor, G, with emission setting; i.e., calibration curve for G. The samples used were 10^{-4} M 2AMP in 0.1 N H_2SO_4 excited at 285 nm, and 10^{-3} M DNSA (1-dimethylaminonaphthalene-5-sulfonamide) in 50 percent ethanol, excited at 330 nm. G was calculated from I_{HV}/I_{HH}. From Chen [52].

5. Scattering. If scatter signal reaches the detector, the polarization will be anomalously high. Scatter can be corrected with a suitable blank, but such blanks may not be available. For example, in obtaining the polarization of the intrinsic emission from a protein, the blank should have the same light-scattering properties without being fluorescent. In turbid solutions, scatter may indirectly lower the observed fluorescence by causing the excitation to appear to reach the sample from many directions due to multiple reflections. For the most accurate measurements, the solutions should be clarified by centrifugation or filtration.

6. Depolarization by radiative energy transfer. In concentrated solutions of substances with considerable overlap of their absorption and emission spectra, depolarization can result from secondary fluorescence which has been excited by self-absorption of radiation. The effect can be detected by the increase in P upon dilution, and can be minimized by the use of small path length cells. Dyes with high absorption coefficients, like fluorescein and Rhodamine B, have been reported to exhibit concentration depolarization in solutions as dilute as 4×10^{-6} M [56].

d. Standards for Polarization.—Standards for fluorescence polarimetry would be helpful to evaluate the performance of a given instrument, but such well-defined standards do not appear to exist. There are considerable variations in reported polarization values for given solutions. The variations are as great as in the area of reported quantum yield values. In the absence of such standards, it is necessary to be certain that the apparatus registers zero polarization for nonviscous solutions of compounds with long lifetimes. Anthracene or other aromatic hydrocarbons in ethanol or cyclohexane may serve this purpose. At the other end of the scale, a sample having nearly the theoretical maximum polarization of 0.5 is desirable. An instrument could read zero for the polarization of a nonviscous solution, but might well give erroneously low polarizations for viscous solutions. Alkaline fluorescein, or Rhodamine B, in glycerol were reported to have polarizations between 0.4 and 0.5 and are therefore often used to test the performance of fluorescence polarimeters. The polarizations reported by various workers are given in table 2. Note

Table 2. Polarizations of dilute dye solutions in glycerol

Sample	Exciting wavelength (nm)	P	Reference
Fluorescein.....	366	0.28	Chen and Bowman [13]
Do.....	366	.424	Price at al. [57]
Do.....	430–520	.477±0.01	Chen and Bowman [13]
Do.....	436	.440	Weber [56]
Do.....	436	.446	Price et al. [57]
Do.....	436	.4922	Szalay et al. [58]
Rhodamine B.....	366	−0.17	Chen and Bowman [13]
Do.....	366	−.0655	Weber [56]
Do.....	366	−.091	Price et al. [57]
Do.....	366	−.17	Kaye[59]
Do.....	436	−.020	Chen and Bowman [13]
Do.....	436	−.0244	Weber [56]
Do.....	436	0.0	Price et al. [57]
Do.....	436	−0.03	Kaye [59]
Do.....	546	0.462	Chen and Bowman [13]
Do.....	546	.444	Weber [56]
Do.....	546	.441	Price et al. [57]
Do.....	546	.462	Singleterry and Weinberger [27]
Do.....	546	.44	Kaye [59]

that there is considerable variation in these values. The best agreement is for Rhodamine B excited at

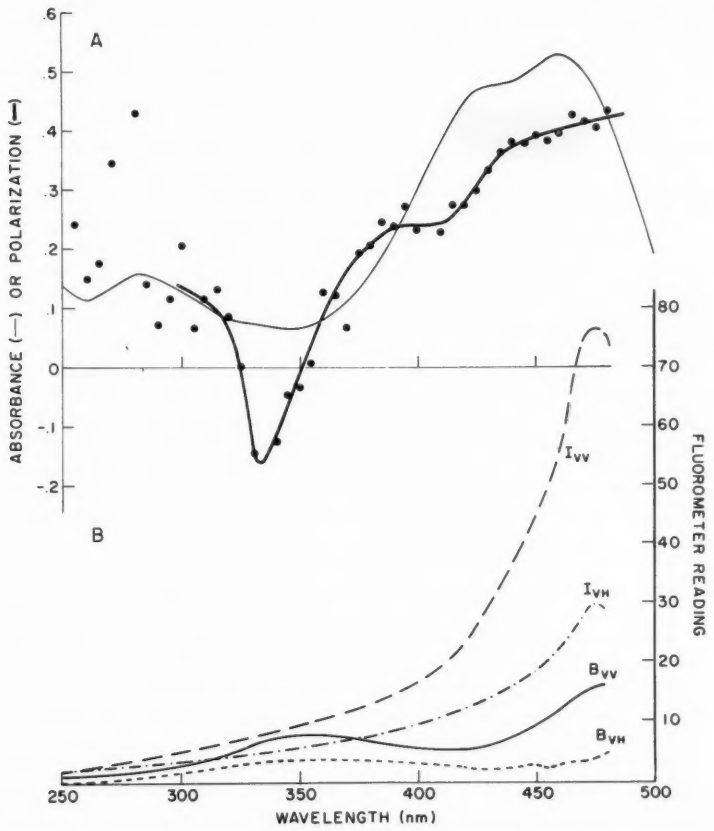

FIGURE 9. Example showing significance of blanks in polarization measurements. In A are shown the absorption (light line) and polarization spectrum (heavy line and points) of bilirubin bound to rabbit serum albumin. The polarization was calculated, using $G = 0.960$, from the data of Part B, which gives the apparent excitation spectra of the sample (I) and blank (B). Subscripts refer to orientation of the polarizer and analyzer. The emission was monitored at 520 nm. From Chen [52].

546 nm: the P values are 0.45 ± 0.01. Poor agreement is found for the values of polarization of Rhodamine B excited at 366 nm.

Useful polarization standards should have polarization which is independent of the emission wavelength. We have found this to be the case for Rhodamine B, fluorescein, and other compounds. However, we found [21] that quinine polarization decreases with wavelength in the emission band (fig. 3).

In many biochemical systems, the emission arises from several fluorophors such as dyes or tryptophans in different parts of a single protein. The polarization therefore depends on both the exciting and emission wavelengths. Much of the early work on the polarization of dye conjugates was obtained with fluorometers where the emission was isolated by a cut-off filter. Such data cannot be duplicated on a spectrofluorometer which detects only a segment of the emission band.

4. *Fluorescence Lifetimes.*

The fluorescence decay time, or lifetime, τ, is defined by $I = I_0 e^{-t/\tau}$ where I_0 is the fluorescence intensity at time $t = 0$ following a delta function exciting pulse, and I is the intensity at subsequent time t. The lifetime is thus the time required for decay of the fluorescence to a value of I_0/e.

The decay times of organic molecules in solution which are of interest to biochemists lie in the range of 0.1 to 100 ns. The accurate measurement of such short times requires complex electronic equipment, but there have been many recent advances in this field. There were no commercially produced instruments for the measurement of τ until 1966. However, numerous laboratory-built instruments had been designed and described. The features of such instruments have been reviewed by Birks and Munro [60].

Two basic types of instrument have been employed. (a) Phase and modulation fluorometers. Here the sample is excited by light which is sinusoidally modulated at megacycle frequencies. The fluorescence thus also fluctuates at these frequencies, but lags behind the excitation by a certain time which is detected electrically as a phase shift with reference to the exciting light. From the phase shift, one can calculate the lifetime value if fluorescence is assumed to decay as a single exponential. The fluorescence decay is also manifested as a decrease in the degree of modulation, and the lifetime can be obtained from this parameter quite apart from the electrical phase shift. Müller et al. [61] reported that a phase fluorometer could be constructed wholly from commercially available components. Spencer and Weber [62] have also constructed a modern phase and modulation fluorometer. Both of these instruments are said to have a very high time resolution, of the order of 0.02 nsec. Therefore, the accuracy of lifetime measurements can be said to exceed the accuracy of absolute determinations of quantum yield. No phase fluorometers have ever been marketed. (b) Nanosecond pulse instruments. By repetitively exciting a sample with a short pulse of light, it is possible to obtain directly, with the aid of a fast oscilloscope, the curve of the fluorescence decay. Ideally, the light flash should be infinitely short; the observed fluorescence should then decay exponentially. Practically, lamp pulses have a finite duration with widths at half maximum intensity of 1 to 10 ns, and the pulse shape may be irregular. The fluorescence decay is also a complex function from which the lifetime must be extracted by any of several mathematical procedures. Advances in lamp design and the use of mode-locked lasers with picosecond pulses may in the future avoid the need for such manipulations, since the excitation will be much shorter than the fluorescence.

The two instruments which are currently available from commercial sources for lifetime determinations are both based on the nanosecond pulse method. In 1966, TRW Instruments introduced a decay time apparatus consisting of a nanosecond fluorometer with a "decay time computer" and requiring a dual-gun oscilloscope. One gun of the oscilloscope was used to display the signal from the sample chamber, while the other channel was connected to the computer, which in turn consisted of a variable waveform signal generator and an analog circuit. The computer was used to compare the shapes of the waveforms derived from the lamp pulse and from a fluorescent sample. The difference between the waveforms was analyzed by the computer to give the corresponding decay time directly. The instrument has been described in some detail [63, 64], is still available, and can be fitted with different kinds of lamps for excitation at different wavelengths. Although originally designed for long lifetimes such as those associated with solid laser materials, the instrument was shown to be capable of measuring lifetimes less than 2 ns [65].

Recently, ORTEC, Inc. (Oak Ridge, Tenn.) has produced a nanosecond pulse instrument based on the so-called single photon counting principle. The important feature of the system is the method used to detect and record the signal from the sample chamber. The low intensity, very fast, nanosecond flash lamp is made weaker still by attenuators so that for each repetitive pulse, no more than one photon which leaves the fluorescent sample causes a response in the photodetector. By timing the interval between the flash and the arrival of the photon at the detector, a histogram of counts versus time is built up and stored in a multichannel analyzer. After sufficient counts have been accumulated, the curve can be displayed on an oscilloscope or digitized for computer analysis. The advantage of the system is the extreme sensitivity, the good time resolution, the use of a lamp, which because of its low output can be made very fast, and then recording the actual undistorted decay. The system theoretically can be used to determine multiple lifetimes present in the fluorescence.

Lifetime measurements by any of the instruments mentioned require only a single standard, namely, a reflecting or scattering substance serving as a standard with $\tau=0$. No comparison with substances of known lifetimes is needed, so each lifetime measurement is, in fact, an absolute determination. There are now several compilations of lifetimes which can be used by investigators to test the accuracy of their instruments [60, 66].

Some lifetimes of fluorescence standards are listed in table 3. Many developers of lifetime instruments have examined fluorescein in aqueous base, and a lifetime of 4.5 ± 0.3 ns agrees with most of the values listed. Curiously, the value of 3.83 ns was obtained by Müller et al. [61] with an instrument estimated to be accurate to 0.02 ns. Several values for quinine lifetime have been reported and are listed in table 3. In 1.0 N H_2SO_4 the lifetime of quinine obtained by averaging the tabulated data is 19.9 ns with an average deviation of 0.5 ns or 2.5 percent. The agreement for this compound is as impressive as any listed by Birks and Munro [60], so quinine is probably the best lifetime standard now available.

However, some caution is required in the use of quinine, because we have now found that not only the quantum yield, but the lifetime too, is dependent on the concentration of sulfuric acid (table 3) present.

III. Summary and Conclusions

In biochemistry, many of the same principles for measuring absolute fluorescence parameters are used which are employed in any other area of physical chemistry. Perhaps the only differences are the general use of aqueous solutions, the greater need for commercially available instrumentation, and the diverse types of measurement needed. The range and quality of available instruments have improved. There are still many problems regarding standards to be used for quantum yields, polarization, and spectra. Quinine,

Table 3. Lifetimes of some fluorescence standards

Sample	Lifetime (ns)	Reference
Quinine, 0.1 *N* H_2SO_4	19.5	Weber [67]
Quinine, 1.0 *N* H_2SO_4	19.2	Berlman [66]
Do	19.4	Ware and Baldwin [40]
Do	20.1	Birks and Dyson [41]
Do	20.5	Metcalf, cited in [41]
Quinine, 10.0 *N* H_2SO_4	21.8	Present work
Quinine, 1.0 *N* H_2SO_4	20.4	Do.
Quinine, 0.1 *N* H_2SO_4	19.0	Present work, also [65]
Quinine, 0.2 *M Tris*-NO_3^-, pH 8	17.2	Do.
Fluorescein, dilute NaOH or KOH.	4.62	Ware and Baldwin [40]
Do	4.6	Szymanowski [68]
Do	4.6	Metcalf [69]
Do	4.8	Bennett [70]
Do	4.8	Brody [73]
Do	4.8	Kirchhoff [74]
Do	4.8	Maercks [75]
Do	4.5	Bailey and Rollefson [71]
Do	4.5	Chen et al. [65]
Do	4.2	Weber [67]
Do	4.0	Brewer et al. [72]
Do	4.0	Strickler and Berg [39]
Do	3.83	Müller et al. [6]
9,10-Diphenylanthracene, cyclohexane, not de-aerated.	6.7	Present work
9,10-Diphenylanthracene, cyclohexane, de-aerated.	9.35	Berlman [66]
Do	10.0	Amata et al. [76]
2-Aminopyridine, 0.1 *N* H_2SO_4	12.7	Present work
1-Dimethylaminonaphthalene-5-sulfonate, 0.1 *M* $NaHCO_3$.	13.8	Chen et al. [65]
Do	13.6	Förster and Rokos [77]

the universal standard, has been shown to undergo changes in emission spectrum, quantum yield, polarization, and lifetime depending on factors such as the wavelength of excitation and the sulfuric acid concentration. To determine what the "true" values are for a given compound, further reporting of such values is to be encouraged. It is suggested that collaborative efforts might speed up the "certification" of values for fluorescence standards.

IV. References

[1] Weber, G., Biochem. J. **51**, 145 (1952).
[2] Weber, G., Biochem. J. **51**, 155 (1952).
[3] Perrin, F., J. Phys. **7**, 390 (1926).
[4] Levshin, V. L., Z. Physik **26**, 274 (1924).
[5] Chen, R. F., Edelhoch, H., and Steiner, R. F., in Physical Principles and Techniques of Protein Chemistry, Part A, S. J. Leach, Ed., pp. 171–244 (Academic Press, N.Y., 1969).
[6] Velick, S. F., J. Biol. Chem. **233**, 1455 (1958).
[7] Chen, R. F., and Kernohan, J. C., J. Biol. Chem. **242**, 5813 (1967).
[8] Förster, T., Ann. Phys. (Leipzig) **2**, 55 (1948).
[9] Lerman, L. S., Proc. Nat. Acad. Sci. **49**, 94 (1963).
[10] Weber, G., and Anderson, S., Biochemistry **8**, 361 (1969).
[11] Witholdt, B, and Brand, L., Biochemistry **9**, 1948 (1970).
[12] Bowman, R. L., Caulfield, P. A., and Udenfriend, S., Science **122**, 32 (1955).
[13] Chen, R. F., and Bowman, R. L., Science **147**, 729 (1965).
[14] Chapman, J. H., Förster, T., Kortum, G., Parker, C. A., Lippert, E., Melhuish, W. H., and Nebbia, G., Appl. Spectroscopy **17**, 171 (1963).
[15] Melhuish, W. H., J. Opt. Soc. Am. **52**, 1256 (1962).
[16] Chen, R. F., Anal, Biochem. **20**, 339 (1967).
[17] Lee, J., and Seliger, H. H., Photochem. Photobiol. **4**, 1015 (1965).
[18] Argauer, R. F., and White, C. E., Anal. Chem. **36**, 368 (1964).
[19] Børresen, H. C., Acta Chem. Scand. **19**, 2089 (1965).
[20] Gill, J. E., Photochem. Photobiol. **9**, 313 (1969).
[21] Chen, R. F., Anal. Biochem. **19**, 374 (1967).
[22] Fletcher, A. N., J. Phys. Chem. **72**, 2742 (1968).
[23] Scott, T. G., Spencer, R. D., Leonard, N. J., and Weber, G., J. Am. Chem. Soc. **92**, 687 (1970).
[24] Hughes, E., Jr., Wharton, J. H., and Nauman, R. V., J. Phys. Chem. **75**, 3097 (1971).
[25] Galley, W. C., and Purkey, R. M., Proc. Nat. Acad. Sci. **67**, 1116 (1970).
[26] Weber, G., and Teale, F. W. J., Trans. Faraday Soc. **53**, 646 (1957).
[27] Singleterry, C. R., and Weinberger, L. A., J. Am. Chem. Soc. **73**, 4574 (1951).
[28] Almgren, M., Photochem. Photobiol. **8**, 231 (1968).
[29] Paoletti, J., and La Pecq, J.-B., Anal. Biochem. **31**, 33 (1969).
[30] Windsor, W. R., and Dawson, M. W., J. Phys. Chem. **72**, 3251 (1968).
[31] Demas, J. N., and Crosby, G. A., J. Phys. Chem. **75**, 991 (1971).
[32] Melhuish, W. H., J. Phys. Chem. **65**, 229 (1961).
[33] Melhuish, W. H., N. Zeal. J. Sci. Technol. **37B**, 142 (1955).
[34] Eastman, J. W., Photochem. Photobiol. **6**, 55 (1967).
[35] Drobnik, J., and Yearghers, E., J. Mol. Spectr. **19**, 454 (1966).
[36] Fletcher, A. N., J. Mol. Spectr. **23**, 221 (1967).
[37] Rusakowicz, R., and Testa, A. C., J. Phys. Chem. **72**, 793 (1968).
[38] Förster, T., Fluoreszenz Organischer Verbindungen, p. 158 (Vandenhoeck u. Rupprecht, Göttingen, 1951).
[39] Strickler, S. J., and Berg. R. A., J. Chem. Phys. **37**, 814 (1962).
[40] Ware, W. R., and Baldwin, B. A., J. Chem. Phys. **40**, 1703 (1964).
[41] Birks, J. B., and Dyson, D. J., Proc. Roy. Soc. **A274**, 135 (1963).
[42] Shore, V. G., and Pardee, A. B., Arch. Biochem. Biophys. **62**, 355 (1956).
[43] Teale, F. W. J., and Weber, G., Biochem. J. **65**, 476 (1957).
[44] Chen, R. F., Anal. Lett. **1**, 35 (1967).
[45] Børresen, H. C., Acta Chem. Scand. **21**, 920 (1967).
[46] Bridges, J. W., and Williams, R. T., Biochem. J. **107**, 225 (1968).
[47] Eisinger, J., Photochem. Photobiol. **9**, 247 (1969).
[48] Rusakowicz, R., and Testa, A. C., J. Phys. Chem. **72**, 2680 (1968).
[49] Weisstuch, A., and Testa, A. C., J. Phys. Chem. **72**, 1982 (1968).
[50] Parker, C. A., and Rees, W. T., Analyst **85**, 587 (1960).
[51] Azumi, T., and McGlynn, S. P., J. Chem. Phys. **37**, 2413 (1962).
[52] Chen, R. F., Anal. Lett. **4**, 459 (1971).
[53] Weber, G., and Bablouzian, B., J. Biol. Chem. **241**, 2558 (1966).
[54] Deranleau, D. A., Anal. Biochem. **16**, 438 (1966).
[55] Rosén, C.-G., Acta Chem. Scand. **24**, 1849 (1970).
[56] Weber, G., J. Opt. Soc. Am. **46**, 962 (1956).
[57] Price, J. M., Kaihara, M., and Howerton, H. K., Appl. Opt. **1**, 521 (1962).

[58] Szalay, L., Gáti, L., and Sárkány, B., Acta Phys. Acad. Sci. (Hungary) **14,** 217 (1962).
[59] Kaye, W., Appl. Spectr. **18,** 9 (1964).
[60] Birks, J. B., and Munro, I. H. in G. Porter, ed., Progress in Reaction Kinetics **4,** 239 (1967).
[61] Müller, A., Lumry, R., and Kokubun, H., Rev. Sci. Instr. **36,** 1214 (1965).
[62] Spencer, R. D., and Weber, G., Ann. N.Y. Acad. Sci. **158,** 361 (1969).
[63] Chen, R. F., Arch. Biochem. Biophys. **133,** 263 (1969).
[64] Meserve, E., in R. F. Steiner and I. Weinryb, eds., Excited States of Proteins and Nucleic Acids, Plenum Press, N.Y., 1971, p. 57.
[65] Chen, R. F., Vurek, G. G., and Alexander, N., Science **156,** 949 (1967).
[66] Berlman, I. B., *Handbook of Fluorescence Spectra of Aromatic Molecules,* Academic Press, N.Y. 1965; 2d Ed., 1971.
[67] Weber, G., Methods in Enzymol. **16,** 393 (1969).
[68] Szymanowski, W., Z. Physik **95,** 450 (1935).
[69] Metcalf, W. S., J. Chem. Soc. 3726 (1960).
[70] Bennett, R. G., Rev. Sci. Instr. **31,** 1274 (1960).
[71] Bailey, E. A., and Rollefson, G. K., J. Chem. Phys. **21,** 1315 (1953).
[72] Brewer, L., James, C. G., Brewer, R. G., Stafford, F. E., Berg, R. A., and Rosenblatt, G. M., Rev. Sci. Instr. **33,** 1450 (1962).
[73] Brody, S. S., Rev. Sci. Instr. **28,** 1021 (1957).
[74] Kirchhoff, W., Z. Physik **116,** 115 (1940).
[75] Maercks, O., Z. Physik **109,** 685 (1938).
[76] Amata, C. D., Burton, M., Helman, W. P., Ludwig, P. K., and Rodemeyer, S. A., J. Chem. Phys. **48,** 2374 (1968).
[77] Förster, Th., and Rokos, K., Chem. Phys. Lett. **1,** 279 (1967).

(Paper 76A6–744)

JOURNAL OF RESEARCH of the National Bureau of Standards—A. Physics and Chemistry
Vol. 76A, No. 6, November–December 1972

Newer Fluorometric Methods for the Analysis of Biologically Important Compounds

G. G. Guilbault

Department of Chemistry, Louisiana State University, New Orleans, La. 70122

(June 15, 1972)

Newer fluorometric methods for the analysis of biologically important compounds will be discussed: enzymes such as LDH, alkaline phosphatase, lipase and cholinesterase, and substrates such as glucose, urea and uric acid. These methods are based on the production of fluorescence initiated by an enzymic reaction.

New reagentless fluorescence methods will be described for enzymes and substrates. These methods are highly precise (1%), fast (less than 1 minute) and involve no preparation of reagents. These methods, as adapted to clinical laboratory procedures, will be discussed.

Key words: Enzymes, fluorometric analysis; fluorometry of enzymes; fluorometry of substrates; silicone pad; solid surface fluorometry.

I. General

Enzymes are biological catalysts which enable the many complex chemical reactions, necessary to the existence of life, to take place at ordinary temperatures. Because enzymes work in complex living systems, one of their outstanding properties is specificity. Thus, an enzyme is capable of catalyzing a particular reaction of a particular "substrate" to produce a characteristic and measurable reaction end product. This specificity of enzymes and their ability to catalyze reactions of substrates at extremely low concentrations is of significant use in biochemical analyses.

Enzyme catalyzed reactions have long been used for such analytical purposes for determining the presence of specific substrates, enzyme activators, enzyme inhibitors, and enzymes themselves, and in determining the concentration of these substances. Numerous methods have been described for the determination of enzymic activity between an enzyme and a substrate. Until recently, however, the disadvantages associated with the use of enzymes in these analytical techniques have seriously limited their usefulness.

A detailed discussion of the use of enzymes for analysis can be found in review articles by Guilbault [1–3] and books by Guilbault [4] and Bergmeyer [5].

The concentration of substrate participating in an enzyme reaction can be calculated in one of two general ways. The first method measures, by chemical, physical, or enzymatic analysis, either the total change that occurs in the end product or the unreacted starting material. In this method, large amounts of enzyme and small amounts of substrate are used to insure a complete reaction. In the second method, which is a kinetic method, the initial rate of reaction is measured, in one of many conventional ways, by following the production of product or the disappearance of the substrate. In this method, the rate of reaction is a function of the concentration of substrate, enzyme, inhibitor and activator.

On the other hand, because enzymes are catalysts, and as such affect the rate and not the equilibrium of reactions, their concentration and activity must be measured by the rate or kinetic method. Similarly, activators and inhibitors that affect the enzyme's catalytic effect can be measured only by the rate method. While, as pointed out above, the substrate can be measured either by a total change or a rate method, the latter method is faster because the initial reaction can be measured without waiting for equilibrium to be established. The accuracy and precision of both methods are comparable.

In the past, manometric methods, pH procedures, and spectrophotometry have been used for determining enzyme activity. Spectrophotometry has been generally preferred because of its simplicity, its rapidity and the capability of measuring lower enzyme and substrate concentrations. Spectrophotometry embraces the use of colorimetric methods where colored products are produced as a result of enzyme activity, and fluorescent methods where fluorescent compounds are produced as a result of enzyme activity. Fluorescent procedures are several orders of magnitude more sensitive than colorimetric methods and thus have replaced the colorimetric methods in numerous instances.

Previous fluorometric methods, although they have

been improvements over other prior art methods of determining enzyme activity have not eliminated all of the problems associated with enzymic analyses. Fluorometric analysis depends on the production of a fluorescent compound as a result of enzyme activity between a substrate and enzyme. The rate of production of the fluorescent compound is related to both the enzyme concentration and substrate concentration. This rate can be quantitatively measured by exciting the fluorescent compound as it is produced and by recording the quantity of fluorescence emitted per unit of time with a fluorometer.

The prior methods for fluorometrically measuring enzyme reaction rates, however, have been wet chemical methods and rely on reacting a substrate solution with an enzyme solution. Wet chemical methods involve time-consuming and wasteful preparation of costly substrate solutions and enzyme solutions. For example, when determining the presence and concentration of an enzyme, a substantial amount of substrate must be accurately weighed and dissolved in a large amount of buffer solution usually about 100 ml to prepare a stock solution. The enzyme reaction is then usually carried out by measuring, for example, 3 ml of stock substrate solution into an optical cuvet, adding a measured amount of the enzyme solution to the substrate solution, and recording the change in fluorescence eminating from the resultant solution per minute with a fluorometer. This standard wet chemical method is costly and wasteful because laboratory trained technicians' time and relatively large quantities of expensive substrate are required.

II. Solid Surface Fluorescence Monitoring System

Solid-surface fluorometric methods, using a reagentless system, have been developed for the assay of clinically important enzymes, substrates, activators and inhibitors. The method comprises forming a solid reactant film of one of the reactants on an inert silicone matrix pad, contacting the film of the first reactant with a solution of the second reactant (substance to the measured) to produce a fluorescent material, and monitoring the change of fluorescence with time to determine the concentration of the second reactant.

The reactant film may be formed by dissolving the reagents in a solvent, depositing the reactant solution on the silicone pad so that the solution spreads evenly over the pad, and evaporating the solvent from solution. The reagent may be applied to the pad either from an acetone solution if a substrate or in a polymeric film such as polyacrylamide if an enzyme. Either substrate or enzyme and/or coenzyme can be deposited on the pad in film form depending upon whether the substance to be assayed is an enzyme or a substrate.

After the pad is formed (fig. 1), it is attached to a slide made of a rigid material, such as a glass or metal slide, by applying an adhesive to the slide and overlying the pad on the adhesive. The pads are placed approximately 1 or 2 cm from the bottom of the slide (fig. 2).

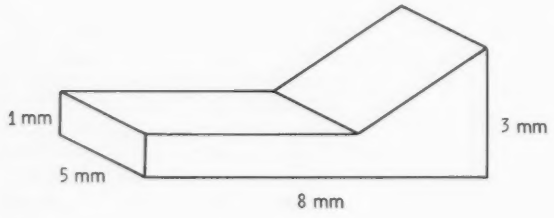

FIGURE 1. Pad support (all measurements are in mm).

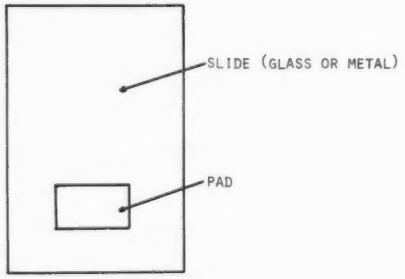

FIGURE 2. Slide support.

The fluorescent cell consists of a rectangular cell made of ordinary sheet metal, wood or plastic material (fig. 3), having portholes to allow radiation to enter and leave the cell cavity. The top of the cell is provided with guides at opposite sides so that the slide containing the reagents can be reproducibly placed within the cell. In order to obtain as low a background as possible, the cell is painted with a black optical paint having a dull finish.

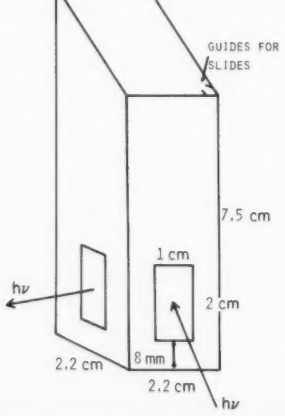

FIGURE 3. Fluorescence attachment used to hold pads (all measurements are in cm).

Before the enzyme solution is added, the glass slide is put into the fluorometer and a background reading is taken. A blank rate is taken using all components of the system, except the unknown. The slide is then removed from the fluorometer and 20 μl of a solution of the substance to be assayed is applied to the slide. The recorder (100 mV input) is started immediately, the slide is placed back into the fluorometer, and the rate is recorded. A calibration plot of the change in fluorescence units per minute versus concentration is prepared and used for subsequent analyses of enzyme or substrate.

After a run is completed, the pad can be peeled from the slide, and the slide cleaned and stored for subsequent use.

The physical properties of the silicones and the stability of the reactant films of enzyme and substrate in the presence of silicones further make these materials ideally suited for use. The silicone materials can retain a reactant film on their surfaces for an indefinite time and permit the direct measurement of fluorescence from its surface when an appropriate second reagent solution is dropped onto the first reactant film. Background interference due to light scattering and nonspecific fluorescence are minimal compared to other materials.

The number of enzyme systems that could be monitored by this type of solid-surface device are as numerous as the number of enzyme systems known. Some of the more clinically important systems that will be studied and for which methods have been developed are as follows.

III. Assay of Clinically Important Enzymes

A. Cholinesterase

Low levels of cholinesterase (ChE) are found in individuals with anemia, malnutrition, and pesticide poisoning. High levels indicate a nephrotic syndrome.

Preliminary results have indicated that cholinesterase in solution can be monitored using a film of *N*-methyl indoxyl acetate on the surface of a silicone rubber pad:

$$N\text{-Methyl indoxyl acetate} \xrightarrow{\text{ChE}} N\text{-Methyl Indoxyl}$$

(Fluorescent—$\lambda_{ex} = 495$ nm, $\lambda_{em} = 525$ nm)

The rate of production of *N*-methyl indoxyl is followed and is proportional to the cholinesterase concentration. Attempts have been made to develop methods for the direct assay of ChE in blood and body tissue. The reproducibility and accuracy obtainable using several configurations of pad and various experimental conditions have been compared and the optimum system developed. A linear region of 10^{-4} to 1 unit has been obtained [6].

Preliminary studies have indicated that pads made from either method were stable for at least 60 days (table 1), if kept in a cold dark place.

TABLE 1. Pad stability data[a]

Day[b]	Rate, ΔF/min[c]
0	3.10
2	3.04
4	3.08
10	3.20
30	3.00
60	3.00

[a] A 500 μg/ml solution of cholinesterase was freshly prepared for each day. Twenty microliters of a 0.1 *M* substrate solution were applied to the pad and allowed to evaporate to dryness.

[b] Days after preparation of pad.

[c] Rates were an average of at least three runs.

B. Alkaline Phosphatase

High levels of alkaline phosphatase are observed in rickets, Paget's disease, obstructive pandicea, and metastatic carcinoma.

The fluorogenic substrate naphthol-AS-BI-phosphate was used for the assay of alkaline phosphatase in serum. Guilbault et al. [7, 8] found that this substrate is the best for the direct assay of alkaline phosphatase in serum. A solution method was used and an accuracy and precision of about 2 percent was obtained. The deep green fluorescent naphthol AS-BI formed is measured. Attempts have been made to monitor this reaction on a solid surface. A drop of serum to be assayed has been added directly to the naphthol AS-BI-phosphate on the surface and the rate monitored. No solutions are required. From 10^{-6} to 10 units are assayable [9].

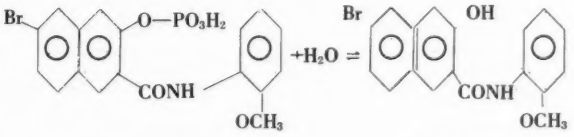

Naphthol AS-BI-Phosphate (Non-Fluorescent) — Naphthol AS-BI (Fluorescent)

Further attempts have been made to extend the usefulness of this method for a wide variety of biological samples.

The color of the silicone rubber however, affects both the background and reaction rates. With any of the filter systems, the background and reaction rates increase in the order black<grey<clear<white. Each possible combination of pad color and filter was examined and it was found that the most accurate results could be obtained if a combination of 7–54 filter and grey silicone rubber pads were used.

Table 2 shows the results obtained from a series of serum samples. Over 80 serum samples were analyzed with a relative error of ± 5 percent.

TABLE 2. Determination of serum alkaline phosphatase

Units alkaline phosphatase taken [a]	Units alkaline phosphatase found [a-c]
20	21.5
22	19
24	24.5
26	23
28	25
30	31
31	31
33	37
37	34
39	40
41	39
43	42
48	49
53	[d] 54
61	[d] 60
64	[d] 64

[a] Units expressed as μmol phenolphthalein liberated min^{-1} l^{-1} serum.

[b] Obtained by multiplying the rate by 31.5.

[c] Average from 3 or more different samples—each analysis in duplicate.

[d] One sample—average of 2 determinations.

Figure 4 shows the correlation between the serum alkaline phosphatase values obtained from the "solid surface" method and alkaline phosphatase values obtained from a solution method employing phenolphthalein phosphate. The graph shows good agreement between the two methods over a wide range of serum values. If the serum values are expressed as μmol phenolphthalein liberated min^{-1} l^{-1} serum, then normal serum has 27–105 units.

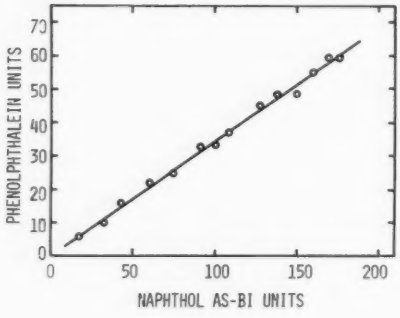

FIGURE 4. Correlation between results obtained with naphthol AS-BI method and phenolphthalein method.

Table 3 shows the alkaline phosphatase values obtained from highly jaundiced serum compared to the phenolphthalein phosphate method. All the results from these samples were low and implied a limitation on the method. It is, however, possible to predict which samples will give low results. Generally, it is those samples which are very dark yellow or orange-yellow in color. The light-yellow serum gave good results as did haemolyzed serum. The low values obtained from jaundiced serum is the main limitation of the method, but it is possible to recognize these solutions and carry out the analysis by an alternative method.

TABLE 3. Analytical results obtained from jaundiced serum samples

Units alkaline phosphatase taken [a]	Units alkaline phosphatase found [a, b]
27	18
34	21
59	30
86	21
135	44
185	115
200	138

[a] Units expressed as μmol phenolphthalein liberated min^{-1} l^{-1} serum.

[b] Average of 3 results.

C. Lipase

A low plasma lipase indicates vitamin A deficiency and some malignancies. Lipase assay is most important in diagnosis of pancreatitis.

Two fluorogenic substrates have been evaluated for the assay of lipase: *N*-methyl indoxyl myristate, a substrate developed by Guilbault and Hieserman [10], and 4-methyl umbelliferone myristate, a substrate recently prepared in our labs.

The production of the green fluorescent naphthol AS–BI or the blue 4-methyl umbelliferone myristate can be followed on the surface.

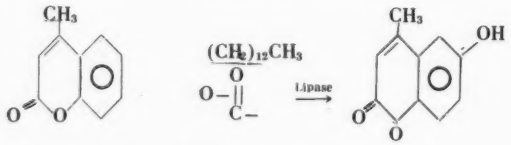

4-Methyl Umbelliferone Myristate ⟶

4-Methyl Umbelliferone $\lambda_{ex} = 340$ nm
$\lambda_{em} = 450$ nm

A direct assay of lipase (10^{-4} to 10 units) in serum and pancreas can be effected.

D. Lactate Dehydrogenase

Levels of this enzyme are elevated in individuals with acute and chronic leukemia in relapse, myocardial infarctions and carcinomatosis.

Fluorometric analysis of dehydrogenases in the past have been based on measurement of NADH fluorescence. Guilbault and Kramer [11] have described a fluorometric method of coupling reduced nicotinamide adenine dinucliotide (NADH) to an electron acceptor (resazurin) in the presence of the cofactor phenazine methosulfate (PMS).

$$\text{Lactate} + \text{NAD} \xrightarrow{\text{LDH}} \text{NADH} + \text{pyruvate}$$

$$\underset{\text{(Non-Fluorescent)}}{\text{NADH} + \text{Resazurin}} \xrightarrow{\text{PMS}} \underset{\text{(Fluorescent)}}{\text{Resorufin} + \text{NAD}}$$

A semisolid state fluorescence method for the analysis of lactic dehydrogenase (LDH) has been developed [12]. The commercially available enzyme in aqueous solution, and the enzyme in blood serum were studied. The serum analysis is compared to a method described by Bergmeyer, et al. [13]. As little as 160 units of LDH per milliliter of blood serum can be analyzed with an accuracy of better that 3 percent.

The reaction system used was:

$$\text{Li Lactate} + \text{NAD} \overset{\text{LDH}}{\rightleftarrows} \text{NADH} + \text{Pyruvic Acid.} \quad \text{(I)}$$

The rate of production of the fluorescent product NADH was monitored.

Some of the results obtained in the assay of LDH in serum using the solid surface method are shown in table 4. An average relative error of 2.3 percent was obtained.

IV. Assay of a Clinically Important Substrate

A. Glucose

High levels of glucose may indicate diabetes.

Guilbault et al. [14] have described a fluorometric assay system for glucose using glucose oxidase, peroxidase, and *p*-hydroxyphenylacetic acid. The rate of production of fluorescence is proportional to the amount of glucose present.

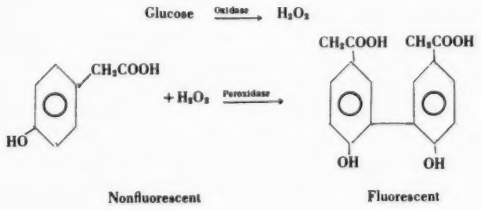

To develop a reagentless surface method for assay of glucose, the enzymes glucose oxidase and peroxidase, and the substrate *p*-hydroxyphenylacetic acid were placed on the surface. The addition of glucose initiates the reaction; fluorescence is produced and its rate of production will be proportional to the glucose present in blood [15]. A range of 10^{-5} to 10^{-1} *M* glucose can be assayed.

TABLE 4. Data and results of the assay of serum LDH using the proposed method

Rate, ΔF/min.	Concentration taken	u/ml Found	Relative error (percent)
6.6	160	168	+4.9
7.3	190	189	−0.3
7.2	200	186	−6.5
10.1	280	276	−1.3
13.2	360	372	+3.3
13.9	380	394	+3.4
15.3	440	437	−0.6
16.0	460	459	− .2
17.2	500	496	− .8
18.8	560	546	−2.5
21.4	620	626	+1.0
		Average relative error	2.3

B. Advantages of Solid Surface Method

The advantages of this radically new system for the clinical laboratory are:

1. The time required for analysis by present methods is 30 to 60 min to prepare reagents plus 10 to 20 min per assay. If a sample is available at 1 a.m., the technician must proceed through the regular preparation and analysis routine. The solid surface method requires 10 bottles of pads, one for each of 10 common tests. The technician would open the bottle marked "LDH test," pick out a pad, put it in the instrument on the strip holder, add a 10 μl sample of blood or urine, and read out the results directly in mg percent urea. Total time is about 2 min.

2. The accuracy of current methods (mostly spectrophotometric) are limited to an error of about 2 to 3 percent over a narrow range (0.15 to 0.85 Abs units). Because fluorescence methods are based on the production of a signal over zero signal, the accuracy of these methods is independent of scale reading, and have an accuracy of 1 percent over a 3 to 4 fold linear range of concentrations.

3. Temperature must be controlled in all enzyme assays based on a kinetic approach. This is expensive and bothersome. The solid surface fluorescence method proposed is not temperature dependent, since the silicone rubber pad used to support the sample is nonheat conductive. Thus, provided the sample of blood is at the same temperature as used to prepare the calibration plot (generally room temperature, 25 °C) the temperature of the environment does not affect the results. For example, in the assay of alkaline phosphatase, we obtained the same rate at 10, 15, 20, 25, 30, 35, and 40 °C external temperature, provided

474-414 O - 73 - 5

we added the blood from a sample kept at 25 °C. This represents a significant improvement.

4. The reagents used in present clinical procedures are unstable, and new solutions must be prepared daily. *o*-Toluidine and peroxidase in glucose assay, or NAD in LDH assay are examples of this. Yet when the reagents are placed in *solid form* on a surface, they can be kept for months with *no deterioration*. In our ChE, alkaline phosphatase and LDH assays, we found we could use our pads for 90 days, using the same calibration plot everyday.

5. Many clinical methods are subject to interferences because of (a) protein absorption in the near UV-visible or (b) absorbing impurities in the reagents. By using reagents that fluoresce in the visible, and reagents in a solid form, these two interferences are eliminated.

V. References

[1] Guilbault, G. G., Anal. Chem. **38,** 527R (1966).
[2] Guilbault, G. G., Anal. Chem. **40,** 459R (1968).
[3] Guilbault, G. G., Anal. Chem. **42,** 334R (1970).
[4] Guilbault, G. G., Enzymatic Methods of Analysis, (Pergamon Press, 1970).
[5] Bergmeyer, H., Methods of Enzymatic Analysis (Verlag Chemie, Germany, 1965).
[6] Guilbault, G. G., and Zimmerman, R., Anal. Letters **3,** 133 (1970).
[7] Guilbault, G. G., and Vaughn, A., Anal. Letters **3,** 1 (1970).
[8] Guilbault, G. G., and Vaughn, A., Anal. Chem. **43,** 721 (1971).
[9] Guilbault, G. G., and Vaughn, A., Anal. Chem. Acta **55,** 107 (1971).
[10] Guilbault, G. G., and Hieserman, J. Anal. Chem. **41,** 2006 (1969).
[11] Guilbault, G. G., and Kramer, D. N., Anal. Chem. **36,** 2497 (1964).
[12] Guilbault, G. G., and Zimmerman, R., Anal. Chim. Acta, **58,** 75 (1972).
[13] Bergmeyer, H., Bernt, E., and Hass, B., in Methods of Enzymatic Analysis, H. Bergmeyer, Ed, (Academic Press, New York, 1963), p. 736.
[14] Guilbault, G. G., Brignac, P., and Zimmer, M., Anal. Chem. **40,** 1256 (1968).
[15] Guilbault, G. G., and Tang, D., unpublished results.

(Paper 76A6–745)

JOURNAL OF RESEARCH of the National Bureau of Standards—A. Physics and Chemistry
Vol. 76A, No. 6, November–December 1972

Inorganic Ions in Glasses and Polycrystalline Pellets as Fluorescence Standard Reference Materials*

R. Reisfeld

Department of Inorganic and Analytic Chemistry, Hebrew University of Jerusalem, Jerusalem, Israel

(June 15, 1972)

The absorption and fluorescence of inorganic glasses and polycrystalline disks doped by heavy metal ions is discussed, and their use as fluorescence standards is evaluated. The advantages of the glass standards over other media is summarized.

The glass standards are divided into two groups (1) glasses doped by trivalent rare earths such as Gd^{3+}, Tb^{3+}, Eu^{3+}, Sm^{3+}, and Tm^{3+} which have narrow band optical spectra as a result of intraconfigurational transitions, and (2) glasses and polycrystalline disks doped by ions such as Tl^{+}, Pb^{2+}, Ce^{3+}, and Cu^{+} which have broad spectral bands since the optical spectra originate from interconfigurationally allowed transitions. Optical and physical parameters, including matrix effects, quantum efficiencies, decay characteristics, Stokes' shifts and spin-orbit versus orbit-lattice interactions due to the different transitions will be discussed.

Group (1) glasses are suitable for use as standards where a narrow well-defined fluorescence range is required, and group (2) glasses are suitable for use as standards whenever a substance with a wide range of fluorescence is measured. Special emphasis will be placed on energy transfer between donor and acceptor ions.

Key words: Fluorescence standards, inorganic ions; glass standards in fluorescence; rare-earth-doped glasses.

Introduction

The use of fluorescence and phosphorescence as experimental tools has increased immensely in the last decade. The fluorescence technique is used now as a common tool of research by physical chemists, physicists, analytical chemists, biochemists and biophysicists. The kinds of analyses which have been performed to date using fluorescence have varied, including such methods as trace metal determination, analysis for traces of organic materials and particularly for determination of trace constituents of biological systems. It provides some of the most sensitive and selective methods of qualitative and quantitative analysis. (Lower limits of detectability using fluorescence analysis lie often in subpart per million (ppm) and part per billion (ppb) range.) Fluoresence analysis especially, has many practical applications in the field of organic, inorganic, agricultural, biological and clinical chemistry.

The reader interested in the principles and applications of fluorescence in analysis is referred to two recently published books [1, 2][1] on this subject and to a very comprehensive review on measurements of photoluminescence quantum yield in solutions written by Demas and Crosby. [3]

The following are a few examples in which fluorescence is used in health and environmental problems.

Organic Compounds

Many organic compounds fluoresce and/or phosphoresce and these properties have been widely used for analysis. An understanding of the basic aspects of the luminescence of organic compounds can greatly enhance its efficiency as an analytical tool.

The ability of proteins to luminesce has now been fairly thoroughly investigated and is mostly due to the presence of the fluorescent aromatic amino acids tryptophan and tyrosine, [4, 5]. Any biological process can be inhibited, stimulated or altered through photochemical methods by inducing electronic excited states in proteins and nucleic acids. In the investigation of these excited states by photoabsorption and luminescence techniques, a great deal of information can be obtained, not only about the number of biopolymeric molecules in the system, but also about their environment.

Significant qualitative and quantitative information concerning molecular structure can be obtained through fluorescence. When one considers that information of this kind can be obtained rapidly from the interior of the undamaged, usually functioning cell, one realizes the special importance of spectral lumi-

* This work was performed under NBS contract G-103.

[1] Figures in brackets indicate the literature references at the end of this paper.

nescence research techniques in biology. An example of fluorimetric methods in this area is: the fluorescent tags for labeling proteins [6] and amino acids [7–10] which have proven useful in immunochemistry, virology, bacteriology, parasitology, and mycology.

Agriculture

Determining factors in the degree of pest control by chemicals are (1) efficiency of application, (2) the loss by spray particle drift to immediate areas not intended to be treated, and (3) the effective life of the chemical on plants, animals and in soils after application. In this respect, fluorescence has made an outstanding contribution in pesticide analysis. The excitation and emission spectra, decay times, analytical curves, and limits of detection, have been obtained for many pesticides in media such as milk, animal feeds, fruits and vegetables, tissues, etc. [11]. Fluorescent tracer studies of spray and dust deposits on plants and soils have been reported [12, 13].

Biomedical Research

In this area, fluorescence spectroscopy has been used largely as an analytical tool for the assay of many materials of biological origin, [14] such as the examination of carcinogenic materials in the environment, [15] in metabolic studies of aromatic hydrocarbon carcinogens [16] and the determination of drugs, enzymes and proteins.

Of great interest are the experimental observations of the luminescence of cells and tissues in such pathological states as carcinogenesis, inflammation, psychic diseases and muscle atrophy due to denervation. Investigators have sought a correlation between luminescence intensity and the pathological process. However, more information about the structural chemical organization of the protoplasm during the development of the pathological process will be obtained if the comparison involves, not merely the intensity of the fluorescence of various cells, but the magnitude of the changes in fluorescence intensity due to several factors. The use of luminescence to a successfully selected set of experimental treatments will prove to be a useful technique in the field of molecular and cell biology and primarily in the field of practical medicine [17].

The mechanism of cancer induction by aromatic hydrocarbons is of particular interest and it is possible that the initial interaction is a complex formation between the hydrocarbon and a vital cell constituent, such as the nucleic acids which may be determined by changes in fluorescence spectra and parameters [18–20]. Various aromatic hydrocarbons may fluoresce at widely differing frequencies, a fact which is of considerable analytical importance. A history of fluorescense work with carcinogenic hydrocarbons was included in a lecture by Cook in 1950 [21]. Presently, fluoroscence analysis is used in many studies to determine qualitatively and quantitatively the presence of polynuclear hydrocarbons in the environment, usually after separation by thin-layer chromatography [22].

A method for binding dyes to nucleic acids is widely used in staining biological tissues for fluorescence microscopic examination and is used as a screening procedure for cancerous tissue [23].

Fluorometric techniques have made great inroads in the clinical laboratory as the basis of sensitive analytical methods [24, 25].

A. General

In all research and measurements in which fluorescence is involved, it is of utmost importance to measure the true wavelength (energy) of excitation and emission, and the fluorescence efficiency. To determine fluorescence efficiency directly, it is necessary to measure the rate of emission at all wavelengths and in all directions. In practice, this is a difficult measurement to perform with accuracy. In view of the difficulties associated with absolute methods, and the ease with which the fluorescence efficiency may be determined by reference to a standard, a search for a suitable standard is of great importance in spectrofluorimetry. The requirements for a good reference compound to be used as a standard are stringent. It should have a well-defined fluorescence and excitation spectrum, a relatively high quantum efficiency, it should be of the same geometry as the samples to be measured and should be stable. There should be little or no overlap between the absorption and the emission spectrum. The reference compound used in any instance should have its absorption and fluorescence in the same general region as the compound being studied. This last restriction is needed because most spectrofluorimeters record spectra which are not corrected for instrumental parameters.

Fluorescence measurements are mainly made on liquids in aqueous or organic solvents, using glass or quartz cuvettes, and in the solid phase with single crystals, in pellets [26] and in solvent glasses [27]. It would therefore be desirable that the standard reference material also be made of the same or similar material having a similar refractive index, thus avoiding the refractive index correction (discussed later). It is also essential that the standard have a small absorption, since a higher absorption introduces an error in the efficiency determination. This arises from the following consideration: The optically dilute measurement rests on Beer's Law $I_0B = I_0(1-10^{-AL})$ where B is the fraction of light absorbed by the sample, I_0 (quanta/sec · cm²) is the irradiance of incident light, A is the absorbance/cm, and L(cm) is the path length [3]. By expanding this expression in a power series we obtain $B = 1-[1-2.303\,AL]+[2.303\,AL]^2/2+ \ldots\ldots \simeq 2.303\,AL$. For solutions that are optically dilute, (absorbance less than 0.05) we can truncate the series and the following approximation is true: $B \simeq 2.303\,AL$. Thus at low solute concentrations, the fluorescence intensity is proportional to concentration.

With these criteria in mind we have attempted to prepare glass and pellet standards. The results of

our work are described in this paper. For the latest references to liquid standards the reader is referred to reference [3], for a sodium salicylate standard to reference [28], and for quantum yield determinations of powder phosphors to reference [29].

In this paper the physical parameters of doped glasses and alkali halides suggested as standards will be described. In order that such materials be used as standards, and the use be at optimal conditions for a fluorescence measurement, the following knowledge is needed:

1. Absorption and/or excitation spectrum.
2. Fluorescence spectrum.
3. Oscillator strength or molar absorptivity at the excitation wavelength.
4. Quantum efficiency for different excitation wavelengths.
5. Fluorescence output as a function of dopant concentration.
6. Lifetimes of fluorescence.
7. Quenching of fluorescence by additional processes such as energy transfer of radiation-induced color centers.
8. Stability.

The principles upon which the determination of quantum efficiencies is based will be discussed. Quantum yields of glasses and pellets prepared in this laboratory, for excitation to various electronic levels and the oscillator strengths of absorption to these levels will also be presented. The concentration dependence of quantum efficiency will be shown.

A short theory of the fluorescence of the material is also outlined for each group of proposed standards in order to simplify the choice of proper materials.

B. Determination of Quantum Yields

The luminescence quantum yield of a compound is defined as the fraction of excited molecules that luminesce after direct excitation by a light source.

The quantum yield, η, which is actually the ratio of probabilities of radiative transitions, ΣA_i^r to the sum of the probabilities of radiative and nonradiative transitions, A_i^{nr}, is defined as:

$$\eta = \frac{\text{number of photons emitted}}{\text{number of photons absorbed}} = \frac{\sum A_i^r}{\sum A_i^r + \sum A_i^{nr}} \tag{1}$$

The quantum yield would equal unity if there were no nonradiative transitions.

The terms "quantum yield," "luminescence quantum efficiency," and "fluorescence yield" are used interchangeably.

Formula (1) serves as a basis of determination of quantum efficiency.

The determination of absolute quantum yields by this formula is difficult as mentioned in the introduction, hence a relative technique is often employed.

1. Comparative Method

Here, the fluorescence of an unknown is compared with the fluorescence of a compound whose fluorescence yield is well known. For dilute solutions, the following equation has been used [30]:

$$\eta_u = \eta_s \frac{n_u F_u A_s}{n_s F_s A_u} \tag{2}$$

where η_u and η_s are quantum yields of unknown and standard respectively, n the index of refraction, A the absorbance at the wavelength of absorption and F the integrated fluorescence output in quanta/unit wavelength. This equation is valid for equal numbers of photons incident on u and s. More often the following equation is used:

$$\eta_u = \eta_s \frac{F_u A_s I(\lambda_s)}{F_s A_u I(\lambda_u)} \frac{n_u^2}{n_s^2} \tag{3}$$

In this equation, F is the integrated area under the corrected emission spectrum, and $I(\lambda)$ is the relative irradiance of the exciting light at wavelength λ. A is the absorbance.

Equations (2) and (3) differ in the ratio $\frac{n_u}{n_s}$ and $\frac{n_u^2}{n_s^2}$. As we see by comparison of the two formulae, refraction corrections can be substantial, modifying quantum yield results by factors of 2 or more. Therefore, one should be especially careful when applying the refractive index correction. A comprehensive discussion on this correction can be found in reference [3], p. 1018. As mentioned in the introduction, when the fluorescence of the unknown is compared with a standard of the same refractive index and geometry, the refractive index correction is avoided.

2. Determination of Quantum Yields from Lifetime Measurements

An alternative method is the determination of quantum yields by measurements of the lifetime of fluorescence and the natural lifetime of the state. Here we use the parameters appearing in eq (1)

$$\eta = \frac{\sum A_i^r}{\sum A_i^r + \sum A_i^{nr}} = \frac{\sum \frac{1}{\tau_{\text{nat}}}}{\frac{1}{\tau_{\text{exp}}}} = \sum \frac{\tau_{\text{exp}}}{\tau_{\text{nat}}} \tag{4}$$

where τ_{exp} is the experimentally determined lifetime from the level in question and $\Sigma \tau_{\text{nat}}^{-1}$ is the sum of natural lifetimes, corresponding to the sum of the inverse of the radiative transition rates from this level. One term, A_j^r, appearing in the sum ΣA_i^r is equal to $\frac{1}{\tau_{\text{inat}}}$ and is obtained directly from the absorbance spectra as shown below. The other terms in the sum are then obtained from the relative areas

in the corrected emission spectra. A detailed example of these calculations is presented below for Eu(III) doped glasses.

The natural radiative lifetime is related to the Einstein coefficient of spontaneous emission. Using this relation, several authors developed expressions relating the natural lifetime of fluorescence to the absorption spectrum of the compound [31].

Here, a distinction can be made between two cases: 1. When the absorption and emission of a compound occur at close wavelengths, that is, zero or very small Stokes shifts are observed, and the spectrum is narrow as in the cases of rare earths in various media, one can use an approximation developed for atomic spectra. Using this approximation [32], one obtains for the natural lifetime the following expression, which is valid for a transition between two levels:

$$\tau_{\text{nat}}^{-1} = 2.880 \times 10^{-9} n^2 (g_l/g_u) < \nu^2 > \int \epsilon(\nu) d\nu \qquad (5)$$

where n is the index of refraction, $< \nu^2 >$ the average squared wave number for the absorption maximum, g_u and g_l the degeneracies in the upper and lower states, respectively, and $\epsilon(\nu)$ the molar absorptivity as a function of wave number.

In the case where there is a considerable Stokes shift between the absorption and emission as a result of strong vibronic coupling, for example in transition metal ions, mercury-like ions and organic compounds, a modified equation can be used for τ_{nat} [33], namely

$$\tau_{\text{nat}}^{-1} = 2.880 \times 10^{-9} n^2 < \nu_f^{-3} >_{\text{av}}^{-1} \frac{g_l}{g_u} \int \frac{\epsilon(\nu) d\nu}{\nu}. \qquad (6)$$

The quantity $<\nu_f^{-3}>_{\text{av}}^{-1}$ is given by

$$<\nu_f^{-3}>_{\text{av}}^{-1} = \frac{\int F(\nu)\ \alpha\nu}{\int F(\nu) \nu^{-3} d\nu} \qquad (7)$$

where $F(\nu)$ is the fluorescence output in photons as a function of wave number and ν is the wave number of $F(\nu)$.

3. *Doped Glasses*

The materials which we suggest as versatile standards for spectrofluorimetry and which were studied in this laboratory will be now described. They are divided in the text into four major groups: I. The rare-earth-doped glasses. II. Thallium-doped alkali halides. III. Glasses doped with thallium. IV. Glasses doped with Ce^{3+}, Pb^{2+}, and Cu^{+}.

I. The Rare-Earth-Doped Glasses

The characteristic spectra of the trivalent rare earths are attributable to the presence of deep lying $4f$ shells in the ions. The electrons of these shells are screened by the outer shell electrons, and as a result they give rise to a number of discrete energy levels. The presence of the surrounding lattice has little effect on the position of these levels; therefore, a close resemblance between the energy level diagram of the free ion and that of the incorporated ion exists (fig. 1).

Considerable attention has been paid in the past few years to the study of both the absorption and emission spectra of the rare earths [34, 35].

Trivalent rare-earth ions incorporated in inorganic solids exhibit luminescence owning to the intraconfigurational transitions of the $4f$ electron shell. The optical excitation of this luminescence can be governed by one of three possible mechanisms:

(a) excitation in the narrow $4f$ levels of the rare-earth ion;
(b) excitation in the broad levels due to $4f$-$5d^*$ transitions, or charge transfer processes;
(c) absorption of the host followed by energy transfer from the host to the rare earth activator.

While the first mechanism is operative in all the rare earths showing fluorescence, the second is well known mainly in europium and terbium. In the case of Eu^{3+}, this band is due to a charge transfer process between the Eu^{3+} ion and oxygen center. In the case of Tb^{3+}, however, the band is due to a $4f$-$5f$ transition in the Tb^{3+} ion. (Samarium also was found in some cases to exhibit a charge transfer type of excitation at wavelengths shorter than 220 nm.)

The narrow band emission of the trivalent rare earths in various media is always due to an inner f shell electronic transition. Intra-f-orbital transitions are parity forbidden in the free ion. In a solid, glass or liquid in the absence of a center of symmetry, the parity selection rule may be relaxed by the mixing of the $4f$ configuration with appropriate levels of configuration of opposite symmetry using odd terms in the static or dynamic crystal field expansion. There will also be an additional interaction owing to the influence of the crystal field of the host which produces broadening and splitting of the levels. As in the transition metal ions, which have been treated extensively by the ligand field theory, an increase in separation of a field-split degenerate level indicates an increase in the ligand field seen by the rare earth ion. The crystal field splittings in the rare earths are, however, much smaller than the transition ion splittings, and are not more than a few hundred wave numbers. For transitions between two nondegenerate levels, increasing the rare-earth-ligand interaction displaces both levels toward lower energies. The displacement of the upper, less shielded, level is usually greater, and thus the stronger perturbation causes shifts to longer wavelengths.

The electrostatic perturbation of a rare-earth ion should be directly related to its binding energy in the host medium. As a first approximation, this energy may be derived from a hard-sphere ionic model by the Born equation:

$$E = \sum \frac{Z_i Z_j}{r_{ij}} + \frac{b}{r^n} \qquad (8)$$

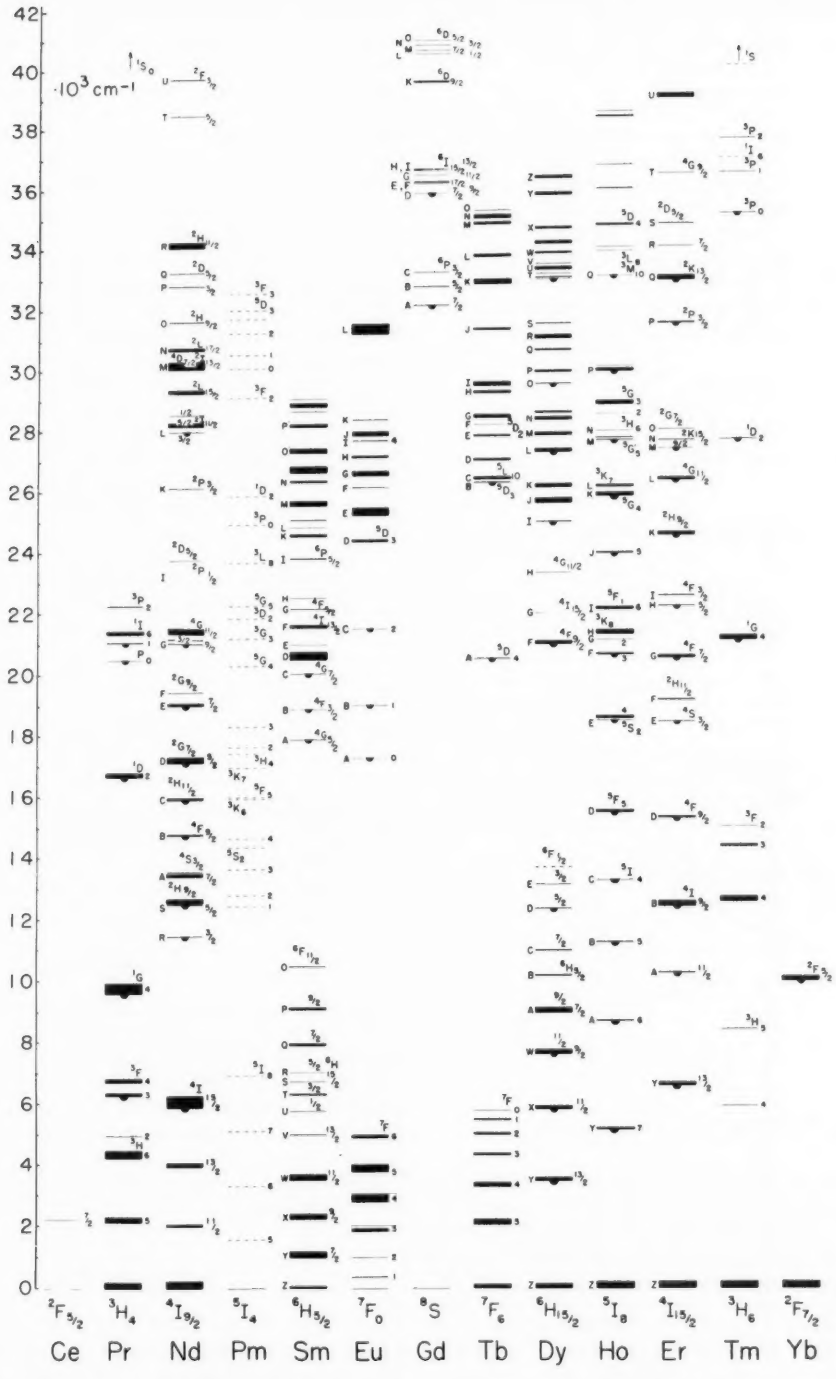

FIGURE 1. Energy level diagram of the rare-earth ions after G. H. Dieke, in Spectra and Energy Levels of Rare Earth Ions, H. M. Crosswhite and H. Crosswhite, Eds. (John Wiley & Sons, New York, N.Y., 1968), p. 142.

E = coulombic potential of the active ion; Z_i = charge on the active ion; Z_j = charge on the matrix ions: b = repulsion coefficient: r = distance between active ion and nearest anion; $n = 4$ to 10.

It was shown in a series of papers by Reisfeld et al. [36–40], that the behavior of rare earths in glasses is similar to that of rare earths in inorganic crystals of low symmetry except for inhomogeneous broadening of the spectra due to a multiplicity of rare-earth sites in glasses. According to our theory [39] a rare-earth ion occupies a center of a distorted cube comprised of four tetrahedra of borate, phosphate or silicate. Two oxygens belonging to such a tetrahedron produce an edge of the cube (fig. 2). The coordination

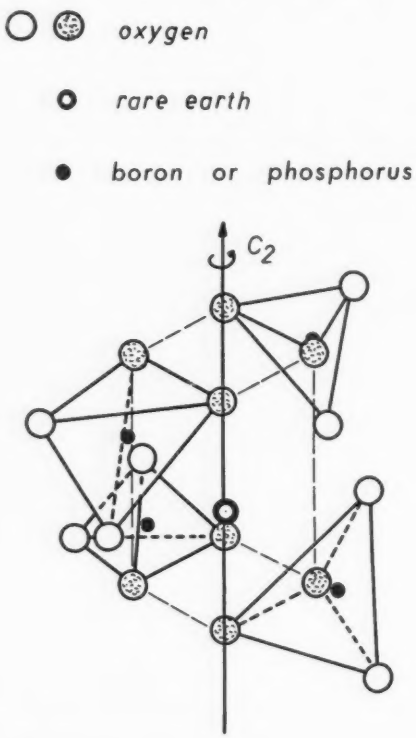

FIGURE 2. Proposed rare-earth site model.

of the rare earth in such an arrangement is with eight oxygens. The observed broadening in the spectrum can occur due to the existence of nonuniform, nonidentical ligand fields caused by slightly different values of rare-earth oxygen distances. An average rare-earth oxygen distance was calculated by assuming a rare-earth sits in a center of a regular cube. In a cube made of borate tetrahedra, in which the boron-oxygen distance is 1.48 Å and the oxygen-oxygen distance 2.4 Å, the rare-earth oxygen distance is 2.1 Å. In a cube made of phosphate tetrahedra in which the phosphorus-oxygen distance is 1.57 Å and the oxygen-oxygen distance is 2.56 Å, the rare-earth oxygen distance is 2.22 Å. It should be realized that in reality the symmetry is lower than cubic, and for the particular cases studied it was found to be of C_s symmetry Eu^{3+} in phosphate glass, [40] and C_2 for Tm^{3+} is phosphate and borate glasses [39]. As a result of this lower symmetry, forced electric dipole transitions become possible and absorption and fluorescence is observed.

The fluorescence can, in some cases, be quenched due to transfer of electronic excitation energy to the vibrations of the surrounding medium. Such interactions reduce the fluorescence quantum yield. In general the larger the energy difference between the two electronic states, the smaller the nonradiative transition probability between them [41]. For rare-earths, the energy difference between the electronic levels below which considerable quenching occurs is about four vibrational quanta (phonons). The nonradiative decay of the higher excited levels in the glasses is generally assisted by the phonons of the glass. The particular vibrational frequencies which are responsible for the quenching are the following:

bond	stretching frequency ν cm^{-1}	bond length Å
silicate, Si−0	1010–1115	1.62
metaphosphate, P−0	1140–1300	1.57
borate, B−0	1310–1380	1.39 (trigonal) 1.48 (tetrahedral)

from which we conclude that in borate glasses, quenching will occur between levels that are separated by about 5000 cm^{-1}, while in silicate by about 4000 cm^{-1}.

We shall now show how this general theory works for specific cases.

A. Europium

The observed optical absorption and emission spectra of Eu^{3+} in glasses are characteristic of transitions between the lower energy levels of the $4f^6$ configuration of this ion. The oscillator strengths of the characteristic absorption bands in a phosphate glass together with the assignments of the transitions are given in table 1.

The oscillator strength was calculated from the well-known equation

$$f = 4.32 \times 10^{-9} \int \epsilon(\nu)\, d\nu \qquad (9)$$

where ϵ is the molar absorptivity at the energy ν (cm^{-1}). The values of f presented in table 1 were corrected for population distribution of total concentration in $^7F_0$, $^7F_1$, and $^7F_2$. Using a Boltzmann distribution correction, the relative concentration for the three levels at room temperature were $C_0 = 0.792$, $C_1 = 0.200$ and $C_2 = 0.008$, respectively.

TABLE 1. Oscillator strengths and quantum yields of fluorescence of Eu^{3+} in phosphate glass

Transition assignment	Wave number cm^{-1}	Wavelength nm	Oscillator strength $\times 10^7$	Percent quantum yield of D_0 fluorescence
$^7F_2 \rightarrow {}^5D_0$	16319	612.8	1.544	
$^7F_1 \rightarrow {}^5D_0$	16771	592.2	0.351	
$^7F_0 \rightarrow {}^5D_0$	17256	579.6	.006	0.95
$^7F_1 \rightarrow {}^5D_1$	18700	534.7	.505	
$^5F_0 \rightarrow {}^5D_1$	18993	526.4	.146	.91
$^7F_0 \rightarrow {}^5D_2$	21493	465.3	1.248	.88
$^7F_0 \rightarrow {}^5D_3$	24009	416.5	.547	.87
$^7F_0 \rightarrow {}^5L_6$	25380	394.0	8.981	.87
$^7F_1 \rightarrow {}^5G_5, {}^5G_6$	26041	384.0	6.019	
$^7F_0 \rightarrow {}^5G_3$	26507	377.2	2.726	
$^7F_1 \rightarrow {}^5L_8$	27285	366.5	.391	
$^7F_0 \rightarrow {}^5D_4$	27567	362.7	1.926	
$^7F_1 \rightarrow {}^5H_3$	30464	328.2	1.242	
$^7F_1 \rightarrow {}^5H_5$	31152	321.0	3.001	
$^7F_0 \rightarrow {}^5H_6$	31397	318.5	6.776	

Fluorescence was observed from the $^5D_0$ level and much weaker fluorescence (by a factor of three orders of magnitude) from the $^5D_1$ level. The corrected $^5D_0$ fluorescence to the ^7F ground state multiplet for Eu^{3+} in phosphate glass is given in figure 3. The corrected excitation spectrum of the fluorescence is also presented in this figure. The assignments, and relative intensities of the transitions are presented in table 2. (The transitions from the $^5D_0$ excited level to the $^7F_5$ and $^7F_6$ ground states are very weak, less than 1 percent of the total intensity, and are not included.) The $^5D_0 \rightarrow {}^7F_1$ emission band for Eu^{3+} are magnetic dipole-allowed transitions; the other fluorescence bands arise from forced electric-dipole transitions. The large ratio of the fluorescence intensities for the $^5D_0 \rightarrow {}^7F_2$ and $^5D_0 \rightarrow {}^7F_1$ transitions implies a low symmetry field at the europium sites.

Quantum efficiencies of fluorescence from the $^5D_0$ level of Eu^{3+} in phosphate [41] and silicate glasses [42] were obtained by two independent methods, (a) lifetime measurements, and (b) comparison with a liquid standard.

a. Lifetime measurements. The quantum yield determination based on lifetime measurements is calculated from eq (4). The measured lifetime of the $^5D_0$ excited state in silicate glass was 2.69 ± 0.03 ms

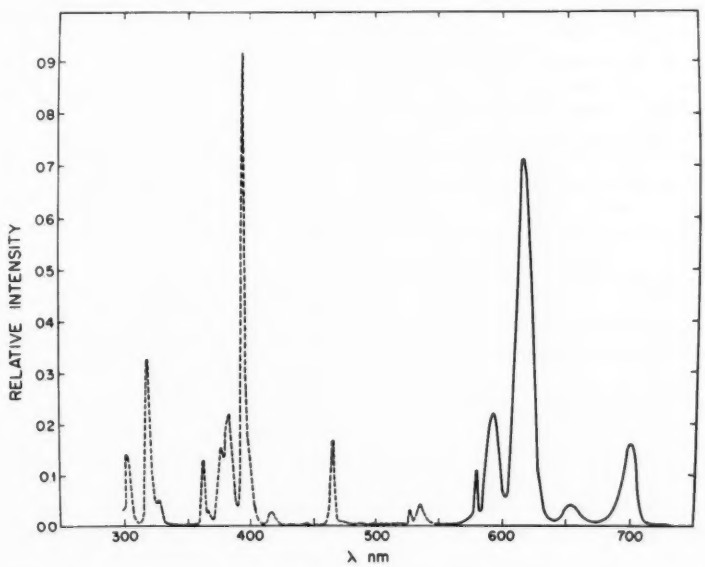

FIGURE 3. Corrected excitation (broken line) and emission (full line) spectrum of the $^5D_0$ fluorescence of Eu^{3+} in phosphate glass.

and in phosphate glass was 2.83 ± 0.03 ms.

The natural radiative lifetime was calculated using eq (5). In this equation, ϵ was corrected for the relative population of the $^7F_0$ level, which was taken as 0.771 in silicate and 0.792 in phosphate. Using the calculated value for $A(^7F_0 \rightarrow {}^5D_0)$ the ratio of the intensities of fluorescence and the fact that $A(^7F_0 \rightarrow {}^5D_0) = A(^5D_0 \rightarrow {}^7F_0)$, the sum of radiative transition probabilities is expressed by:

$$\sum \frac{1}{\tau_{nat}} = \sum A_r = A(^5D_0 \rightarrow {}^7F_0) \left[1 + \frac{S(^5D_0 \rightarrow {}^7F_1)}{S(^5D_0 \rightarrow {}^7F_0)} + \frac{S(^5D_0 \rightarrow {}^7F_2)}{S(^5D_0 \rightarrow {}^7F_0)} + \frac{S(^5D_0 \rightarrow {}^7F_3)}{S(^5D_0 \rightarrow {}^7F_0)} + \frac{S(^5D_0 \rightarrow {}^7F_4)}{S(^5D_0 \rightarrow {}^7F_0)} \right] \quad (10)$$

where S is the area of the relevant emission bands obtained from the corrected emission spectrum.

TABLE 2. Emission wavelength and relative areas of the $^5D_0 \rightarrow {}^7F_i$ transitions for Eu^{3+} in phosphate glass

Transition assignments	Wavelength	Relative fluorescence (areas)
$^5D_0 \rightarrow {}^7F_0$	578.5	0.036
$^5D_0 \rightarrow {}^7F_1$	591.9	1.000
$^5D_0 \rightarrow {}^7F_2$	612.1	3.000
$^5D_0 \rightarrow {}^7F_3$	654.7	0.219
$^5D_0 \rightarrow {}^7F_4$	692.3	1.026

For Eu^{3+} in phosphate glass, the quantum yield obtained by this method was 0.95 [41] and for Eu^{3+} in silicate, 0.90 [42]. Europium-doped glasses do not show concentration quenching of the $^5D_0$ fluorescence [43].

b. Determination of Quantum Yield by Comparison Method. Here, the comparison was made with a solution of $Eu(NO_3)_3$ with a known quantum efficiency of 4 percent [41]. The fluorescence spectra were taken on a Turner Model 210 spectrofluorimeter[2] which gives corrected emission spectra in quanta/unit bandwidth, and excitation spectra corrected to constant energy [44]. The glasses were of the same geometry (standard cuvette form) as the cells in which the fluorescence of the solution of europium nitrate was measured.

Equation (11), which is a modification of eq (3) for use with a corrected spectrofluorimeter [45], was used:

$$\eta_u = \eta_s [(F_u A_s d_u \lambda_{ex.s} n_u^2)/(F_s A_u \lambda_{ex \cdot u} d_s \cdot n_s^2)] \quad (11)$$

where all the symbols have the same meaning as in eq (3); subscripts u and s refer to the unknown and standard, respectively; d is the dilution factor denoting the ratio of the fluorescence species concentration in the sample used for absorbance measurements to that used for fluorescence measurements: λ is the excitation wavelength.

The quantum efficiency determined by direct excitation to the $^5D_0$ level obtained by this method was 0.95 ± 0.03 for the phosphate glass, [41] and 0.93 ± 0.05 for the silicate glass [42].

The very similar values for the quantum yield obtained by the two independent methods suggests use of the phosphate glass as a reliable fluorescence standard at wavelengths similar to those for the fluorescence of europium, as summarized in table 2.

To obtain this quantum efficiency, it is necessary to excite the $^5D_0$ level of europium from the $^7F_0$ level at 580 nm, or from the $^7F_1$ level at 591 nm. Excitation to higher levels results in a decrease of fluorescence yield from the $^5D_0$ level, as additional paths for radia tive and nonradiative transitions become possible.

The quantum yields of fluorescence upon excitation to selected levels in phosphate glass are presented in table 1 [41]. The values of quantum efficiencies for fluorescence monitored by $^5D_0$ emissions when excited to higher levels, as listed in the table, were obtained from the ratio of the area under the excitation spectrum to the ratio of the area under the absorption band for a given level using eq (12). No corrections were made for the change of refractive index with wavelength.

$$\text{Q.Y.}^b = \frac{F_b/A_b}{F_a/A_a} \frac{\lambda_{ex\,a}}{\lambda_{ex\,b}} \text{Q.Y.}^a \quad (12)$$

Q.Y.^{b}	Quantum efficiency of $^5D_0$ fluorescence by excitation to a given level
Q.Y.^{a}	Quantum efficiency of $^5D_0$ fluorescence by excitation to the $^5D_0$ level
F_b	peak area of a given level in excitation spectrum
A_b	peak area of a given level in the absorption spectrum
F_a	peak area of $^5D_0$ in excitation spectrum
A_a	peak area of $^5D_0$ is absorption spectrum
$\lambda_{ex\,a}$	wavelength of $^5D_0$ absorption (581 nm)
$\lambda_{ex\,b}$	wavelength of absorption for given transition.

Therefore, europium glass is proposed as a standard where the emission of the unknown is close to the emission of Eu^{3+} (table 2) and the excitation wavelength is also near one of the excitation wavelengths of europium (table 1).

The fluorescence of europium shows a linear dependence on concentration up to 7 weight percent and no quenching is observed. Therefore, the concentration of the standard used will be governed by the desired wavelength of excitation because of different oscillator strengths. For excitation at 580 or 591 nm, 1–2 weight percent of Eu^{3+} in glass is suggested. The europium glass standard is suitable for compounds having narrow fluorescence in the wavelength range of 600–700 nm.

[2] In order to adequately describe materials and experimental procedures, it was occasionally necessary to identify commercial products by manufacturer's name or label. In no instances does such identification imply endorsement by the National Bureau of Standards, nor does it imply that the particular product or equipment is necessarily the best available for that purpose.

B. Gadolinium

Gadolinium has a comparatively simple optical absorption and emission spectrum because the trivalent gadolinium has a half-filled configuration corresponding to $7-4f$ electrons. The ground state is $^8S_{7/2}$, which is not split in a crystal field. Its first excited state lies around 3200 cm^{-1}, which corresponds to the 312 nm band. Gadolinium is the only rare-earth ion whose spectrum consists only of bands lying in the UV region. The emission spectrum of gadolinium in borate glass [46] has a major band with maximum at 312 nm due to the $^6P_{7/2}$–$^8S_{7/2}$ transition (fig 4), which is essentially unchanged in other matrices [47]. The oscillator strength of this transition and of transitions to higher levels from $^6P_{7/2}$ are tabulated in table 3. The quantum yield of the 312 nm fluorescence was computed by taking a ratio of the measured lifetime of $^6P_{7/2}$ fluorescence, which is 4.10 ± 0.01 ms, to the natural lifetime of this transition obtained by use of formula (5). The calculated lifetime was found to be 4.10 ms. The quantum yield thus obtained equals 1 with an estimated error of ± 1 percent. The quantum yield of $^6P_{7/2}$ fluorescence at excitation to higher levels was obtained relative to the quantum yield of excitation at $^6P_{7/2}$ using eq (12).

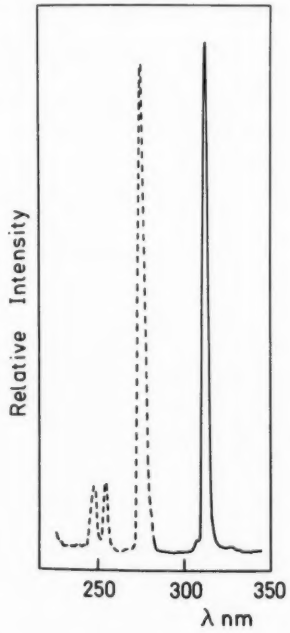

FIGURE 4. Corrected excitation (broken line) and emission (full line) spectrum of the $^6P_{7/2}$ fluorescence of Gd^{3+} in borate glass.

The quantum efficiencies of the 312 nm fluorescence of gadolinium in borate glass are tabulated in table 3.

Borate glass containing gadolinium can be used as a standard for fluorescent materials having emissions around 312 nm and excitation peaks around 250 and 273 nm. Because of the narrowness of the band, it is suitable for materials with narrow fluorescence. Gadolinium in borate glass shows a linear fluorescence output as a function of concentration from the ppm range [48] to 7 weight percent (the highest concentration introduced).

C. Terbium

The electronic configuration of Tb^{3+} is $4f^8$. The absorption spectrum of Tb^{3+} arises from the transitions from the ground $^7F_6$ state to higher levels of the f orbital giving rise to sharp bands of absorption due to f-f^* transitions. In glasses, an additional broad band occurs in the UV due to the $4f^8 \rightarrow 4f^75d$ transition. The oscillator strengths of Tb^{3+} together with the quantum efficiencies of the $^5D_4$ level are presented in table 4.

Terbium fluorescence is observed in the glass from the $^5D_4$ and $^5D_3$ excited states. The $^5D_3$ fluorescence, around 378–369 nm, is quenched at higher concentrations of Tb^{3+} due to $Tb^{3+} - Tb^{3+}$ interactions. The $^5D_4$ fluorescence consists of seven bands due to the transitions: $^5D_4 \rightarrow {}^7F_{6,5,4,3,2,1,0}$. The wavelengths for maxima of these bands together with their relative peak areas are presented in table 5. The corrected emission

TABLE 3. Oscillator strengths and quantum yields of fluorescence of Gd^{3+} in borate glass

Transition assignment	Wavelength nm	Wave number cm^{-1}	Oscillator strength $\times 10^6$	Quantum yield of $^6P_{7/2}$ fluorescence
$^8S_{7/2} \rightarrow {}^6P_{7/2}$	313.0	31949	0.176	1
$^6P_{5/2}$	307.0	32573	.074	
$^6I_{7/2}$	280.25	35682	.117	
$^6I_{9/2}$, $^6I_{17/2}$, $^6I_{11/2}$	277.0	36101	.781	
$^6I_{13/2}$	274.3	36456	1.679	0.870
$^6I_{15/2}$				
$^6D_{9/2}$	253.6	39432	0.406	.735
$^6D_{7/2}$	247.6	40388	.385	.735
$^6D_{3/2}$				
$^6D_{5/2}$	245.5	40733	.099	.590

TABLE 4. Oscillator strengths and quantum yields of $^5D_4$ fluorescence of Tb^{3+} in borate glass

Transition assignment	Wavelength nm	Wavenumber cm^{-1}	Oscillator strength $\times 10^7$	Quantum yield
$^7F_6 \rightarrow {}^5D_4$	485.5	20597	0.633	1
$^5D_3$, $^5G_6$, $^5L_{10}$	378.9	26392	3.812	0.60
	368.7	26954	7.204	
$^5G_5$, $^5G_2$, $^5G_4$, $^5L_9$	352.5	28369	7.622	.62
$^5G_3$, $^5L_8$, $^5L_7$, $^5L_6$, $^5G_2$	340.6	29360	5.764	.256
$^5D_1$	325.7	30703	0.407	
$^5D_0$, $^5H_7$	318.5	31397	4.405	.197
$^5H_6$	303.4	32960	5.249	.06
$^5H_4$, $^5H_5$, $^5H_3$, $^5I_8$, $^5F_4$	283.6	35261	1.787	
$4f^8 \rightarrow 4f^75d$	220.5	45351	385×10^4	

TABLE 5. Emission wavelength and relative areas of the $^5D_4$ level of Tb^{3+} in borate glass

Transition assignments	Wavelength nm	Relative fluorescence (areas)
$^5D_4 \rightarrow {}^7F_6$	486	0.040
$^5D_4 \rightarrow {}^7F_5$	541	.150
$^5D_4 \rightarrow {}^7F_4$	585	.033
$^5D_4 \rightarrow {}^7F_3$	624	.019

spectrum from the $^5D_4$ level and the corrected excitation spectrum are presented in figure 5.

No quenching of the $^5D_4$ terbium fluorescence was observed in our work with borate glasses from the ppm range to 6 weight percent [49].

The lifetime of the $^5D_4$ fluorescence of terbium follows a simple exponential with an e^{-1} decay time of 2.80 ± 0.05 ms.

The quantum yields of $^5D_4$ fluorescence on excitation to this level were obtained using the measured

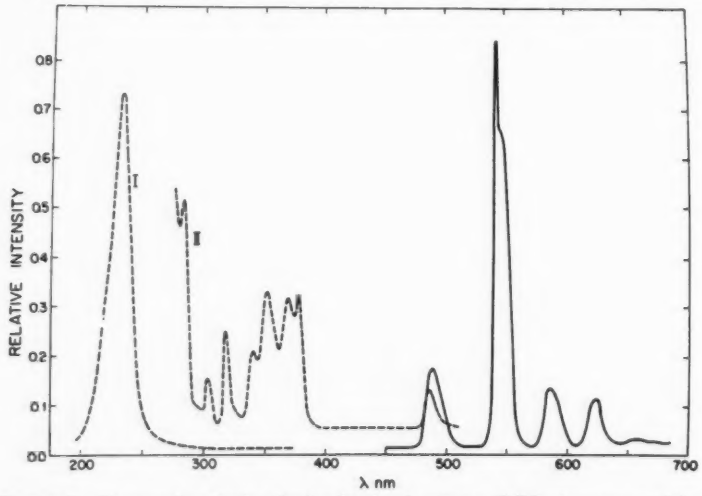

FIGURE 5. Corrected excitation (broken line) and emission (full line) spectrum of the $^5D_4$ fluorescence of Tb^{3+} in borate glass. I = the intensity decreased by a factor of 30.

lifetime and absorption and emission spectra in a similar way as the quantum yields for europium, using eqs (4), (5), and (10).

The radiative probability for the $^7F_6 \rightarrow {}^5D_4$ transition was calculated using eq (5) and equals 57.6 s^{-1}.

The total radiative transition probability, from the $^5D_4$ level, $\sum A_i' [^5D_4]$ is given by:

$$\sum A_i' [^5D_4] = \sum_{i=0}^{6} A [^5D_4 \rightarrow {}^7F_i].$$

From the emission spectrum we found that

$$\sum A_i' [^5D_4] = 6A [^5D_4 \rightarrow {}^7F_6];$$

thus, the total radiative transition rate from the $^5D_4$ level is 345 s^{-1}, which is equivalent to

$$\left[\sum \frac{1}{\tau_{nat}}\right]^{-1}$$

2.9 ms. Hence the quantum yield

$$\text{Q.Y.} = \frac{2.8}{2.9} = 0.97$$

with an estimated error of about 3 percent.

The quantum yields of the $^5D_4$ level on excitation to higher levels were obtained as they were for Eu^{3+} and Gd^{3+}; i.e., by taking ratios of the areas under the excitation spectrum to the areas in the absorption spectra, and multiplying by the ratio of excitation wavelength at 480 to the wavelength for the given excitation. Equation (12) was used for this calculation.

Terbium can be used as a standard for compounds which fluoresce at approximately 480, 543, 587, and 624 nm.

D. Samarium

The electronic configuration of Sm^{3+} is $4f^5$. Its absorption spectrum arises from transitions from the ground $^6H_{5/2}$ level to higher levels of the $4f^5$ configurations. The oscillator strengths of Sm^{3+} in phosphate glass are presented in table 6.

The excitation and emission spectra of Sm^{3+} in phosphate glass are presented in figure 6. The visible fluorescence of Sm^{3+} arises from the transitions from the $^4G_{5/2}$ level to the ground ^6H multiplet. The relative fluorescence intensities to each level in the multiplet are presented in table 7. The fluorescence arising from these transitions is linear with concentration up to about 0.6 weight percent. At higher concentrations an ion-ion energy transfer occurs. This multipolar interaction can be represented systematically (see ref. [35], p. 97):

$$[^4G_{5/2} \rightarrow {}^6F_{9/2}] \rightarrow [^6H_{5/2} \rightarrow {}^6F_{9/2}] \text{ or}$$

$$(Sm^{3+}\,{}^4G_{5/2})^* + (Sm^{3+}\,{}^6H_{5/2}) \rightarrow 2(Sm^{3+}\,{}^6F_{9/2})^*.$$

Therefore, if samarium glass is to be used as a fluorescence standard for the wavelength range presented in table 7, a glass containing less than 0.6 weight percent of this element should be used.

The quantum yield of the $^4G_{5/2}$ fluorescence of samarium in phosphate and borate glasses was calculated by use of eqs (4), (5), and (10). The radiative transition probability from $^6H_{5/2}$ to $^4G_{5/2}$ in phosphate glass as obtained from the absorption spectrum, using eq (5), is 41.3 s^{-1}. The total radiative transition probability from the $^4G_{5/2}$ level, $\Sigma A_i'[^4G_{5/2}]$, is given by

TABLE 6. Oscillator strengths and quantum yields of $^4G_{5/2}$ fluorescence of Sm^{3+} in phosphate glass

Energy level	Wave number cm^{-1}	Wavelength nm	Oscillator strength $\times 10^6$	Quantum yields
$^4G_{5/2}$	17467–18348	545.0–572.5	0.0476	0.950
$^6F_{3/2}$	18779–19047	525.0–532.5	.0115	
$^4G_{7/2}$	19800–20100	497.5–505.0	.0183	
$^4I_{9/2}$, $^4M_{15/2}$, $^4I_{11/2}$	20181–21621	462.5–496.0	1.5370	.653
$^4I_{13/2}$	21267–21978	455.0–470.0	0.1388	
$^4F_{5/2}$	21978–22346	447.5–455.0	.0273	.491
$^4M_{17/2}$, $^4G_{9/2}$, $^4I_{15/2}$	22321–23255	430.0–448.0	.2169	
$(^6P, ^4P)_{5/2}$	23255–24630	406.0–430.0	1.0039	.213
$^4L_{17/2}$, $^6F_{7/2}$, $^6P_{3/2}$ $^4K_{11/2}$, $^4M_{21/2}$, $^4L_{15/2}$	24242–25316	395.0–412.5	4.0749	.264
$^4G_{11/2}$, $^4D_{1/2}$, $^6P_{7/2}$	25252–26109	383.0–396.0	0.2298	.249
$^4L_{17/2}$, $^4K_{13/2}$, $^6F_{9/2}$	26109–27173	368.0–383.0	1.2246	.224
$^4D_{3/2}$, $(^4D, ^6P)_{5/2}$	27173–28089	356.0–368.0	1.2230	.226
$^4H_{7/2}$ $^4K_{15/2}$, $^4H_{9/2}$, $^4D_{7/2}$	27972–28368	352.5–357.0	0.0264	
$(^4K, ^4L)_{17/2}$, $^4L_{19/2}$ $^4H_{11/2}$	28490–29450	340.0–351.0	.7457	.155

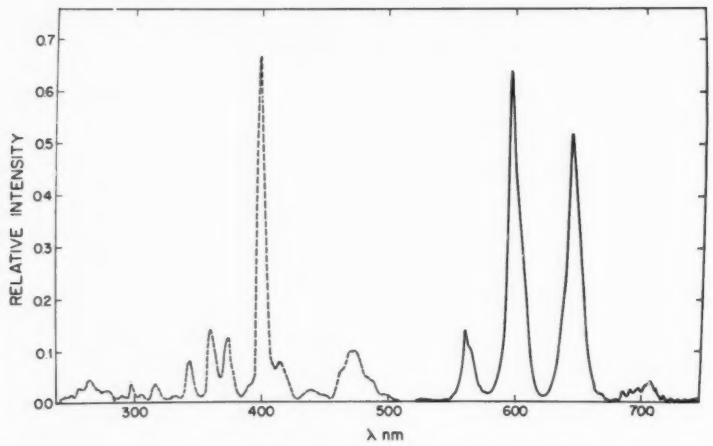

FIGURE 6. Corrected excitation (broken line) and emission (full line) of the $^4G_{5/2}$ fluorescence of Sm^{3+} in phosphate glass.

TABLE 7. Emission wavelength and relative areas of fluorescence from the $^4G_{5/2}$ level of Sm^{3+} in phosphate glass

Transition assignments	Wavelength nm	Relative areas
$^4G_{5/2} \rightarrow {}^6H_{5/2}$	562	1.000
$^4G_{5/2} \rightarrow {}^6H_{7/2}$	597	5.128
$^4G_{5/2} \rightarrow {}^6H_{9/2}$	645	4.856
$^4G_{5/2} \rightarrow {}^6H_{11/2}$	707	0.574
$^4G_{5/2} \rightarrow {}^6H_{13/2}$*	830	0.487
$^4G_{5/2} \rightarrow {}^6H_{15/2}$*	900	

*These two transitions were obtained by calculation assuming quantum yield of level $^4G_{5/2}$ to be 0.95.

$$\sum A_i'[^4G_{5/2}] = \sum_{i=5/2}^{15/2} {}^4G_{5/2} \rightarrow \sum {}^6H_i.$$

The measured lifetime of the fluorescence from the $^4G_{5/2}$ level is 1.91 ms. By assuming the quantum efficiency of fluorescence from this level to be 0.95, we can calculate the transition rate $^4G_{5/2} \rightarrow {}^6H_{13}$, $^6H_{15}$, which is out of the range of measurements, by use of the formula[3]

$$\text{Q.Y.} = \tau_{exp}\left[A(^6H_{5/2} \rightarrow {}^4G_{5/2}) \times (1 + \frac{A(^4G_{5/2} \rightarrow {}^6H_{7/2})}{A(^6H_{5/2} \rightarrow {}^4G_{5/2})} + \frac{A(^4G_{5/2} \rightarrow {}^6H_{9/2})}{A(^6H_{5/2} \rightarrow {}^4G_{5/2})} + \frac{A(^4G_{5/2} \rightarrow {}^6H_{11/2})}{A(^6H_{5/2} \rightarrow {}^4G_{5/2})} + x)\right]$$

$$0.95 = 0.00191[41.3(1.000 + 5.128 + 4.856 + 0.5744 + x)].$$

$$x = \frac{A(^4G_{5/2} \rightarrow {}^6H_{13/2})}{A(^6H_{5/2} \rightarrow {}^4G_{5/2})} + \frac{A(^4G_{5/2} \rightarrow {}^6H_{15/2})}{A(^6H_{5/2} \rightarrow {}^4G_{5/2})}$$

The numbers in parenthesis are the relative fluorescence intensities of the transitions $^4G_{5/2} \rightarrow {}^6H_i$ as given in table 7. The relative areas of $^4G_{5/2} \rightarrow {}^6H_{13/2}$, $^6H_{15/2}$ thus calculated amount to about 4 percent of the total emission of the $^4G_{5/2}$, hence the assumption that the quantum yield equal 0.95 is justified. The estimated error in Q.Y. here is about 3 percent.

The quantum yields of the $^4G_{5/2}$ fluorescence on excitation to higher levels were calculated by eq (12) using as an internal standard the fluorescence yield on direct excitation to the $^4G_{5/2}$ level. They were independently calculated by use of Eu^{3+} glass as standard. The values of quantum yield are presented in table 6.

Glasses containing small concentrations of Sm^{3+} can be used as fluorescence standards for compounds which fluoresce at around 560, 602, and 640 nm.

By examining the quantum efficiencies of Eu^{3+}, Gd^{3+}, Tb^{3+}, and Sm^{+} in glasses, we see that the fluorescence quantum yields from the lowest excited fluorescing levels approach unity. This is because the differences between these levels and the ground levels (or multiplets) are more than five phonons. In such cases, the electronic transitions are almost totally radiative.

E. Thulium

The electronic configuration of trivalent thulium is $4f^{12}$. It possesses more than one strongly emitting level and selective excitation of the various fluorescent levels have been achieved in both phosphate and borate glasses [50]. Because part of the fluorescence occurs in the infrared, we were unable to obtain the relative quantum efficiency of fluorescence of thulium for various levels. It was found, however, that an estimation of an "apparent quantum efficiency" of these glasses could be of practical use if the materials are used as fluorescence standards. Therefore, these parameters will be presented here.

Oscillator strengths of Tm^{3+} in phosphate and borate glasses are presented in table 8. They were obtained by gaussian analysis of the absorption spectrum.

TABLE 8. Oscillator strengths, f, of $T_m{}^{+3}$ in borate and phosphate glasses

Transition assignments	Borate			Phosphate		
	Wave number cm^{-1}	Wavelength nm	$f\times10^6$	Wave number cm^{-1}	Wavelength nm	$f\times10^6$
$^3H_6 \rightarrow {}^3H_4$	5847 to 6134	1630.0 to 1710.0	3.94	5714	1750.0	.....
$^3H_6 \rightarrow {}^3H_5$	8257	1211.0	2.09	8250	1212.0	1.82
$^3H_6 \rightarrow {}^3F_4$	12626 to 12903	792.0 to 775.0	4.39	12626	792.0	3.00
$^3H_6 \rightarrow {}^3F_3$	14619	684.0	4.02	14550	687.2	2.53
$^3H_6 \rightarrow {}^3F_2$	15100	662.0	0.70	15060	664.0	0.22
$^3H_6 \rightarrow {}^1G_4$	21231 to 21505	471.0 to 465.0	2.19	21052	475.0	1.58
				21505	465.0	
$^3H_6 \rightarrow {}^1D_2$	27855 to 28050	356.5 to 355.0	3.75	27855	359.0	3.06
$^3H_6 \rightarrow {}^1I_6$	34246 to 34662	292.0 to 288.5		33057	302.5	
				34364	291.0	
			4.14			31.87
$^3H_6 \rightarrow {}^3P_0$	35082	285.0		35057	286.0	
$^3H_6 \rightarrow {}^3P_1$	36363	275.0		36166	276.5	
$^3H_6 \rightarrow {}^3P_2$	37950 to 38387	262.5 to 260.5	6.13	38095	262.5	14.46

The absorption occurs from the ground $^3H_6$ state. The emission spectra of Tm^{3+} at various excitation wavelengths are presented in table 9. The excitation spectrum of the 453 nm fluorescence

TABLE 9. Emission spectrum of Tm^{3+} at various excitation wavelengths

Excitation (nm)	Assigned transition	Emission			
		borate		phosphate	
		λ(nm)	R.A.*	λ(nm)	R.A.*
468.0($^1G_4$)	$^1G_4 \rightarrow {}^3H_4$			651.50	1.000
	$^1G_4 \rightarrow {}^3H_5$			752.75	0.114
	$^3F_2 \rightarrow {}^3H_6$			665.50	.083
	$^3F_3 \rightarrow {}^3H_6$			690.00	.708
358.0($^1D_2$)	$^1D_2 \rightarrow {}^3H_4$	456.00	1.000	453.00	1.000
	$^1D_2 \rightarrow {}^3H_5$	517.00	0.008	513.00	0.011
	$^1D_2 \rightarrow {}^3F_4$	665.00	.127	663.50	.034
	$^1G_4 \rightarrow {}^3H_6$	478.00	.118	478.00	.063
	$^1G_4 \rightarrow {}^3H_4$	652.50	.180	651.50	.074
	$^3F_2 \rightarrow {}^3H_6$	665.50	.014	665.50	.009
288.0($^3P_0$)	$^1I_6 \rightarrow {}^3H_4$	355.00	.446	350.00	1.000
	$^1I_6 \rightarrow {}^3H_5$	385.00	.125	383.00	0.094
	$^3P_0 \rightarrow {}^3F_4$, $^1I_6 \rightarrow {}^3F_4$	465.00	.155	463.00	.200
	$^1I_6 \rightarrow {}^3F_3$	500.00	.110	498.00	.060
	$^3P_0 \rightarrow {}^3F_3$, $^1I_6 \rightarrow {}^3F_2$	530.00	.061	521.50	.094
	$^3P_0 \rightarrow {}^1G_4$, $^1I_6 \rightarrow {}^1G_4$	705.00	.754	701.00	1.000
	$^1D_2 \rightarrow {}^3H_5$	367.50	.275	365.00	0.133
	$^1D_2 \rightarrow {}^3H_4$	456.00	1.000	453.00	.455
	$^1D_2 \rightarrow {}^3H_5$	517.00	0.067	513.00	.044
	$^1D_2 \rightarrow {}^3F_4$	.....			
	$^1G_4 \rightarrow {}^3H_6$	480.00	.190	478.00	.105
	$^1G_4 \rightarrow {}^3H_4$	.....			
	$^3F_2 \rightarrow {}^3H_6$	.....			
	$^3F_3 \rightarrow {}^3H_6$	.....			

*Relative areas; for each excitation the areas are given relatively to the strongest emission band which is taken as unity.

$(^1D_2 \rightarrow {}^3H_4)$ and the emission spectrum with excitation at 262 nm $(^3H_6 \rightarrow {}^3P_0)$ are presented in figure 7.

The "apparent quantum yield," (A.Q.Y.), of 450–478 nm fluorescence of Tm^{3+} was calculated by the comparative method, using Tb^{3+} as a standard. The A.Q.Y. of Tm^{3+} is defined by eq [12a]:

$$\text{A.Q.Y. } Tm^{3+} = \left\{ \frac{F\left[(^1G_4 \rightarrow {}^3H_6) + (^1D_2 \rightarrow {}^3H_4)\right]\left[A(^7F_6 \rightarrow {}^5D_4)\right]}{\left[F\left(^5D_4 \rightarrow \sum_{i=6}^{i=0} {}^7F_i\right) A\,(^3H_6 \rightarrow {}^1D_2)\right]} (\text{Q.Y. } Tb^{3+}) \right\} \quad [12a]$$

in which $F[(^1G_4 \rightarrow {}^3H_6) + (^1D_2 \rightarrow {}^3H_4)]$ is the sum of the corresponding fluorescence intensities (expressed as areas under the emission spectrum) of Tm^{3+}; $A\,(^3H_6 \rightarrow {}^1D_2)$ is the absorbance for the 358 nm band of Tm^{3+}; $F(^5D_4 \rightarrow \Sigma\,{}^7F_i)$ is the sum of fluorescence intensities of the $^5D_4$ fluorescence of Tb; $A\,(^7F_6 \rightarrow {}^5D_4)$ is the absorbance for the Tb^{3+} band at 358 nm; and Q.Y. Tb^{3+} is the quantum efficiency of Tb^{3+} taken as 0.63. The apparent quantum efficiency for 10 weight percent of Tm^{3+}, calculated in this way, is 0.037 in borate and 0.043 in phosphate glasses.

Here, not all the transitions of Tm^{3+} were taken into account, but since the relative transitions to each level are constant for a given host, Tm^{3+} doped glasses can be used as standards for fluorescence around 450–480 nm and excitation around 358 nm. This small value of A.Q.Y. is not surprising since it is known [50] that at one weight percent of Tm^{3+} the concentration quenching of fluorescence is about 50 percent due to multipolar transitions between neighboring thulium ions. It should also be remembered that the fluorescence around 455–475 nm is one of seven transitions from $^1D_2$ and one of the six $^1G_4$ transitions.

Because of its low A.Q.Y. value, use of Tm^{3+} in the region of 450–480 nm fluorescence has no obvious advantage over Tb^{3+} as a standard. However, it can be used as an internal standard for Tm^{3+}. This fluorescence can be used to determine the apparent yield at 355 nm $(^1I_6 \rightarrow {}^3H_4)$, 385 nm $(^1I_6 \rightarrow {}^3H_5)$ and 367 nm $(^1D_2 \rightarrow {}^3H_6)$, upon excitation to 288 nm $(^3P_0)$ or 265 nm $(^3P_2)$, which is of practical value as a standard in the UV region.

II. Thallium-Doped Alkali Halides and Glasses

While the rare-earth ions have characteristic sharp fluorescence bands largely independent of the host, due to f–f^* transitions, mercury-like ions in general and thallium in particular have much broader fluorescence, with the fluorescence maxima strongly dependent on the composition of the host matrix. The quantum efficiency also is dependent on the host as described below. Monovalent thallium is a well-known fluorescence emitter in the UV region and was used in our studies in various matrices as a possible standard for UV fluorescence.

The absorption spectrum of thallium consists of three main bands: A, B, and C. A review of the absorption and luminescence of this element can be found in references [51] and [52]. The absorption band A, which is discussed here, is assigned to the spin-forbidden transition $^1A_{1g} \rightarrow {}^3T_{1u}$ $(^1\Gamma_1 - {}^3\Gamma_4^o)$, equivalent to $^1S_0 \rightarrow {}^3P_1$ in the free thallous ion (see fig. 8), which is triply degenerate. It can be split in a cubic field by a dynamic Jahn-Teller effect [54], or the degeneracy can be lifted when the symmetry is decreased in glasses [55] from cubic to tetragonal or lower. The oscillator strengths, f, for the maxima of the A bands are presented in table 10. It was shown by Scott and Hu [53] that when the chloride ligand is replaced by an oxygen ligand in aqueous solution, the maxima of the band is shifted towards a shorter wave-

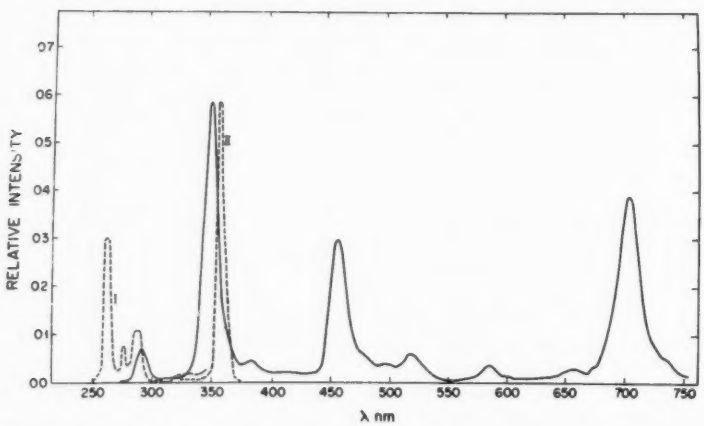

FIGURE 7. Corrected excitation spectrum of the $^1D_2$ fluorescence (broken line—II decreased by a factor of 2) and emission spectrum (full line) excited at $^3P_2$ band of thulium in phosphate glass.

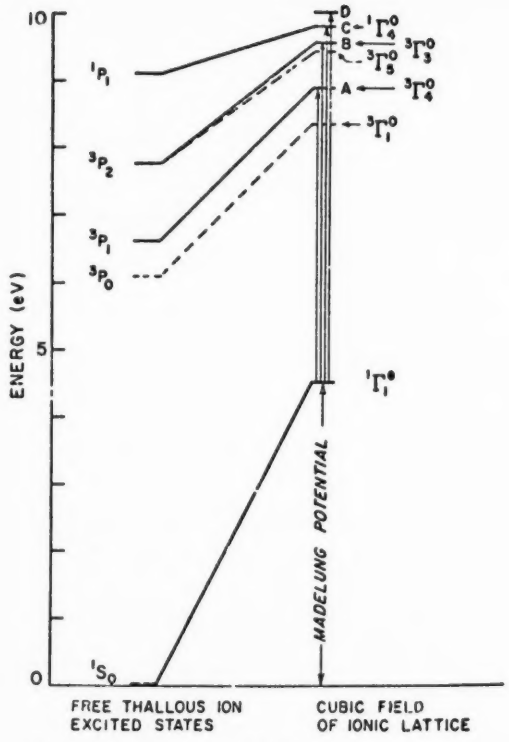

FIGURE 8. The energy of thallous ion in a cubic field.

length. The fluorescence occurs at a somewhat longer wavelength due to the Stokes' shift.

The relation between absorption and fluorescence can be most easily explained by the use of the configurational coordinate diagram, given in figure 9 [56]. The potential energy of the luminescent center in a crystal lattice is plotted here as a function of the configurational coordinate r. The quantity r represents a mean distance between the luminescence center and the surrounding ligands. The horizontal lines represent the vibrational states of the metal-oxygen bond vibrations.

At a temperature of absolute zero the luminescent center will occupy the lowest vibrational level of the ground state. The ions surrounding the central ion vibrate about their equilibrium positions situated at a distance r_0 from the central ion. At higher tempera-

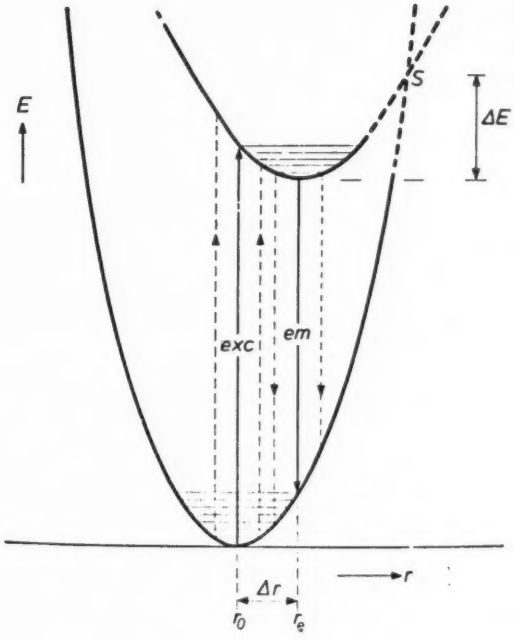

FIGURE 9. Configurational coordinate diagram of a luminescent center. The potential energy E of the center in the lattice is plotted as a function of the configurational coordinate r for the ground state and the first excited state. In practice, r is identified with the distance between the central cation and the surrounding anions. Vibrational states are represented schematically by horizontal lines in the parabolae. The excitation and emission transitions correspond to vertical transitions between the two curves. Since $\Delta r \neq 0$, the emission shows a Stokes' Shift (wavelength of the emission is longer than that of the excitation). Since the center can be in various vibrational states both at the ground level and at the excited level, and since $\Delta r \neq 0$, the transitions occur in a broad band of energies (schematically indicated by vertical dashed lines). Nonradiative return from the excited state to the ground state is possible via the point of intersection, S, of the two curves. This requires an activation energy ΔE, which can be supplied at higher temperatures (thermal quenching of the emission). In the region where the two parabolae intersect, the curve is marked by dashes since the situation is actually more complicated than is indicated here. This is due to interaction between the ground and the excited state at the situation of the intersection point. The present treatment is not invalidated by this.

TABLE 10. Quantum efficiencies (QE) of thallium in 4 matrices

Matrix	Max. absorption nm	Max. excitation nm	Max. emission nm	Oscillator strength, f [35]	QE	Stokes' shift (cm^{-1})
Borax	230	248	325	0.072	0.19	12709
Phosphate	212.5	230	300	.080	.23	13726
KCl	247	247	300	.074	.5	7153
KBr	261	261	320	.097	.44	7064

474-414 O - 73 - 6

tures, higher vibrational levels may be occupied. In figure 9, the horizontal lines represent vibrational states. Due to the absorption of radiation of the appropriate wavelength (in this case UV radiation) the center is raised to an excited state. Since the equilibrium distance r_e of the excited state will not in general be equal to that of the ground state, and since the center may be at different vibrational levels, this transition will correspond to a fairly broad absorption band. The fact that the optical absorption corresponds to a vertical transition in figure 9 is attributable to the rapid nature of electronic transitions as compared to vibrational transitions which involve the heavier nuclei (Franck-Condon effect).

Once in an excited state, the system will relax towards the equilibrium state (of the excited level) by dissipation of heat. From this state or nearby levels the system returns to the ground state by emitting radiation. The emission, therefore, also consists of a broad band. Line emission is found only in the exceptional case where the configurational-coordinate curves are identical in shape and have the same equilibrium distance, as in the case of the rare-earth ions. Because of the heat dissipation, the emission always lies at a lower energy than the absorption. This displacement of emission with respect to absorption is known as the Stokes' shift.

With the aid of the simple model in figure 9 (the Mott-Seitz model) one can explain:

(a) the broad-band character of the emission and absorption of many centers;
(b) the shift of the emission to lower wavelengths; and,
(c) the temperature dependence of the emission.

If the equilibrium configuration of the excited state lies outside the curve of the ground state (fig. 10), then, after excitation, the intersection point of both curves is reached before the above-mentioned equilibrium configuration is reached, and the system relaxes nonradiatively to the ground state. No emission is then possible. The radiationless return to the ground state is temperature-independent. This is the model which Seitz proposed to explain the absence of luminescence in certain cases [57]. In other words, the condition for the absence of luminescence is a large difference between the equilibrium distance of the excited state and that of the ground state.

Dexter, Klick, and Russell later proposed a different model [58] which shows that even under less rigorous circumstances than in figure 10, nonradiative transitions to the ground state may occur (fig. 11). The characteristic feature of the situation in figure 11 is that the intersection point S of the two curves is lower than the level reached after excitation. When, after excitation, the system now relaxes while vibrating, to the equilibrium position of the excited state, the intersection point of the two curves is passed. Here too, a temperature-independent, radiationless return to the ground state can take place.

We learn from these models that the difference, Δr, between the equilibrium configuration of the excited

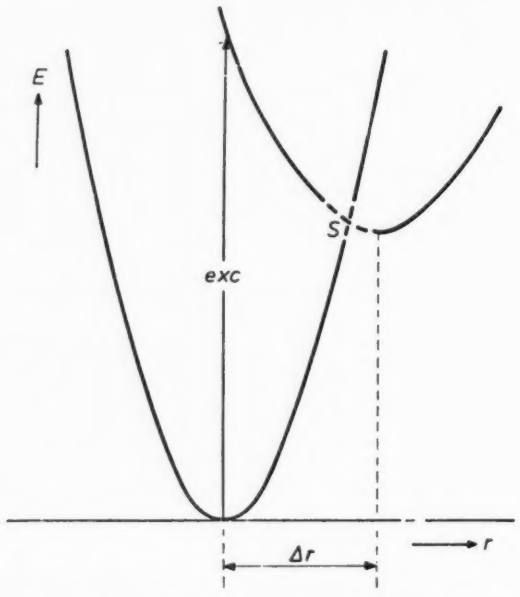

FIGURE 10. The Seitz model for explaining the absence of luminescence; see figure 9. The minimum of the curve for the excited state lies outside the curve for the ground state; luminescence is then not possible.

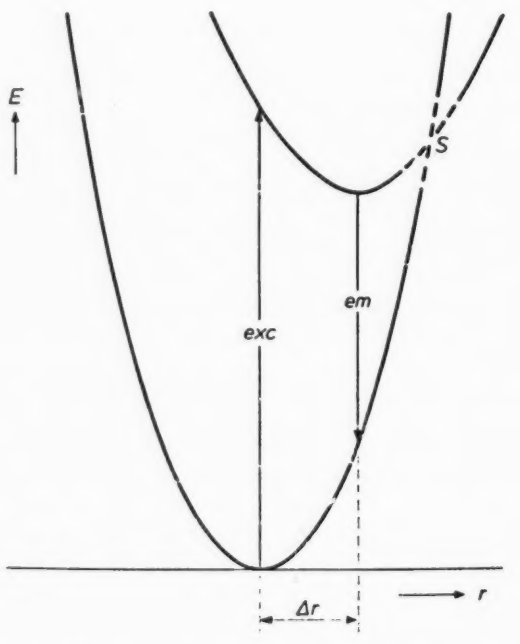

FIGURE 11. The Dexter-Klick-Russel model for explaining a low luminescence efficiency or the absence of luminescence. The intersection point S of the two curves lies below the vibrational level reached after excitation. The nonradiative return to the ground state requires no activation energy (as it did in fig. 9).

state and that of the ground state must be small if luminescence is to occur.

Because of the well-defined and broad fluorescence of thallium in the UV region, we have determined the optimum conditions for preparation of thallium doped alkali halide pellets in phosphate and borate glasses. Also, the dependence of fluorescence efficiency on concentration of Tl^+ was measured. It is shown that the thallium doped pellets and glasses can be used as fluorescence standards. The detailed results of the measurements are given.

A. Thallium Doped Potassium Chloride Disks

Polycrystalline pellets were used [52] as mentioned in the introduction. Such pellets are used in biomedical research for fluorescence measurements.

The optical absorption and fluorescence of alkali halides containing thallium has been widely studied; references can be found in a review paper by Teegarden [51].

The absorption band *A* with maximum around 247 nm in potassium chloride, arises from the spin-forbidden transition $^1A_g \rightarrow {}^3T_{1u}$ (corresponding to $^1S_0 \rightarrow {}^3P_1$ in a free thallous ion), and is accompanied by the fluorescence with band maximum at 300 nm. Because of large half-widths, the absorption and fluorescence are suitable for quantum-yield studies.

1. Preparation of Disks

Baker Analyzed KCl was ground for 1 h with an automatic mortar and pestle and dried for 48 h at 120 °C. TlCl (BDH Analytical Grade) was then added and the mixture was homogenized in an electric vibrator. In order to obtain low concentrations, the stock mixture was diluted twice with dry KCl powder. Prior to diffusion, the homogenized mixture was ground in an agate mortar with a small amount of triple-distilled water, and redried at 120 °C for 24 h.

As known from previous work [59, 60], only thallium that has undergone diffusion has an absorption band at 247 nm. The completeness of diffusion was checked by heating the mixtures at different temperatures for various periods and measuring the absorbance. The diffusion was then carried out by heating the mixtures at 400 °C for 4 h. Under these conditions, all of the thallium introduced diffuses into the KCl powder.

The absorption measurements were made on a Cary 14 spectrophotometer, with a KCl disk as blank. The effect of the emission on the absorbance readings was negligible, mainly because the solid angle subtended by the photomultiplier was small (0.005 rad), as compared to the full sphere (4π rad) over which emission occurs.

2. Preparation of Quinine Sulfate

Fisher Reagent Grade quinine sulfate was recrystallized from water five times and dried in a vacuum oven at 60 °C. Stock solutions were prepared by dissolving the purified quinine sulfate in 0.1 N H_2SO_4, analytical grade. The water used for the stock solutions was distilled, passed through an ion-exchange column, and then doubly distilled from a quartz still. Special low-fluorescence 1 mm quartz cells were used to hold the standard solutions.

3. Emission Measurements

The corrected emission was measured on a Turner 210 spectrofluorimeter in which the regular 1 cm cell was replaced by a special sample holder adapted to hold disks and cells of 1 mm thickness. The sample holder could be rotated to permit continuous variation of the angle of incidence of the exciting light. Because of the optical arrangement of the spectrofluorimeter, it was necessary to place a black-velvet screen between the sample and the collecting mirror to reduce reflections. All measurements were made at constant excitation energy and at room temperature.

Some representative A-band absorption curves are shown in figure 12. A plot of thallium concentration versus absorbance is linear, as can be seen in figure 13.

The oscillator strength, f, was calculated from the generalized formula of Smakula, (13), given by Patek (ref. [35], p. 72).

$$f = 0.82 \times 10^{17} \frac{n}{(n^2+2)^2} \frac{V}{N} \alpha(E)dE \qquad (13)$$

where n is the refractive index, $\left(\frac{V}{N}\right)^{-1}$ the concentration of the ions per cm^3, α the absorbance in cm^{-1} and E the energy in electron volts. The refractive index of a KCl crystal was taken from Landoldt-Bornstein [61] as 1.59. Multiplying 1.59 by the ratio of the pressed disk density (1.690 g/cm^3) to the crystal density (1.984 g/cm^3) yields an index of refraction value for the pressed disk of 1.57.

The oscillator strength was 0.074 ± 0.002. Figure 14 shows the corrected emission spectra. The linear concentration dependence of the emission-peak height is shown in figure 15.

The quantum yield was determined by use of eq (11) using quinine sulfate as a standard [52].

The quantum yield of 0.508 for quinine sulfate in 0.1 N H_2SO_4 used as a standard was taken from the data of Melhuish at $\lambda_{exc} = 366$ nm. Fletcher showed that the quantum yield was constant to within 5 percent over the wavelength range 240–290 nm, excluding a minimum at 270 nm. The refractive index n_s was taken as a weighted mean of the refractive indices of the standard solution and the quartz windows of the cell.

The excitation wavelength for the unknown and the standard was 247.5 nm. The emission-peak height was critically dependent on the angle of incidence of the exciting light, so that the small but inevitable difference of the angles of the sample and reference could cause a considerable error. On the other hand, the shape factor of the emission (ratio of emission-peak area to peak height) was independent of the angle. To eliminate the error, we found the maximum peak height by

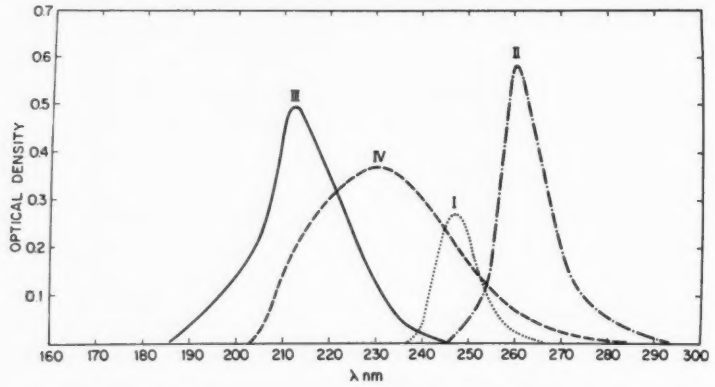

FIGURE 12. A band absorption spectra. I. KCl:Tl^+ 20 ppm; II. KBr:Tl^+, 20 ppm; III. Phosphate:Tl^+, 50 ppm; IV. Borax:Tl^+, 100 ppm.

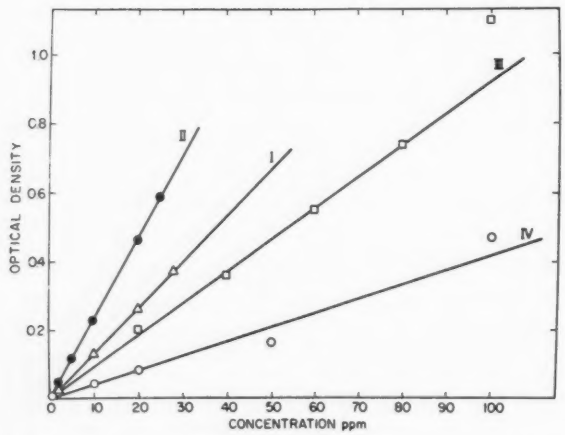

FIGURE 13. Absorbance versus concentration of Tl^+ in I. KCl; II. KBr; III. Phosphate; IV. Borax.

varying the angle of incidence and multiplied it by the shape factor to obtain the emission-peak area, A.

The quantum yield obtained in this way was 0.50 ± 0.03.

Pressed polycrystalline KCl:Tl disks differ only slightly in their density from KCl:Tl crystals, and they have the same optical characteristics. All of the thallium diffuses into the polycrystalline disks, and they can therefore be prepared to the predetermined uniform concentration. The linear concentration dependence of the absorbance (fig. 13) gives a check on the reproducibility of the samples, and the agreement of the oscillator strength of the disks with that of the crystals permits their use as a substitute for crystals. From the linear concentration dependence of the emission, it is concluded that the quantum yield is constant over the concentration range 2–30 ppm. Pressed polycrystalline KCl disks doped by diffusion with TlCl can therefore be used as UV luminescence standards at room temperature. The recommended

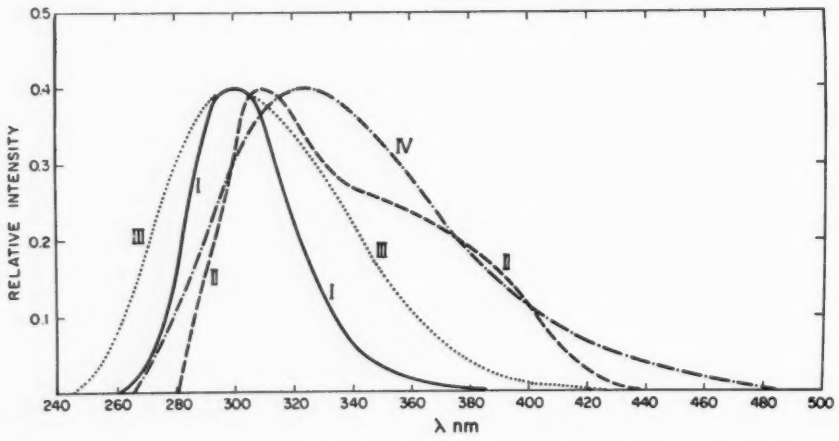

FIGURE 14. Corrected emission spectra I. KCl:Tl^+; II. KBr:Tl^+; III. Phosphate:Tl^+; IV. Borax:Tl^+.

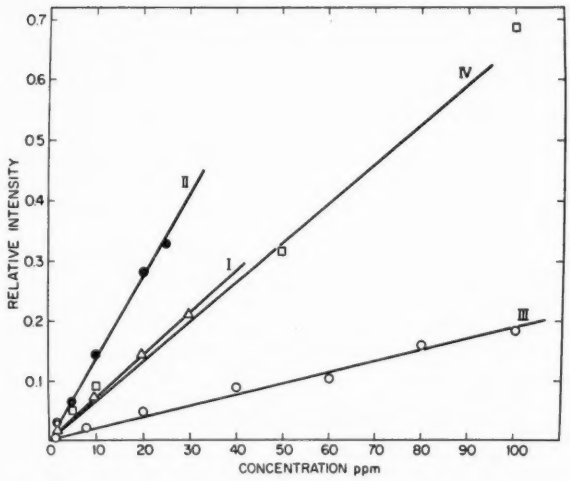

FIGURE 15. The dependence of fluorescence output on Tl^+ concentration: I. KCl; II. KBr; III. Phosphate; IV. Borax.

concentration is 2 ppm, corresponding to 0.624×10^{-6} mol/mol.

B. Thallium-Doped Potassium Bromide Disks

The absorption spectrum of KBr : Tl in polycrystalline disks and single crystals is well known [60, 62] and is presented in figure 12. The concentration dependence of the absorption maximum is presented in figure 13. The corrected emission spectrum of the A band is presented in figure 14. The dependence of fluorescence intensity on concentration is presented in figure 15.

The oscillator strength was calculated by use of Smakula's equation (13), and was found to be 0.097 ± 0.003. The quantum yield of the A band in KBr : Tl was calculated using KCl : Tl as a standard.

The emission and excitation spectra of the disks were measured on a spectrofluorimeter built in this laboratory, the description of which may be found in reference [36]. The emission spectra were corrected using standard compounds and their reported spectra. To correct for the difference of excitation energy in the standard and the unknown, a correction factor was introduced into eq (11).

The refined formula for the use with this spectrofluorimeter is of the form:

$$\eta_u = \eta_s \frac{F_u A_s d_s \lambda_s n_u^2}{F_s A_u d_u \lambda_u n_s^2} \times \frac{F_s^B F_u^T}{F_s^T F_u^B} \qquad (14)$$

in which the parameters have the same meaning as in (11). F_S^B is the relative fluorescence output at peak maximum in the excitation spectrum of the standard measured with our apparatus; F_S^T is the relative fluorescence output at peak maximum in the excitation spectrum of the standard measured on the Turner Model 210 spectrofluorimeter; F_u^B is the output at peak maximum of the unknown in the excitation spectrum of the standard measured in our apparatus; F_u^T is the output at peak maximum of the unknown measured in the excitation spectrum of the standard on the Turner Model 210 spectrofluorimeter. The density of the pressed KBr disk is 2.67 g/cm³.

We used as a standard a KCl:Tl disk with a quantum yield of 0.50. The quantum yield obtained for the KBr : Tl disk is 0.44 ± 0.03. All data concerning KBr : Tl disks are presented in table 10.

Because of the linear dependence of absorption and emission on the Tl^+ concentration, it is concluded that the quantum yield is independent of the concentration in the 0.5–25 ppm range. Pressed polycrystalline KBr:Tl and KCl:Tl disks can easily be prepared to predetermined concentrations for use as UV fluorescence standards at room temperature. The recommended Tl concentration is 2 ppm, corresponding to 0.837×10^{-6} mol/mol KBr:Tl and 0.624×10^{-6} mol/mol in KCl.

III. Thallium-Doped Glasses

To compare our results in glasses with the corresponding data of alkali halides, we have prepared and measured glasses doped with thallium.

Glasses were prepared from sodium phosphate monobasic and from borax. Glasses, 1 mm thick and 12 mm in diameter were obtained by molding the melt on a tile.

The absorption spectra were recorded on a Cary 14 spectrophotometer using undoped glasses or disks as blanks, and are presented in figure 12. The concentration dependence of the absorption is presented in figure 13.

1. *Excitation and Emission Spectra*

Excitation and emission spectra were taken on a spectrofluorimeter built in this laboratory [36]. The spectra were corrected with respect to light characteristics and spectral distribution of the photomultiplier by comparison with a similar spectrum taken on the Turner Model 210 spectrofluorimeter using standard compounds (quinine sulfate, fluoresceine, etc.).

The corrected emission spectra are presented in figure 14. The concentration dependence of the emission is presented in figure 15. The quantum efficiencies were obtained by comparison of the glasses with alkali halide-thallium-doped disks using eq (14), the results of which are presented in table 10.

When a pellet or a glass containing thallium is excited through absorption into the A band at room temperature, the emission is composed of two time components, one with a short lifetime of about 25 ns and one with a long component of 400 ns. We have proposed an explanation for the two decay constants [55].

The proposed explanation is as follows: The absorption is from $^1S_0$ ground state to $^3P_1$ excited state. The emission occurs also between these two levels and is followed by a Stokes' Shift (see table 10). It is an allowed emission with a short lifetime. However, part

of the population of the $^3P_1$ level is rapidly depleted by a radiationless process to the metastable $^3P_0$ state (see fig. 16). This assumption is proven by an experiment of Tomura [63], who had observed a decay of 2 − 1 ms at 20 K due to this transition. At an elevated temperature, the vibronic modes promote tunnelling from $^3P_0$ back to $^3P_1$. This process occurs with an activation energy of 0.06 eV in KCl. The next process is the delayed emission from $^3P_1$. The rate of this process is the rate of tunnelling which controls the population of $^3P_1$. Since both the instant and delayed emission occurs from the $^3P_1$ state, the wavelength of emission for both decays is the same. Also, the delayed fluorescence is not polarized [63] because the memory of polarization is lost during tunnelling. To determine the quantum yield from the lifetime measurement, additional calculations have to be made because of this delayed fluorescence.

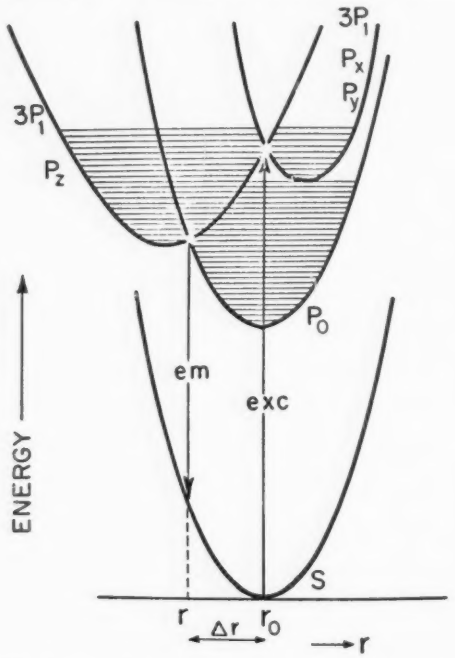

FIGURE 16. Configurational coordinate diagram of Tl^+ in a tetragonal symmetry.

In this mechanism, for all four cases described here, the broadening of the emission in KBr:Tl is due to emission from P_x, P_y and another emission from P_z, and not from P_0. Splitting of the various P orbitals by the Jahn-Teller effect is stronger the heavier the anion of the host lattice.

The shift of the absorption band to longer wavelength in the order Tl^+-phosphate, Tl^+-borax, Tl^+-KCl and Tl^+-KBr (also Tl^+-Kl) indicates that the ligand field acting on Tl^+ increases in the same order. The stronger the ligand field the smaller the difference between the excited and ground state and hence the absorption occurs at longer wavelengths. This also indicates that, in the case of borax, the electrons of the oxygen participating in the thallium-oxygen bond are shifted more to the Tl (stronger polarization of the bond), which is due to stronger electron affinity of phosphorus (0.78 eV) than of boron (0.33 eV).

IV. Glasses Doped by Pb^{2+}, Ce^{3+}, and Cu^+

In a search for standards to cover the fluorescence range from the UV region to the red region, it was found that in addition to thallium doped glasses [64], glasses containing Ce^{3+} [65], Pb^{2+} [66], and Cu^+ [67] lead^{2+} and copper$^+$ are suitable for standards, considering the positions of their emission wavelengths and half bandwidths.

The corrected emission spectra of various glasses containing these ions are presented in figure 17. The

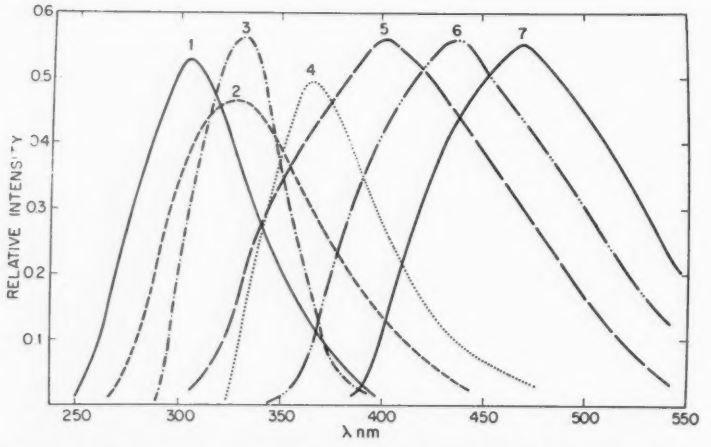

FIGURE 17. Matrix effects on position of emission band of Tl^+, Ce^{3+}, Pb^{2+}, and Cu^+. I. Phosphate:Tl^+; II. Borax:Tl^+; III. Phosphate:Ce^{3+}; IV. Borax:Ce^{3+}; V. Borax:Pb^{2+}; VI. Germanate: Pb^{2+}; VII Phosphate: Cu^+.

absorption spectra of Ce^{3+} and Cu^{+} in phosphate glass and Pb^{2+} in borax glass are presented in figure 18. The absorption is linear with concentration in the range measured (1–1000 ppm). The dependence of fluorescence on concentration is linear as shown in figure 19, and this range of concentration can be used for preparation of the standards. The maximum emission and excitation wave lengths of the glasses and the half bandwidths of the emission are presented in table 11.

The determinations of quantum yields of these glasses are now undergoing research. For these determinations, doped potassium chloride disks are used as standard references [64–67]. For the quantum

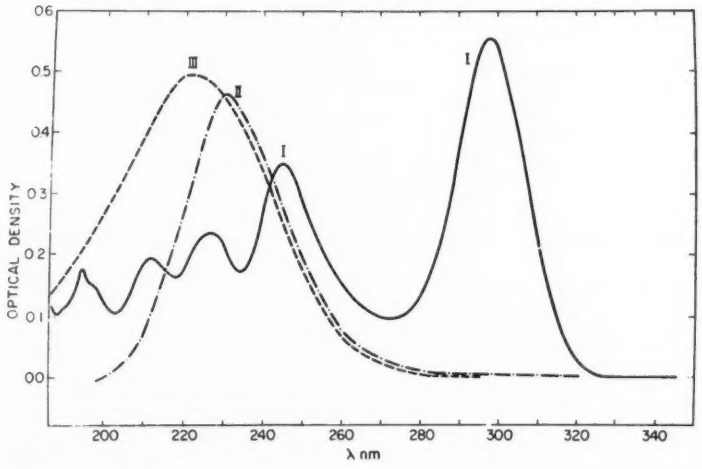

FIGURE 18. Absorption spectrum of I. Ce^{3+} in phosphate, 400 ppm; II. Pb^{2+} in borax, 100 ppm; III. Cu^{+} in phosphate, 50 ppm.

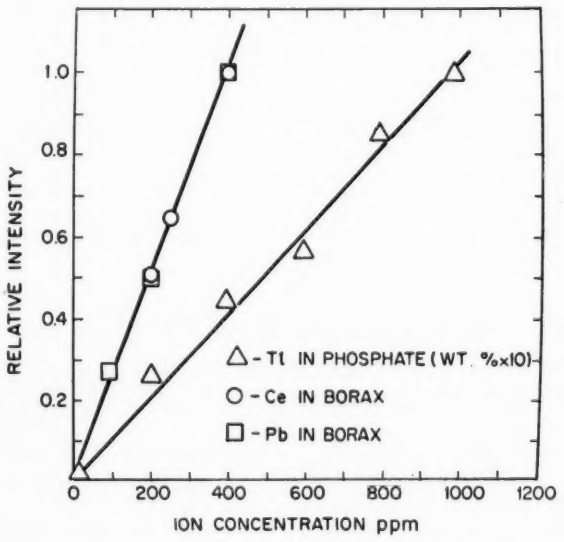

FIGURE 19. The dependence of fluorescence intensity on concentration I. Tl^{+} in phosphate; II. Ce^{3+} in borax; III. Pb^{2+} in borax.

yield determination of Tl in phosphate and borate glasses, and Ce^{3+} in phosphate glasses, quinine sulfate was used as a relative standard [68].

Conclusions

Rare-earth-doped glasses are suggested as relative standards for use with compounds having narrow band excitation and emission of fluorescence. Thallium-doped alkali halides are standards suitable for determination of substances in alkali halide pellets, while thallium doped glasses can be used as standards for glassy substances or liquids in quartz cells. Other varieties of glass standards and pellets are now under investigation. Energy transfer studies which are of great importance in understanding quantum efficiencies will be summarized in a separate review.

The assistance of E. Greenberg in preparation of this paper is gratefully acknowledged. I wish also to express my thanks to Y. Eckstein and L. Boehm for fruitful discussions, and E. Hoffman for providing relevant literature on fluorescence in biomedical systems. I especially wish to express my gratitude to Menis who suggested the topic for this paper.

TABLE 11. Emission and excitation wavelength dependence on matrix for lead, cerium, thallium and copper

Ion	Matrix	Wavelength, nm		Emission half-bandwidths, nm
		Excitation	Emission	
Tl^{+}	KCl	247.5	300	40
Tl^{+}	Phosphate	219.0	302	70
Tl^{+}	Borate	233.0	325	90
Ce^{3+}	Phosphate	297.0	334	55
Ce^{3+}	Borate[a]	310.0	364	80
Ce^{3+}	Borax[b]	311.0	365	65
Ce^{3+}	Silicate	317.0	380	85
Pb^{2+}	Phosphate	241.5	309	70
Pb^{2+}	Borate[a]	261.0	424	140
Pb^{2+}	Borax[b]	241.0	425	165
Pb^{2+}	Germanate	295.0	440	125
Cu^{+}	Phosphate	270.0	445	120

[a] Mixture of boric acid and boric oxide. [b] Sodium borate only.

VI. References

[1] Parker, C. A., Photoluminescence of Solutions (Elsevier Publishing Co., New York, N.Y. 1968); Hercules, D. M. Ed., Fluorescence and Phosphorescence Analyses. (Interscience Publishing Co., New York, N.Y., 1966); B. Becker, R. S., Theory and Interpretation of Fluorescence and Phosphorescence (John Wiley & Sons, Inc., New York, N.Y., 1969).
[2] White, C. E., and Argaver, R. J., Fluorescence Analysis (M. Dekker, Inc., New York, N.Y. 1970); Berlman, I. B., Handbook of Fluorescence Spectra of Aromatic Molecules, (Academic Press, New York, N.Y., 2nd Edition 1971).
[3] Demas, J. N., and Crosby, G. A., J. Phys. Chem. **75,** 991 (1971).
[4] Edelman, G. M., and McClure, W. O., Accounts. Chem. Res. **1(3),** 65 (1968).
[5] Strayer, L., Science **162,** 526 (1968).
[6] Rinder-Knecht, H., Nature **193,** 167 (1962).
[7] Hartley, B. S., and Massey, V., Biochim. Biophys. Acta **21,** 58 (1956).
[8] Deyl, Z., and Rosmus, J., J. Chromatogr. **20,** 514 (1965).
[9] Pataki, G., and Strasky, E., Chimia **20,** 361 (1966).
[10] Chen, R. F., Arch. Biochem. Biophys. **120,** 609 (1967).
[11] Moye, H. A., and Winefordner, J. D., J. Agr. Food Chem. **13,** 516 (1965).
[12] Staniland, L. N., J. Agr. Eng. Res. **4,** 110 (1959).
[13] Staniland, L. N., J. Agr. Eng. Res. **5,** 42 (1960).
[14] Udenfriend, S., Fluorescence Assay in Biology and Medicine (Academic Press, New York, N.Y., Vols. I and II, 1962, 1969).
[15] Van Duuren, B. L., J. Natl. Cancer Inst. Monograph No. 9, 135 (1962).
[16] Van Duuren, B. L., Acta Unio Intern. Contra Cancrum **19,** 524 (1963).
[17] Konev, S. V., Fluorescence and Phosphorescence of Proteins and Nucleic Acids, (Plenum Press, New York, 1967), p. 171.
[18] Booth, J., et al., J. Chem. Soc. 598 (1954).
[19] De Santis, F., et al., Nature **191,** 900 (1961).
[20] Liquori, A. M., et al., J. Mol. Biol. **5,** 521 (1962).
[21] Cook, J. M., J. Chem. Soc. London, 1210 (1950).
[22] Sawicki, E., et al., Talanta **14,** 431 (1967).
[23] Van Bertalanffy, L., et al., Cancer **11,** 873 (1958).
[24] Rubin, M., Fluorimetry in Clinical Chemistry, American Instrument Co., Silver Spring, Maryland.
[25] Phillips, R. E., Ed., Manual of Fluorimetric Clinical Procedures, G. K. Turner Assoc., Inc., Palo Alto, California.
[26] Van Duuren, B. L., and Bardi, C. E., Anal. Chem. **35,** 2198 (1963).
[27] Winefordner, J. D., and St. John, P. A., Anal. Chem. **35,** 2211 (1963).
[28] Samson, J. A. R., Techniques of Vacuum Ultraviolet Spectroscopy (John Wiley & Sons, Inc., New York, 1967), p. 212–216.
[29] Bril, A., Luminescence of Organic and Inorganic Materials (John Wiley & Sons, Inc., New York, N.Y. 1962), p. 477.
[30] Birks, J. B., and Dyson, D. J., Proc. Roy. Soc. **275A,** 135 (1963).
[31] Seybold, P. G., Gouterman, M., and Callis, J., Photochemistry and Photobiology **9,** 229 (1969).
[32] Lewis, G. N., and Kasha, M., J. Am. Chem. Soc. **67,** 994 (1945).
[33] Strickler, S. J., and Berg, R. A., J. Chem. Phys. **37,** 814 (1962).
[34] Wybourne, B. G., Ed., Spectroscopic Properties of the Rare Earths (Interscience Publ., New York, N.Y. 1965).
[35] Patek, K., Glass Lasers, Edwards, J. G., Ed., London (Butterworth & Co., 1970).
[36] Reisfeld, R., Honigbaum, A., Michaeli, G., Harel, L., and Ish-Shalom, M., Israel J. Chem. **7,** 613 (1970).
[37] Reisfeld, R., Greenberg, E., Kirshenbaum, L., and Michaeli, G., Proc. 8th Rare Earth Conference **2,** 743 (1970).
[38] Reisfeld, R., and Hormadaly, J., Proc. 9th Rare Earth Conference, **1,** 123 (1971).
[39] Reisfeld, R. and Eckstein, Y., Solid State Chem. **5,** 174 (1972).
[40] Reisfeld, R., Velapoldi, R. A., Boehm, L., and Ish-Shalom, M., J. Phys. Chem. **75,** 3981 (1971).
[41] Reisfeld, R., Velapoldi, R. A., and Boehm, L., J. Phys. Chem. **76,** 1293 (1972).
[42] Velapoldi, R. A., Reisfeld, R., and Boehm., L., Proc. 9th Rare Earth Res. Conf. **2,** 488 (1971).
[43] Reisfeld, R., and Greenberg, E., Anal. Chem. **47,** 155 (1969).
[44] Turner, G. K., Science **146,** 183 (1964).
[45] Fletcher, A. N., J. Mol. Spectry. **23,** 221 (1967).
[46] Reisfeld, R., Greenberg, E., Velapoldi, R. A., and Barnett, B., J. Chem. Phys. **56,** (4) 1698 (1972).
[47] Reisfeld, R., Glasner, A., and Mustaki, A., Proc. Int. Colloqu. Optic and Spectroscopic Phenomena in Ionic Crystals, Bucharest, 1968; Mustachi, A., Reisfeld, R., and Glasner, A., Israel J. Chem. **7,** 627 (1970).
[48] Reisfeld, R., and Biron, E., Talanta **17,** 105 (1970).
[49] Reisfeld, R., Arye, Z. Gur., and Greenberg, E., Anal. Chim. Acta **50,** 249 (1970).
[50] Reisfeld, R., and Eckstein, Y., Anal. Chim. Acta **56,** 461 (1971).
[51] Teegarden, T., in Luminescence of Inorganic Solids, Goldberg, P., Ed. (Academic Press, New York, N.Y., 1966), p. 83.
[52] Reisfeld, R., Honigbaum, A., and Velapoldi, R. A., J. Opt. Soc. Am. **61,** 1422 (1971).
[53] Scott, A. B., and Hu, K. H., J. Chem. Phys. **23,** 1830 (1955).
[54] Sturge, M. D., Solid State Physics **20,** 91 (1967).
[55] Reisfeld, R., Greenberg, E., Deinum, T., Werkhoven, C. J., and van Voorst, J. D. W., to be published.
[56] Blasse G., and Bril, A., Philips Technical Review **31,** 304 (1970).
[57] Seitz, F., Trans. Faraday Soc. **35,** 74 (1939).
[58] Dexter, D. L., Klick, C. C., and Russel, G. A., Phys. Rev. **100,** 603 (1955).

[59] Glasner A., and Reisfeld, R., J. Phys. Chem. Solids **18,** 345 (1961).
[60] Glasner, A., Rejoan, A., and Reisfeld, R., J. Phys. Chem. Solids **19,** 331 (1961).
[61] Landolt-Bornstein, Zahlenwerte und Funktionen, Bd. **2,** Teil 8, Optische Konstanten (Springer, Berlin, 1962).
[62] Reisfeld, R., and Honigbaum, A., 1972, unpublished results.
[63] Tomura, M., and Nishimura, H., J. Phys. Soc. Japan, **21,** 2081 (1966).
[64] Reisfeld, R., and Morag, S., J. Appl. Phys. Letters **21,** 57 (1972).
[65] Reisfeld, R., Hormodaly, J., and Barnett, B., Chem. Phys. Letters.
[66] Reisfeld, R., and Lieblich, N., unpublished results.
[67] Reisfeld, R., and Kosloff, R., unpublished results.
[68] Reisfeld, R., Velapoldi, R. A., and Greenberg, E., unpublished results.

(Paper 76A6–746)

JOURNAL OF RESEARCH of the National Bureau of Standards—A. Physics and Chemistry
Vol. 76A, No. 6, November–December 1972

Development of a New Fluorescent Reagent and Its Application to the Automated Assay of Amino Acids and Peptides at the Picomole Level *

Sidney Udenfriend

Roche Institute of Molecular Biology, Nutley, New Jersey 07110

(June 15, 1972)

Methods for the assay of amino acids and peptides are most important in elucidating the structure of proteins and peptides. In many important areas of research such as in endocrinology, neurobiology, and genetics, methods are needed with sensitivity higher than is available with the widely used colorimetric ninhydrin procedure. A short while ago, we noted that all primary amines react with ninhydrin and phenylacetaldehyde to give a ternary product which is highly fluorescent. The chemistry of that reaction has now been elucidated and the conditions have been modified and improved so that essentially quantitative yields of fluorescent products are formed with all primary amines. The reaction has been automated and is being used as the detecting system for chromatography of amino acids, peptides and amines in the 10 to 100 picomole range. Problems concerning the fluorescence instrumentation and the isolation and chromatography of these compounds in the picomole range will be discussed.

Key words: Fluorometry, amino acids; fluorometry, peptides; picomole fluorometry.

Collaborative studies by biologists and chemists at Nutley have led to the development of a new fluorometric reagent for amino acids and peptides and its application to their automated assay at the picomole level. The origin of these studies, as well as the chemistry and the analytical applications, are presented in this report.

A number of years ago McCaman and Robins [1][1] reported a highly specific and sensitive fluorometric method for blood phenylalanine assay. The procedure is now generally used for the diagnosis of phenylketonuria. In this method, fluorescence develops when phenylalanine is treated with ninhydrin and a peptide. The other amino acids which are normally found in plasma and protein hydrolyzates give no fluorescence. On the other hand, almost any peptide can be used in the phenylalanine assay.

These very unusual requirements led us to investigate the reaction with the possibility of reversing the conditions to assay peptides fluorometrically by adding ninhydrin plus phenylalanine. When this was tried it worked. Other than phenylalanine, the only α-amino acid which yielded fluorescence (although of far less intensity) was α-aminobutyric acid. This amino acid is not normally present in tissues.

On further investigation, it was found that phenylalanine itself was not the active agent, but was first oxidized and decarboxylated by ninhydrin to phenylacetaldehyde. The latter, in the presence of additional ninhydrin, combined with primary aliphatic amines to yield highly fluorescent derivatives. It was found that several other aldehydes yielded fluorophors with ninhydrin and amines but that the most intense fluorescense by far was obtained with phenylacetaldehyde.

The products obtained on reacting amines, amino acids and peptides with ninhydrin and phenylacetaldehyde all exhibit the same excitation and emission spectra (fig. 1). Excitation maxima are at 275 nm and 390 nm with emission at 480 nm.

To investigate the mechanism of the reaction further, the fluorophor formed on reacting phenylacetaldehyde and ninhydrin with a simple amine, such as ethylamine, was prepared. The purifled product could not be obtained in crystalline form, but was shown to be in equilibrium with a nonfluorescent congener which was apparently a lactone. The latter was crystallized and yielded a molecular ion with the highest mass at 305. This and other findings suggested that the product was the result of a ternary reaction involving one molecule each of amine, phenylacetaldehyde and ninhydrin.

The purified fluorophor obtained with ethylamine was used as a standard to show that under the conditions of the reaction the yield of fluorescent product was about 50 percent. There was considerable variation in the fluorescence obtained with various other amino acids. Much of this was due to differences in quantum yield as well as to completeness of reaction.

* This article is based on studies carried out in collaboration with Wallace Dairman, Keijiro Samejima, Manfred Weigele, Willy Leimgruber, Stanley Stein, and Peter Böhlen.

[1] Figures in brackets indicate the literature references at the end of this paper.

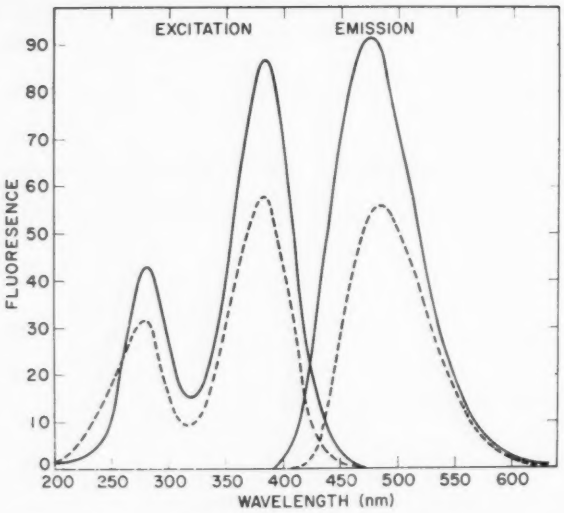

FIGURE 1. Spectral properties of fluorophor obtained on reacting an amino acid with ninhydrin and phenylacetaldehyde.

The procedure was automated with the use of appropriate pumps and a flow cell cuvette in an Aminco Microfluorometer.[2] Application of this automated procedure was made for amino acid analysis. The sensitivity at this stage with most amino acids was found to be below the nanomole level. This compares to a limit of 10 nanomoles for most commercial amino acid analyzers which utilize the colorimetric ninhydrin procedure.

Details of the procedure utilizing ninhydrin and phenylacetaldehyde have been published [2, 3]. It possesses the sensitivity and many other qualities which could have made it a useful analytical procedure. However, elucidation of the mechanism of the reaction [4] led to the development of a new reagent and made it obsolete.

Weigele and Leimgruber and their colleagues at Hoffmann-La Roche in Nutley had been collaborating with us in our studies. They concentrated on the mechanism of the ninhydrin phenylacetaldehyde reaction utilizing mass spectrometry, x-ray crystallography and other procedures on a number of crystalline derivatives. The structure of the fluorophor obtained with ethylamine was proven to be as shown in figure 2. The condensation with ninhydrin and phenylacetaldehyde also yielded two nonfluorescent products which could be converted to the fluorophor by treatment with base.

Brilliant deduction led Weigele and Leimgruber[3] to synthesize the compound, 4-phenylspiro [furan-2(3H), 1^1-phthalan]-3,3^1-dione, RO 20–7234. This compound was found to react with amines to form the identical

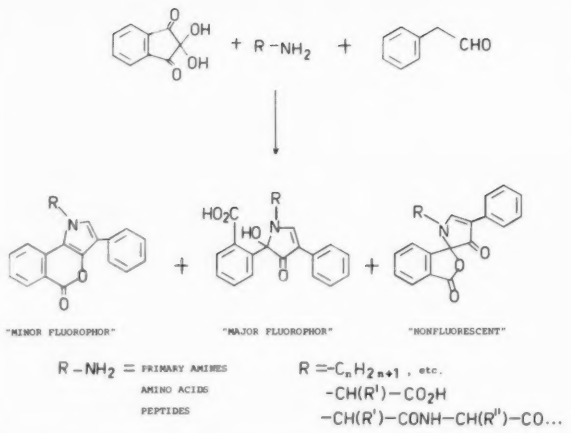

FIGURE 2. Formation of fluorophor from ninhydrin, phenylacetaldehyde and ethylamine.

fluorophor obtained with ninhydrin and phenylacetaldehyde (fig. 3). With this new reagent the reaction is a

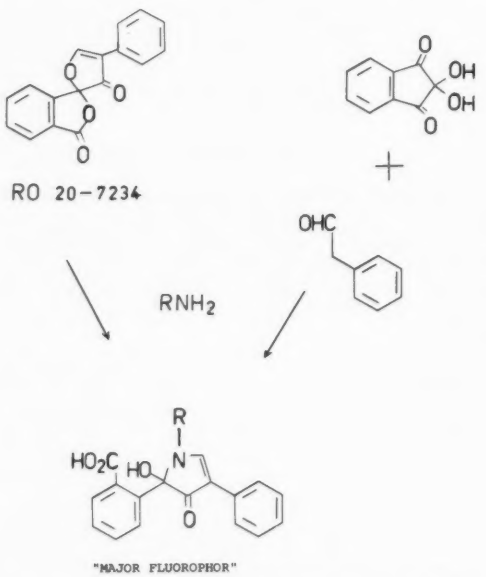

FIGURE 3. Comparison of reactions of amines with RO 20–7234 and with ninhydrin and phenylacetaldehyde.

binary one rather than a ternary one. The resulting advantages are many-fold. The ternary reaction with ninhydrin does not go to completion; about 45 percent with ethylamine and much less for aspartic acid. Yields with the new reagent are almost quantitative with all amines, amino acids and peptides. The ternary reaction is run at 65° for 25 min. The binary reaction is instantaneous at room temperature. In both cases the reagents are nonfluorescent. In the ternary reaction, ammonia does not react at all. With the new reagent, ammonia reacts to a slight extent (one thousandth as

[2] In order to adequately describe materials and experimental procedures, it was occasionally necessary to identify commercial products by manufacturer's name or label. In no instances does such identification imply endorsement by the National Bureau of Standards, nor does it imply that the particular product or equipment is necessarily the best available for that purpose.

[3] Weigle, M., and Leimgruber, W., to be published.

much as a typical amino acid). The conditions of the binary reaction lead to several times more intense fluorescence for the same amount of fluorophor.

The fluorophor obtained with peptides (fig. 4) are

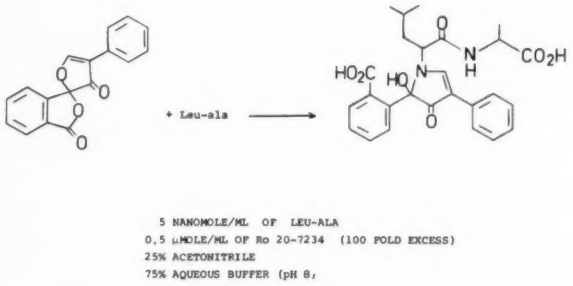

FIGURE 4. Formation of fluorophor with a peptide and the reagent RO 20–7234.

more intensely fluorescent than the fluorophors formed from the corresponding amino acids. This may be due to a greater quantum yield. The free carboxyl group close to the fluorophoric group may quench the fluorescence. Whatever the reason, this is a decided advantage for peptide assay.

The new reagent is ideally suited to detect amino acids and peptides in the automated assay of column effluents. Such assays have now been set up and even with relatively unsophisticated pumping systems and fluorescence instrumentation, it has been possible to carry out analyses in the picomole range. Figure 5 shows the chromatographic separation of an amino acid mixture (neutral and acidic), 250 picomoles of each. Figure 6 shows the chromatographic separation of 50 picomoles each of the basic amino acids.[4]

A number of applications have already been made which make use of this great sensitivity. It has been possible to measure the peptides oxytocin and vasopressin in an aliquot of an extract of a *single* rat pituitary (fig. 7). Thus, the method will be of great

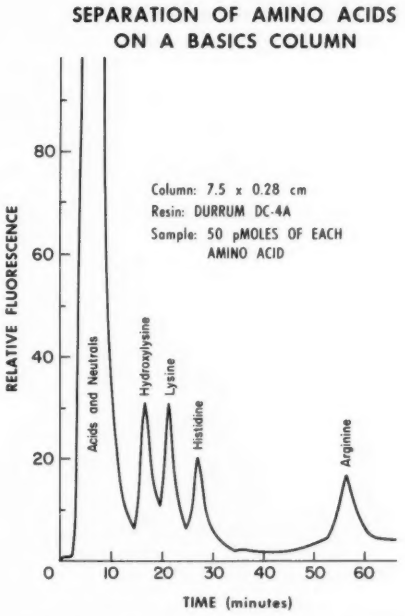

FIGURE 6. Chromatography of basic amino acids in the picomole range.

importance in the isolation and characterization of physiologically active peptides and their metabolites. Another important application has been to the assay of spermine and spermidine. The sensitivity in this case is so great and the tissue levels so high that microgram quantities of brain tissue are sufficient for assay. Most important, the simplicity of the apparatus required to operate in the picomole region using fluorescence should make it possible to devise relatively inexpensive commercial equipment. It is hoped that commercial instruments, which make use of this reagent, will soon be available.

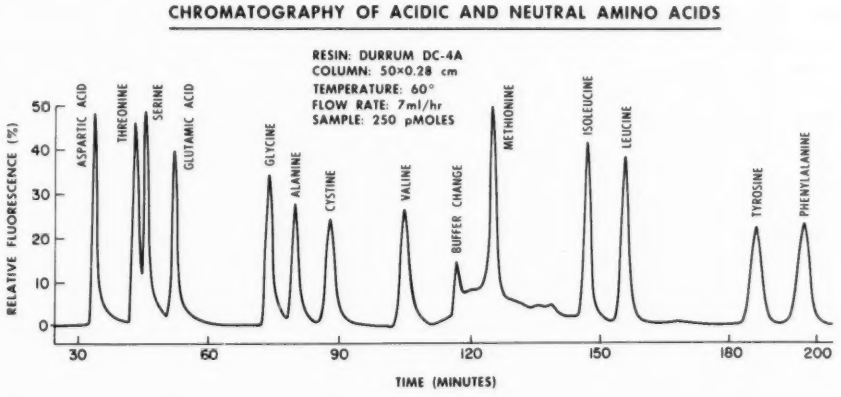

FIGURE 5. Chromatography of neutral and acidic amino acids in the picomole range.

[4] Details of these procedures will be published in a subsequent paper.

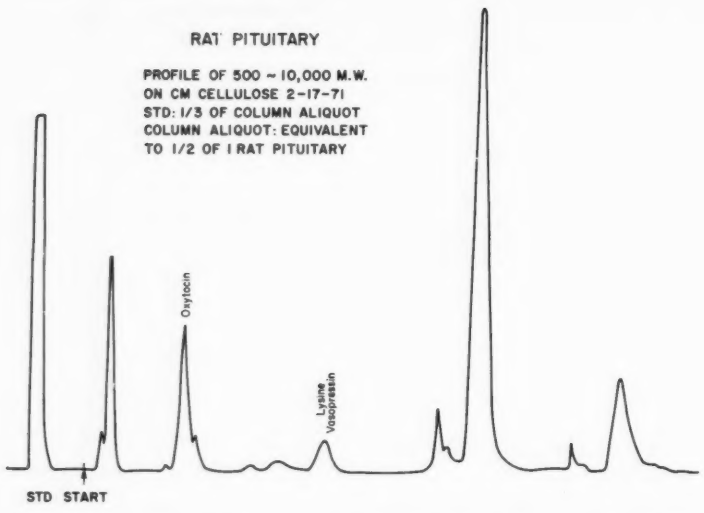

FIGURE 7. Chromatographic separation of the oxytocin and vasopressin in an extract of one rat pituitary.

References

[1] McCaman, M. W., and Robins, E., J. Lab. Clin. Med. **59,** 885 (1962).

[2] Samejima, K., Dairman, W., and Udenfriend, S., Anal. Biochem. **42,** 222 (1971).

[3] Samejima, K., Dairman, W., Stone, J., and Udenfriend, S., Anal. Biochem. **42,** 237 (1971).

[4] Weigele, M., Blount, J. F., Tengi, J. P. Czajkowski, R. C., and Leimgruber, W., J. Am. Chem. Soc. **94,** 4052 (1972).

(Paper 76A6-747)

JOURNAL OF RESEARCH of the National Bureau of Standards—A. Physics and Chemistry
Vol. 76A, No. 6, November–December 1972

Considerations on Organic Compounds in Solution and Inorganic Ions in Glasses as Fluorescent Standard Reference Materials

R. A. Velapoldi

Institute for Materials Research, National Bureau of Standards, Washington, D.C. 20234

(June 30, 1972)

The use of various organic compounds in solution and inorganic ions in glasses has been investigated as possible fluorescence Standard Reference Materials. Emphasis was placed on measuring physical and chemical parameters such as stability, reproducibilities of absorbance and fluorescence measurements, relative quantum efficiencies as a function of excitation wavelength, etc., for quinine derivatives and selected organic compounds. A brief discussion is included on the use of rare earth and non-rare earth inorganic ions in glasses as standards.

Key words: Emission spectra; excitation spectra; fluorescence; fluorescence standards; glass standards; quinine derivatives; rare earths; relative quantum efficiencies; solution standards.

I. Introduction

The rapid growth of publications in fluorimetric research and applications during the last two decades, and the variability of data and results in those publications, underline the need for standardization of fluorescence nomenclature and data presentation. These needs were discussed previously by investigators [1–3][1], who collectively presented a proposal for fluorescence standardization [4]. The main objective of this proposal was to supply a firm basis for reporting fluorimetric results so that comparisons of data among laboratories would be meaningful.

There are basically two methods which can be used for the presentation of data: (a) in absolute radiative or energy units, and (b) by comparing fluorescence data of the compound under study with data obtained for an accepted standard. Very few laboratories are equipped to make absolute radiant energy measurements; however, comparative spectra of standards run under the same experimental conditions on the same instrument can be easily done. This latter method, which effectively corrects for instrumentally dependent perturbations on the true fluorescence spectra is most widely used and applicable provided the users know the limitations, not only of their instrumentation, but also of the standard.

Not included here are fluorimetric measurements obtained on "uncorrected" instruments which are presented without units of intensity or benefit of comparative measurements. Many of these types of published results have led to confusion and are often of no quantitative value.

Fluorescence standards can be used to (a) correct spectra for instrumental parameters such as the wavelength dependence of exciting lamp intensity, monochromator transmission and detector response, (b) determine comparative quantum efficiencies, (c) compare data among laboratories, (d) determine periodically "in house" instrumental stabilities, (e) calibrate fluorescent lifetime determinations, and (f) calibrate polarization value measurements.

The requirements for a "general" fluorescence standard are quite specific. It should:

(a) have broad fluorescence spectra,
(b) be easily purifiable,
(c) be stable in solution or as the solid,
(d) have as little overlap as possible between the excitation (absorbance) and emission spectra,
(e) not be subject to oxygen quenching,
(f) have a constant quantum efficiency as a function of exciting wavelength,
(g) have isotropic emission,
(h) have the same emission spectrum shape independent of exciting wavelength,
(i) be soluble in aqueous and organic solvents, and
(j) absorb and emit in the same general regions as the compound under study.

No single compound exhibits all these desirable characteristics. In fact, the last requirement precludes the use of a single standard, for although absorbance may occur over a wide range (e.g. rhodamine B absorbs from 200 nm to about 560 nm), emission is usually limited to one small wavelength interval (for rhodamine B, 550 nm to 650 nm with maximum at 573 nm).

For this reason, in addition to the fact that fluores-

[1] Figures in brackets indicate the literature references at the end of this paper.

cence spectra are composites of true spectra and instrumental parameters dependent on wavelength, it is necessary to have available a series of fluorescence standards with emission maxima that covers the wavelength range of current interest. With the wide use of lasers and interest in radiative measurements in the near-infrared, this range now extends from 250 nm to 1100 nm.

One of the major objectives of the fluorescence program at the National Bureau of Standards is the selection, production, and certification of a series of fluorescence standards (Standard Reference Materials) which can be used for the standardization and comparison of data and methodologies among laboratories [5, 6]. It is essential that these Standard Reference Materials (SRM's) be certified with absolute values. Data reported here, however, are in relative units and not absolute since instrumentation for absolute measurements is not available at the present time. Absolute measurements will be made and values assigned to the SRM's as soon as instrumentation becomes available.

The work at NBS is following two parallel investigative paths: (a) the use of solutions of organic molecules and metal chelates in various solvents, and (b) in close collaboration with Reisfeld, The Hebrew University, Jerusalem, the use of inorganic ions in solid matrices. Group (b) may be further split into rare earth and non-rare earth inorganic ions. The investigative work on the inorganic ions has been covered extensively earlier in this series of papers by Reisfeld [7]. Discussion here, then, will be restricted primarily to the use of comparative standards in solution and some of the factors which affect quantum yields and spectra.

Since quinine and its derivatives are probably the most widely used comparative standards [13], and since a great deal of controversy exists as to their usefulness as standards, the emphasis of this paper is on the reproducibility, stability, and effects of wavelength excitation and acid concentration on the spectra and quantum efficiencies of the quinines.

I would like to digress briefly and discuss some of the equations and assumptions which have to be made in using comparative techniques and standards. Two types of solutions may be employed: optically dense and optically dilute. With optically dense solutions and front surface excitation and emission, Vavilov's experimental set up with some modifications is generally used [1, 8–12]. This method is not as widely utilized as the optically dilute method since stray light is high, compounds with large emission and excitation overlap give erroneous results, and only compounds with a high molar absorptivity can be used easily [13].

The optically dilute method is based on the Beer-Lambert Law and several assumptions. Combining the definition of quantum efficiency [14], eq (1),

$$Q=\frac{I_F}{I_A} \tag{1}$$

where Q = luminescence quantum efficiency
I_F = rate of fluorescence emission in quanta/s.
I_A = rate of light absorption in quanta/s.

with the Beer-Lambert Law, eq (2),

$$\frac{I_T}{I_0}=e^{-\epsilon cl} \tag{2}$$

where I_0 is the radiative flux of the exciting light in quanta/s,
I_T is the radiative flux of the transmitted light in quanta/s.
ϵ is the molar absorptivity in liter, mole^{-1}, cm^{-1},
c is the concentration in moles/liter,
l is the path length of the cell in cm,

and expanding the exponential term in a power series, the expression for the rate of light emission becomes [3, 13, 15]:

$$I_F=I_0(2.3\epsilon cl)\left[1-\frac{2.3\epsilon cl}{2}+\frac{(2.3\epsilon cl)^2}{6}-\cdots\right]Q. \tag{3}$$

For dilute solutions (i.e. absorbances less than 0.05), eq (3) may be approximated with only slight error by eq (4) [15],

$$I_F=I_0(2.3\epsilon cl)\,Q. \tag{4}$$

In determining comparative quantum efficiencies, a term for the index of refraction of the solvent is added [16–18], resulting in the final form of the applicable equation:

$$Q_u=Q_s\left(\frac{FA_u}{FA_s}\right)\left(\frac{A_s}{A_u}\right)\left(\frac{I_{0s}}{I_{0u}}\right)\left(\frac{\eta_u^2}{\eta_s^2}\right) \tag{5}$$

where Q is the quantum efficiency,
FA is the integrated fluorescence area (Σ quanta/unit bandwidth),
I_0 is the radiative flux of the exciting light in quanta/s,
η is the average refractive index of the solvent over the emission wavelength range, and
u and s refer to the unknown and standard, respectively.

In the studies reported here, comparative quantum efficiencies were calculated using eq (6) [20]:

$$Q_u=Q_s\left(\frac{FA_u}{FA_s}\right)\left(\frac{A_s}{A_u}\right)\left(\frac{\lambda_{ex_s}}{\lambda_{ex_u}}\right)\left(\frac{\eta_u^2}{\eta_s^2}\right) \tag{6}$$

where $\lambda_{ex_s}/\lambda_{ex_u}$ replaces I_0 and converts from an instrumentally produced constant energy to quanta/s.

The assumptions have been made, however, that (a) instrumental geometries are the same for the unknown and standard, (b) emission is isotropic, (c) the exciting light is monochromatic if excitation for both samples is

at different wavelengths, (d) no reabsorption and re-emission occur, and (e) the absorption is less than 0.04. (Recent work permits solutions with absorbances of 0.2 to 1.0 to be measured by the sideview technique [21, 22].) In addition, use of dilute solutions minimizes factors (d) and (e), and use of the same instrument and cuvette minimizes factor (a). Anisotropic emissions (polarization effects) may cause large measurement errors which may be corrected [13, 23]; but the easiest way to avoid polarization problems is to use a standard which emits isotropically.

Assuming then that corrected spectra may be obtained [11, 12, 15], the fundamental problem in spectrofluorimetry is the lack of well-characterized standards. Table 1 lists various organic compounds which have been suggested for possible inclusion in a series of fluorescence standards [1, 3, 10, 24, 25]. Some may not be suitable as general standards. Fluorescein undergoes degradation in sodium hydroxide, and solutions should be prepared and used within 12 hours. The purification of β-naphthol by recrystallization in air results in some discoloration due probably to oxidation. Aromatics such as anthracene and pyrene have narrow emission and/or excitation spectra (25 nm or less) and are not suitable as standards for fluorimeters which use wide slits since fluorescence spectra, as absorption spectra [26], are bandpass dependent [27, 28]. Other factors, such as acid concentration or excitation wavelength, are reported to affect the fluorescence of quinine and quinidine sulfates [21, 28–37] and 3-aminophthalimide [38]. The presentation and discussion of some of these factors and their effects, follow. The experimental section is presented as addendum A.

TABLE 1. Compounds proposed as fluorescence standards [1, 3, 8–10]

Compound	Emission maxima (nm)
β-Naphthol	354, 402
2-Aminopyridine	368
Anthracene	383, 404, 428, 454
Pyrene	390
Quinine sulfate	454
Quinidine sulfate	454
3-Aminophthalimide	510[a]
Fluorescein	518
N,N-Dimethylamino-*m*-nitrobenzene	542
Rhodamine 6G	557
Aluminum(III)-PBBR-chelate	635
4-Dimethylaminonitrostilbene	742

[a] Value is average.

The following abbreviations are used in this paper: Q – quinine; QS – quinine sulfate; QDS – quinidine sulfate; 3-APT–3-aminophthalimide; N,N-DMAMNB–*N,N*-dimethylamino-*m*-nitrobenzene. Quinine samples are designated A, B, C, etc. and are listed in addendum A.

II. Results and Discussion

A. Quinine Sulfate and Related Compounds

1. Physical and Chemical State

It has been reported that the history of the quinine determines its optical characteristics [24, 35]. A report by Fletcher [28], however, suggests this is not the case, and that the observed differences were probably due to the presence of varying amounts of hydrated water. Although quinine sulfate is obtained as the dihydrate, varying amounts of water are definitely present. Table 2 summarizes the weight losses as determined by thermogravimetric (TGA) measurements for various quinine derivatives before and after vacuum drying. It can be seen that with no

TABLE 2. Water weight losses of various quinine derivatives as a function of pretreatment

Sample[a]		Percent weight loss	Calculated molecular formula
F	No drying	4.24	QS[b]·5.4H_2O
C	No drying	4.96	QS·5.7H_2O
E	No drying	[c]4.37	QS·5.0H_2O
E	Vacuum dried, in desiccator for 6 months	0.18	QS·2.1H_2O
E	Vacuum dried within 24 hours	.03	QS·2.0H_2O
H	No drying	4.36	QDS[d]·5.4H_2O
H	Vacuum dried within 24 hours	0.02	QDS·2.0H_2O
J	No drying	.00	Q[e]·2.0H_2O

[a] See experimental section for designation.
[b] QS = quinine sulfate.
[c] Average of two determinations.
[d] QDS = quinidine sulfate.
[e] Q = quinine.

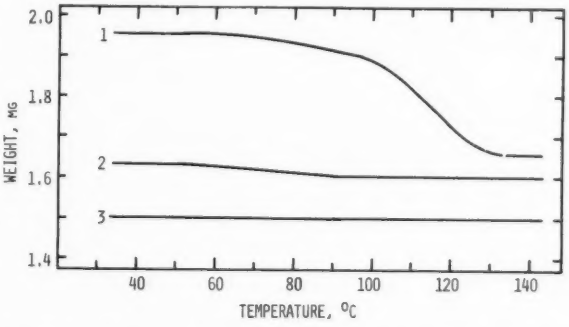

FIGURE 1. Thermogravimetric analyses of quinine sulfate (Sample E). 1. undried after recrystallization; 2. dried in vacuo at 55 °C for 18 hours, placed in desiccator, removed periodically to obtain sample; 3. freshly dried as 2. Heating rate was 5.0 °C/min in dry air. Weight scale offset 10 mg.

474-414 O - 73 - 7

drying, approximately 5 to 6 waters of hydration per molecule rather than 2 are actually present. Figure 1 shows three TGA curves obtained for $QS \cdot 2H_2O$, sample E. There is a slight loss of water for the vacuum dried sample that had been kept in a desiccator for six months and removed periodically to obtain samples which shows the hygroscopic nature of $QS \cdot 2H_2O$. As pointed out by Fletcher [28], insufficient drying can cause variations in absorbance values, leading investigators to propose the inequivalence of quinine derivatives. For this reason, samples used for the following studies were predried as outlined in the experimental section.

2. *Absorbance Measurements*

Average weight absorptivities for various $QS \cdot 2H_2O$ samples from different suppliers with varying recrystallizations were calculated from eq (7), and the results are summarized in table 3.

$$WA = \frac{A}{cl} \tag{7}$$

where WA is the weight absorptivity.
A is the absorbance.
c is the sample concentration in grams solute/gram solvent.
l is the path length of the cell in cm.

Sample F gave consistently high weight absorptivities, but was included in the statistical analyses. The average weight absorptivities at 317.0, 347.5, and 365.0 nm for samples A to F differ from previous data [28] by −1.2 percent, +0.5 percent, and −2.3 percent in that order. Values for the average of all samples, including E, differ from previous data by −1.0 percent, −0.5 percent, and −1.0 percent in that order.

TABLE 3. Determination of weight absorptivities for quinine sulfate with varying recrystallizations in 0.1 N H_2SO_4 from different suppliers

Sample[a,b]	Rx[c]	Weight absorptivities × 10^4			
		365.0 nm	347.5 nm	317.0 nm	250.0 nm
A	0	0.922	1.430	1.148	7.720
B	0	.916	1.418	1.146	7.700
C	0	.918	1.428	1.145	7.710
D	3	.922	1.438	1.140	7.820
F	4	.941	1.454	1.162	7.920
E	6	.925	1.436	1.152	7.820
E'[d]	6	.947	1.445	1.146	7.717
Average[e]		0.924	1.434	1.149	7.782
σ		.009	0.012	0.008	0.086
Percent σ		.97	.84	.66	1.12

[a] All samples vacuum dried at 50–60 °C for 24 hours.
[b] See experimental section for sample designation.
[c] Times recrystallized.
[d] Absorbances measured on Cary 16, others on Cary 14, see addendum A.
[e] For samples A–F only (excluding E').

Determination of the weight absorptivities at 347.5 nm for three individual weighings of sample E yielded a value of 1.436 ± 0.005. Weight absorptivities and molar absorptivities are also given for $QDS \cdot 2H_2O$ in

TABLE 4. Molar and weight absorptivities (× 10^4) of quinine and quinidine sulfates in 0.1 N H_2SO_4

Compound	Concentration $M \times 10^{-5}$	Sample	Wavelength							
			365.0 nm		347.5 nm		317.0 nm		250.0 nm	
			ϵ[c]	WA[d]	ϵ[c]	WA[d]	ϵ[c]	WA[d]	ϵ[c]	WA[d]
Quinine sulfate[a]	2.554	E	0.7235	(0.924)	1.1228	(1.434)	0.8996	(1.149)	6.0930	(7.782)
Quinidine sulfate[b]	3.269	H	.7189	(0.918)	1.1257	(1.438)	.8902	(1.138)	6.0110	(7.676)

[a] Average for 6 determinations, samples A–F, table 2.
[b] Average for two determinations.
[c] l, mol^{-1}, $cm^{-1} \times 10^4$.
[d] $g_{solvents}, (g_{solute})^{-1}$, $cm^{-1} \times 10^4$.

table 4. As expected, the molar and weight absorptivities for $QS{\cdot}2H_2O$ agree with those for $QDS{\cdot}2H_2O$ since they are stereoisomers (structures for quinine and quinidine are I and II, respectively).

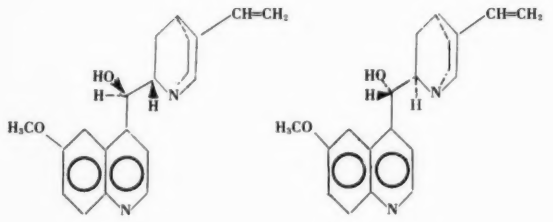

I. Quinine II. Quinidine

A single determination for the molar or weight absorptivities for quinine dihydrate gave results which, as a function of wavelength, were consistently 3 to 5 percent low as compared to the values for QS and QDS after correction for the difference in molecular weights. Plotting relative absorbances, i.e. A_λ/A_{250nm} versus wavelength, however, resulted in good agreement among the three spectra, figure 2, indicating the probable presence of a systematic error in the determination of the absorptivities for quinine dihydrate. These values are being redetermined.

Values of the ratios for several absorbance peaks of QS in 0.1 *N* sulfuric acid have been calculated from the literature [28–30, 33, 36, 46–48], and these values and those from the present work are reported in table 5. Although systematic errors exist since various spectrophotometers were used, comparison of the average of the literature values and the present work show differences to be +2.77, +0.25 and +0.62 percent. The first value is for the A_{250}/A_{347} ratio, and measurements in the ultraviolet are usually not as accurate or precise as those in the visible. Statistical evaluation (again

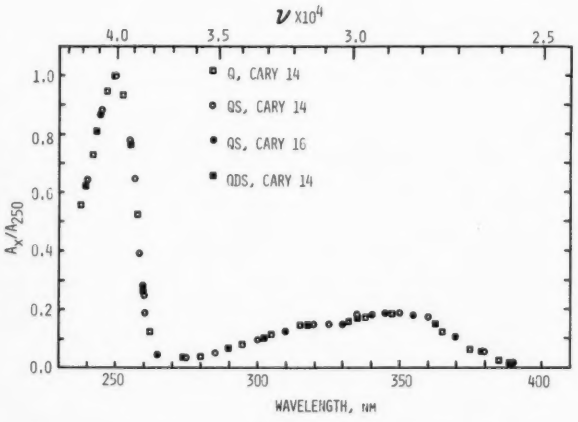

FIGURE 2. Normalized absorbance spectra of quinine (Q), quinine sulphate (QS), and quinidine sulfate (QDS) in 0.1 *N* H_2SO_4 using absorbance at 250.0 nm as 1.0. Temperature, 25.0 °C.

TABLE 5. Absorbance ratios for quinine sulfate dihydrate in 0.1 *N* sulfuric acid

Spectrophotometer	A_{250}/A_{346}	A_{317}/A_{346}	A_{365}/A_{346}	Ref.
Cary 16	5.340	0.793	0.655	this work
Cary 14	5.43	.80	.64	this work
Cary 14	5.38	.78	.65	[33]
Cary 14	5.36	.80	.62	[30]
Beckman D.U		.82	.63	[47]
Beckman D.U	5.43	.80	.59	[29]
Bausch and Lomb	5.23	.80	.63	[30]
Turner 210	5.4	.82	.66	[28]
	5.0	.75		[46]
	5.25	.80	.65	[48]
	5.10	.82	.69	[36]

including systematic errors) of all the ratios shows, however, that any individual ratio may be as much as 4 or 5 percent high or low at only the 68 percent confidence level. It is essential that accurate data be obtained for absorbance measurements, especially since the determinations of relative quantum efficiencies depend on these measurements, eqs (5) and (6).

The instruments used for the absorbance measurements in the present work were checked for accuracy by comparison against optically neutral filters supplied by Mavrodineanu [26]. Absorbance measurements were also made on solutions of QS and 3-APT in 0.1 *N* sulfuric acid at peak maxima using various instruments. The results are summarized in table 6. Good agreement was observed for these solutions. No

TABLE 6. The determination of absorbances of quinine sulfate and 3-aminophthalimide in 0.1 *N* H_2SO_4 using various spectrophotometers

QS A, 250.0 nm	3-APT A, 385.0 nm	Instrument
	0.9164	NBS [26]
0.7506	.9158	Cary 16
.751	.919	Cary 14
.749	.914	Turner 210

apparent fluorescence artifact was observed as shown by comparing absorbances from the first three instruments with those of the last instrument which has a monochromator between the sample and the detector [20, 23].

Differences as large as 8 percent, however, were observed when absorbances were measured on slopes in absorbance spectra. Care must therefore be used when absorbance measurements are made on slopes of peaks since small errors in wavelength (and also large bandwidths if the slope is steep) result in inaccurate absorbance values.

3. *Fluorescence Measurements*

Studies were made to determine fluorescence reproducibility of measurements on quinine sulfate dihydrate (sample E) in 0.1 *N* sulfuric acid. Table 7 summarizes results of repetitive measurements on five different quinine sulfate solutions.

474-414 O - 73 -

TABLE 7. Reproducibility of repetitive fluorescence measurements on different solutions of quinine sulfate dihydrate

(Sample E) in 0.1 *N* sulfuric acid[d]

Concentration (ppm)	Average emission peak area	σ	Percent σ
0.5[a]	0.053	0.002	2.83
1.0[a]	.104	.002	1.92
1.0[b]	.104	.001	1.09
2.5[a]	.260	.002	0.85
5.0[a]	.706	.003	.42
5.0[b]	.518	.001	.22
10.0[a]	.915	.007	.78
10.0[b]	.911	.003	.32
5.0[c]	.517	.003	.59

[a] Dilution by volume, four sample weighings.
[b] Dilution by weight, three sample weighings.
[c] Quinidine sulfate dihydrate (Sample H) dilution by weight.
[d] λ_{ex}, 350 nm.

Fairly large standard deviations were obtained with the 0.5 and 1.0 ppm solutions, probably due to instrumental noise resulting from increased instrumental sensitivity. As can be seen, dilution by weight yields results for which standard deviations are approximately two times lower than those for dilution by volume. Similar results were obtained for solutions of quinidine sulfate [38]. All weighings of the vacuum-dried solid samples were made in air. Weighing in a dry nitrogen atmosphere should result in lower percent standard deviations since the dried material is somewhat hygroscopic.

Similar fluorescence measurements made on solutions of quinine sulfate samples from two different sources (samples A, B, D, and F), results summarized in table 8, show that the relative integrated area under the fluorescence peak may be considered to be the same if percent standard deviations of 1 to 3.0 percent are acceptable.

TABLE 8. Measurement of fluorescence peak areas using quinine sulfate dihydrate from two sources[a]

Sample	Emission peak areas: One day average	Three day average
A	0.555	0.554
B	.542	.544
D	.552	.556
F	.564	.558
Average	.553	.553
σ	.009	.006
Percent σ	1.64	1.12

[a] λ_{ex}, 350.0 nm; °C = 25.0.

Studies were also initiated to determine the stability of quinine sulfate (sample E) in 0.1 *N* sulfuric acid since little definitive data exist concerning the stability of QS in solution [43, 44, 49]. Table 9 summarizes results for "stabilities" during two "short time" (1 to 10 h) tests, while table 10 and figure 3 summarize results for longer periods of time (25 to 35 days). As might be expected, the results in table 9 show stabilities are better for the 1 hour determinations than for those stretching over a 10 hour period. From table 10, it is observed that glasses give more repeatable values and thus lower percent standard deviations. It is evident from the data in tables 9 and 10 and figure 3 that the results are actually composites of quinine sulfate solution stability and instrumental stability. The latter was maximized by using the overlapping solution method, and the results from this study are graphically illustrated in figure 4.

TABLE 9. Statistical analyses for fluorescence determinations[c] of quinine sulfate dihydrate (Sample E) in 0.1 *N* H_2SO_4 during two "short" time intervals

Concentration (ppm)	1.0[a]	5.0[a]	10.0[a]	1.0[b]	2.0[b]	2.0[b]
H_2SO_4, *N*	0.1	0.1	0.1	0.1	0.1	0.01
$\bar{A}$, peak area	.105	.557	1.116	.411	.816	.848
σ	.004	.003	.005	.001	.002	.001
Percent σ	4.34	.59	.49	.21	.24	.14

[a] Eleven determinations during a 10 hour span (same solution).
[b] Four determinations during a 1 hour span (same solution).
[c] λ_{ex} = 350.0 nm; °C = 25.0.

TABLE 10. Fluorescence peak areas of quinine sulfate and a uranium doped glass as a function of time on corrected and uncorrected instruments

	Instrument A, corrected [20] QS, Sample E[a,b]	Instrument B, uncorrected QS, Sample E[a,c]	Instrument B, uncorrected Uranium glass[c]
Average peak area	0.739	0.398	0.383
σ	.011	.027	.018
Percent σ	1.49	6.89	4.80

[a] 2.0 ppm in 0.1 *N* H_2SO_4.
[b] Fifteen measurements covering 26 days.
[c] Fourteen measurements covering 37 days. The uranium glass was too concentrated for use in the corrected instrument.

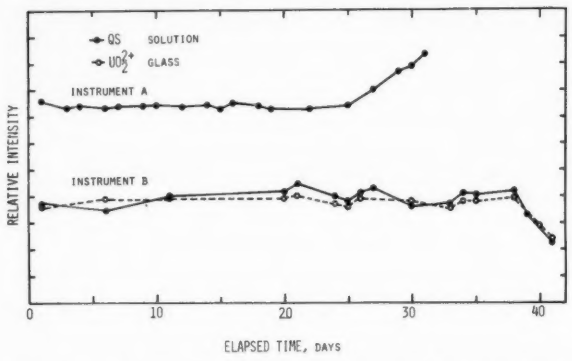

FIGURE 3. Instrumental and compound stability determinations using 2 ppm (μg solute/g solvent, 2.55×10^{-6} *M*) quinine sulfate in 0.1 *N* H_2SO_4 and a uranyl glass on corrected (instrument A) and uncorrected (instrument B) spectrofluorimeters.

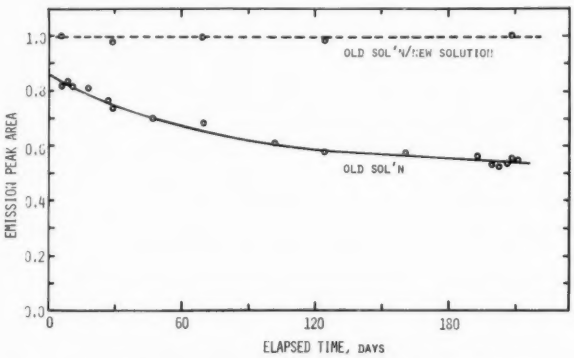

FIGURE 4. 2 ppm (2.55×10^{-6} *M*) quinine sulfate stability test in 0.1 *N* H_2SO_4 using relative emission peak areas as a function of time, designated by solid line and overlapping solution method (peak area original solution/peak area fresh solution), designated by broken line.

A 37 percent decrease in relative peak area as a function of time was observed (solid line) which, on face value, would indicate instability of the quinine sulfate in solution. Preparing new solutions, however, and comparing the peak areas to those of the "aged" solution gave ratios of one (designated by dashed line) proving quinine sulfate stability in solution over this period of time. The assumption was made that dried QS in a desiccator in the dark was stable over the 6-month period of time. Absorbance measurements for the freshly prepared QS solutions agreed within the standard deviations presented in table 3. The observed 37 percent decrease in peak area was due therefore to an instrumental factor and not QS instability.

No long term data as to the stability of quinine sulfate in a 0.1 *N* sulfuric acid solution in light have been established; however, preliminary results indicate that a 2 ppm solution is stable for 2 weeks if irradiated by typical laboratory fluorescent lighting [38]. Excitation in this study was done at 350 nm and emission peak areas were measured in the usual manner. However, Melhuish [50] reports a 25 percent decrease in fluorescence intensity upon irradiation of the QS solution with 313 nm light (and excitation at 313 nm). Excitation at this wavelength also resulted in a deviation of quantum efficiency as a function of excitation wavelength [13, 21]. The problems which arise when this wavelength is used should be investigated.

4. Corrected Excitation and Emission Spectra

To insure consistency in relative quantum efficiency measurements with instruments that give corrected spectra, the excitation spectrum should be compared with the absorbance spectrum and the emission spectrum compared with corrected spectra obtained by other investigators.

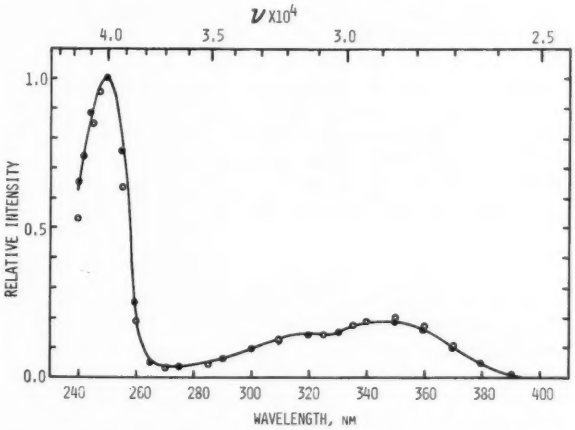

FIGURE 5. Normalized intensities which show equivalency of absorbance spectrum (solid line) and excitation spectrum (circles). Quinine sulfate solution 20 ppm (2.55×10^{-5} *M*) for absorbance spectrum and 2 ppm (2.55×10^{-6} *M*) for excitation spectrum, both in 0.1 *N* H_2SO_4; excitation bandwidth, 25 Å, emission bandwidth, 100 Å; temperature, 25.0 °C.

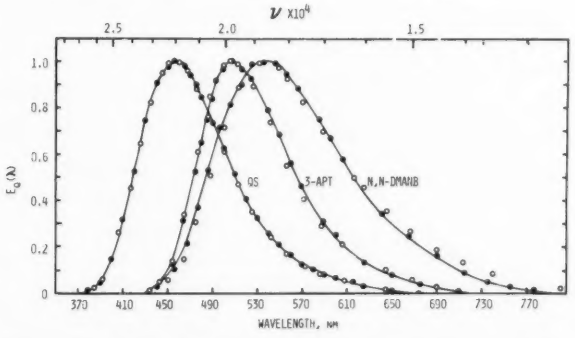

FIGURE 6. Relative $E_q(\lambda)$ versus wavelength for quinine sulfate [2 ppm (2.55×10^{-6} *M*) in 0.1 *N* H_2SO_4], 3-aminophthalimide [5.64 ppm (2.68×10^{-5} *M*) in 0.1 *N* H_2SO_4], and N,N-dimethylamino-*m*-nitrobenzene [2.76 ppm (9.34×10^{-6} *M*) in 70 percent *n*-hexane: 30 percent benzene, V/V] ● = this study, ○ = Lippert, et al., [1] corrected from $E_q(\nu)$ to $E_q(\lambda)$ [50].

The equivalency of the excitation spectrum and absorbance spectrum is shown in figure 5, which has, as a direct consequence, the constancy of quantum efficiency as a function of excitation wavelength (discussed later). Some deviation is seen at wavelengths >350 nm as might be expected with the reported shift in emission maximum as a function of excitation wavelength [29, 31]. The emission spectra of QS and 3-APT in 0.1 *N* sulfuric acid and N,N-DMAMNB are given in figure 6 as $E_q(\lambda)$ versus λ in which $E_q(\lambda)_{max}=1$. Data show good agreement with those taken from Lippert, et al. [1] which were corrected to $E_q(\lambda)$ from $E_q(\nu)$ by multiplying $E_q(\nu)$ by λ^{-2} [50].

5. *Relative Quantum Efficiencies*

a. Intercomparative Study.—To verify the validity of the relative quantum efficiency (QE) measurements, an intercomparative study was undertaken using QS, fluorescein, pyrene, rhodamine B, and 3-APT in various solvents as comparison "standards." Table 11 summarizes the results of this study. The values of the quantum efficiencies for quinine or its derivatives in sulfuric acid have been reported to be in the range 0.40 to 0.70 [12, 21, 32, 34, 35, 37, 43–45]. Melhuish [43] and Dawson and Windsor [21] have measured the absolute quantum efficiency for QS in 1.0 *N* sulfuric acid and obtained excellent agreement (0.546 and 0.54 ± 0.02, respectively, $\lambda_{ex}=365$ nm). Measurements by Eastman [35] tend to support these findings. Systematic errors [13] have been suggested to explain low values of 0.46 or less by Rusakowicz and Testa [24] and Drobnik and Yeargers [34]. The quantum efficiencies chosen for this comparative study are the widely used and accepted values of 0.55 and 0.51 in 1.0 and 0.1 *N* sulfuric acid, respectively [43].

It is difficult to reconcile the results of this intercomparative study and many others with those of Scott, et al. [37], who recently reported the quantum efficiency of QS in 0.1 *N* sulfuric acid, based on lifetime measurements, as 0.70. It has been reported that QS has an anomalous lifetime [45, 51], and thus basing quantum efficiencies on this measurement alone is questionable. In addition, Scott, et al., suggest that the discrepancies in quantum efficiencies may be explained if previous investigators had ignored the red "tail" (>550 nm) of the corrected emission spectrum. An examination of the corrected emission spectra, however, figure 6 [1], shows that the spectra extend quite far into the red (>650 nm).

Quantum efficiencies for fluorescein in sodium

TABLE 11. Results of the intercomparative quantum efficiency (QE) study [e]

	Solvent	QE	QE (lit.)
QS[a]	0.1 *N* H_2SO_4	0.51 ± 0.01	0.508[43]
QDS[b]	.1 *N* H_2SO_4	$.52\pm0.01$	
Fluorescein[c]	.1 *N* NaOH	$.87\pm0.03$	[d] .88
Pyrene[b]	Toluene	$.57\pm0.04$	.60[21], 0.32[51]
Rhodamine B [b]	Ethanol	$.72\pm0.02$	.69[3], 0.71[13]
3-Aminophthalimide[b]	0.1 *N* H_2SO_4	$.47\pm0.02$	

[a] Determined by intercomparison study with fluorescein, pyrene and rhodamine B.
[b] Duplicate determinations, duplicate measurements.
[c] Quadruplicate determinations, duplicate measurements.
[d] Average of 16 literature values, see text.
[e] Temperature, 25.0 ± 0.1 °C.

TABLE 12. Dependence of the relative quantum efficiencies of quinine and quinidine sulfates on sulfuric acid concentrations [a]

	Quantum efficiencies				
	$QS\cdot 2H_2O$				$QDS\cdot 2H_2O$
$[H^+]$, *N*	This work	[21]	Percent [c]	Percent [32]	This work
0.01	0.52 ± 0.01		+1.97		
.02	.52		+1.57		
.10	[b] .51	0.50	—		0.52
.50	.54		+5.71		
1.02	$.55\pm0.01$	.54	+7.68	6	.55
2.00	.57		+9.84		
3.56	$.60\pm0.01$	.60	+17.72	13	.59

[a] Temperature, $25.0\pm.1$ °C, $\lambda_{ex}=350.0$ nm.
[b] Reference.
[c] Using 0.51 as 100 percent.

hydroxide have been reported to cover the range 0.76 to 0.96 [3, 9, 21, 23, 52–61]; however, the most widely accepted value is 0.90 plus or minus five percent [13]. The values quoted for pyrene and rhodamine B are less widely accepted: e.g. values of 0.97 and 0.92 have been reported for rhodamine B [23, 57], although it was reported the measurements in these cases were not made with a red-sensitive photomultiplier [13].

b. Acid Concentration.—The variability of quantum efficiency of quinine sulfate as a function of three sulfuric acid concentrations has been reported [21, 32]. These studies were extended to cover eight acid concentrations, as summarized in table 12. The results for the 0.1, 1.0, and 3.5 *N* sulfuric acid concentrations agree well with those reported by Dawson and Windsor [21] and Eisenbrand [32], although the latter reported a constant quantum efficiency for sulfuric acid concentrations from 0.01 to 0.2 *N*. The increases for acid concentrations less than 0.1 *N* are small, but apparently real, since Chen also observed this same phenomenon and suggested that this was due to less quenching by the sulfate ion at low acid concentrations [62]. Although the weight absorptivities of QS and QDS in three different acid concentrations agree within experimental error, table 13, a slight trend towards lower absorbances

TABLE 13. Weight absorptivities [a] of quinine and quinidine sulfates as a function of H_2SO_4 concentration [b]

	WA [a] × 10^4 at 347.5 nm	
$[H_2SO_4]$ *N*	QS	QDS
0.10	1.43	1.44
1.02	1.40	1.41
3.55	1.39	1.40

[a] See equation (7).
[b] Temperature 25.0 °C.

may be noted. Coupled with the increased fluorescence area as $[H^+]$ increases, the observed increase in quantum efficiency may be explained simply by ionization changes; however, discussions by Chen [29, 62] appear to negate this explanation. Further work is being done to resolve these discrepancies.

The increase in quantum yield of QS as a function of acid concentration is paralleled by QDS as might be expected due to their similarities in spectra, figure 2 [30, 47] and molar absorptivities, tables 4 and 13.

c. Excitation Wavelength.—The quantum efficiencies of quinine sulfate, figure 7, rhodamine B, and rhodamine 6G, figure 8 (others discussed later) were found to be independent of excitation wavelength (±5 percent). The largest deviations for QS were found from 260 to 280 nm where the absorbance is at a minimum and larger errors would be expected. Several investigators [21, 29, 36] reported a variation in quantum efficiency of fluorescence intensity as a

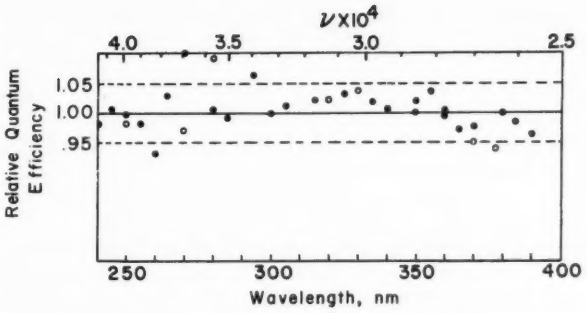

FIGURE 7. Relative quantum efficiencies of quinine sulfate as a function of excitation wavelength (● = this work), quinine sulfate concentrations: λ_{ex} = 240–290 nm, 0.1 ppm (1.28×10^{-7} *M*) and 0.5 ppm in 0.1 *N* H_2SO_4; λ_{ex} = 260–390 nm, 2.0 and 2.5 ppm (6.39×10^{-7} *M*) in 0.1 *N* H_2SO_4; excitation bandwidth, 25 Å; emission bandwidth, 100 Å; temperature, 25.0 °C; ○=Fletcher [28].

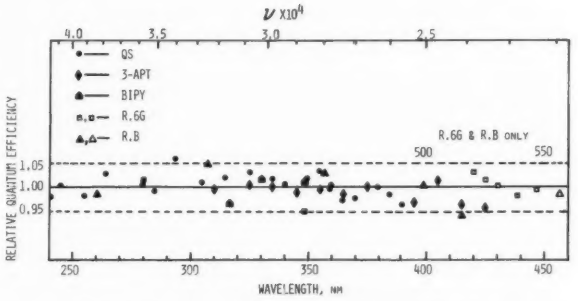

FIGURE 8. Relative quantum efficiencies as a function of excitation wavelength: quinine sulfate—same conditions as figure 7;3-aminophthalimide, 5.64 ppm (2.68×10^{-5} *M*) in 0.1 *N* H_2SO_4; bipyrenyl (BIPY), 0.14 ppm (2.98×10^{-7} *M*) in toluene; rhodamine 6G (R.6G), 0.12 ppm (2.08×10^{-7} *M*) and 0.025 ppm (4.43×10^{-8} *M*) in ethanol; rhodamine B (R.B.), 0.13 ppm (2.15×10^{-7} *M*) in ethanol. Emission bandwidth, 100 Å; excitation bandwidth, 25 Å; temperature, 25.0 °C.

function of excitation wavelength. Fletcher [28], however, found no more than ±5 percent quantum yield deviation for excitation wavelengths from 240 to 400 nm (except for 272 nm region, selected values in fig. 7), and other investigators also report essentially no variation in quantum yield at two excitation wavelengths [33–35].

B. Aromatic Hydrocarbons

Another large group of compounds with relatively high quantum yields are the aromatic hydrocarbons. Series of possible standards may be made by simply adding aromatic rings to the base compound, e.g. benzene and naphthalene fluoresce in the UV, anthracene exhibits blue fluorescence, naphthacene fluoresces in the green, and pentacene in the red. Anthracene has been studied quite extensively in ethanol and benzene, and the quantum efficiencies

reported from these studies vary from 0.25 to 0.33 [3, 18, 21, 23, 43, 57, 63–67].

We have studied pyrene derivatives [42] to determine if these compounds are suitable as fluorescence standards and to determine if substituents on more condensed systems exhibit the same trends in emission wavelengths, intensities and quantum efficiencies as the substituted naphthalenes. Corrected excitation and emission spectra for the pyrene derivatives are presented in figure 9. The 1-chloro-, 1-bromo-, and 1-nitropyrene compounds showed little, if any, fluorescence but would be expected to phosphoresce at low temperatures if the substituent "heavy atom" effect is followed for the substituted pyrenes as in the case of the naphthalenes [68]. The results for the quantum efficiency calculations and data taken from Berlman [51] for the naphthalenes and pyrenes are summarized in table 14. As can be seen, fairly good agreement was obtained with the quantum efficiency values from Berlman for the bipyrenyl. Better agreement for pyrene, however, was obtained with values from Förster and Seidel [69], probably due to the use of the same solvent, toluene, rather than benzene. The value for the quantum efficiency of pyrene by Dawson and Windsor [21] was obtained using ethanol as the solvent. The differences observed here may be due to some of the problems associated in the general use of aromatic hydrocarbons as standards since aromatics (a) usually show oxygen quenching, (b) have fairly large emission-excitation spectra overlap, (c) are very sensitive to extremely small amounts of impurities, (d) have narrow emission bandwidths, necessitating use of narrow slits, and (e) must have large index of refraction corrections made (as in this work) when quantum efficiencies are compared to compounds dissolved in aqueous media.

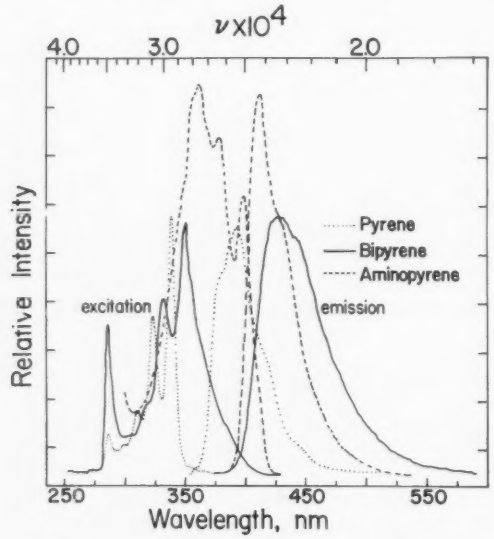

FIGURE 9. Relative intensities (emission spectra: quanta/unit bandwidth) versus wavelength for 0.13 ppm (5.69×10^{-7} *M*) pyrene, 0.47 ppm (1.84×10^{-6} *M*) 1-aminopyrene and 0.14 ppm (2.98×10^{-7} *M*) bipyrenyl in toluene. Excitation bandwidth, 25 Å, emission bandwidth, 100 Å; temperature, 25.0 °C.

Similar trends in quantum efficiencies are noted upon comparing pyrene and naphthalene to bipyrenyl and binaphthalenyl. The dimeric species have quantum efficiencies that are higher than the monomeric species which may be directly attributable to the lifetimes—i.e. 2 to 3 ns for the dimers and 100 to 600 ns for the monomers [51, 70]. The dimeric species have more asymmetry than the monomeric species and thus possess higher transition probabilities.

C. 3-Aminophthalimide

Although the compound 3-APT in 0.1 *N* sulfuric acid has been suggested as a fluorescence standard [1], care should be taken in its use. We have found that the absorption (excitation) spectrum, figure 10, and the quantum efficiency, table 15, are dependent on the acid concentration [38]. The decrease in the weight absorptivities at 385 nm with increasing acid concentration, coincides with the increased absorbance of a peak at 296 nm.

The quantum efficiency of 3-APT in ethanol reported by Alentsov [52] was 0.6. A quantum efficiency of 0.47 in 0.1 *N* sulfuric acid is not unreasonable in view of the difference in solvent. The observed decreases in the quantum efficiencies as a function of acid concentration are consistent with the presence of more than one species, allowing additional radiationless transitions such as energy transfer between the species to occur.

TABLE 14. Quantum efficiencies (QE) of some pyrene derivatives compared to similar naphthalene derivatives

Compound	Solvent	λ_{ex}	$\lambda_{em(max)}$	QE
Pyrene	Toluene	338.5	394	0.48, [a]0.52, [b]0.32, [c]0.53
1-Aminopyrene	Toluene	401	413	.43
1,1′-Bipyrenyl	Toluene	349	428	.78, [b]0.84
Naphthalene[a]	Cyclohexane	276	322	.23
1-Aminonaphthalene [a]	Cyclohexane	319	376	.46
1,1′-Binaphthyl[a]	Cyclohexane	284, 294	361	.77

[a] Ref. [70].
[b] Ref. [51].
[c] Ref. [21].

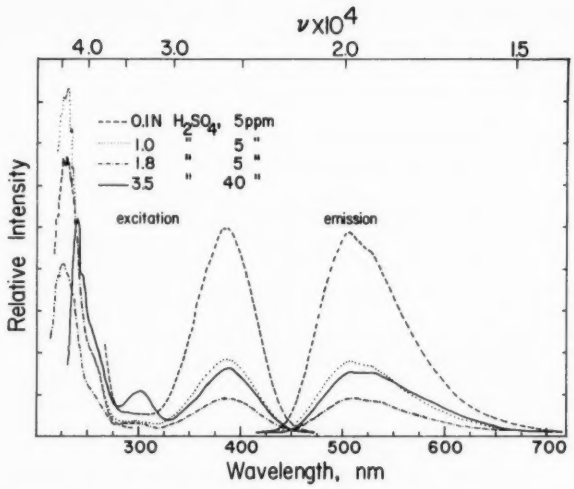

FIGURE 10. Relative intensities (emission spectra: quanta/unit bandwidth) versus wavelength for 5 ppm (2.38×10^{-5} *M*) and 40 ppm (1.90×10^{-4} *M*) 3-aminophthalimide in 0.1 *N*----, 1.0 *N*·····, 1.8*N* -·-·- and 3.5 *N*—H_2SO_4. Excitation bandwidth. 25 Å; emission bandwidth, 100 Å; temperature, 25.0 °C.

TABLE 15. Dependence of absorbance at 385 nm and quantum efficiency for 3-aminophthalimide as a function of sulfuric acid concentration

	WA[a] × 10^4		
$[H_2SO_4]$, *N*	385 nm	296 nm	Quantum efficiencies[b]
0.10	2.36	0.39	0.45 ± 0.01
1.02	1.29	.78	.31 ± 0.02
1.75	0.82	.94	.23 ± 0.02
3.55	.32	1.02	.15 ± 0.01

[a] See equation (7).
[b] λ_{ex}=385 nm; °C = 25.0; reference = QS · $2H_2O$ in 0.1 *N* H_2SO_4.

This work is in progress and will be reported later in more detail. The quantum efficiency for 3-APT in 0.1 *N* sulfuric acid is constant within ± 5 percent over the excitation wavelength range of 310 to 425 nm, figure 8.

D. Other Fluorescence Standards

N,*N*-dimethylamino-*m*-nitrobenzene has also been suggested as a standard [1] and, although the quantum efficiency appears to be relatively constant as a function of excitation wavelength [38], it is quite low and not very suitable as a standard. In addition, as mentioned before, a solvent system of 70:30, V:V of hexane:benzene is not desirable since fluorescence analyses in the biochemical areas [71] require use of compounds which are soluble in aqueous media.

Chen [62] has suggested standards which can be used in aqueous solutions and are suitable for biochemical applications. Other compounds which might be added to this list that cover the "red" region, include rhodamine B and rhodamine 6G, both used as quantum counters and both having relatively constant quantum efficiencies over a wide excitation wavelength range (250 to 600 nm), figure 8 [13, 72]. Studies should be made of these compounds in aqueous rather than alcoholic media, although aggregation in water has been reported [73].

E. Inorganic Ions in Glass or Polycrystalline Matrices

The use of inorganic ions in glass matrices as cuvette or disc shaped samples, figure 11, is attractive, especially when one considers ease of handling which may result in decreased methodological errors [74, 75]. The inorganic ions may be split into two classes determined by their absorption and emission spectra.

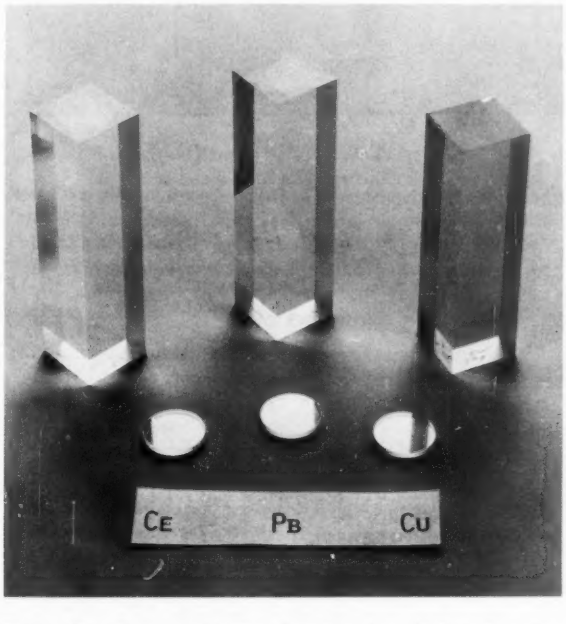

FIGURE 11. Cuvette and disc shaped cerium, lead, and copper doped silicate glasses.

The non-rare earths and cerium(III) have broad spectra with little structure due to interconfigurational electronic transitions, making them prime candidates for fluorescence standards. The rare earths in the +3 oxidation states, on the other hand, have sharp spectra due to intraconfigurational electronic transitions (less than 25 nm bandwidths), and may be used for wavelength calibration, spectral resolution of instruments, and, in special cases, as quantum yield standards.

The non-rare earth inorganic ions interact to a greater extent with the matrix than the rare earth ions. Thus changing the glass matrix from borate to silicate results in fairly large shifts of emission maxima.

Figure 12 shows these shifts for lead-doped phosphate, borate, and silicate glasses.

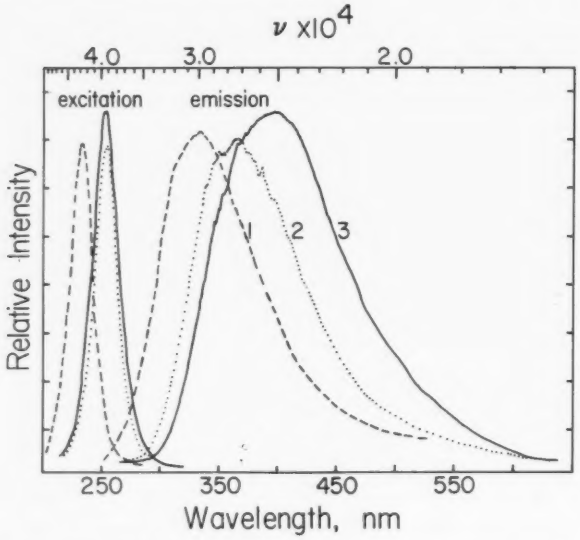

FIGURE 12. Relative intensity (emission spectra: quanta/unit bandwidth) versus wavelength for lead doped phosphate, 1; borate, 2; and silicate, 3; discs. Emission and excitation bandwidths, 100 Å; temperature, 25.0 °C; angle of disc with exciting beam, 15° [74, 75].

Table 16 summarizes ranges of emission maxima for the non-rare earth ions in glass or polycrystalline matrices. For an in-depth discussion of these effects and information concerning the rare earths, see reference [7] and the references listed therein.

TABLE 16. Ranges of emission maxima for cerium and non-rare earth inorganic ions in various solid matrices [a]

Inorganic Ion	Emission Range (nm)
Tl^{+}	290–325
Ce^{3+}	325–400
Pb^{2+}	350–450
UO_2^{2+}	475–550
Cu^{+}	475–550
Mn^{2+}	500–600

[a] For emission spectra, see reference [7].

F. Summary

In summary then, substantiative data are being accumulated as to the applicability of various compounds for use as fluorescence standards. The next major step would appear to be interlaboratory testing and comparison of data leading to the acceptance of either a single or a series of standards which are widely available for general use. Quinine sulfate, due to its desirable fluorescence characteristics, overall applicability, and widespread use and study, should probably be the first material selected for an interlaboratory comparison study.

III. Addendum A. Materials and Instrumentation

In order to adequately describe materials and experimental procedures, it was occasionally necessary to identify commercial products by manufacturer's name or label. In no instances does such identification imply endorsement by the National Bureau of Standards, nor does it imply that the particular product or equipment is necessarily the best available for that purpose.

A. Materials

The following reagents were used in this study:

Perchloric Acid: National Bureau of Standards, purified reagent, double distilled, lot 111103 [39].

Sulfuric Acid: Ultrex Grade, J. T. Baker Chemical Co., Phillipsburg, N.J. Used as obtained.

Sodium Hydroxide: Reagent Grade, J. T. Baker Chemical Co., address above. Used as obtained.

Distilled Water: Distilled water was passed through an ion exchange column (IWT Research Column, Rockford, Illinois), followed by double distillation from a quartz still.

Toluene: Certified, Fisher Chemical Co., Fairlawn, N.J., was shaken with cold concentrated sulfuric acid, water, aqueous 5 percent sodium hydroxide, water, and dried over calcium sulfate in that order. It was then distilled from sodium under nitrogen.

Benzene and *n*-Hexane: Spectrograde, Eastman Chemical Co., Rochester, N.Y. Used as obtained.

Ethanol, 95 and 100 percent: Pharmco Distributing Co., Publicker Industries, Philadelphia, Pa. Used as obtained.

Quinine Sulfate Dihydrate: Sample A—Aldrich Chemical Co., lot 032007; sample B—N. F. Grade, Fisher Chemical Co.; sample C—Pfalz and Bauer, 31–20 College Point Causeway, Flushing, N.Y.; sample D—sample A recrystallized three times from warm water; sample E—sample A recrystallized six times from warm water; sample F—sample B recrystallized four times from warm water.

Quinidine Sulfate Dihydrate: Sample G—Aldrich Chemical Co., lots 032781 and 062607; sample H—sample G recrystallized four times from warm water.

Quinine Dihydrate: Sample J—Aldrich Chemical Co., lot 071491 dissolved in dilute sulfuric acid, precipitated by neutralizing with dilute ammonium hydroxide. Washed with water twice.

All quinine derivatives were dried at 55–60 °C under vacuum for a minimum of 18 h before use [28].

Fluorescein: Aldrich Chemical Co., purified three times by the method of Koch [40].

Rhodamine B and Rhodamine 6G: Samples obtained from R. A. Keller [41]. Rhodamine 6G was purified by repeated recrystallizations, using ethyl acetate:

ethanol followed in one case by elution from a silica column (purification by R. A. Keller).

3-Aminophthalimide: Eastman Organic Chemicals. Recrystallized three times from ethanol, mp-260 °C [1].

N,N-Dimethylamino-*m*-nitrobenzene: Eastman Organic Chemicals. Recrystallized twice from chloroform and once from acetone-benzene [1].

Pyrene, bipyrenyl, 1-aminopyrene, 1-chloropyrene, and 1-nitropyrene prepared as designated [42].

B. Instrumentation

Absorbance spectra were obtained using Cary 14 and Cary 16 spectrophotometers, and a Turner Model 210 "Spectro" in the absorbance mode [20]. The spectrophotometers (except Model 210) were equipped with constant temperature cell blocks. Spectra were recorded or read at 25.0 ± 0.1 °C. Matched quartz cuvettes of 0.1, 1.0, and 5.0 cm were used.

Fluorescence spectra were obtained using a Turner Model 210 "Spectro" which gives corrected excitation and emission spectra [20], and a Farrand spectrofluorimeter which gives uncorrected spectra. Unblackened quartz spectrofluorimeter cells were used. Solvents were always run to determine baselines.

Before quantum efficiencies or band positions were measured, the accuracy of the wavelength scales for the emission and excitation monochromators were checked using a mercury lamp. A polished aluminum block cut at an angle of 45° was placed in the sample compartment. The monochromators were calibrated at 253.6, 435.8, and 546.1 nm. If necessary, the wavelength scales were adjusted so that accuracies of ±0.2 nm over the 253.6 to 546.1 nm range were obtained. A special Schlenk type [76] quartz cell was constructed, figure 13, by H. Deleonibus, Glassblowing Section, 129.06, National Bureau of Standards.

Stopcock and stopper were of polytetrafluoroethylene to avoid contamination. The solution was placed in the cylindrical sidearm and alternately frozen using liquid nitrogen and evacuated and thawed at room temperature at least five times to deoxygenate the solution. A test which repeated this cycle ten times resulted in a solution weight loss of less than 0.1 percent. Fluorescence studies, unless noted, were made on the corrected instrument. Quantum efficiencies were determined in duplicate, except where noted. All fluorescence measurements were made with 25 Å excitation bandwidth, 100 Å emission bandwidth, and at 25.0 ± 0.1 °C, except where noted.

Thermogravimetric measurements were run using dry nitrogen on a Model 950 TGA, E. I. DuPont de Nemours & Co., Wilmington, Delaware, by T. Sterling or S. Wicks, Section 310.04, Analytical Chemistry Division, National Bureau of Standards.

The glasses mentioned were prepared by the Inorganic Glass Section, 313.02, W. Haller, head, National Bureau of Standards. They were cut to size and polished by the Optical Shop, Section 129.05, S. Gerner, National Bureau of Standards.

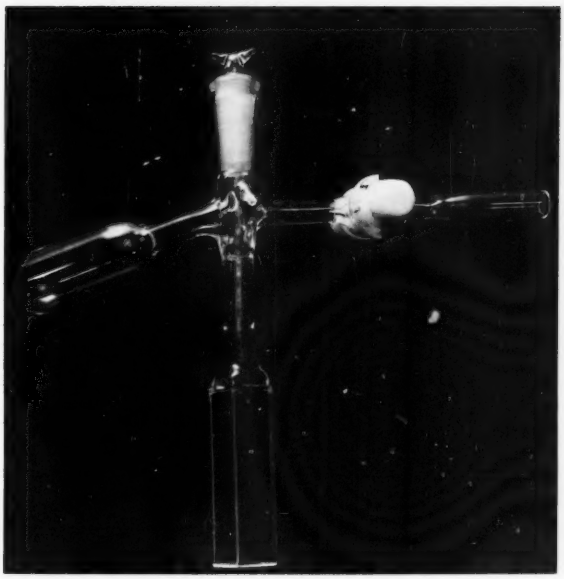

FIGURE 13. Schlenk type [76] spectrofluorimeter cell used with nitrogen manifold for degassing solutions.

The author would like to acknowledge the useful discussions in fluorescence with G. H. Atkinson, NBS, and the encouragement and support of O. Menis and J. I. Shultz, NBS.

IV. References

[1] Lippert, E., Nägele, W., Seibold-Blankenstein, I., Staiger, W., and Voss, W., Z. Anal. Chem. **170,** 1 (1959).
[2] Melhuish, W. H., J. Phys. Chem. **64,** 762 (1960).
[3] Parker, C. A., and Rees, W. T., Analyst **85,** 587 (1960).
[4] Chapman, J. H., Förster, Th., Kortüm, G., Lippert, E., Melhuish, W. H., Nebbia, G., and Parker, C. A., Z. Anal. Chem. **197,** 431 (1963).
[5] Velapoldi, R. A., Nat. Bur. Stand. (U.S.), Tech. Note 544 (O. Menis and J. I. Shultz, Eds.) 151 pages (Sept. 1970).
[6] Velapoldi, R. A., Nat. Bur. Stand. (U.S.), Tech. Note 584 (O. Menis and J. I. Shultz, Eds.) 175 pages (Dec. 1971).
[7] Reisfeld, R., "Inorganic Ions in Glasses and Polycrystalline Pellets as Fluorescence Standard Reference Materials, J. Res. Nat. Bur. Stand. (U.S.), **76A** (Phys. and Chem.), No. 6, (Nov.–Dec. 1972).
[8] Vavilov, S. I., Z. Phys. **22,** 266 (1924).
[9] Vavilov, S. I., Z. Phys. **42,** 311 (1927).
[10] Melhuish, W. H., J. Opt. Soc. Amer. **54,** 183 (1964).
[11] Melhuish, W. H., J. Opt. Soc. Amer. **52,** 1256 (1962).
[12] Melhuish, W. H., New Zealand J. Sci. Tech. **37,** 142 (1955).
[13] Demas, J. N. and Crosby, G. A., J. Phys. Chem. **75,** 991 (1971).
[14] No distinction is made here between luminescence quantum yield, quantum efficiency, or quantum yield.
[15] Parker, C. A., Photoluminescence of Solutions (Elsevier Publishing Co., New York, N.Y., 1968).
[16] Förster, Th., Fluoreszenz Organischer Verbindungen (Vandenhoeck-Ruprecht, Göttingen, Germany, 1951).
[17] Gilmore, E. H., Gibson, G. E., and McClure, D. S., J. Chem. Phys. **23,** 399 (1955).
[18] Fletcher, A. N., J. Mol. Spectry. **23,** 221 (1967).
[19] Hermans, J. J. and Levinson, S., J. Opt. Soc. Amer. **41,** 460 (1951).
[20] Turner, G. K., Science **146,** 183 (1964).

[21] Dawson, W. R. and Windsor, M. W., J. Phys. Chem. **72,** 3251 (1968).
[22] Gill, J. E., Appl. Spectry. **24,** 588 (1970).
[23] Weber, G. and Teale, F. W. J., Trans. Faraday Soc. **53,** 646 (1957).
[24] Rusakowicz, R. and Testa, A. C., J. Phys. Chem. **72,** 2680 (1968).
[25] Argauer, R. J. and White, C. E., Anal. Chem. **36,** 368 (1964).
[26] Mavrodineanu, R., Nat. Bur. Stand. (U.S.), Tech. Note 544, 151 pages, Sept. 1970 and 584, 175 pages, Dec. 1971 (O. Menis and J. I. Shultz, Eds.).
[27] Dawson, W. R. and Kropp, J. L., J. Opt. Soc. Amer. **55,** 822 (1965).
[28] Fletcher, A. N., Photochem. Photobiol. **9,** 439 (1969).
[29] Chen, R. F., Anal. Biochem. **19,** 374 (1967).
[30] Gill, J. E., Photochem. Photobiol. **9,** 313 (1969).
[31] Fletcher, A. N., J. Phys. Chem. **72,** 2742 (1968).
[32] Eisenbrand, J., Z. Anal. Chem. **179,** 170 (1961).
[33] Rosen, P., and Edelman, G. M., Rev. Sci. Instrum. **36,** 809 (1965).
[34] Drobnik, J., and Yeargers, E., J. Mol. Spectry. **19,** 454 (1966).
[35] Eastman, J. W., Photochem. Photobiol. **6,** 55 (1967).
[36] Börreson, H. C., Acta Chem. Scand. **19,** 2089 (1965).
[37] Scott, T. G., Spencer, R. D., Leonard, N. J., and Weber, G., J. Amer. Chem. Soc. **92,** 687 (1971).
[38] Velapoldi, R. A., and Kenigsberg, D. R., unpublished results.
[39] Murphy, T. J., Section 310.06, Analytical Chemistry Division, National Bureau of Standards, Washington, D.C. 20234.
[40] Koch, L., J. Assoc. Off. Agr. Chem. **42,** 149 (1959).
[41] Samples obtained from R. A. Keller, Section 316.03, Physical Chemistry Division, National Bureau of Standards, Washington, D.C. 20234.
[42] Fatiadi, A., and Velapoldi, R. A., unpublished data.
[43] Melhuish, W. H., J. Phys. Chem. **65,** 229 (1961).
[44] G. K. Turner Associates, Notes on the Determination of Quantum Efficiency with the Model 210 "Spectro", Feb. 1966.
[45] Birks, J. B., and Dyson, D. J., Roy. Soc. (London) Proc. **A275,** 135 (1963).
[46] Moss, D. W., Clin. Chim. Acta **5,** 283 (1960).
[47] Grant, H. S., and Jones, J. H., Anal. Chem. **22,** 679 (1950).
[48] Bartholomew, R. J., Rev. Pure Appl. Chem. Australia **8,** 265 (1958).
[49] Bowman, E. J., and Wokes, F., Fluorescence of Solutions (Longmans Green, London, p. 77, 1953).
[50] Ejder, E., J. Opt. Soc. Amer. **59,** 223 (1969). See also Discussion by W. H. Melhuish, Absolute Spectrofluorometry, J. Res. Nat. Bur. Stand. (U.S.), **76A** (Phys. and Chem.), No. 6, 547–560 (Nov.–Dec. 1972).
[51] Berlman, I. B., Handbook of Fluorescence Spectra of Aromatic Molecules, 2d ed., p. 383 (Academic Press, New York, N.Y., 1971).
[52] Alentsov, M. A., National Res. Council of Canada. Tech. Trans., TT–433 from Zhur. Eskp. i. Teoret. Fiz. **21,** 133 (1951).
[53] Forester, L. S., and Livingston, R., J. Chem. Phys. **20,** 1315 (1952).
[54] Hellstrom, H., Arkiv. Kemi. Mineral. Geol. **12A,** 17 (1937).
[55] Umberger, J., and LaMer, V., J. Amer. Chem. Soc. **67,** 1099 (1945).
[56] Bridges, J. W., and Williams, R. T., Nature **196,** 59 (1962).
[57] Roberts, B. G., and Hirt, R. C., Ann. ISA Conf. Proc. **19** (III), 2.2.2.64 (1964).
[58] Hercules, D. M., and Frankel, H., Science **131,** 1611 (1960).
[59] Latimer, P., Bannister, T. T., and Rabinowitch, E., Science **124,** 585 (1956).
[60] Forester, L. S., and Dudley, D., J. Phys. Chem. **66,** 838 (1962).
[61] Seybold, P. G., Gouterman, M., and Callis, J., Photochem. Photobiol. **9,** 229 (1969).
[62] Chen, R. F., Measurements of Absolute Values in Biochemical Fluorescence Spectroscopy, J. Res. Nat. Bur. Stand. (U.S.), **76A** (Phys. and Chem.), No. 6, 593–606 (Nov.–Dec. 1972).
[63] Parker, C. A., and Joyce, T., Trans. Faraday Soc. **62,** 2785 (1966).
[64] Medinger, T., and Wilkinson, F., Trans. Faraday Soc. **61,** 620 (1965).
[65] Drushel, H. V., Sommers, A. L., and Cox, R. C., Anal. Chem. **35,** 2167 (1963).
[66] Bridges, J. W., and Williams, R. T., Nature **196,** 59 (1962).
[67] Himel, C. M., and Mayer, R. T., Anal. Chem. **42,** 130 (1970).
[68] Wehry, E. L., and Rogers, L. B., in Fluorescence and Phosphorescence Analyses, D. M. Hercules, Ed., p. 81 (Interscience Publishers, New York, N.Y., 1966).
[69] Förster, Th., and Seidel, H. P., Z. Phys. Chem. (N.F.) **48,** 58 (1965).
[70] Birks, J. B., Photophysics of Aromatic Molecules, p. 128 (J. Wiley & Sons, Ltd., New York, N.Y., 1970).
[71] Udenfriend, S., Fluorescence Assay in Biology and Medicine (Academic Press, New York, N.Y., Vols. I and II, 1962, 1969).
[72] Yguerabide, J., Rev. Sci. Instrum. **39,** 1048 (1968).
[73] Selwyn, J. E., and Steinfeld, J. I., J. Phys. Chem. **76,** 762 (1972).
[74] Velapoldi, R. A., and Reisfeld, R., Nat. Bur. Stand. (U.S.), Tech. Note 584 (O. Menis and J. I. Shultz, Eds.) 175 pages (Dec. 1971).
[75] Reisfeld, R., Honigbaum, A., and Velapoldi, R. A., J. Opt. Soc. Amer. **61,** 1422 (1971).
[76] Schlenk, W., and Thal, A., Ber. Deut. Chem. Ges. **46,** 2840 (1913).

(Paper 76A6–748)

JOURNAL OF RESEARCH of the National Bureau of Standards—A. Physics and Chemistry
Vol. 76A, No. 6, November–December 1972

Ion-Molecule Reactions in Isopropanol: Implications for Its Radiolysis *

R. Gorden, Jr., and L. W. Sieck

Institute for Materials Research, National Bureau of Standards, Washington, D.C. 20234

(June 21, 1972)

The photoionization of isopropanol (*i*-PrOH) at 11.7 eV has been investigated in the NBS high pressure photoionization mass spectrometer over the pressure range 0.1 to approximately 200 millitorr. The major primary ion, CH_3CHOH^+, reacts with a total rate coefficient of $1.1 \pm 0.1 \times 10^{-9}$ cm³/molecule-s to yield mainly $(i\text{-PrOH})H^+$ and $CH_3(i\text{-}C_3H_7)COH^+$. At pressures in excess of a few millitorr consecutive reactions of $(i\text{-PrOH})H^+$ and $CH_3(i\text{-}C_3H_7)COH^+$ were also detected, including the overall dehydration process

$$(i\text{-PrOH})H^+ + i\text{-PrOH} \rightarrow H_2O + (i\text{-}C_3H_7)_2OH^+$$

These data are interpreted in light of a recent radiolysis study, and a thermal cationic chain mechanism for production of $(I\text{-}C_3H_7)_2O$ consistent with those results is proposed. The value for the proton affinity of SF_6 is also discussed in some detail.

Key words: Gas-phase kinetics; ion-molecule reactions; mass spectrometry; photoionization; proton affinity; radiolysis.

1. Introduction

Although the positive ion chemistry of the lower aliphatic alcohols has been extensively investigated in the vapor phase by mass spectrometric techniques, little is known concerning the reactions occurring in isopropanol (*i*-PrOH) at higher densities. Beauchamp and co-workers [1],[1] using electron impact ionization, have reported the only detailed study of this system, and although many reaction channels were defined, those experiments were restricted to pressures less than approximately 0.1 millitorr. The vapor phase radiolysis of *i*-PrOH has also been investigated by Van der Linde and Freeman [2] at high temperatures (> 400 K) and pressures (P > 100 torr), and chemical evidence was obtained for the production of di-isopropyl ether via a cationic chain mechanism. To our knowledge, no other studies have been reported.

Recent studies in our laboratory [3] have revealed that rather dramatic changes may occur in the positive ion mechanism at pressures in excess of a few millitorr, and this information is often of fundamental importance in unraveling the behavior characteristic of much higher densities. In order to bridge the gap between the studies mentioned above and provide information which might be useful for interpreting the radiolysis data, we will report here a study of *i*-PrOH in the NBS high pressure photoionization mass spectrometer over the pressure range 0.1 to approximately 200 millitorr.

2. Experimental Procedure

All experiments were carried out with the NBS high pressure photoionization mass spectrometer described in detail elsewhere [4]. The methods used for deriving rate coefficients and other kinetic parameters have also been discussed previously [5].

3. Results

3.1. Primary Mass Spectrum

The following primary mass spectrum, given as percentages of the total ionization, was obtained when *i*-PrOH was photoionized at 106.7–104.8 nm (henceforth referred to as 11.7 eV); *m/e* 60 (parent) (~ 2%), *m/e* 59 (~ 3%), *m/e* 45 (85%), and *m/e* 44 (~ 10%). Essentially the same composite spectrum may be derived from the data of Rafaey and Chupka [6] using their fractional photoionization cross-section curves and assuming a photon energy of 11.7 eV. The major primary ion produced in this system is the protonated acetaldehyde ion (*m/e* 45), which results from simple C—C cleavage in the α position:

*This work was supported by the U.S. Atomic Energy Commission.
[1] Figures in brackets indicate the literature references at the end of this paper.

$$(CH_3)_2CHOH^{+*} \rightarrow CH_3CHOH^+ + CH_3. \quad (1)$$

Elimination of methane to give *m/e* 44, which has been suggested to have the oxonium ion structure [6] also occurs to some extent,

$$(CH_3)_2CHOH^{+*} \rightarrow CH_2CHOH^+ + CH_4 \quad (2)$$

as well as loss of H from the parent to give *m/e* 59, $(CH_3)_2COH^+$. The fractional yield of parent ions, *m/e* 60, which do not dissociate at 11.7 eV is quite small (≤ 2%), reflecting the reported ease with which loss of CH_3 and CH_4 occurs from the molecular ion even at excitation energies only slightly in excess of the ionization threshold.

3.2. Ion-Molecule Reactions—Reactions of Primary Ions

As the pressure in the ionization chamber is increased a number of reaction sequences are initiated by primary ions. The general behavior is displayed in figure 1, which gives a representation of the composite mass spectrum obtained (major ions only) when *i*-PrOH is photoionized at 11.7 eV over the pressure range 0.1 to approximately 200 millitorr. When the fractional intensity of the major primary ion, CH_3CHOH^+, is plotted versus pressure over the range 0.1 to 2 millitorr a straight line is obtained for the decay curve from which an absolute rate coefficient of $1.1 \pm 0.1 \times 10^{-9}$ cm³/molecule-s may be derived for the process

$$CH_3CHOH^+ + i\text{-PrOH} \rightarrow \text{Products other than } CH_3CHOH^+ \quad (3)$$

Two major overall reaction channels are found for CH_3CHOH^+, proton transfer to yield *m/e* 61, $(i\text{-PrOH})H^+$, and condensation with loss of H_2O to give *m/e* 87 [most likely protonated methyl-isopropyl ketone]:

$$CH_3CHOH^+ + i\text{-PrOH} \rightarrow (i\text{-PrOH})H^+ + CH_3CHO \quad \Delta H = -13\,[7] \quad (4a)$$

$$\rightarrow (\text{Me})(i\text{-Pr})COH^+ + H_2O \quad \Delta H = -38 \quad (4b)$$

[(Me)(*i*-Pr)CO = methyl-isopropyl ketone]. In the low pressure range, under conditions where consecutive ion-molecule reactions are negligible (pressures <1 millitorr, fig. 1) the proton transfer reaction (process 4a) is favored by approximately a factor of three over process 4b. Processes 4a and 4b have also been observed by Beauchamp and co-workers [1a].

The other major primary ion, *m/e* 44, which is assumed to have the initial structure CH_2CHOH^+, is also reactive towards *i*-PrOH ($k \sim 10^{-9}$ cm³/molecule-s). The only reaction product which can be uniquely assigned to this precursor is *m/e* 62, which must have the empirical formula $C_2H_6O_2^+$. The production of this ion may correspond to an overall process involving elimination of C_3H_6 from the collision complex and the concurrent formation of the ethylene glycol molecular ion, $(CH_2OH)_2^+$, although other plausible structures for $C_2H_6O_2^+$ may also be written. The products resulting from the interactions of *m/e* 60 (parent ion) and *m/e* 59 (parent minus H) could not be determined from our data due to the low relative abundance of these ions in the primary mass spectrum.

3.3. Reactions Occurring at Higher Pressures

At pressures ≥ approximately 0.7 millitorr the appearances of *m/e* 121, $(i\text{-PrOH})_2H^+$ and *m/e* 103, $(i\text{-PrOH})_2H^+$ minus H_2O [most likely protonated diisopropyl ether $(i\text{-Pr})_2OH^+$] are first noted. These products result from the further interactions of $(i\text{-PrOH})H^+$ as follows:

$$(i\text{-PrOH})H^+ + i\text{-PrOH} \rightarrow (i\text{-PrOH})_2H^+ \quad (5)$$

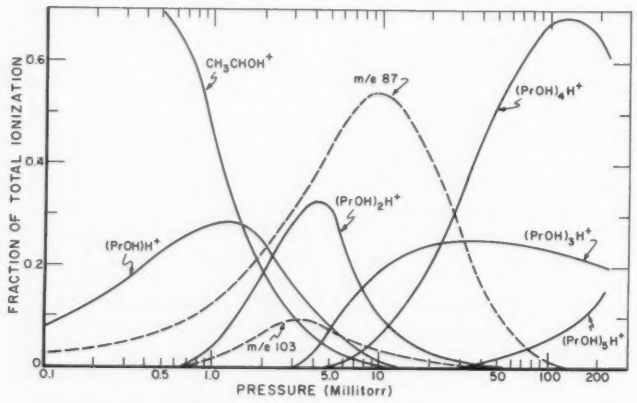

FIGURE 1. *Composite mass spectrum obtained (major ions only) when* i-PrOH *is photoionized at 106.7–104.8 nm (11.7 eV) as a function of pressure.*

$$(i\text{-PrOH})H^+ + i\text{-PrOH} \rightarrow (i\text{-PrOH})_2H^{+*}$$

$$\rightarrow (i\text{-Pr})_2OH^+ + H_2O \quad \Delta H = -8. \qquad (6)$$

Overall dehydration processes analogous to 6 have been observed mass spectrometrically in methanol [8] and ethanol [9] as well as *i*-PrOH [1a].

As the pressure in the reaction chamber is increased above 2–3 millitorr a number of higher order solvation reactions are observed yielding ionic products which will be designated simply as $(i\text{-PrOH})_3H^+$, $(i\text{-PrOH})_4H^+$, and $(i\text{-PrOH})_5H^+$ with the experimental order of appearance matching the apparent proton solvation number. Although the exact kinetic order of the various processes leading to the formation of these entities cannot be defined from our data due to the indeterminate effect of nonreactive scattering of ions at higher pressures, several general comments concerning the behavior under these conditions are warranted.

a. The fractional yield of *m/e* 103 $(i\text{-Pr})_2OH^+$, exhibits a maximum at approximately 3 millitorr, which is slightly below the maximum found for $(i\text{-PrOH})_2H^+$ (see fig. 1). In addition, there is no evidence over the entire pressure range for the formation of *m/e* 163, which would be the product ion obtained if *m/e* 103 was removed via simple addition of a molecule of *i*-PrOH. These observations may be taken as evidence for collisional stabilization of those internally excited $(i\text{-PrOH})_2H^+$ entities which dissociate according to process 6 (loss of H_2O) at lower pressures. An alternative process for removal of $(i\text{-Pr})_2OH^+$, bimolecular proton transfer to *i*-PrOH

$$(i\text{-Pr})_2OH^+ + i\text{-PrOH} \rightarrow (i\text{-PrOH})H^+ + (i\text{-Pr})_2O \quad \Delta H = +12 \qquad (7)$$

is endothermic as written for ground state reactants by approximately 12 kcal/mol. However, the overall exothermicities of the two consecutive reactions responsible for production of $(i\text{-Pr})_2OH^+$, process 4a followed by process 6, are exothermic by 13 and 8 kcal/mol respectively, and we cannot rule out the possibility that the $(i\text{-Pr})_2OH^+$ ion retains sufficient internal energy to overcome the energy barrier for reaction 7. In any event, the overall process

$$(i\text{-Pr})_2OH^+ + 2i\text{-PrOH} \rightarrow (i\text{-Pr})_2O + (i\text{-PrOH})_2H^+ \qquad (8)$$

will certainly be exothermic as written due to the change in the solvation energy of H^+ when two molecules of *i*-PrOH are involved. Although the bimolecular reaction involving one *i*-PrOH molecule is endothermic (process 7), an adequate quantity of additional energy is provided by the solvation reaction process

$$(i\text{-PrOH})H^+ + i\text{-PrOH} \rightarrow (i\text{-PrOH})_2H^+. \qquad (5)$$

Processes analogous to 8 have been reported from this laboratory for a number of polar systems [10].

b. The fractional yield of *m/e* 87, $(\text{Me})(i\text{-Pr})COH^+$, reaches a maximum at approximately 10 millitorr and decreases at higher pressures. Again, as in the previous case, the bimolecular proton transfer reaction

$$(\text{Me})(i\text{-Pr})COH^+ + i\text{-PrOH} \rightarrow (i\text{-PrOH})H^+ + (\text{Me})(i\text{-Pr})C{=}O \quad \Delta H = +10 \qquad (9)$$

is endothermic as written for ground state reactants by approximately 10 kcal/mol. However, the process responsible for production of *m/e* 87 (process 4b) is exothermic by 38 kcal/mol, and the possibility exists that retention of internal energy in the ionic reaction product is sufficient to drive the process to completion. Overall processes analogous to process 8 involving two molecules of *i*-PrOH will always be exothermic for ground state reactants. The appearance of *m/e* 147, which corresponds to the solvation of *m/e* 87 with one molecule of *i*-PrOH, was also noted at pressures above 5 millitorr.

c. At pressures in excess of 20 millitorr the major ionic species present in the system are $(i\text{-PrOH})_3H^+$, $(i\text{-PrOH})_4H^+$, and, at much higher pressures, $(i\text{-PrOH})_5H^+$. If one applies the empirical rule originally proposed by Munson [11] stating that the maximum proton solvation number in a system which can form hydrogen bonds will usually be one more than the number of hydrogens bonded to the heteratom, then one would expect the solvation number for the most stable structure in *i*-PrOH to be three. Assuming the validity of this empiricism, which does appear to be valid at least for the solvation reactions occurring in the methylamines [12], the observation in this study of $(i\text{-PrOH})_4H^+$ and $(i\text{-PrOH})_5H^+$ suggests that $(i\text{-PrOH})_3H^+$ rearranges to give isomeric alcohols or ketones which can readily incorporate additional solvent molecules. It is interesting to note in this context that the fractional yield of $(i\text{-PrOH})_3H^+$, the anticipated stable form, decreases in relative abundance much more slowly as a function of pressure than $(i\text{-PrOH})H^+$, $(i\text{-PrOH})_2H^+$, and $(i\text{-PrOH})_4H^+$. However, whether or not this apparent reduction in reactivity is associated with the stability of the unrearranged trisolvated form cannot be ascertained from our data.

4. Discussion

4.1. Implications for the Radiolysis of Isopropanol

The vapor phase radiolysis of *i*-PrOH has been reported by Van der Linde and Freeman [2] from 125 to 400 °C and over a range of pressures from 100 to 2000 torr. The significant result of their study was evidence for production of diisopropyl ether, $(i\text{-Pr})_2O$, via a chain mechanism. Energy (G) values as high as 1000 were obtained under certain conditions, and the overall chain length was found to increase with increasing temperature and decreasing pressure. In order to account for their findings a cationic chain mechanism was proposed having as an initiation step a bimolecular proton transfer reaction involving the parent molecular ion

$$i\text{-PrOH}^+ + i\text{-PrOH} \rightarrow (i\text{-PrOH})H^+ + C_3H_7O^+. \quad (10)$$

It was suggested that process was followed by conversion of $(i\text{-PrOH})H^+$ into $(i\text{-PrOH})_nH^+$ via successive collisions, with the rate controlling step in the chain mechanism corresponding to process 6

$$(i\text{-PrOH})H^+ + i\text{-PrOH} \rightarrow (i\text{-PrOH})_2H^{+*}$$

$$\rightarrow (i\text{-Pr})_2OH^+ + H_2O \qquad \Delta H = -8. \quad (6)$$

The mechanism for production of neutral $(i\text{-Pr})_2O$, as well as the subsequent reactions of $(i\text{-Pr})_2OH^+$, was not specified.

Although it is difficult to extrapolate the behavior observed in our experiments, which were carried out at 298 K, to that characteristic of temperatures in the range 400 to 700 K, our data does suggest a possible cationic chain for production of $(i\text{-Pr})_2O$ which is consistent with the radiolysis results. The formalism follows.

It is evident that the role of parent molecular ions, $i\text{-PrOH}^+$, will be negligible at temperatures above 400 K due to the fact that the activation energy for dissociation is on the order of only 0.15 eV [6]. Although the exact identities and relative yields of the various fragment ions produced under radiolysis conditions cannot be specified, consideration of the fragmentation pattern of *i*-PrOH produced both by high energy electron impact [13] and photoionization [6] over a wide range of temperatures indicates that the major ionic species present initially will most probably be CH_3CHOH^+ (the major ion in our study) with smaller contributions from $C_2H_3^+$, $C_3H_7^+$, $C_2H_5^+$, etc., as well as fragments containing oxygen atoms. Most, if not all, of the primary ions will react via proton transfer with parent molecules at higher temperatures

$$XH^+ + i\text{-PrOH} \rightarrow (i\text{-PrOH})H^+ + X \quad (11)$$

(XH^+ denotes any of the primary fragment ions).

Under radiolysis conditions, the $(i\text{-PrOH})H^+$ ions so formed will rapidly initiate a series of sequential, competing processes including reactions 5, 6, and 8. Since cationic production of $(i\text{-Pr})_2O$ must be related to the formation of $(i\text{-Pr})_2OH^+$, which is in turn related exclusively to the decomposition of internally excited $(i\text{-PrOH})_2H^+$, it follows that the rate controlling step in any chain mechanism must involve the competition between process 6 and the conversion of $(i\text{-PrOH})_2H^+$ into more highly solvated (or rearranged) ions which cannot yield $(i\text{-Pr})_2OH^+$ as a decomposition product. Once formed, $(i\text{-Pr})_2OH^+$ ions will be quickly converted to $(i\text{-Pr})_2O$ via either

$$(i\text{-Pr})_2OH^+ + i\text{-PrOH} \rightarrow (i\text{-PrOH})H^+ + (i\text{-Pr})_2O \qquad \Delta H = +12 \quad (7)$$

or

$$(i\text{-Pr})_2OH^+ + 2i\text{-PrOH} \rightarrow (i\text{-Pr})_2O + (i\text{-PrOH})_2H^+. \quad (8)$$

According to this mechanism, the chain carrier is either $(i\text{-PrOH})H^+$ or $(i\text{-PrOH})_2H^+$. The fact that Van der Linde and Freeman [2] observed a substantial decrease in the yields of $(i\text{-Pr})_2O$ at higher pressures (temperature held constant) is consistent with this sequence since collisional deactivation of $(i\text{-PrOH})_2H^+$ or further solvation of this ion prior to dissociation will be favored at higher densities. Alternatively, an increase in temperature at constant pressure will serve to increase the rate of dissociation of $(i\text{-PrOH})_2H^+$ into $(i\text{-Pr})_2OH^+$.

4.2. Some Comments on the Proton Affinity of SF_6

Van der Linde and Freeman [2] also reported a number of experiments involving the radiolysis of *i*-PrOH-additive mixtures. The additives included H_2O, C_3H_6, SF_6, $(CH_3)_2CO$, and NH_3, all of which inhibited ether formation to some extent. These authors concluded, on the basis of a plot of the proton affinity of the additive versus the ether yield, that the proton affinity of SF_6 was on the order of 184 kcal/mol. The absolute value for the proton affinity of SF_6 is an important quantity for kineticists since this molecule is used extensively as a thermal electron scavenger in ionized systems in order to modify the charge neutralization mechanism [14]. In order to offer an independent measurement of this quantity we have carried out several additional experiments. An upper limit for the proton affinity of SF_6 may be estimated by determining whether or not a hypothetical ion MH^+ (in which the proton affinity of M is known) will undergo the following reaction

$$MH^+ + SF_6 \rightarrow SF_6H^+ \text{ (or dissociative proton transfer products)} + M. \quad (12)$$

A series of possible proton donors (MH^+) were investigated via photoionization of SF_6—hydrocarbon mixtures at 11.7 eV, since at this energy ionization occurs only in the hydrocarbon component (I.P. SF_6 = 15.3 eV). Although the results will not be presented in detail, we were unable to find any evidence for the occurrence of process 12 for MH^+ ions in which the proton affinity of M was as low as 146 kcal/mol (the lower limit available to us as a possible reactant). This limit was established by determining that the reaction

$$C_2H_6^+ + SF_6 \rightarrow C_2H_5 + SF_6H^+ \quad (13)$$

did not occur for ground state reactants, and assuming a value of 146 kcal/mol for the proton affinity of C_2H_5. Since this general method has been used successfully in several laboratories [7b] to establish limits for proton affinities, we are forced to conclude that the proton affinity of SF_6 is less than 146 kcal/mol and that the assumptions of Van der Linde and Freeman [2] are in error. An upper limit of this magnitude indicates that the addition of SF_6 will not materi-

ally effect the positive ion chemistry occuring in hydrocarbons during radiolysis.

In order to resolve what effects the addition of SF_6 to *i*-PrOH might have had in the radiolysis study we also carried out a number of experiments in which various *i*-PrOH–SF_6 mixtures were photoionized at 11.7 eV over the pressure range covered by figure 1. Again (all of the results were negative in the sense that) we were unable to detect any reaction between SF_6 and any of the ions resulting from the photoionization of *i*-PrOH, including higher molecular weight products such as $(i\text{-PrOH})_2H^+$, $(i\text{-PrOH})_3H^+$, $(i\text{-Pr})_2OH^+$, etc. This finding is consistent with the general assumption that SF_6 exhibits an extremely low reactivity towards positive ions, and on this basis we cannot offer any rationale for the effects observed in the radiolysis experiments.

We are indebted to P. Ausloos for his advice and counsel during the course of this study.

5. References

[1a] Beauchamp, J. L., and Dunbar, R. C., J. Am. Chem. Soc. **92,** 1477 (1970).
[1b] Lehman, T. A., Elwood, T. A., Bursey, J. T., Bursey, M. M., and Beauchamp, J. L., ibid, **93,** 2108 (1971).
[2] Van der Linde, H. J., and Freeman, G. R., J. Am. Chem. Soc. **92,** 4417 (1970).
[3a] Sieck, L. W., and Ausloos, P., J. Chem. Phys. **56,** 1010 (1972).
[3b] Sieck, L. W., and Ausloos, P., J. Res. Nat. Bur. Stand. (U.S.), **76A** (Phys. and Chem.), No. 3, 253–262 (May–June 1972).
[3c] Sieck, L. W., Searles, S., and Ausloos, P., J. Chem. Phys. **54,** 91 (1971).
[3d] Searles, S. K., Sieck, L. W., and Ausloos, P., ibid, **53,** 849 (1970).
[4] Sieck, L. W., Searles, S. K., and Ausloos, P., J. Am. Chem. Soc. **91,** 7627 (1969).
[5] Sieck, L. W., and Searles, S. K., J. Am. Chem. Soc. **92,** 2937 (1970).
[6] Rafaey, K. M. A., and Chupka, W. A., J. Chem. Phys. **48,** 5205 (1968).
[7] Overall heats of reaction are calculated from thermodynamic data contained in the following publications:
[7a] Franklin, J. L., Dillard, J. L., Rosenstock, H. M., Herron, J. T., Draxl, K., and Field, F. H., Nat. Stand. Ref. Data Ser., Nat. Bur. Stand. (U.S.), **26,** 289 pages (June 1969).
[7b] Beauchamp, J. L., Ann. Rev. Phys. Chem. **22,** 527 (1971).
[7c] Ausloos, P., and Lias, S. G., Radiation Chemistry of Organic Compounds. Ionic Processes (M. I. T. Press (U.S.), 1972).
[8a] Munson, M. S. B., J. Am. Chem. Soc. **87,** 5313 (1965).
[8b] Henis, J. M. S., ibid, **90,** 844 (1968).
[9] Sieck, L. W., Futrell, J. H., and Abramson, F. P., J. Chem. Phys. **45,** 2859 (1966).
[10a] Hellner, L., and Sieck, L. W., J. Res. Nat. Bur. Stand. (U.S.), **75A** (Phys. and Chem.), No. 5, 487–492 (September-October 1971).
[10b] Sieck, L. W., and Searles, S. K., J. Chem. Phys. **53,** 2601 (1970).
[11] Munson, M. S. B., J. Phys. Chem. **70,** 2034 (1966).
[12] Hellner, L., and Sieck, L. W., Int. J. Chem. Kinetics, in press.
[13] Friedman, L., Long, F. A., and Wolfsberg, M., J. Chem. Phys. **27,** 613 (1957). and references cited therein.
[14] See, for example, Fundamental Processes in Radiation Chemistry, P. Ausloos, Ed. (John Wiley & Sons, Inc., New York, N. Y., 1968).

(Paper 76A6–749)

JOURNAL OF RESEARCH of the National Bureau of Standards — A. Physics and Chemistry
Vol. 76A, No. 6, November–December 1972

Excitation of $O_2\ ^1\Delta_g$ by Electron Impact*

P. S. Julienne and M. Krauss

Institute for Materials Research, National Bureau of Standards, Washington, D.C. 20234

(June 21, 1972)

The total and differential cross sections as a function of energy were calculated for electron impact excitation of the $O_2{}^1\Delta_g$ state from the ground $^3\Sigma_g^-$ state. The Ochkur-Rudge approximation was used for the exchange amplitude, which was calculated using Hartree-Fock wave functions with a Gaussian basis. There is good agreement with the experimental total cross section except near threshold.

Key words: Ab initio Gaussian wave functions; electron impact excitation; exchange amplitude; $O_2\ ^1\Delta_g$ state; Ochkur-Rudge approximation.

Optically forbidden molecular transitions involving a change in electron spin may be excited by electron impact through electron exchange. Such processes are particularly of interest for common atmospheric molecules. We have calculated total and differential cross sections for the excitation of the $^1\Delta_g$ state of O_2 from the ground $^3\Sigma_g^-$ state using the Ochkur-Rudge approximation [1, 2, 3]. This is essentially a first order Born approximation for the exchange amplitude in which distortion of the incident electron wave function and polarization of the molecule are neglected. However, in calculations of excitation cross sections for triplet states in H_2 [4] and for the $B^3\Pi_g$ state of N_2 [5, 6] this approximation gives reasonable agreement with experimental total cross sections. This report summarizes the results of our calculation of the $O_2\ ^1\Delta_g$ cross section and makes a comparison with experimental data [7, 8, 9].

In the Ochkur-Rudge approximation the differential cross section for excitation from a state i to a state f is given in atomic units (a_0^2/sr) by the following expression

$$I(\theta) = 4\frac{g_f}{g_i}\frac{K_f}{K_i}\frac{1}{T^4}\,|A|^2$$

where g_i, g_f are degeneracy factors, K_i and K_f the magnitudes in atomic units (a_0^{-1}) of the initial and final wave vectors, and T and A are defined by

$$T = \sqrt{K_i^2 + \epsilon}$$

$$A(K) = \int \psi_f^* \psi_i e^{i\mathbf{K}\cdot\mathbf{r}} d\,\mathbf{r}.$$

Here ϵ is the ionization potential of the initial state in Rydbergs and

$$\mathbf{K} = \mathbf{K}_f - \mathbf{K}_i$$

is the momentum transfer vector having magnitude

$$K = \sqrt{K_i^2 + K_f^2 - 2K_iK_f\cos\theta'}$$

where $\theta' = \pi - \theta$ is the angle between K_i and K_f. The total cross section

$$\sigma = 2\pi\int_0^\pi I(\theta)\,\sin\theta d\theta$$

is expressed in terms of an integration over K as

$$\sigma = \frac{4}{K_i^2T^4}\frac{g_f}{g_i}\int_{K_{\min}}^{K_{\max}} |A(K)|^2\,KdK$$

where $K_{\min} = K_f - K_i$ and $K_{\max} = K_f + K_i$.

For molecular transitions the wave functions ψ_i and ψ_f are total wave functions including the vibrational and rotational motion. However, we wish to consider here only the cross section averaged over initial and final rotational and vibrational states, and therefore calculate $A(K)$ at the equilibrium position of the nuclei. This is reasonable for the $O_2X^3\Sigma_g^- - a\ ^1\Delta_g$ transition since the 0–0 Franck-Condon factor is 0.986 [7].

The dominant single configuration representing the molecular oxygen $X^3\Sigma_g^-$ and $A^1\Delta_g$ states is

$$1\sigma_g^2 1\sigma_u^2 2\sigma_g^2 2\sigma_u^2 3\sigma_g^2\ 1\pi_u^4 1\pi_g^2$$

with $1\pi_g^2$ coupled $^3\Sigma^-$ in the former and $^1\Delta$ in the latter. The transition is possible since the incident electron can couple with each of these states to produce a

* This work was supported by the Naval Research Laboratory, Washington, D.C.

doublet. A detailed consideration of these antisymmetrized doublet wave functions show that the matrix element A may be written as

$$|A| = \frac{3}{\sqrt{6}} < 1\pi_g^y\ (\Sigma)\ |e^{i\mathbf{K}\cdot\mathbf{r}}|\ 1\pi_g^x\ (\Delta) >$$

where $\pi^{\pm 1} = (\pi^x \pm i\pi^y)/\sqrt{2}$. This matrix element was evaluated analytically using a Gaussian expansion basis for the $1\pi_g$ orbitals, which were determined by a Hartree-Fock self-consistent field procedure [10]. The Gaussian basis, which is derived from the atom results of Huzinaga [11], contained a total of 48 functions and should represent the orbitals well. A subsequent multi-configuration self-consistent field calculation using a Slater trial orbital expansion basis [12] indicates that neglecting electron correlation near R_e probably does not introduce an error in A greater than 20 percent or so.

$A(K)$ was evaluated between $K=0$ and 5 a_0^{-1} at equal intervals of 0.25 a_0^{-1}. This, plus an accurate numerical interpolation formula, permitted the evaluation of $I(\theta)$ and σ for a number of incident electron energies. The results for the total cross section are shown in figure 1, which also includes the experimental points of Trajmar et al. [7]. As may be expected for a Born-type approximation, the high energy tail is calculated fairly well, whereas the low energy calculated cross sections differ appreciably from the experimental values. The source of this difference is clear when one examines the differential cross section. The present approximation necessarily predicts no forward peaking in $I(\theta)$, whereas Trajmar et al., observe strong forward peaking, as shown in figure 2. The major difference between the calculated and experimental total cross sections below 10 eV results from the difference in the small angle differential cross section. (However, the contribution to the total cross section from forward peaking is somewhat reduced by the volume element $\sin\theta d\theta$).

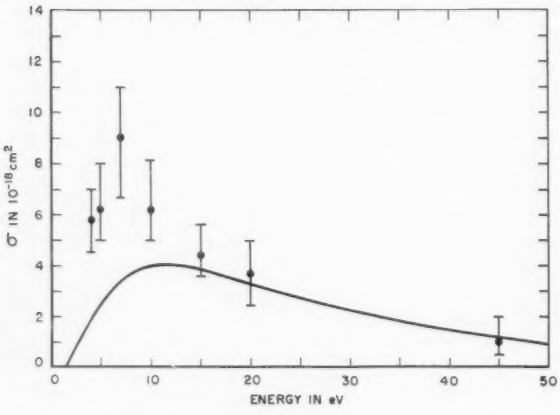

FIGURE 1. *Calculated total cross section for excitation of $^1\Delta_u$ as a function of incident electron energy.*

The experimental points of Trajmar et al., are also shown.

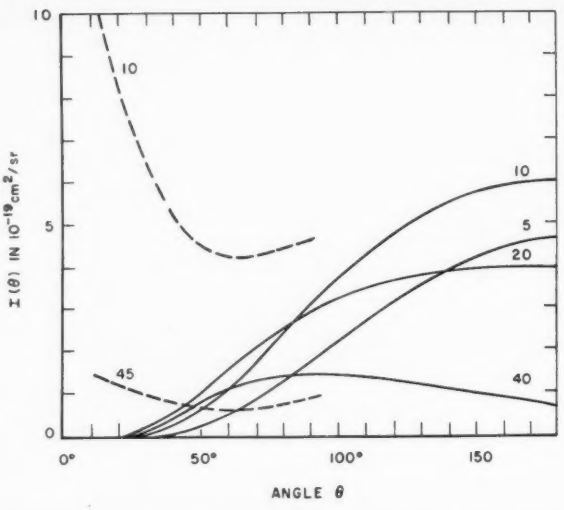

FIGURE 2. *Calculated differential cross section for excitation of $^1\Delta_g$ for incident electron energies of 5, 10, 20, and 40 eV.*

Experimental values of Trajmar et al., at 10 and 45 eV are also shown.

The total cross section has also been measured above 20 V by Konishi et al. [9]. Although their values differ appreciably from those of Trajmar et al., the latter authors point out that there is not necessarily any inconsistency between the two results if the error limits on both measurements are taken into consideration. The differential cross section has been measured at an incident energy of 30 eV by Suzuki et al. [8]. Their large angle cross section does not differ from the present result or that of Trajmar et al. (estimated by interpolation) by more than a factor of 2 or so. However, they do not observe the forward peaking of the latter authors. Their cross section for angles less than about 30° is decreasing and appears to be tending towards zero.

The large peak in the total cross section around 7 eV has been ascribed [13] to scattering through excited states of O_2^-. Only the $^2\Pi_u$ state can contribute by a first-order exchange mechanism. This state can also decay by dissociation to $O(^3P)+O^-(^2P)$ and back to the ground state of O_2. Since the $^2\Pi_u$ state is expected to have a small electronic width, it is not certain that this resonance state contributes substantially to the forward peaking and total cross section at low energies. But this mechanism shows how inaccurate the Ochkur-Rudge approximation can be at low energies.

This simple approximation appears to provide a useful estimate of the total cross section for the exchange scattering as observed by all who have applied it. At the equilibrium separation the Gaussian basis SCF wave functions also appear to be sufficiently accurate as long as the inherent approximate nature of the method is realized.

References

[1] Ochkur, V. I., Zh. Eksp. Teor. Fiz. **45,** 734 (1963) [Sov. Phys. JETP **18,** 503 (1964)].
[2] Rudge, M. R. H., Proc. Phys. Soc. (London) **85,** 607 (1965); **86,** 763 (1965).
[3] Truhlar, D. G., Cartwright, D. C., Kuppermann, A., Phys. Rev. **175,** 113 (1968).
[4] Cartwright, D. C., Kuppermann, A., Phys. Rev. **163,** 86 (1967).
[5] Chung, S., Lin, C. C., Ap. Optics **10,** 1790 (1971).
[6] Cartwright, D. C., Phys. Rev. **A2,** 1331 (1970).
[7] Trajmar, S., Cartwright, D. C., Williams, W., Phys. Rev. **A4,** 1482 (1971).
[8] Suzuki, H., Wakiya, K., Takayanagi, T., Okino, T., Studies of Atomic Collisions and Related Problems in Japan. Progress Report, Institute of Space and Aeronautical Science, University of Tokyo, March 1971, p. 8.
[9] Konishi, A., Yamamoto, K. W., Suzuki, H. J. Phys. Soc. Japan **29,** 526 (1970).
[10] The present calculations were made with a computer program IBMOL2, that was written by E. Clementi and A. Veillard, and modified to suit the open-shell problem. See E. Clementi and D. R. Davis. J. Comput. Phys. **1,** 223 (1966).
[11] Huzinaga, S., J. Chem. Phys. **42,** 1293 (1965).
[12] Julienne P. S., and Krauss, M., unpublished.
[13] Larkin, I. W., and Hasted, J. B., J. Phys. **B5,** 95 (1972).

(Paper 76A6–750)

JOURNAL OF RESEARCH of the National Bureau of Standards—A. Physics and Chemistry
Vol. 76A, No. 6, November–December 1972

Vibrational and Electronic Oscillator Strengths of LiO*

M. Marchetti, P. S. Julienne, and M. Krauss

Institute for Materials Research, National Bureau of Standards, Washington, D.C. 20234

(July 28, 1972)

Electronic energies and wave functions of ground and excited states of LiO are calculated in the Hartree-Fock approximation. The vibrational oscillator strengths of the $X^2\Pi$ and $A^2\Sigma^+$ valence states are calculated for $v=0$ to 1 and 1 to 2 transitions. Electronic oscillator strengths are also presented for transitions to the quantum number two Li Rydbergs. Reasons are presented to support the use of the Hartree-Fock approximation.

Key words: $A^2\Sigma$; electronic transition probabilities; Hartree-Fock; LiO, vibrational transition probabilities; $X^2\Pi$.

1. Introduction

Refractory metal oxides have proved to be difficult experimental subjects. For even one of the simplest, LiO, little is known about the system beyond the ground state properties of the $X^2\Pi$ state. In particular there is no experimental information on the infrared intensities and the ultraviolet spectrum. Interest in the radiative properties of LiO has prompted a number of theoretical calculations. Accurate Hartree-Fock (H-F) and configuration interaction (CI) results [1][1] have been reported for the $X\,^2\Pi$ and the low-lying $^2\Sigma^+$ excited states. These results show that the properties of this molecule are accessible to theoretical calculation. This paper will apply the Hartree-Fock technique to some remaining problems of the properties of LiO.

The Hartree-Fock self-consistent-field variational calculations are based upon an anti-symmetrized product of one-electron orbitals that are determined by the averaged field of all the other electrons. The lack of correlation in this model leads to large absolute errors in the energy. But the applicability of the Hartree-Fock technique must not be rejected out of hand without an examination of the problem at question since correlated wave functions are obtained at high cost. There are four calculations considered in this paper: (1) the energy curve of the ground state and the vertical excitation energies of the low-lying excited states, (2) the infrared intensities of the $X^2\Pi$ and $^2\Sigma^+$ states, (3) the oscillator strengths for excitation from the ground state to all the low-lying excited states, and (4) the Λ doubling matrix elements.

The limitations of the Hartree-Fock method can lead to significant and unknown errors in the calculation of excitation energies when the correlation energies are very different in the ground and excited states. However, it is clear from the monovalent character of the Li and the ionic behavior of the molecule in the neighborhood of the equilibrium internuclear separation, that the $X^2\Pi$ and $A^2\Sigma^+$ states are best described as different orientations of the $O^-(^2P)$ orbital angular momentum relative to the molecular axis. Hartree-Fock and correlated results should agree for relative energies and this is found in the recent accurate CI results [1b]. The present study supplements this work done on the $X^2\Pi$ and $A^2\Sigma^+$ states and repeats sufficient work to show substantial agreement in the areas that overlap.

2. Self-Consistent-Field Solutions

The present calculations were performed with a Gaussian-type function (GTF) constructed by augmenting the 9/5 basis of Huzinaga [3] with three $2p$ Li functions that are suitable for representing the ^2P excited state of Li. The configurations can be represented:

$$1\sigma^2 2\sigma^2 3\sigma^2 4\sigma^2 1\pi^3 \qquad X^2\Pi$$

$$1\sigma^2 2\sigma^2 3\sigma^2 4\sigma\ 1\pi^4 \qquad A^2\Sigma^+$$

The $X^2\Pi$ and $A^2\Sigma^+$ were calculated at five distances for which the energies and dipole moments are given in table 1. There is a crossing of these states near

* This research was supported in part by the Advanced Research Projects Agency of the Department of Defense under the Strategic Technology Office.

[1] Figures in brackets indicate the literature references at the end of this paper.

TABLE 1. LiO *Energy as a function of internuclear separation*[a]

	$X^2\Pi$		$A^2\Sigma^+$	
R(a.u.)	$-E$	μ	$-E$	μ
2.7	82.2493	2.49	82.2586	2.19
2.9	82.2706	2.63	82.2699	2.37
3.184	82.2817	2.84	82.2716	2.64
3.4	82.2815	2.99	82.2668	2.85
3.6	82.2774	3.14	82.2598	3.04

[a] Energy and dipole moment given in atomic units: E, 1 a.u. = 27.2097 eV; μ, 1 a.u. = $2.54158.10^{-18}$ esu cm.

2.9 a.u. which is in accord with the united atom character of these states. At large internuclear separation the $^2\Sigma^+$ state correlates with $O(^3P)+Li(^2P)$ while the $^2\Pi$ state correlates with ground state atoms. Since the SCF configurations do not go correctly asymptotically there is little point in determining dissociation energies.

The Rydberg orbitals were obtained by direct variation at $R=3.184$ a.u. of the Rydberg states to the $^3\Sigma^-$ and $^1\Sigma^+$ ions. These states were chosen as representative by consideration of the ion atom interaction at long distance. Adiabatic correlation rules predict that the interaction of $Li^+(^1S)$ and $O(^3P)$ yields $^3\Sigma^-$ and $^3\Pi$ states for which the $^3\Sigma^-$ is attractive and $^3\Pi$ repulsive with respect to the ion-quadrupole interaction. Similarly, the interaction of $Li^+(^1S)$ and $O(^1D)$ yields $^1\Delta$, $^1\Pi$, and $^1\Sigma^+$ for which only the $^1\Delta$ state is attractive with respect to the ion-quadrupole interaction. The most attractive ion states were considered with 2*s* and 2*p* Rydberg Li electrons as given in the list above. Analysis of the wave functions shows very little difference between Rydberg orbitals obtained between the Rydbergs for the $^3\Sigma^-$ and $^1\Sigma^+$ states. The different orientation of the quadrupole of the oxygen atom will affect the energy position but the transition probabilities for a number of Rydberg transactions can be estimated from the orbitals calculated from a few representative states.

3. Discussion

A. $X^2\Pi$ and $A^2\Sigma^+$ Energies

Polarization functions were not included in the present calculation. Comparison with the accurate Hartree-Fock results of Yoshimine [1b] show that the error increases to smaller internuclear separation as expected. Polarization is more important as the atoms approach each other. However, the error induced in the spectroscopic properties is not substantial. This calculation obtained $\omega_e=804.4$ cm^{-1}, $R_e=3.275$ a.u., and $\omega_e x_e=6.1$ cm^{-1} for $X^2\Pi$ and $\omega_e=877.5$ cm^{-1}, $R_e=3.076$ a.u., and $\omega_e x_e=10.5$ cm^{-1} for $A^2\Sigma^+$. The largest error is about 5 percent in the ω_e of $X^2\Pi$. Note that the accurate CI spectroscopic constants are in very close agreement with the H-F results [1b]. Fortuitously, the present results are in better agreement with the reported experimental results [2] for the $X^2\Pi$ state. The ω_e for $^2\Sigma^+$ is within 7 cm^{-1} of the H–F value and the improved shape is related both to the fact that the asymptote of the $^2\Sigma^+$ H-F state is not ionic which diminishes the asymptotic error and to the σ character of the open shell orbital. The GTF basis is more flexible for the σ orbitals and the polarization error is accordingly less.

B. Infrared Intensities

The dipole moment values are within 10 percent at worst in absolute agreement with the accurate CI values [1]. More important all the curves are very ionic and linear. The slopes of the present results agree with the CI results to within 2 to 3 percent.

Vibrational oscillator strengths were calculated from the equation

$$f=\frac{2}{3}\Delta E\,|<\Psi_{v'}|\mu(R)|\Psi_{v''}>|^2$$

$$=\frac{2}{3}\Delta E\,I^2.$$

The vibrational energies and f numbers for the $0\rightarrow 1$ and $1\rightarrow 2$ transitions are given in table 2. The infrared

TABLE 2. LiO *vibrational oscillator strength*

State	Vibrational transition	ΔE(cm^{-1})	Band strength (I^2)	$f\cdot 10^5$
$X^2\Pi$	0–1	792	0.0082	2.0
	1–2	780	.0165	3.9
$A^2\Sigma^+$	0–1	856	.0128	3.3
	1–2	836	.0260	7.4

transitions are strong for both states as expected for an ionic system. These values are in moderate agreement [4] with values obtained from the CI calculation. Since the dipole moment function is linear the $0\rightarrow 2$ transition is very weak.

The vibration-rotational levels of the $X^2\Pi$ state are perturbed by the $A^2\Sigma^+$. The Λ-doubling matrix element is readily evaluated since the electronic matrix element $<\Psi(\pi)\,|\,L^+\,|\,\Psi(\Sigma^+)>$ does not vary with internuclear separation and is equal in magnitude to the pure precessing value. The matrix element $<\Psi_v(^2\Pi)\,|\,V\,|\,\Psi_{v'}(^2\Sigma^+)>$, where

$$V=\frac{1}{\sqrt{2}\mu R^2},$$

is given in table 3. The sensitivity of these values with vibrational quantum number would caution that they be considered quite approximate considering the level of accuracy of the energy curves.

TABLE 3. LiO Λ-*doubling matrix element* [a]

$v(^2\Pi)$ $v'(^2\Sigma^+)$	0	1	2	3	4
0	1.25	1.03	0.69	0.43	0.25
1	−0.96	0.47	.90	.83	.62
2	0.40	−0.99	−0.008	.65	.81
3	−0.09	0.57	−.89	−0.29	.39
4	0.0007	−0.14	0.67	−.77	−0.44

[a] Matrix element $< \psi_v(^2\Pi)|\hbar^2/\sqrt{2}\mu R^2|\psi_{v'}(^2\Sigma^+) >$ in cm^{-1}.

C. Electronic Oscillator Strengths

The low-lying ion states of LiO^+ can be represented:

$$1\sigma^2 2\sigma^2 3\sigma^2 4\sigma^2 1\pi^2 \qquad {}^3\Sigma^-, {}^1\Delta, {}^1\Sigma^+$$

$$1\sigma^2 2\sigma^2 3\sigma^2 4\sigma 1\pi^3 \qquad {}^3\Pi, {}^1\Pi$$

Rydberg Li 2*s* and 2*p* orbitals were generated in the field of the $^3\Sigma^-$ and $^1\Sigma^+$ SCF approximations to the ions. Since these states are most widely separated in energy and the Rydberg orbitals were determined to be substantially the same for both ion cores, the Rydberg 5σ(Li 2*s*), 6σ(Li 2*p*), and 2π(Li 2*p*) orbitals were used to determine oscillator strengths for the $^3\Sigma^-$, $^1\Delta$, $^3\Pi$, and $^1\Pi$ Rydbergs. The $^1\Sigma^+$ state will require substantial mixing of the $4\sigma^2 1\pi^2$ and $1\pi^4$ configurations and, in any case, is the highest energy of these ion states.

Asymptotic correlations are given in table 4 for several of the lower asymptotes that can correlate with the valence and quantum number 2 Rydbergs. It is apparent that the asymptotic behavior of the Rydberg states is complicated since a sizable fraction must become valence. However, at the R_e of the ground state the single Rydberg configuration should be a good approximation to the true wave function.

TABLE 4. *Adiabatic correlation of molecular states of* LiO

Molecular states [a]	Atomic states [b]	Asymptotic energy (eV)
$^{2,4}\Sigma^+$, $\Sigma^-(2)$, $\Pi(2)$, Δ	$Li(^2P_u) + O(^3P_g)$	3.83
$^{2,4}\Sigma^-$, Π	$Li(^2S_g) + O(^3P_g)$	3.37
$^2\Pi(3)$, Σ^-, $\Sigma^+(2)$, Φ $\Delta(2)$, Φ	$Li(^2P_u) + O(^1D_g)$	2.57
$^2\Delta$, Σ^+, Π	$Li(^2S_g) + O(^1D_g)$	1.97
$^{2,4}\Sigma^-(2)$, $\Pi(2)$, Δ, Σ^+	$Li(^2P_u) + O(^3P_g)$	1.85
$^{2,4}\Sigma^-$, Π	$Li(^2S_g) + O(^3P_g)$	0

[a] $^{2,4}\Sigma^-$, Π signifies $^2\Sigma^-$, $^4\Sigma^-$, $^2\Pi$, $^4\Pi$.

[b] Atomic states and energies, from C. E. Moore, Atomic Energy Levels, Nat. Stand. Ref. Data Ser., Nat. Bur. Stand. (U.S.), 35, Vol. 1, 359 pages (Dec. 1971).

From the asymptotic behavior and the calculated energies at $R = 3.184$ a.u., we can deduce that these Rydberg states will probably be photodissociated. Both the $^4\Sigma^-$ and $^2\Sigma^-$ that arise from the ground state atoms will correlate with the $1\pi^2 5\sigma$ configuration and the $^4\Sigma^-$ state is at least 0.6 eV above the asymptote. The $^2\Delta$ state correlates to $Li(^2P) + O(^3P)$ and is calculated to be about 1.0 eV above this asymptote. The ion states go formally correctly to the asymptote, and the configuration mixing required to insure that the excited valence asymptotes are correctly obtained should only be important at large internuclear separation. The excitation energy is, therefore, meaningful within the error due to the lack of polarization functions. The error in the $X^2\Pi$ state at R_e is about 0.027 a.u. and the $^2\Delta$ state would still be repulsive at this distance. The $^2\Sigma^-$ and $^2\Pi$ Rydbergs that can go asymptotically to $Li(^2P) + O(^3P)$ should be above the $^4\Sigma^-$ in energy and, even with the polarization error, would be photodissociated. Without a configuration mixing calculation it is impossible to be certain but the present analysis would indicate that the vertical excitation of LiO from either $X^2\Pi$ or $A^2\Sigma^+$ would lead to dissociation throughout the Rydberg region.

Transition probabilities are calculated from both the $X^2\Pi$ and $A^2\Sigma^+$ states by forming the appropriate symmetry-adapted linear combination of determinants. In order to avoid estimating the excitation energy, the oscillator strengths were obtained with an expression using the product of the dipole length and velocity matrix elements [5],

$$f = \frac{2}{3} |< \mathbf{r} >^2 < \mathbf{p} >^2|^{1/2} \, (2 - \delta_{0\Lambda_i}\delta_{0\Lambda_f})/(2 - \delta_{0\,\Lambda_i}),$$

after summing over all initial and final state degeneracies, averaging over the degeneracies of the initial state, including the Λ-doublet substates [6], and using the fact that the sum of Franck-Condon factors to final vibrational states is unity.

There are no strong transitions apparent in table 5. The strong $2s \rightarrow 2p$ resonance transition of Li is not involved here since the ground state is so ionic that all low-lying transitions originate on the O^- atom and the overlap through the dipole operator is relatively small.

The electronic oscillator strength for the transition from the ground $X^2\Pi$ state to the $A^2\Sigma^+$ state is calculated to be about $4 \cdot 10^{-7}$. This extremely small value reflects the ionic character of the two states. The transition is between different orientations of the O^- ion which has no dipole moment.

TABLE 5. LiO *spectral distribution from* $X^2\Pi$ *and* $A^2\Sigma^+$ *states*

Transitions [a]			$\lvert<r>\rvert$	$\lvert<\nabla>\rvert$	$f(r, \nabla)$
	Final state	Ion Rydberg			
$^2\Pi \rightarrow$	($^2\Pi$;	$^3\Pi$, $^2\Sigma^+$)	0.0217	0.00271	3.94×10^{-5}
$^2\Pi \rightarrow$	($^2\Pi$;	$^3\Pi$, $^2\Sigma^+$)	.0193	.00639	8.26×10^{-4}
$^2\Pi \rightarrow$	($^2\Pi$;	$^1\Pi$, $^2\Sigma^+$)	.125	.0156	1.31×10^{-3}
$^2\Pi \rightarrow$	($^2\Pi$;	$^1\Pi$, $^2\Sigma^+$)	.111	.0368	2.75×10^{-3}
$^2\Pi \rightarrow$	($^2\Sigma^+$;	$^1\Pi$, $^2\Pi$)	.0415	.0179	4.97×10^{-4}
$^2\Pi \rightarrow$	($^2\Sigma^-$;	$^1\Pi$, $^2\Pi$)	.0415	.0179	4.97×10^{-4}
$^2\Pi \rightarrow$	($^2\Sigma^+$;	$^3\Pi$, $^2\Pi$)	.0239	.0103	1.65×10^{-4}
$^2\Pi \rightarrow$	($^2\Sigma^-$;	$^3\Pi$, $^2\Pi$)	.0239	.0103	1.65×10^{-4}
$^2\Pi \rightarrow$	($^2\Delta$;	$^1\Pi$, $^2\Pi$)	.0587	.0254	9.94×10^{-4}
$^2\Pi \rightarrow$	($^2\Delta$;	$^3\Pi$, $^2\Pi$)	.0678	.0293	1.32×10^{-3}
$^2\Pi \rightarrow$	($^2\Sigma^-$;	$^3\Sigma^-$, $^2\Sigma^+$)	.207	.0209	2.89×10^{-3}
$^2\Pi \rightarrow$	($^2\Sigma^-$;	$^3\Sigma^-$, $^2\Sigma^+$)	.258	.0812	1.40×10^{-2}
$^2\Pi \rightarrow$	($^2\Delta$;	$^1\Delta$, $^2\Sigma^+$)	.254	.0256	4.34×10^{-3}
$^2\Pi \rightarrow$	($^2\Delta$;	$^1\Delta$, $^2\Sigma^+$)	.316	.0995	2.10×10^{-3}
$^2\Pi \rightarrow$	($^2\Pi$;	$^3\Sigma^-$, $^2\Pi$)	.243	.0279	4.52×10^{-3}
$^2\Pi \rightarrow$	($^2\Pi$;	$^1\Delta$, $^2\Pi$)	.297	.0342	6.79×10^{-3}
$^2\Sigma^+ \rightarrow$	($^2\Pi$;	$^1\Pi$, $^2\Sigma$)	.308	.0548	2.26×10^{-2}
$^2\Sigma^+ \rightarrow$	($^2\Pi$;	$^1\Pi$, $^2\Sigma$)	.236	.1012	3.18×10^{-2}
$^2\Sigma^+ \rightarrow$	($^2\Sigma^+$;	$^3\Pi$, $^2\Sigma$)	.0535	.0095	3.39×10^{-4}
$^2\Sigma^+ \rightarrow$	($^2\Sigma^+$;	$^3\Pi$, $^2\Sigma$)	.0409	.0175	4.79×10^{-4}
$^2\Sigma^+ \rightarrow$	($^2\Sigma^+$;	$^1\Pi$, $^2\Pi$)	.143	.0111	1.06×10^{-3}

TABLE 5. LiO *spectral distribution from* $X^2\Pi$ *and* $A^2\Sigma^+$ *states*—Continued

Transitions [a]			$\lvert<r>\rvert$	$\lvert<\nabla>\rvert$	$f(r, \nabla)$
	Final state	Ion Rydberg			
$^2\Sigma^+ \rightarrow$	($^2\Sigma^+$;	$^3\Pi$, $^2\Pi$)	0.248	0.0192	3.19×10^{-3}
$^2\Sigma^+ \rightarrow$	($^2\Pi$;	$^1\Sigma^+$, $^2\Pi$)	.0571	.0226	1.72×10^{-3}

[a] The transition $^2\Pi \rightarrow$ ($^2\Pi$; $^3\Pi$, $^2\Sigma^+$) designates the following: initial state → (final state; ion state, Rydberg orbital symmetry).

4. References

[1a] Wahl, A. C., (private communication). Energy and spectroscopic constants reported in reference [2].
[1b] Yoshimine, M., J. Chem. Phys. to be published.
[2a] Freund, S. M., Herbst, E., Mariella, R. P., and Klemperer, W., J. Chem. Phys. **56,** 1467 (1972).
[2b] White, D., Seshadri, K. S., Dever, D. F., Mann, D. E., and Linevsky, M. J., J. Chem. Phys. **39,** 2463 (1963).
[3] Huzinaga, S., J. Chem. Phys. **42,** 1293 (1965).
[4] Liu, B., private communication, to be published.
[5] Hansen, A. E., Mol. Phys. **13,** 425 (1967).
[6] Schadee, A., J. Quant. Spectr. Rad. Trans. **7,** 169 (1967).

(Paper 76A6–751)

JOURNAL OF RESEARCH of the National Bureau of Standards—A. Physics and Chemistry
Vol. 76A, No. 6, November–December 1972

Publications of the National Bureau of Standards*

Citations with Selected Abstracts

H105-1. (Revised 1972). **Specifications and tolerances for reference standards and field standard weights and measures. 1. Specifications and tolerances for field standard weights (NBS class F),** T. M. Stabler, Nat. Bur. Stand. (U.S.), Handb. 105-1, 12 pages (July 1972) 25 cents, SD Catalog No. C13.11:105-1.

Key words: Field standard weights; specifications; test weights; tolerances; weights and measures inspection; weights used by servicemen.

These specifications and tolerances are recommended as minimum requirements for standards used in the field by State and local weights and measures officials in examination of weighing devices. Revision of NBS Handbook 105-1, Apr. 1969.

H110-1. **National Electrical Safety Code. Part 1. Rules for the installation and maintenance of electrical supply stations and equipment,** Nat. Bur. Stand. (U.S.), Handb. 110-1, 43 pages (June 1972) 30 cents, SD Catalog No. C13.11:110-1.

Key words: Electrical safety; electrical supply station; electrical utility station; high voltage safety; power station equipment; power station safety.

This Handbook contains Part 1 of the National Electrical Safety Code and supersedes NBS Handbook H31 and pages 31 through 75 of the NBS Handbook H30. Part 1 of this Code covers the electric conductors and equipment in electrical supply stations along with the associated structural arrangements employed, for example, by an electrical or railway utility in the exercise of its function as a utility and accessible only to properly qualified personnel. It also covers similar electric conductors and equipment in electrical supply stations when owned by and installed in an industrial establishment, where the electrical supply stations are under the control of and accessible only to properly qualified persons. Examples of such industrial establishments are the paper and steel industries.

H111. **American National Standard. Radiation safety for x-ray diffraction and fluorescence analysis equipment.** Nat. Bur. Stand. (U.S.), Handb. 111, 20 pages (June 1972) 30 cents, SD Catalog No. C13.11:111.

Key words: Radiation safety; x-ray equipment.

This standard reviews the types of injuries resulting from accidental exposure to ionizing radiation resulting from the operation of x-ray diffraction and fluorescence analysis equipment, establishes equipment design criteria, sets up requirements for approved operating procedures and recommends the establishment of health surveillance, and personnel monitoring programs. The circumstances under which operation of equipment must be limited to specially designated areas equipped with radiation barriers and warning signs are set forth. Maximum permissible dose limits established by the National Council on Radiation Protection and Measurement are stated. A list of references to selected articles on various aspects of radiation safety is given and notes on the detection and measurement of radiation from x-ray diffraction and fluorescence analysis equipment are included in an appendix.

SP260-33. **Standard reference materials: Comparison of original and supplemental SRM 705, narrow molecular weight distribution polystyrene,** H. L. Wagner, Nat. Bur. Stand. (U.S.), Spec. Publ. 260-33, 30 pages (May 1972) 35 cents, SD Catalog No. C13.10:260-33.

Key words: Characterized polymers; narrow molecular weight polystyrene; polystyrene standard; Standard Reference Material 705.

Because the supply of the original batch of narrow molecular weight distribution polystyrene, SRM 705, is almost exhausted, another supply of polystyrene, reported to be from the same batch as the original has been characterized to determine whether it is the same as the original as far as the properties listed on the certificate are concerned. No difference in molecular weight as measured by light scattering, osmometry, or gel-permeation chromatography could be found. The limiting viscosity numbers were also the same. It was also shown from solution viscosity measurements that pellet to pellet variation in molecular weight is negligible.

SP260-36. **Standard reference materials: A referee method for the determination of calcium in serum,** J. P. Cali, J. Mandel, and L. Moore, Nat. Bur. Stand. (U.S.), Spec. Publ. 260-36, 136 pages (May 1972) $1.25, SD Catalog No. C13.10:260-36.

Key words: Accuracy; atomic absorption spectrometry; calcium in serum; clinical chemistry; referee method for calcium.

The first referee method of analysis (a method of known accuracy) in clinical chemistry has been developed by a team of experts from clinical chemistry, 8 cooperating clinical chemistry laboratories, and scientists from the National Bureau of Standards. Subject to the limitations and provisos stated, calcium in serum can be determined by the referee method to within ± 2% of the "true or absolute" value. Also discussed are: (1) What Constitutes a Meaningful Measurement System; (2) Theory of Operation and Practice Required to Develop a Referee Method; (3) History of the Actual Work; the Referee Method Protocol; (4) Results; (5) The Isotope-Dilution Mass Spectrometry Work; (6) Discussion, Conclusions, and Recommendations for Future Referee Method Developments.

SP260-37. **Standard reference materials: Methods of analysis of NBS clay standards,** J. I. Shultz, R. K. Bell, T. C. Rains, and O. Menis, Nat. Bur. Stand. (U.S.), Spec. Publ. 260-37, 86 pages (June 1972) 75 cents, SD Catalog No. C13.10:260-37.

Key words: Atomic absorption; ceramics; classical procedures; clay materials; flame emission; refractories; Standard Reference Materials.

This publication brings together a compilation of methods used at NBS for the analysis of two complex standard reference clay materials. The methods were selected to give the best obtainable results for those elements normally found in clays. In some instances, more than one procedure was employed for an element as a cross-check on the precision and accuracy of the results. The procedures are presented in two parts. Part I is concerned with the determination of the major

constituents by the classical analytical procedures. Part II covers the minor elements which are determined instrumentally by flame emission and atomic absorption spectrometry. These clay materials serve as analytical composition standards to provide quality control of the basic raw materials which are used in the ceramics and refractories industries.

SP260-38. **Standard reference materials: Preparation and calibration of standards of spectral specular reflectance,** J. C. Richmond and J. J. Hsia, Nat. Bur. Stand. (U.S.), Spec. Publ. 260-38, 57 pages (May 1972) 60 cents, SD Catalog No. C13.10:260-38.

Key words: Aluminum; gold; infrared reflectance; interferometer; mirrors; reflectance; reflectance standards; spectral reflectance; spectral specular reflectance; specular reflectance; standards; ultraviolet reflectance.

This report describes in detail the preparation and calibration of Standard Reference Materials 2001 through 2008. These standards of spectral specular reflectance were prepared commercially by vacuum depositing opaque coatings of gold and aluminum, respectively, onto polished substrates of fine-annealed borosilicate glass. The near-normal (9° from normal) spectral specular reflectance was measured by the multiple-reflection technique. Four different combinations of source, spectrometer, and detector were used to cover the wavelength range from about 0.25 μm to 30 μm and beyond.

SP260-39. **Standard reference materials: The eddy current decay method for resistivity characterization of high purity metals,** A. F. Clark, V. A. Deason, J. G. Hust, and R. L. Powell, Nat. Bur. Stand. (U.S.), Spec. Publ. 260-39, 53 pages (May 1972) 55 cents, SD Catalog No. C13.10:260-39.

Key words: Apparatus; characterization; eddy current decay; electrical resistivity; high purity metals; homogeneity; low temperature.

Characterization of high purity metals by resistivity measurements at low temperatures is discussed. In particular, the eddy current decay method of resistivity measurement is described in detail. The advantages and limitations are presented along with the theoretical basis of the method. Detailed instructions are given for constructing and operating the apparatus.

SP300. Vol. 5. **Precision measurement and calibration. Selected NBS papers on frequency and time,** B. E. Blair and A. H. Morgan, Editors, Nat. Bur. Stand. (U.S.), Spec. Publ. 300, Vol. 5, 565 pages (June 1972) $6.00, SD Catalog No. C13.10:300.

Key words: Atomic beams; atomic clocks; atomic standards; atomic time; clock synchronization; coordinated U.T. dissemination of frequency and time; flicker noise; frequency and time standards; frequency measurement; frequency stability; international comparison of atomic standards; lasers; masers; radio frequency measurements; satellite timing; spectral density; standard frequency and time broadcasts; statistics of frequency and time measurements; time scales; time synchronizations; TV timing; VLF timing.

This is one of a series of volumes consisting of a group of selected papers and monographs by NBS authors, and abstracts of papers by non-NBS and NBS authors, dealing with the precision measurement of specific physical quantities and related topics. The contents should be useful to those in the scientific community who are engaged in frequency and time measurements or are otherwise interested in these physical quantities.

This volume contains selected reprints, and abstracts of very general papers, printed in chronological order in most cases from January 1960 through June 1969, covering the following general topics: Frequency and Time Standards, Time Scales, Distribution of Frequency and Time Signals, Statistics of Frequency and Time Standards, and Selected Frequency and Time References.

SP300. Vol. 9. **Precision measurement and calibration. Selected NBS papers on colorimetry,** I. Nimeroff, Editor, Nat. Bur. Stand. (U.S.), Spec. Publ. 300, Vol. 9, 460 pages (June 1972) $5.50, SD Catalog No. C13.10:300.

Key words: Appearance evaluation: colorimetry; color spacing; color vision; gloss; metamerism; spectrophotometry; standards; uncertainty; variability.

This volume is one of an extended series which brings together the previously published papers, monographs, abstracts, and bibliographies by NBS authors dealing with the precision measurement of specific physical quantities and the calibration of the related metrology equipment. The contents have been selected as being useful to the standards laboratories of the United States in tracing to the NBS standards the accuracies of measurement needed for research work, factory production, or field evaluation.

Volume 9 treats the field of Colorimetry. It contains 37 reprints on Colorimetry and Spectrophotometry assembled in 8 sections: (1) Spectrophotometry, (2) Color Vision, (3) Color Specification, (4) Sources and Instrumentation, (5) Color Spacing and Metamerism, (6) Variabilities and Uncertainties, (7) Appearance and Gloss, (8) List of Publications, LP39 (in part), Colorimetry and Spectrophotometry Publications by the Staff of the National Bureau of Standards, January 1957 through August 1969.

SP305. Supplement 3. **Publications of the National Bureau of Standards 1971 catalog. A compilation of abstracts and key word and author indexes,** B. L. Oberholtzer, Nat. Bur. Stand. (U.S.), Spec. Publ. 305 Suppl. 3, 342 pages (July 1972) $3.00, SD Catalog No. C13.10:305.

SP362. **Chemical kinetics in the C-O-S and H-N-O-S systems: A bibliography—1899 through June 1971,** F. Westley, Nat. Bur. Stand. (U.S.), Spec. Publ. 362, 68 pages (Apr. 1972) 70 cents, SD Catalog No. C13.10:362.

Key words: Bibliography; carbon oxysulfides; carbon sulfides; chemical kinetics; gas phase; hydrogen; nitrogen; nitrogen oxides; oxygen; sulfur; sulfur hydrides; sulfur oxides.

A bibliography, a reaction oriented list of references, is provided for published papers and reports containing rate data for reactions of COS, COS_2, CS, CS_2, CS_3, D_2S, H_2S, H_2S_2, HSO_2, S, SH, SO, SO_2, SO_3, SO_4, S_2, S_2O_2, S_4, S_6 and S_8 with each other and with CO, CO_2, D, D_2, H, H_2, H_2O, N, N_2, N_2O, N_2O_3, NO, NO_2, NO_3, NOS, O, OH, O_2, O_3, R and RH. Three lists of critical reviews dealing with the above reactions are included. 317 papers covering 240 reactions are listed. The period covered extends from 1899 through June 1971.

SP363. **Bibliography on atomic energy levels and spectra, July 1968 through June 1971,** L. Hagan and W. C. Martin, Nat. Bur. Stand. (U.S.), Spec. Publ. 363, 103 pages (June 1972) $1.00, SD Catalog No. C13.10:363.

SP365. **Metric conversion card,** J. V. Odom, Nat. Bur. Stand. (U.S.), Spec. Publ. 365, 2 pages (July 1972) 10 cents ($6.25 for 100 copies), SD Catalog No. C13.10:365.

AMS62. **Cyclic designs,** J. A. John, F. W. Wolock, H. A. David, J. M. Cameron, and J. A. Speckman, Nat. Bur. Stand. (U.S.), Appl. Math. Ser. 62, 79 pages (Apr. 1972) 75 cents, SD Catalog No. C13.32:62.

Key words: Analysis of variance; cyclic designs; design of experiments; designs for calibration; incomplete block designs.

Cyclic designs are incomplete block designs based on cyclic development of an initial block or blocks. Their flexibility, ease in

conduct of the experiment and natural grouping for elimination of heterogeneity make them worthy of attention in their own right even though their analysis does not possess the ease of computation of the more common completely balanced or partially balanced incomplete block designs with two associate classes. Methods for construction and analysis of the designs are given along with a numerical example. Applications of the designs are discussed and an appendix on their use in calibration is given.

NSRDS-NBS40. **A multiplet table of astrophysical interest, (Revised Edition), Part I—Table of multiplets and Part II—Finding list of all lines in the table of multiplets,** C. E. Moore, Nat. Stand. Ref. Data Ser., Nat. Bur. Stand. (U.S.), 40, 253 pages (Feb. 1972) $2.00, SD Catalog No. C13.48:40.

Key words: Atomic spectra, multiplet table; finding list, atomic spectra; multiplet table; spectra, atomic.

Pending the completion of a current edition, the 1945 Multiplet Table is being reprinted here to meet continuing demands. The leading lines in 196 atomic spectra of 85 chemical elements are listed in related groups called multiplets. Estimated intensities, excitation potentials and multiplet designations are given for the individual lines, and each multiplet is assigned a number. An extensive bibliography covers the source material used for the compilation.

The Table is presented in two parts: Part I includes the multiplets, with the spectra of each element being given in order of increasing ionization, and the elements in order of increasing atomic number. Part II is a Finding List in which all the lines in Part I are entered in order of increasing wavelength, with their multiplet numbers.

The range of the Table is from 2951 Å to 13164 Å. A supplementary table of "Forbidden Lines" extends from 2972 Å to 12645 Å. Reprint of NBS Technical Note 36 (PB151395).

BSS41. **Performance of a single-stack DWV system utilizing low-angle stack-branch confluence and bottom shunt venting,** R. S. Wyly and G. C. Sherlin, Nat. Bur. Stand. (U.S.), Bldg. Sci. Ser. 41, 24 pages (Apr. 1972) 35 cents, SD Catalog No. C13.29/2:41.

Key words: Criteria for plumbing; hydraulic test loads; performance of plumbing; single stack plumbing.

Among the more important criteria for hydraulic and pneumatic performance of sanitary drain-waste-vent systems are (1) maintenance of water seals in fixture traps, (2) limitation of pneumatic pressures, (3) limitation of hydrostatic and hydrodynamic pressures, and (4) limitation of cross-flow between horizontal branches or trap arms.

Recent tests of a single-stack drainage system proposed for a high-rise apartment project in Fairfax County, Virginia have produced the following findings with respect to these performance criteria: (1) test loads (total discharge rates) ranging up to magnitudes greater than predicted loads yielded reasonable average trap-seal retention; (2) the use of trap-seal retention as a measure of performance appears to be more meaningful than the traditional pneumatic-pressure measure; (3) fitting geometry and branch arrangement can be more critical in single-stack systems than in conventional vented systems, and (4) present procedures for selecting test loads, for making tests, and for reporting and interpreting measured values need improvement and standardization.

BSS42. **Design loads for inserts embedded in concrete,** T. W. Reichard, E. F. Carpenter, and E. V. Leyendecker, Nat. Bur. Stand. (U.S.), Bldg. Sci. Ser. 42, 28 pages (May 1972) 35 cents, SD Catalog No. C13.29/2:42.

BSS43. **Paper honeycomb sandwich panels as lightweight structural components,** T. W. Reichard, Nat. Bur. Stand. (U.S.), Bldg. Sci. Ser. 43, 7 pages (Apr. 1972) 25 cents, SD Catalog No. C13.29/2:43.

Key words: Adhesives; paper honeycomb; sandwich facings; sandwich panels.

This paper presents a resume of current practice in the U.S. with regard to the use of sandwich panels in single-story buildings. A description and the properties of typical paper honeycomb cores are given. Some of the factors which are considered in choosing sandwich facings and adhesives are given.

PS52-71. **Polytetrafluoroethylene (PTFE) plastic tubing,** L. H. Breden, Technical Standards Coordinator, Nat. Bur. Stand. (U.S.), Prod. Stand. 52-71, 12 pages (Apr. 1971) 20 cents, SD Catalog No. C13.20/2:52-71.

Key words: Chemical, mechanical, and electrical tubing; fluorocarbon plastic tubing; plastic tubing, polytetrafluoroethylene; PTFE tubing; tubing, PTFE-fluorocarbon.

This Voluntary Product Standard covers commercially available PTFE tubing intended for chemical, mechanical, and electrical applications. Included are requirements and methods of test for materials, dimensions, and physical and chemical properties. A method for identifying products which comply with this Standard is provided.

PS53-72. **Glass-fiber reinforced polyester structural plastic panels,** L. H. Breden, Technical Standards Coordinator, Nat. Bur. Stand. (U.S.), Prod. Stand. 53-72, 13 pages (Apr. 1972) 20 cents, SD Catalog No. C13.20/2:53-72.

Key words: Glass-fiber reinforced polyester panels; panels, glass-fiber reinforced polyester; plastic panels, structural; structural panels.

This Voluntary Product Standard covers two types of plastic panels furnished in three weights and seven geometrical configurations, including flat panels, intended for use in structural applications. The Standard covers requirements for the sizes, configurations, weights, and squareness of the panels. Included are requirements for materials, appearance, color uniformity, light transmission, transverse load, bearing load, flammability, packing, and marking. Methods for identifying products that conform to this Standard are also included. Information on chemical resistance and available panels is provided in an appendix.

TN594-1. **Optical radiation measurements: Fundamental principles of absolute radiometry and the philosophy of this NBS program (1968 to 1971),** J. Geist, Nat. Bur. Stand. (U.S.), Tech. Note 594-1, 59 pages (June 1972) 60 cents, SD Catalog No. C13.46:594-1.

Key words: Absolute detector radiometry; electrically calibrated detectors; International Pyrheliometric Scale; irradiance; radiometry.

The philosophy of the present NBS program in realizing a scale of total irradiance with electrically calibrated (absolute) detectors, a theoretical analysis of the sources of error in such a scale realization, a description of the electrically calibrated detector developed from 1968 to 1971, and participation in the Third International Pyrheliometer Comparison are presented.

TN614. **Longitudinal magnetoresistance in polar semiconductors,** R. L. Peterson, Nat. Bur. Stand. (U.S.), Tech. Note 614, 47 pages (Apr. 1972) 50 cents, SD Catalog No. C13.46:614.

Key words: Magnetophonon effect; magnetoresistance; semiconductors; transport theory.

The magnetophonon effect due to resonant interactions of charge carriers with optical phonons in nondegenerate polar semiconductors

is studied when several elastic scattering mechanisms are simultaneously active also. The simple model of the band structure, and the displaced Maxwellian distribution function are used. Analytical expressions for drift mobility are given for $B=0$ and the quantum limit, and are compared with the results of other techniques where possible. The numerical calculations show that whenever magnetophonon oscillations are seen in the ohmic regime, maxima occur near the resonance magnetic fields for all lattice temperature and strengths of scattering mechanisms which compete with the optical phonon scattering. This is in contrast with typical experimental findings, in which minima usually (but not always) appear near the resonance fields for ohmic, longitudinal, conditions. The explanation of the minima must therefore be sought in the use of a distribution function in which carrier-carrier scattering is less important.

TN615. **WR15 thermal noise standard,** W. C. Daywitt, W. J. Foote, and E. Campbell, Nat. Bur. Stand. (U.S.), Tech. Note 615, 154 pages (Mar. 1972) $1.25, SD Catalog No. C13.46:615.

Key words: Error analysis; millimeter wave; noise; Nyquist's theorem; thermal noise standard.

This note describes the design and construction of a WR15 thermal noise power standard. The standard is designed to operate around the Silver Point Temperature (963.19 °C) with a noise temperature output accurate to approximately ± 2 K.

Complete details of the theory, design, construction, and performance tests are given.

TN616. **Frequency standards and clocks: A tutorial introduction,** H. Hellwig, Nat. Bur. Stand. (U.S.), Tech. Note 616, 69 pages (Apr. 1972) 70 cents, SD Catalog No. C13.46:616.

Key words: Cesium beam; clocks (atomic); crystal oscillator; frequency accuracy; frequency stability; frequency standards; hydrogen maser; quartz crystal; rubidium gas cell; timekeeping.

The topic of frequency standards and clocks is treated in a tutorial and nonmathematical way. The concepts of time, frequency, frequency stability, and accuracy are introduced. The general physical principles and design features of frequency standards and clocks are described. The design, performance, and limitations of quartz crystal oscillators and atomic devices (cesium, hydrogen, rubidium) are discussed in detail and critically compared for laboratory devices as well as for devices intended for field usage.

TN617. **Thermophysical properties of parahydrogen from the freezing liquid line to 5000 R for pressures to 10,000 psia.** R. D. McCarty and L. A. Weber, Nat. Bur. Stand. (U.S.), Tech. Note 617, 169 pages (Apr. 1972) $1.50, SD Catalog No. C13.46:617.

Key words: Density; dielectric constant; enthalpy; entropy; equation of state; fixed points; heat transfer coefficients; hydrogen; index of refraction; Joule-Thomson; latent heat; melting point; Prandtl number; specific heat; speed of sound; surface tension; thermal conductivity; thermal diffusivity; vapor pressure; viscosity; volume.

Tables of thermophysical properties of para hydrogen are presented for temperatures from the melting line to 5000 R for pressures from 1 to 10,000 psia. The tables include entropy, enthalpy, internal energy, density, volume, speed of sound, specific heat, thermal conductivity, viscosity, thermal diffusivity, Prandtl number and the dielectric constant for 65 isobars. Also included in the isobaric tables are quantities of special utility in heat transfer and thermodynamic calculations: $(\partial P/\partial V)_T$, $(\partial P/\partial T)_V$, $V(\partial H/\partial V)_P$, $V(\partial P/\partial U)_V$, $-V(\partial P/\partial V)_T$, $1/V(\partial V/\partial T)_P$.

In addition to the isobaric tables, tables for the saturated vapor and liquid are given which include all of the above properties, plus the surface tension. Tables for the P-T of the freezing liquid, index of refraction and the derived Joule-Thomson inversion curve are also presented.

TN618. **WR15 microwave calorimeter and bolometer unit,** M. E. Harvey, Nat. Bur. Stand. (U.S.), Tech. Note 618, 41 pages (May 1972) 75 cents, SD Catalog No. C13.46:618.

Key words: Calorimeter; microwave; power; standard.

A microwave calorimeter which serves as the National Bureau of Standards (NBS) standard for power measurements in the frequency range 50 to 75 GHz has been completed and evaluated recently. Included here are descriptions of the principal changes in the calorimeter and bolometer unit from the WR28 models which are of similar design. Also included are construction details, accessory equipment, operation procedure, and error analysis. An improved thermal isolating waveguide section and calorimeter flange are features of this calorimeter.

A careful error analysis permits the determination of the effective efficiency of a standard bolometer unit to estimated limits of systematic uncertainty of $\pm 0.23\%$. The estimated 3σ limit of random uncertainty is 0.05%.

TN710-3. **Building research translation: New regulation on ventilation of dwellings, fixed heating facilities, and flues,** A. Chalandon, M. Schumann, and P. Dechartre, Nat. Bur. Stand. (U.S.), Tech. Note 710-3, 46 pages (May 1972) 50 cents, SD Catalog No. C13.46:710-3.

TN710-4. **Building research translation: Thermal comfort requirement adjacent to cold walls—application to glazed opening,** J. Anquez and M. Croiset, Nat. Bur. Stand. (U.S.), Tech. Note 710-4, 54 pages (May 1972) 55 cents, SD Catalog No. C13.46:710-4.

TN710-5. **Building research translation: Use of an air-to-air heat exchanger to recover heat from air exhausted by mechanical ventilation,** P. Garrivier, Nat. Bur. Stand. (U.S.), Tech. Note 710-5, 62 pages (July 1972) 60 cents, SD Catalog No. 13.46:710-5.

TN715. **Tabulation of published data on electron devices of the U.S.S.R. through December 1971,** C. P. Marsden, Nat. Bur. Stand. (U.S.), Tech. Note 715, 108 pages (June 1972) $1.00, SD Catalog No. C13.46:715.

Key words: Electron devices; electron tubes; semiconductors; U.S.S.R.

This tabulation includes published data on U.S.S.R. electron devices as collected from publications, mostly handbooks, published by the various ministries and institutes of the U.S.S.R. Information is given on all active devices ranging from receiving to microwave devices, semiconductor devices, and miscellaneous devices such as photographic flash tubes and thermistors. Supersedes NBS TN526.

TN719. **A simple correction procedure for quantitative electron probe microanalysis,** K. F. J. Heinrich, R. L. Myklebust, H. Yakowitz, and S. D. Rasberry, Nat. Bur. Stand. (U.S.), Tech. Note 719, 49 pages (May 1972) 55 cents, SD Catalog No. C13.46:719.

Key words: Absorption; atomic number; chemical elements; computation procedure; data reduction; electron probe microanalysis; fluorescence; time-sharing; x-ray analysis.

A calculation technique for data reduction in quantitative electron probe microanalysis is described. This technique is embodied in a computer program, called MULTI8, written in FORTRAN IV for batch processing. Six chemical elements may be determined simultaneously without redimensioning the program. The relative x-ray intensity data are corrected for atomic number, absorption and secon-

dary fluorescence due to the characteristic lines. Options for calculating the mass fraction of one chemical element by difference or by stoichiometry are available in the program. Supersedes and extends NBS TN521.

TN721. **NBS Special Foreign Currency Program in Israel 1970-71,** H. S. Peiser and M. Klein, Nat. Bur. Stand. (U.S.), Tech. Note 721, 175 pages (Apr. 1972) $1.50, SD Catalog No. C13.46:721.

TN722. **Tensile creep of boron epoxy and boron epoxy-reinforced 7075-T6 aluminum alloy,** D. J. Chwirut, Nat. Bur. Stand. (U.S.), Tech. Note 722, 60 pages (May 1972) 60 cents, SD Catalog No. C13.46:722.

Key words: Aluminum alloy; boron/epoxy; composite materials; creep; elastic follow-up technique; sandwich specimen.

Tensile creep tests were performed on twelve specimens of 0° unidirectional boron/epoxy and on twenty-four specimens of 7075-T6 aluminum alloy reinforced with 0° unidirectional boron/epoxy. An analytical procedure for predicting the creep properties of composite-reinforced metals is presented. Agreement between calculated and experimental creep curves varies with test temperature. These discrepancies between experiment and analysis are probably not due to an error in the analysis itself, but rather to uncertainty in the residual stresses in the specimens.

TN723. **A laser technique for investigating the effects of thermal transients on pressure transducer performance characteristics,** P. S. Lederer and J. S. Hilten, Nat. Bur. Stand. (U.S.), Tech. Note 723, 43 pages (May 1972) 45 cents, SD Catalog No. C13.46:723.

Key words: Laser; performance characteristic; pressure transducer; temperature effects; test method; thermal transient.

A simple and repeatable testing technique was developed which makes it practical to obtain information on the zero shift and change in sensitivity of a pressure transducer while it is subjected to a thermal transient generated by a mechanically chopped cw laser beam. Several commercial, flush diaphragm, pressure transducers with ranges from up to 50 psi (3.45×10^6 N/m^2) were tested and showed zero shifts and changes in sensitivity of the order of 20% FS due to thermal transients with power densities up to 100 K W/m^2. The transducer under test can be pressure cycled while it is irradiated. In this way, zero shifts and sensitivity changes may be directly displayed in a procedure which requires a testing time of only about one minute.

TN724. **Properties of selected superconductive materials,** B. W. Roberts, Nat. Bur. Stand. (U.S.), Tech. Note 724, 100 pages (June 1972) $1.00, SD Catalog No. C13.46:724.

Key words: Bibliography; compilation of data; composition; critical field; critical temperature; crystallographic data; low temperature; superconductivity.

This is a noncritical compilation of data on superconductive materials with the exception of data on the elements that has been extracted from a portion of the literature published up to early 1971. The properties concerned are composition, critical temperature, critical magnetic fields, crystallographic data, and the lowest temperature tested for materials specifically explored for superconductivity. The compilation also includes, bibliography, general reference review articles and a special tabulation of high magnetic field superconductors. Supersedes and extends NBS TN482.

TN725. **A neutron moments computer code, moment I,** C. M. Eisenhauer, G. L. Simmons, and L. V. Spencer, Nat. Bur. Stand. (U.S.), Tech. Note 725, 38 pages (May 1972) 50 cents, SD Catalog No. C13.46:725.

TN727. **Methods of measurement for semiconductor materials, process control, and devices. Quarterly report October 1 to December 31, 1971,** W. M. Bullis, Editor, Nat. Bur. Stand. (U.S.), Tech. Note 727, 79 pages (June 1972) 70 cents, SD Catalog No. C13.46:727.

TN728. **Torsional instabilities in composite and composite-reinforced aluminum-alloy thin-walled cylinders,** D. E. Marlowe, Nat. Bur. Stand. (U.S.), Tech. Note 728, 77 pages (June 1972) 70 cents, SD Catalog No. C13.46:728.

Key words: Aircraft structures; boron/epoxy; composite materials; reinforced aluminum; stability; thin shells; torsion buckling.

The elastic buckling strength has been determined for thin-walled aluminum-alloy tubes fabricated with and without unidirectional boron/epoxy and glass/epoxy composite materials applied as reinforcement to their outer surfaces. Three boron/epoxy ply orientations were investigated. The results of these tests have been compared with the buckling strengths predicted by two analytical techniques. It was found that reinforcement of the metal tubes with an equal thickness of the composite material increased the buckling strength about threefold. The effect on buckling strength of the ply angles investigated is small when compared with the overall effect of adding the reinforcement. The analyses have approximately the same degree of accuracy as that generally attributed to Donnell's treatment of isotropic tubes.

TN729. **Design, construction, and testing of a new high accuracy spectrophotometer,** K. D. Mielenz and K. L. Eckerle, Nat. Bur. Stand. (U.S.), Tech. Note 729, 60 pages (June 1972) 60 cents, SD Catalog No. C13.46:729.

Key words: Beam non-uniformity; circular entrance and exit apertures; high accuracy spectrophotometer; linearity; parabolic mirrors; stray radiant energy; transmittance.

A new spectrophotometer is described which has an accuracy of approximately 0.0001 transmittance units. The spectrophotometer utilizes a collimated beam in the sample area. This is accomplished by means of off-axis parabolic mirrors in the monochromator and sample compartment. Also, circular holes are used as entrance and exit apertures in the monochromator. All components of this spectrophotometer were chosen to achieve maximum accuracy. The result of this work is a "state of the art" instrument. The instrument was tested to evaluate its performance. Systematic errors such as detector non-linearity, stray radiant energy, and beam non-uniformity are measured. A correction for non-linearity of the photomultiplier and electronics is applied.

TN730. **Manual and automated fingerprint registration,** J. H. Wegstein, Nat. Bur. Stand. (U.S.), Tech. Note 730, 26 pages (June 1972) 35 cents, SD Catalog No. C13.46:730.

TN731. **Calibration of secondary standard magnetic tape cassettes (computer amplitude reference) Phase I,** S. B. Geller and P. A. Mantek, Nat. Bur. Stand. (U.S.), Tech. Note 731, 60 pages (July 1972) 60 cents, SD Catalog No. C13.46:731.

Key words: Cassette tapes; cassette transport; computer amplitude reference; magnetic tape cassette; secondary standard; standard reference material; unrecorded references.

This Technical Note discusses a method for developing and maintaining a reference system which will produce NBS Secondary Standard Magnetic Tape Cassettes (Computer Amplitude Reference). It describes both centerline tape search procedures and an interim signal amplitude measurement system for the reference magnetic tape cassette candidates. The results of the initial experiments with cassette tapes and transports are given.

TN732. **A computer terminal network for transparent stimulation of the user of an on-line retrieval system,** S. Treu, Nat. Bur. Stand. (U.S.), Tech. Note 732, 39 pages (July 1972) 45 cents, SD Catalog No. C13.46:732.

Key words: Computer terminal network; human characteristics; interactive information retrieval; man-computer interface; transparent stimulation; unobtrusive monitoring.

A computer terminal network to enable "transparent stimulation" of the user of an on-line retrieval system has been designed, implemented, and pilot tested. Its basic purpose is to provide a suitable and effective framework and methodology for experimental identification/validation of those human characteristics which should be recognized/reinforced in man-computer interface design. The rationale behind the transparent stimulation approach is presented and the methodology employed for such real-time, unobtrusive scanning and manipulation of the man-computer dialogue is described. A general overview of the hardware and software features of the implemented stimulation network is included.

TN734. **OMNITAB II. Segmentation structure for the SCOPE operating system,** S. T. Peavy and R. N. Varner, Nat. Bur. Stand. (U.S.), Tech. Note 734, 25 pages (June 1972) 35 cents, SD Catalog No. C13.46:734.

Key words: ANSI FORTRAN; general-purpose computer program; implementation of OMNITAB II; links; OMNITAB II;

OMNITAB II is an interpretive system developed and maintained by the National Bureau of Standards to enable scientists to use a large computer easily, effectively and accurately for numerical, statistical and data analysis without prior computer experience. The system is as machine independent as possible, making implementation relatively easy. Since OMNITAB II has a large memory requirement, segmentation and overlay are virtually essential.

Overlay procedures are dependent upon the operating system of the computer. Changes are necessary to the OMNITAB II program when the overlay procedure requires specific overlay CALL statements to external procedures in other overlay links. This Technical Note describes a method of segmentation and overlay for a particular operating system (CDC-6000 series). The method can readily be adapted to other operating systems with modifications to the control statements.

The following Bibliography Series are available by purchase from the National Technical Information Service (NTIS), Springfield, Va. 22151.

COM-72-10014. Kondratiev, V. N., **Rate constants of gas phase reactions,** translated by L. J. Holtschlag and edited by R. M. Fristom, 433 pages, January 1972. (Johns Hopkins University, Applied Physics Laboratory, Silver Spring, Md.) $8.50.

Key words: Atom reactions; compilation; critical evaluation; gas phase reactions; radical reactions; rate constants.

This survey of the kinetics of biomolecular and termolecular reactions covers the literature to the end of 1969. Gas-phase reactions of neutral particles have been surveyed, rate constants are presented in consistent units and a number of reactions have been critically evaluated. A table of equilibrium constants has been added to the English edition as well as a bibliography of rate constant compilations and sources of evaluated kinetic information.

COM-72-10266. **Index and cumulative list of papers on radiation chemistry,** Vol. IV, Nos. 27-52, July through December 1971, Radiation Chemistry Data Center, Radiation Laboratory, University of Notre Dame, January 1972, $6.00.

The following are outside publications by the NBS staff, as soon after issuance as practical. For completeness, earlier references not previously reported may be included from time to time. The five digit number at the beginning of each entry is used for record keeping only and should not be used when requesting reprints or other information.

12688. Carpenter, B. S., **Quantitative applications of the nuclear track technique** (Proc. Inter/Micro 71 Conf., London, England, Sept. 17-24, 1971), *Microscope* **20,** 175-182 (1972).

Key words: Boron; glasses; image analyzing system; liver; microscopy; neutron activation analysis; nitrogen; nuclear track technique; orchard leaves; steels; track etch method; uranium.

The nuclear track technique has been used since the early 1960's as a means of mapping the location of uranium and boron concentration in several matrices and in geochronology. This technique has now been applied to the quantitative determination of several elements that emit charged particles. The detector sample "sandwich" is exposed to the desired radiation source, fast or thermal neutrons, or high energy photons, and the charged particles emitted are registered in plastic detectors. The elements boron, lithium, nitrogen, thorium and uranium have been determined in various matrices; *e.g.* liver, orchard leaves, tomato leaves, blood, glass, soil, steel and minerals. The amount of material in these matrices is determined in three different ways, the absolute method, the method of standard additions and the comparative method. All three of these methods require that the plastic detectors be chemically etched and the resulting optically visible tracks are then counted with the aid of an image analyzing microscope.

12689. Carpenter, B. S., LaFleur, P. D., **Observing proton tracks in cellulose nitrate,** *Int. J. Appl. Radiat. Isotop.* **23,** 157-159 (1972).

Key words: Activation analysis; cellulose nitrate detectors; nitrogen; nuclear track technique; proton tracks.

Cellulose nitrate is used as a detector to observe monoenergetic proton tracks. These monoenergetic protons are produced from a ^{14}N source placed in contact with the detector and irradiated in a thermal-neutron flux. After irradiation the detectors are chemically etched to produce optically visible tracks.

12690. Clough, R. B., **Mobile dislocation density and velocity in plastically deformed aluminum at room temperature,** *Scr. Met.* **6,** No. 4, 293-298 (1972).

Key words: Aluminum; dislocation velocity; mobile dislocation density.

Recently, Gillis and Hockett have calculated the Gilman drag stress in commercially-pure aluminum as a function of strain and temperature, basing their calculations on a model of yielding by Gillis and Gilman. The purpose of this note is to show that the Gillis-Gilman model used cannot properly be applied to yielding in aluminum at constant strain rate because it leads to an improbable dislocation velocity-stress relationship. Another more satisfactory model is proposed, and in addition it is pointed out that the entropy of plastic flow in aluminum is significant at 300 K.

12691. Codling, K., Madden, R. P., **Resonances in the photoionization continuum of Kr and Xe,** *Phys. Rev. A* **4,** No. 6, 2261-2263 (Dec. 1971).

Key words: Autoionization; far ultraviolet; krypton; photoionization; resonances; xenon.

A total of 153 krypton resonances in the spectral region 500–337 Å, and 254 xenon resonances in the spectral region 600–375 Å are reported. The disposition of the detailed line lists are indicated. The analysis is very incomplete and will require detailed theoretical calculations to advance. In krypton, 45 resonances and in xenon, 56 resonances have been grouped into probable Rydberg series, for which classifications are suggested. In general, the resonances observed are due to the excitation of the inner subshell "*s*" electron ($ns^2np^6 \rightarrow nsnp^6mp$) or to the excitation of two of the outer electrons simultaneously ($ns^2np^6 \rightarrow ns^2np^4mll'$). These high-lying excited states

autoionize, resulting in resonances with window-, asymmetric-, and absorption-type profiles. The detailed lists for the subshell "*s*" electron excitations are given.

12692. Cooper, J. W., LaVilla, R. E., **"Semi-Auger" processes in L_{23} emission in Ar and KCl,** *Phys. Rev. Lett.* **25,** No. 26, 1745-1748 (Dec. 28, 1970).

Key words: Argon; configuration interaction; KCl; radiative process; two electron processes; x-ray L_{23} emission.

X-ray emission studies in Ar and KCl due to formation of an L_{23} vacancy reveal a low-energy satellite below the main emission peak. Comparison with other data on related processes indicates that this satellite is due to two-electron effects (configuration interaction) in the final state of the emission process.

12693. Coxon, B., **Application of internuclear, double-resonance techniques to carbohydrates. Detection of small coupling-constants,** *Carbohydrate Res.* **18,** No. 3, 427-442 (1971).

Key words: General Overhaus effect; internuclear double resonance; long-range coupling; magnetic equivalence factoring; spin-tickling; transient nutations; 6-deoxy-α-D-glucofuranose derivative.

6-Deoxy-1,2:3,5-di-*O*-isopropylidene-α-D-glucofuranose-d_{12} (**1**-d_{12}) has been synthesized by an exchange reaction of its non-deuterated analog (**1**) with acetone-d_6. The p.m.r. spectrum of **1**-d_{12} at 90 MHz has been analyzed iteratively by means of a computer program for magnetic-equivalence factoring. Confirmation of the assignments of lines in the analysis has been investigated by proton-proton, internuclear, double-resonance (indor) techniques, which served also for the detection of a small long-range coupling-constant. Examples of indor spectra containing general Overhauser effects, spin-tickling effects, or transient nutations are shown, and are discussed in relation to the experimental power-levels of the observing and double-resonance frequencies, and their sweep-rates. The mass spectra of **1** and **1**-d_{12} are analyzed and compared.

12694. Dodge, W. R., Murphy, J. J., II, **Ratio of the ^{4}He(γ,*p*) and ^{4}He(γ,*n*) cross sections,** *Phys. Rev. Lett.* **28,** No. 13, 839-843 (Mar. 27, 1972).

Key words: Differential cross section; electrodisintegration; isospin; light nuclei; photonuclear; ratio cross sections.

The ^{4}He(γ,*p*)^{3}H and ^{4}He(γ,*n*)^{3}He cross sections have been determined with a magnetic spectrometer in the energy interval of 30.0 to 51.8 MeV. We find that the average value of $\sigma(\gamma,p)/\sigma(\gamma,n)$ is 1.03 ± 0.04 in the above energy interval. The ^{4}He(γ,*p*) cross section decreases from 1.52 ± 0.13 mb at 31.7 MeV to 0.36 ± 0.03 mb at 51.8 MeV.

12695. Durst, R. A., Staples, B. R., Paabo, M., **Activity standards for ion-selective electrodes,** *Experientia Suppl.* **18,** 275-279 (1971).

Key words: Activity standards; clinical pH; electrodes; ion-selective electrodes; pH; potassium chloride; sodium chloride; standards.

Ion-selective electrodes, like the pH glass electrode, are finding growing use in various biomedical studies for monitoring the activities of ions such as Ca^{2+}, Na^+, K^+, Cl^-, F^-, etc. As in the case of the pH electrode, standards are also required for the reliable application of these sensors to complex biological fluids. Research is in progress to establish ionic activity scales and reference materials to permit the accurate use of ion-selective electrodes for biological and medical studies. At the present time, these investigations are concerned with aqueous standards and will progress to studies of these ions in mixed electrolyte systems and synthetic and real biologic fluids.

Studies are concurrently in progress to certify clinical pH standard buffers based on the tris/tris · HCl system [tris = tris(hydroxymethyl)aminomethane]. This buffer has been exhaustively studied to establish its behavior over wide temperature ranges and buffer ratios.

The standard reference materials resulting from these studies will serve the all-important purpose of calibrating ion-selective electrode analyzer systems for use in many areas of science and technology.

12696. Eisen, H., Rosenstein, M., Silverman, J., **2.00-MeV electron depth-dose measurements in aluminum, copper and tin absorbers using a radiochromic dye film,** *Int. J. Appl. Radiat. Isotop.* **23,** 97-108 (Apr. 1972).

Key words: Absorbed energy; depth dose; electron energy deposition; radiation dosimetry.

The use of radiochromic dye films for electron dosimetry has been extended to absorbers with atomic numbers in the range 13–50. The depth-dose profiles in slab targets of aluminum, copper, and tin irradiated by a plane parallel 2.00-MeV electron beam are presented for incident beams at 0, 30, and 60 degrees with respect to the surface normal. Absolute energy deposition per unit fluence was determined by using calibrated films, a fluence measurement, and a stopping-power ratio correction. The results are compared to the ionization measurements of Nakai and to the theoretical calculations of Berger and Seltzer; all agree within 10 percent. The stopping-power ratio, necessary to convert dose in the dye film to absorber dose at that point, is determined three ways and the results compared. The three techniques range from a detailed computer transport calculation yielding a variable stopping-power ratio with depth to the use of a constant stopping-power ratio obtained from tabulations. It is demonstrated that the use of the constant stopping-power ratio gives depth-dose distributions that differ by no more than 1-2 percent for aluminum, 3-5 percent for copper, and 4-8 percent for tin from the results obtained with the more rigorously evaluated stopping-power ratios.

12697. Fulmer, C. B., Toth, K. S., Williams, I. R., Handley, T. H., Dell, G. F., Callis, E. L., Jenkins, T. M., Wyckoff, J. M., **Photonuclear reactions in iron and aluminum bombarded with high-energy electrons,** *Phys. Rev. C* **2,** No. 4, 1371–1378 (Oct. 1970).

Key words: Aluminum; GeV electrons; iron; photonuclear; production cross sections; radioactivity; spallation.

Previously reported evidence for photofission of iron is investigated by a more extensive study. Thin foils of iron were bombarded with beams of 1.5-, 3-, 5-, and 16-GeV electrons. γ-ray spectroscopy and radiochemical measurements were used to measure yields of radionuclides produced in the targets. The yields of 25 nuclides were measured for the bombarded iron foils; these include eight nuclides in the mass region $22 \leq A \leq 35$. A thin aluminum target was bombarded with 16-GeV electrons, and the yields of seven radionuclides were measured. The yield of ^{24}Na in a thick iron target was measured as a function of target thickness and compared with that of radionuclides produced by cascade-evaporation reactions. The experimental evidence obtained in this series of experiments indicates that nuclides of mass < 35 produced in the iron targets are the result of a fissionlike process. For cascade-evaporation reaction products, there is a decrease in the variation of yield with ΔZ as the bremsstrahlung energy is increased.

12698. Gebbie, H. A., Bohlander, R. A., **Nonresonant cavity as a long path absorption cell,** *Appl. Opt.* **11,** No. 4, 723–728 (Apr. 1972).

Key words: Absorption cell; far infrared; nonresonant cavity; spectroscopy.

We have constructed spherical specularly reflecting nonresonant

cavities for use as absorption cells in far ir spectroscopy. A theory of their performance is developed and shown to be in agreement with experiment. An example is given of their use in a research program to ascertain the composition of water vapor. The essential advantage of these cells is that they give long pathlengths with high energy throughput.

12699. Geltman, S., **A high energy approximation: I. Proton-hydrogen charge transfer,** *J. Phys. B: At. Mol. Phys.* **4,** No. 10, 1288-1298 (Oct. 1971).

Key words: Born approximation; Coulomb wave; electron; excitation; high energy; hydrogen; large angle; theoretical.

The proton-hydrogen ground state charge transfer process is studied in a first order approximation in which the proton-proton interaction is treated as belonging to the unperturbed part of the problem. This results in the appearance of a Coulomb wave rather than a plane wave in the final state of the T matrix. The result is a cross section which lies between the Brinkmann-Kramers and Jackson-Schiff results, with the high energy limit of $0.810\,\sigma_{BK}$.

12700. Hayward, E., Gibson, B. F., O'Connell, J. S., **Consequences of isospin sum rules for photonuclear reactions,** *Phys. Rev. C* **5,** No. 3, 846-852 (Mar. 1972).

Key words: Giant resonance; isoscalar; isospin; isotensor; isovector; photonuclear; sum rules.

Isospin sum rules for photonuclear reactions are derived; they relate the strengths of the two isospin components of the giant resonance to the isoscalar, isovector, and isotensor radii of the nucleus. The connection between these radii and both the number and correlations of excess neutrons is discussed. A semiempirical formula for the fraction of the dipole strength in the $T+1$ giant resonance is derived and various experimental data are discussed in the light of the results obtained using this equation.

12701. MacDonald, R. A., **Neutron scattering due to lattice distortion around point defects,** *J. Phys. F: Metal Phys.* **2,** 209-218 (Mar. 1972).

Key words: Anisotropic elastic continuum; coherent scattering; differential scattering cross-section; elastic scattering; isotropic elastic continuum; lattice; local force model; long wavelength; neutron scattering; point defects; vacancy.

The distortions calculated from four different models of a vacancy, one discrete lattice model, two anisotropic continuum models and one isotropic continuum model are used to calculate the differential cross section for coherent elastic scattering of long wavelength neutrons by a single vacancy in copper. The results of the local force anisotropic continuum model and the isotropic continuum model are distinctly different from those of the discrete lattice and nonlocal force anisotropic continuum models. The effect of the distortion around the vacancy on the differential scattering cross section extends to at least 600 neighbouring atoms.

12702. Moore, G. A., **Recent progress in automatic image analysis,** *J. Micros.* **95,** Pt. 1, 105-118 (Feb. 1972).

Key words: Analysis of microstructures; automatic image analysis; Gestalt of a material; microarchitecture; patternness; scanning microscopes; television microscopes.

The utility of computing devices in stereology is evaluated with regard to three objectives. (1) Computer terminals permit easy and rapid prediction of 2-dimensional measurement distributions characteristic of any mathematically defined spatial structure. (2) The materials engineer can be satisfied by description of a Gestalt which characterizes the material as a whole and which can reasonably be presumed to control the behavior of the material in service. Six stereologically valid parameters are sufficient to define such a Gestalt. These are: volume fraction (V_V), mean free path in the matrix (l_a), mean intercept width of particles (l_β), and measures of material variability, general anisotropy, and degree of patternness. Current scanner models are intrinsically suitable for these measurements but will benefit from standardized data outputs and improvements to increase measuring accuracy. (3) Microarchitectural observations such as counting and measuring, or identifying, individual object sections are inefficient in ordinary computers. Large program effort is required for limited machine intelligence and operating speeds are unsatisfactory. These machine operations are not yet competitive with human observers. New hardware systems appear to be necessary to economically simulate human processes of image recognition. Some proposed systems will be mentioned.

12703. Oneal, G., Jr., Harris, W. P., **Three-terminal cell for thin film dielectric measurements,** (Proc. Electrical Insulation and Dielectric Phenomena, Buck Hill Falls, Pa., Oct. 20-22, 1969), Chapter in *1969 Annual Report of the Conference Electrical Insulation and Dielectric Phenomena*, pp. 164-170 (National Research Council, National Academy of Sciences, Washington, D.C., 1970).

Key words: Dielectric constant; dissipation factor; electrical measurements; FEP fluorocarbon; polyethylene terephthalate; thin films; two fluid.

A new design of dielectric test cell for measuring the dielectric constant and dissipation factor of a thin film has been built. The two fluid principle is used and agreement better than 1% in dielectric constant is obtained. Measurements on films as thin as 1.2 μm (50 gage) and frequencies as high as 1 MHz are practicable. A byproduct of the calculation is the average thickness of the sample. Results of measurements on films such as "FEP" fluorocarbon and polyethylene terephthalate will be presented.

12704. Newman, M., **2-Generator groups and parabolic class numbers,** *Proc. Amer. Math. Soc.* **31,** No. 1, 51-53 (Jan. 1972).

Key words: Fuchsian groups; parabolic classes; 2-generator groups.

It is shown that if x, y are generators of the finite group G such that $x^p=y^q=(xy)^n=1$, where p, q, n are integers >1, $(p, q)=1$, and xy is of true order n, then the order $\mu=nt$ of G satisfies $n \leqq pqt^p$. This result is used to show that if F is a Fuchsian group of genus 0 generated by 2 elliptic elements of coprime order and with 1 parabolic class, then F possesses only finitely many normal subgroups having a given number of parabolic classes.

12705. Reichard, T. W., **Mechanical properties of insulating concretes,** Paper in *American Concrete Spec. Publ. SP 29, Lightweight Concrete*, pp. 253-316 (American Concrete Institute, Detroit, Mich., 1971).

Key words: Cellular concrete; drying shrinkage; foam concrete; low density concrete; perlite concrete; thermal expansion; vermiculite concrete.

A description is given of a series of tests with perlite, vermiculite, and cellular insulating concretes. The tests were designed to develop data for the purpose of determining: (1) Elastic properties and strength as a function of size and shape of specimen, curing method, density, and composition; (2) drying shrinkage; (3) thermally induced movements; and (4) behavior of reinforced insulating concrete slabs under short-term and long-term loads.

Data are presented which show that although the relative strengths of various size specimens were affected by the curing method, the cubical specimen consistently showed a significantly higher strength than a cylindrical one with a height to diameter ratio of about two when their sizes are comparable.

There are significant differences in the drying shrinkages of the 3 types of concretes and also in the shrinkages of the concretes made from the 3 brands of perlite.

12706. Reimann, C. W., **The single crystal spectra of dichlorotetrapyrazolenickel(II), dibromotetrapyrazolenickel(II), and hexapyrazolenickel(II) nitrate,** *J. Chem. Phys.* **73,** No. 3, 561-568 (Feb. 5, 1970).

Key words: Crystal spectra; pyrazole complexes; tetragonal molecular symmetry.

The single crystal spectra of hexapyrazolenickel(II) nitrate, dichlorotetrapyrazolenickel(II), and dibromotetrapyrazolenickel(II) from 6000 to 30,000 cm^{-1} have been measured. The spectra of the halide complexes have been assigned on the basis of tetragonal molecular symmetry using the spectrum of hexapyrazolenickel(II) nitrate as a comparison. The tetragonal splittings in the first octahedral bands are considerably larger than observed in related complexes. These large splittings are related to low values of the effective Dq of the halide ions. Detailed crystallographic data are presented which show that the low effective field of the halide ions arises through an internal hydrogen bond interaction with the coordinated pyrazole molecules.

12707. Ritter, J. J., Coyle, T. D., Bellama, J. M., **Synthesis of ethynylboron halides,** *Chem. Commun.*, pp. 908-909 (1969).

Key words: Acetylenic boranes; ethynyldichloroborane; ethynyldifluoroborane; organoboron halides.

The first examples of organoboron halides containing acetylenic groups have been prepared and characterized. Ethynyldichloroborane, HC_2BCl_2, was obtained by irradiation of *cis*-bis(dichloroboryl)ethylene or trans-2-chlorovinyldichloroborane with a medium pressure mercury lamp (85% 2537 Å). The corresponding fluoride, HC_2BF_2, was prepared by the reaction of boron trifluoride with ethynyltrimethyltin. The compounds were characterized by infrared amd mass spectroscopy and by cleavage of the ethynyl group with propionic acid to produce acetylene. In contrast to most known ethynylboranes, the new compounds are apparently stable as uncomplexed three-coordinate boron species.

12708. Roberts, J. R., Voigt, P. A., **The continuous emission from hydrogen at the bound-to-free transition regions,** *Proc. Xth Int. Conf. Phenomena in Ionized Gases, Oxford, Eng., Sept. 13-18, 1971*, p. 375 (1971).

Key words: Emission coefficient; hydrogen; hydrogen continuum; LTE; Stark broadening.

The continuous emission coefficient of a dense hydrogen plasma is appreciably modified by high density effects such as the lowering of the ionization potential and the merging of broadened higher lines to form a quasicontinuum. Close to a series limit, these effects become quite significant. A method for calculating the hydrogen emission coefficient near a series limit is proposed. The results of this method are in good agreement with the measured intensity distribution of a wall-stabilized hydrogen arc in the Balmer limit wavelength region of the spectrum.

12709. Rosenblatt, J. R., Filliben, J. J., **Randomization and the draft lottery,** *Science* **171,** 306-308 (Jan. 22, 1971).

Key words: Draft lottery; random numbers; random permutations; randomization.

Fifty "random permutations" were prepared for use by the Selective Service System as a basis for a two-stage randomization that preceded the lottery drawing on 1 July 1970. This report identifies the permutations used. It also gives the orders in which calendar dates and numbers were put into and drawn from two drums and the correlations between them.

12710. Rossmassler, S. A., **Federal information programs,** *Chem. Eng. Prog.* **67,** No. 11, 75-76 (Nov. 1971).

12711. Sengers, J. M. H. Levelt, Chen, W. T., **Vapor pressure, critical isochore, and some metastable states of CO_2,** *J. Chem. Phys.* **56,** No. 1, 595-608 (Jan. 1, 1972).

Key words: Burnett method; CO_2; coexistence curve; controlled clearance gage; critical exponent; critical isochore; critical region; metastable states pressure calibration; scaling law; vapor pressure.

An experimental method for obtaining precise PVT properties for gases in the critical region is described. Main features are absence of noxious volumes, small height of sample volumes, precise temperature control, and high pressure sensitivity. Some results are presented for CO_2. The 0 °C fixed point and the vapor-pressure curve have been measured and compared with literature values. Three liquid isochores including their metastable extensions into the two-phase region are also presented. The vapor-pressure data and pressures on the critical isochore above T_c are compared with the predictions of the thermodynamic scaling law and with those of a recently proposed extension of scaling. The equation of extended scaling fits the data between −2 and 46 °C with a standard deviation of 1.5×10^{-3} bar, for a "best" critical exponent $\alpha = 0.09$.

12712. Simmons, J. D., McDonald, J. K., **The emission spectrum of AlN,** *J. Mol. Spectrosc.* **41,** 584-594 (1972).

Key words: AlN; electronic spectrum; emission spectrum; high resolution; hyperfine broadening.

A new system of emission bands has been observed in the visible region of the spectrum. The bands exhibit the characteristic rotational structure of a $^3\Pi_i - {}^3\Pi_i$ electronic transition. Rotational analysis and isotopic studies of these bands indicate that the carrier of the spectrum is the species AlN. The rotational analyses of the (0 − 0) and (0 − 1) $Al^{14}N$ bands yield the following rotational constants, band origins, and lower state vibrational frequency $\Delta G''_{1/2}$

$$\nu_0(0-0) = 19727.37\ cm^{-1};\ \nu_0(0-1) = 18980.44\ cm^{-1};$$

$$B_0' = 0.5811\ cm^{-1};\ B''_0 = 0.5702\ cm^{-1};\ B''_1 = 0.5646\ cm^{-1};$$

$$A_0' \cong -23\ cm^{-1};\ A''_0 \cong -33\ cm^{-1};\ A''_1 \cong -34\ cm^{-1};$$

$$\Delta G''_{1/2} = 746.8\ cm^{-1}.$$

The rotational analysis of the (0 − 0) $Al^{15}N$ band yields:

$$\nu_0(0-0) = 19727.13\ cm^{-1};$$

$$B_0' = 0.5559\ cm^{-1};\ B''_0 = 0.5454\ cm^{-1};$$

$$A_0' \cong -21\ cm^{1};\ A_0'' \cong -31\ cm^{-1}.$$

An interesting pattern of sharp and broadened lines observed throughout the bands will be discussed in terms of unresolved nuclear hyperfine splittings.

12713. Taylor, J. K., Ed., Alvarez, R., Paulson, R. A., Rains, T. C., Rook, H. L., **Interaction of nitrilotriacetic acid with suspended and bottom material,** *Water Pollution Control Research Series 16020 GFR 07-71—Environmental Protection Agency (Progress Report)*, pp. 1-31 (July 1971).

Key words: Detergent; nitrilotriacetic acid; water pollution.

An experimental investigation was made of the possible interaction of residual concentrations of nitrilotriacetic acid in surface waters with metallic elements contained in sediments and bottom materials. Samples of bottom materials from typical bodies of surface waters were analyzed for their major, minor, and trace constituents. Eight representative samples of these were equilibrated with distilled water and with water containing 20 ppm of NTA and the resulting solutions were analyzed by three analytical techniques. Elements showing essentially no increased solubility in the presence of NTA were: barium, antimony, molybdenum, strontium, chromium, silver, tin, iron, lead, cadmium, copper, and mercury. Elements showing small increases in solubility were: nickel, zinc, manganese, and

cobalt. Calcium and magnesium concentrations were increased somewhat above their normal relatively high concentrations.

This report was submitted in fulfillment of Project No. 16020 GFR under sponsorship of the Water Quality Office, Environmental Protection Agency.

12714. Thom, H. C. S., Marshall, R. D., **Wind and surge damage due to hurricane Camille,** *J. Waterways, Harbors, Coastal Eng. Div. Proc. Amer. Soc. Civil Eng.* **WW2,** No. 8144, 355-363 (May 1971).

Key words: Coastal engineering; damage; hurricanes; ocean waves; probability theory; storms; storm surges; wind.

The wind speeds in hurricane Camille are evaluated to provide a structural engineering interpretation. These are compared to published design winds for the area. Similar evaluation is made of the storm surge heights. A new method of probability analysis is applied to the historical surge data for Biloxi. Surveys of the storm and surge damage are considered with reference to actual wind speeds and design values in various parts of the storm area.

12715. von Busch, F., Dunn, G. H., **Photodissociation of H_2^+ and D_2^+: Experiment,** *Phys. Rev. A* **5,** No. 4, 1726-1743 (Apr. 1972).

Key words: D_2^+; experiment; H_2^+; ionization; photodissociation; vibrational state populations.

Measurements are reported of the cross sections for photodissociation of H_2^+ and D_2^+ at 21 wavelengths ranging from 2472 to 13,613 Å. The measurements are compared with theory using normalized Franck-Condon factors for the vibrational populations of the ions. Deviations are found, which are interpreted as a failure of this latter approximation. A least-squares analysis of the data yields vibrational-state populations different from simple Franck-Condon factors and alleged to be those characteristic of high-energy electron-impact ionization of H_2 and D_2. Interpretation of the data using a mechanism requiring that a fraction of the ions formed by electron impact be generated via the autoionization channel can qualitatively lead to the observations of this experiment. However, such an explanation would require about 2/3 of all H_2^+ and D_2^+ to be formed via autoionization—a seemingly unrealistic requirement. Interpretation of the data in terms of a variation with internuclear separation of the electronic matrix element involved in the electron-impact ionization process shows that a matrix element varying as $Q_e(r) = 1 + 0.56(r_{a.u.} - 0.99)^2$ can lead to the experimentally deduced populations of both H_2^+ and D_2^+. This latter interpretation is favored, though one cannot rule out the former or some combination of the two. The data and interpretation are consistent with other related experiments.

12716. Scheer, M. D., Klein, R., **The addition of $O(^3P)$ to olefins. The nature of the intermediate,** *J. Phys. Chem.* **74,** 2732-2733 (1970).

12717. Yakowitz, H., Ballantyne, J. P., Munro, E., Nixon, W. C., **The cylindrical secondary electron detector as a voltage measuring device in the scanning electron microscope,** *Proc. 5th Annual Scanning Electron Microscopy Symp., ITT Research Institute, Chicago, Ill., Apr. 1972,* Part 1, pp. 33-40 (1972).

12718. Ballard, D. B., **Comparison and evaluation of specimens for resolution standard,** *Proc. 5th Annual Scanning Electron Microscopy Symp., ITT Research Institute, Chicago, Ill., Apr. 1972,* Part 1, pp. 121-128 (1972).

12719. Rosenstein, M., McLaughlin, W. L., Silverman, J., **Energy deposition of electron beams in insulating materials,** (Proc. 4th Int. Conf. on Electron and Ion Beam Science and Technology, Los Angeles, Calif., May 1970), Chapter in *Electron and Ion Beam Science and Technology, 4th International Conference,* R. Bakish, ed., pp. 591-604 (The Electrochemical Society, New York, N.Y., 1970).

Key words: Charge deposition; depth dose; dielectrics; dose distribution; dosimetry; dye film dosimeters; electron beams; polystyrene; radiochromic dye.

Experimental depth-dose curves were obtained for semi-infinite thicknesses of ordinary and conducting polystyrene, irradiated in air by a 1.5-MeV electron beam in the dose range 5 to 20 Mrad. Radiochromic dye films were used as spatial dosimeters. By using a calibration of optical density versus dose, a microdensitometric reading of the irradiated dye films gave continuous depth-dose curves. No difference was observed between the depth-dose curves for the ordinary polystyrene and conducting polystyrene at absorbed dose rates between 2.5 and 10 Mrad/min. Within the limits of uncertainty for the present experiment, the results are in agreement with theoretical and experimental depth-dose data for 1.5-MeV electrons in polystyrene. Under the conditions studied, trapped charge does not measurably perturb the energy deposition of electrons in polystyrene.

12720. Powell, C. J., **Structure on the high-energy side of the $KL_{23}M$ Auger peak from solid aluminum: internal photoemission,** *Appl. Phys. Lett.* **20,** No. 9, 335-337 (May 1, 1972).

12721. Carter, G. C., Weisman, I. D., Bennett, L. H., Watson, R. E., **The $AuAl_2$-$AuGa_2$-$AuIn_2$ problem: Knight shifts and relaxation times in their pseudobinary alloys,** *Phys. Rev. B* **5,** No. 9, 3621-3638 (May 1, 1972).

Key words: Alloys; aluminum; gallium; gold; indium; intermetallic compound; Knight shift; relaxation time; soft x-ray spectroscopy; x-ray photoemission spectroscopy.

The nuclear-magnetic-resonance (NMR) and susceptibility behavior of the intermetallic compound $AuGa_2$ differs anomalously from the isoelectric and isostructural compounds $AuIn_2$ and $AuAl_2$. In an effort to test and extend the explanation offered by Jaccarino et al. and by Switendick and Narath, spin-lattice relaxation times and Knight shifts have been measured as a function of temperature and composition for the $AuAl_2$-$AuGa_2$, $AuAl_2$-$AuIn_2$, and $AuGa_2$-$AuIn_2$ pseudobinary alloy systems. At high temperature, the solute X (Al, In, Ga) resonance properties are dominated by the host. Satellite resonances are observed with temperature dependences differing from the main resonance. The results are partially explainable on the basis of an average-band model and partially on a local atom model. The role of the Au d bands is discussed. Metallurgical results on alloying are obtained using the NMR data.

12722. Shapiro, H. M., Bryan, S. D., Lipkin, L. E., Stein, P. G., Lemkin, P. F., **Computer-aided microspectrophotometry of biological specimens,** *Exp. Cell Res.* **67,** No. 1, 81-89 (July 1971).

12723. Semmelroth, C. C., **Adjustment of the Munsell-value and W^*-scales to uniform lightness steps for various background reflectances,** *Appl. Opt.* **10,** No. 1, 14-18 (Jan. 1971).

12724. Bender, P. L., Dicke, R. H., Wilkinson, D. T., Alley, C. O., Currie, D. G., Faller, J. E., Mulholland, J. D., Silverberg, E. C., Plotkin, H. E., Kaula, W. M., MacDonald, G. J. F., **The lunar laser ranging experiment,** (Proc. Conf. on Experimental Tests of Gravitational Theories, Pasadena, Calif., Nov. 1970), *JPL Technical Memo* **33-499,** pp. 178-181 (Jet Propulsion Laboratories, Pasadena, Calif., Nov. 1971).

Key words: Gravity; laser; lunar motion; moon; relativity.

The emplacement of the Apollo II retro-reflector package on the lunar surface has made possible very accurate measurements of the lunar distance. A continuing program of range measurements to the package at nearly all phases of the moon is being carried out by the McDonald Observatory under NASA support. Returned signals have also been obtained by the Pic du Midi Observatory in France and by

U. S. GOVERNMENT PRINTING OFFICE : 1973 O - 474-414

the AFCRL Lunar Laser Observatory near Tucson, Arizona. It is hoped that several other lunar ranging stations will be in operation within the next year or two, including ones in Japan, Hawaii, Russia, and the southern hemisphere.

12725. Semmelroth, C. C., **Prediction of lightness and brightness on different backgrounds,** *J. Opt. Soc. Amer.* **60,** No. 12, 1685-1689 (Dec. 1970).

12726. Mahler, R. J., Phelan, R. J., Jr., Cook, A. R., **High D^*, fast, lead zirconate titanate pyroelectric detectors,** *Infrared Phys.* **12,** 57-59 (1972).

Key words: Infrared; pyroelectric; room temperature detector.

Large area PZT detectors with D^* (500 K, 1, 1,)$=7\times10^8$ cm $Hz^{1/2}/W$ and fast detectors with a response time of at least 5 nsec have been fabricated. The pyroelectric coefficient of 27 nC/cm^2 K and a materials figure of merit of 2.8×10^{-9} C cm/J have been measured for these devices.

12727. Mulholland, J. D., Alley, C. O., Bender, P. L., Currie, D. G., Dicke, R. H., Faller, J. E., Kaula, W. M., MacDonald, G. J. F., Plotkin, H. H., Wilkinson, D. T., **Preliminary results of laser ranging to a reflector on the lunar surface,** (Proc. 13th Plenary Meeting of COSPAR, Leningrad, May 1970), *Space Research XI*, 97-104 (Academy-Verlag, Berlin, 1971).

Key words: Celestical mechanics; geophysics; laser; lunar ephemeris; selenology.

The first Lunar Ranging Experiment (LURE) retroreflector array was placed on the lunar surface during the Apollo 11 mission. Prior to this event, a special high-precision lunar ephemeris (designated LE 16) was developed by means of a composite numeric/analytic process, so as to provide more accurate predictions for use at the telescope. First returns were observed at the Lick Observatory on 1 August 1969 and at the McDonald Observatory shortly thereafter. The observing program is to continue for several years. Preliminary use of these data consists of their comparison with the LE 16 ephemeris, preparatory to a differential correction of the lunar elements. Present indications are that the ephemeris must undergo order-of-magnitude improvements before the full power of the laser data can be utilized. Other parameters in the predictive process are also capable of being corrected; an improvement in the coordinates of the Lick Observatory 120-inch telescope is already indicated.

12728. Sengers, J. V., **Triple collision effects in the transport properties for a gas of hard spheres,** (Proc. Symp. on Kinetic Equations, Cornell University, Ithaca, N.Y., 1969), Paper C-1 in *Kinetic Equations,* R. L. Kiboff and N. Rostoker, eds., pp. 137-193 (Gordon and Breach, New York, N.Y., 1971).

Key words: Collision integrals; hard spheres; thermodynamic conductivity transport properties; triple collisions; viscosity.

A study is made of the effect of successive correlated binary collisions on the transport properties of gases. In particular, triple collision transport integrals are derived for the thermal conductivity and viscosity of a gas of hard spheres. Preliminary numerical estimates for these collision integrals allow us to make an assessment of the contributions from the various triple collision events.

12729. Danos, M., **Baryon resonances in the nuclear ground state: How about double counting?** (Proc. 3d Int. Conf. High-Energy Physics and Nuclear Structure, Columbia University, New York, N.Y., Sept. 7-12, 1969), Chapter in *High-Energy Physics and Nuclear Structure,* pp. 811-815 (Plenum Press, New York, N.Y., 1970).

Key words: Baryon resonances; exchange currents; nuclear magnetic moments; nucleons; π-mesons; relativistic nuclear physics.

In a relativistic treatment of nuclei one encounters serious problems of double or multiple counting. They are associated with the existence of baryon and meson resonances. A procedure is described for overcoming these difficulties.

12730. Flynn, D. R., **Considerations in launching effective noise control programs,** (Proc. EASCON 1971 Conf., Oct. 6-8, 1971, Washington, D.C.), *IEEE Trans. Aerosp. Electron. Syst.,* pp. 53-59 (Nov. 1971).

Key words: Acoustics; environmental control; measurement; noise; pollution; sound.

Measurement plays a pervasive role in assessing the consequences of noise, its effects and control. Both the assessment of noise problems and the assessment of alternative strategies for noise abatement and control ultimately rest on accurate, reliable, and relevant measurement capability. Accurate measurement is required in order to ascertain the effects of a given noise exposure, to establish trends in noise exposure, to permit selection of cost-effective solutions, to monitor the effectiveness of control programs, and to provide the factual (measurement) basis for legal regulation. While considerable information is presently available regarding measurement and monitoring of noise, further work which will lead to more accurate or less expensive measurement methods is clearly needed. This paper will include a brief discussion of the research needs in assessment of the effects of noise on people, in characterization of the noise generation or transmission characteristics of various products or systems, and in development of meaningful correlations between noise exposure and the related human responses.

12731. Nimeroff, I., **The psychology of color,** *Amer. Paint J.*, pp. 65-70 (Jan. 11, 1971).

12732. Yule, H. P., **Study of gamma-ray spectrum distortion by mathematical smoothing,** *Anal. Chem.* **44,** No. 7, 1245-1249 (June 1972).

12733. Rook, H. L., Gills, T. E., LaFleur, P. D., **Method for the determination of mercury in biological materials by neutron activation analysis,** *Anal. Chem.* **44,** No. 7, 1114-1117 (June 1972).

Key words: Activation analysis; biological; environment; mercury; Standard Reference Material.

A method is described for the determination of mercury in a variety of matrices. Three significant improvements over currently used procedures have been achieved: The procedure has a minimum of chemical manipulations, thereby minimizing technique related errors; the radiomercury separation is quantitative, thus eliminating unnecessary errors involved in the determination of chemical yields; the procedure is based on a simple combustion separation of radiomercury allowing the same technique to be used on a wide variety of matrices. The method was tested using radiotracer experiments and by analyzing samples of flour and coal which had been independently analyzed. The procedure has been subsequently used to determine the mercury concentration of two new Standard Reference Materials being offered by the National Bureau of Standards.

12734. Rook, H. L., **Rapid, quantitative separation for the determination of selenium using neutron activation analysis,** *Anal. Chem.* **44,** No. 7, 1276-1278 (June 1972).

Key words: Biological; neutron activation analysis; selenium; standard.

The role selenium plays in the biochemistry of higher animals is complex and as yet, ill defined. A prerequisite for definitive studies is a sensitive, accurate analytical procedure for selenium. Relatively few analytical techniques fulfill both criteria of sensitivity and accuracy in biological and environmental matrices. This work describes

474-414 O - 73 - 9

a simple, effective method for the determination of selenium by neutron activation analysis using a combustion separation of volatile elements followed by liquid nitrogen freezing.

12735. Yates, J. T., Jr., Madey, T. E., **The adsorption of methane by tungsten (100),** *Surface Sci.* **28,** 437-459 (1971).

Key words: Adsorption; field emission; methane; physical adsorption; single crystal; tungsten; work function.

The adsorption of methane by the (100) plane of tungsten has been studied using flash desorption and work function methods. It has been found that CH_4 adsorbs to appreciable coverage as an undissociated molecular species at ~ 100 K. The activation energy for first order desorption from this state is 6.9 kcal/mole (0.30 eV/molecule). This observed binding energy is greater than expected for dispersion forces alone, and added contributions to the binding energy are discussed. An observed work function of − 0.34 eV on adsorption of CH_4 is consistent with the presence of a physically adsorbed CH_4 layer.

Related studies of CH_4 adsorbed on a tungsten field emission tip demonstrate that adsorption of CH_4 proceeds rapidly at 77 K, but is negligible at 300 K. At tungsten temperatures above 1200 K in 10^{-5} Torr of CH_4, decomposition of the CH_4 to form a carbon layer occurs.

It is postulated that at elevated temperatures and at high CH_4 pressures the physically adsorbed state may be sufficiently populated to serve as a source of adsorbed CH_4 species which undergo activated surface decomposition, leading eventually to surface carbides.

12736. Madey, T. E., **Adsorption and displacement processes on W(111) involving CH_4, H_2, and O_2,** *Surface Sci.* **29,** 571-589 (1972).

Key words: Binding energy; chemisorption; displacement; hydrogen; methane; oxygen; tungsten; work function.

Adsorption and displacement processes involving CH_4, H_2, and O_2 on the (111) surface of tungsten have been examined using the thermal desorption method in conjunction with mass spectrometry and work function changes. Methane is physically adsorbed on W(111) at $T \sim$ 125 K and desorbs with a binding energy of 8.0 kcal/mole. Neither adsorption nor decomposition of CH_4 is observed at 300 K on W(111). Hydrogen is chemisorbed on W(111); 4 atomic binding states having desorption energies from 12 kcal/mole to 31 kcal/mole are observed. The influence of oxygen on the binding of both H_2 and CH_4 has been examined. Oxygen specifically blocks the adsorption of certain hydrogen binding states; oxygen causes an increase in the CH_4 binding energy to ~ 10 kcal/mole. Coadsorption of hydrogen and CH_4 also exhibits site specificity.

12737. Comeford, J. J., **The spectral distribution of radiant energy of a gas-fired radiant panel and some diffusion flames,** *Combust. Flame* **18,** 125-132 (1972).

Key words: Diffusion flames; emission spectra; flame spectra; infrared spectra; radiant test panel; radiant test sources.

Measurements were made of the spectral distribution of energy from radiant sources employed in standard test methods of flammability. Radiant sources examined were a gas-fired radiant panel employed in ASTM Test E-162 and the electric heater employed in the Smoke Chamber Test. To afford a basis for comparison, the emission spectra of several diffusion flames in air were measured. The energy distribution of the flames occurred essentially in two narrow wavelength intervals corresponding to emission of carbon dioxide at 4.4 μm and water at 2.7 μm. Luminous diffusion flames containing large amounts of incandescent carbon, such as occur from the combustion of acetylene-in-air, show a blackbody background continuum with CO_2 and H_2O emission peaks superimposed on the continuum. The radiant test sources exhibited an energy distribution approximating that of a blackbody with atmospheric CO_2 and H_2O absorptions superimposed. The gas-fired radiant panel in addition showed a significant emission peak at 4.4 μm due to excited CO_2.

12738. LaVilla, R. E., **$K\alpha$ emission spectrum of gaseous N_2,** *J. Chem. Phys.* **56,** No. 5, 2345-2349 (Mar. 1, 1972).

Key words: Electron bombardment; lead myristate analyzing crystal; M. O. correlation; nitrogen K emission spectrum; resonance radiation; x-ray emission.

The nitrogen $K\alpha$ emission spectrum excited by electron bombardment of nitrogen gas was obtained on a single planar crystal spectrometer with photon counting. The experimental profile is in fair agreement with a calculated profile based on molecular orbital theory and the single vacancy states measured by x-ray photoelectron spectroscopy. Evidence is presented to suggest that some of the emission intensity on the high-energy side of the main peak is due to "resonance radiation." To fix the energy scale of the spectrum, the effective $2d$ spacing of the analyzing lead myristate crystal was experimentally determined.

12739. Okabe, H., **Photodissociation of $OSCl_2$ in the vacuum ultraviolet; the heat of formation of SO,** *J. Chem. Phys.* **56,** No. 7, 3378-3381 (Apr. 1, 1972).

Key words: Heat of formation; $OSCl_2$; photodissociation; SO; vacuum ultraviolet.

The photodissociation of $OSCl_2$ at the Kr (1165-, 1236-Å) lines has resulted in the production of SO $A\ ^3\Pi, B\ ^3\Sigma$. The threshold energy of incident photons to produce the reaction,

$$OSCl_2 \xrightarrow{h\nu} SO A\ ^3\Pi_0 + 2Cl\ ^2P_{3/2},$$

was 9.41 ± 0.03 eV from which $\Delta H_{f0}°(SO) = 1.3 \pm 0.7$ kcal/mole is derived. The I_f/I_0-vs-incident wavelength curve shows many diffuse bands found in the absorption spectrum of $OSCl_2$ indicating that the process is predissociative. Various other methods to obtain $\Delta H_{f0}°(SO)$ are compared. It is concluded that the best value is $1.3 > \Delta H_{f0}°(SO) > 0.8$ kcal/mole.

12740. Stephenson, N. C., Roth, R. S., **The crystal structure of the high temperature form of Ta_2O_5,** *J. Solid State Chem.* **3,** 145-153 (1971).

Key words: Crystallographic shear; crystal structure; high temperature Ta_2O_5; nonstoichiometric.

The structure of the high temperature form of Ta_2O_5 can be stabilized by doping with 2 mole%Sc_2O_3 and single crystals have been prepared from a $Ta_2O_5 - Sc_2O_3$ (98 ± 2) composition by the Czochralski technique. The crystal system which at first appeared to body-centered tetragonal has been determined to be face-centered monoclinic, space group $C2$ with $a = 35.966$ Å, $b = 3.810$ Å, $c = 3.810$ Å, $\beta = 96°7'$. Least squares refinement cycles reduced the reliability index R to 0.089.

The structure of αUO_3-type blocks in which each tantalum atom is surrounded by a pentagonal bipyramid of oxygen atoms. These blocks are infinite in two directions and are separated from similar blocks along a third direction by shear planes. In the vicinity of these shear planes the tantalum atoms are surrounded by distorted octahedral coordination polyhedra.

It is believed that the stabilizing effect of the Sc_2O_3 impurity is due to an increase in the concentration of shear planes. Random shear planes (Wadsley defects) are introduced at approximately 300 Å intervals along the large axis by doping with a substance (Sc_2O_3) which has cations (Sc) large enough to substitute for the host (Ta) but a lower oxygen : metal ratio than the host compound (Ta_2O_5).

12741. Schrack, R. A., Heaton, H. T., II, Schwartz, R. B., **Suppression of after-pulsing in the type 58AVP photomultiplier,** *Nucl. Instr. Methods* **77,** 175-176 (1970).

12742. Thompson, B. A., Lutz, G. J., **Characterization of ancient bronze artifacts by neutron and photon activation analysis,** *Radiochem. Radioanal. Lett.* **9,** No. 5-6, 343-350 (Mar. 1972).

12743. Seltzer, S. M., Berger, M. J., **Response of NaI detectors to high-energy gamma rays,** *Trans. Amer. Nucl. Soc.* **14,** No. 1, 124-125 (June 1971).

12744. Sanchez, I. C., DiMarzio, E. A., **Dilute-solution theory of polymer crystal growth. Some thermodynamic and predictive aspects for polyethylene,** *Macromolecules* **4,** 677-687 (Nov.-Dec. 1971).

Key words: Activity; chain fold; cilia; equilibrium dissolution temperature; equilibrium melting temperature; free energy of crystallization; lamella thickness; nucleation rate; surface free energy; undercooling.

The kinetic theory of polymer crystallization from dilute solution is applied to the system polyethylene-xylene. Prerequisite free energy driving forces are derived for crystallization from solution. These naturally depend on bulk thermodynamic properties and three thermodynamic potentials are derived depending on what melt and crystalline properties are assumed. The commonly used $\Delta H \Delta T / T_m^0$ expression is shown to be an upper bound for all materials and a more accurate expression descriptive of polyethylene is used in the actual calculations. Growth rate and lamella thickness are computed as functions of undercooling, concentration, and molecular weight. It is found that the growth rate varies roughly as concentration raised to a power, the value of the power being a function of both molecular weight and temperature. The isothermal lamella thickness increases only slightly with decreasing molecular weight and is even less dependent on concentration. The isothermal growth rate as a function of molecular weight exhibits a broad maximum. An analysis of the temperature dependence of the growth rate is made in terms of classical nucleation theory using calculations of the present theory as data points. This leads to the concept of an apparent $\sigma\sigma_e$ which is seen to vary as a function of molecular weight. The theory makes definitive, as yet unverified, predictions which can be tested experimentally.

12745. Garvin. D., Evans, W. H., Duncan, B. C., **Some information processing techniques for the small, semi-automated, scientifically-oriented data center,** (Proc. Forum on the Management of Information Analysis Centers, National Bureau of Standards, Gaithersburg, Md., May 17-19, 1971), Chapter in *The Management of Information Analysis Centers,* W. A. Smith, ed., **72-1,** 40-57 (Sponsored by The COSATI Panel Information Analysis Centers) (U.S. Atomic Energy Commission, Oak Ridge, Tenn., Jan. 1972).

Key words: Chemistry; codes for information interchange; editing; information analysis centers; information processing; information retrieval; text handling.

Solutions are presented for several of the problems encountered in handling scientific text in machine-readable form in small data centers. The problems discussed are the selection of an adequate character set for representation of scientific text, the essential and useful features of editing routines, and batch-mode information retrieval.

12746. Bridges, J. M., Richter, J., **Arc measurements of Fe I oscillator strengths with improved accuracy,** *Proc. Xth Int. Conf. on Phenomena in Ionized Gases, Oxford, England, 1971,* p. 384 (Donald Parsons and Company, Ltd., Oxford, England, 1971).

Key words: Arc; *f*-values; iron; oscillator strengths; wall-stabilized.

Measurements of relative Fe I *f*-values have been performed with greatly improved accuracy over similar previous measurements. The lines are measured in emission from a wall-stabilized argon arc, containing admixtures of $FeCl_3$ and hydrogen. Recent modifications of the arc allow better control over the iron density, and lead to improved accuracy in relative intensity measurements as well as in plasma diagnostics required for determination of the arc temperature. Results for some selected lines are given, and the program for further measurements is discussed.

12747. Scheer, M. D., Fine, J., **The positive and negative self-surface ionization of tantalum,** Chapter 39 in *The Structure and Chemistry of Solid Surfaces,* G. A. Somorjai, ed., pp. 39-1—39-15 (John Wiley & Sons, Inc., New York, N.Y., 1969).

Key words: Electron affinities; self-surface ionization; singly charged positive and negative atomic ions; sublimation energies; tantalum.

The sublimation of atoms, singly charged positive, and negative atomic ions of tantalum has been investigated in the 2000-2600 K temperature range with a specially designed mass spectrometer. It was shown that carbon contamination of the tantalum surface could account for the discrepancies previously reported for the energies of atom sublimation. Measurements made on a carbon-free tantalum surface gave values of 7.94 ± 0.09, 11.18 ± 0.11 and 11.2 ± 0.5 eV for the sublimation energies of atoms, positive, and negative ions, respectively. The electron affinity of tantalum was found to be 0.9 ± 0.3 eV. These sublimation processes were shown to be consistent with the assumption of thermal equilibration on the tantalum surface and hence can be described by a generalized form of the Saha-Langmuir equation.

12748. Milligan, D. E., Jacox, M. E., **Infrared and ultraviolet spectroscopic studies of free radicals and molecular ions isolated in inert solid matrices,** Paper in *Molecular Spectroscopy: Modern Research,* pp. 259-286 (Academic Press, Inc., New York, N.Y., 1972).

Key words: Alkali metal reactions; cage effect; flash photolysis; free radicals; infrared spectrum; matrix isolation; molecular ions; molecular orbitals; photolysis; ultraviolet spectrum.

The principles of the matrix isolation technique are reviewed, and results of experiments leading to the stabilization of free radicals in inert solid matrices in concentration sufficient for direct infrared and ultraviolet spectroscopic observation are surveyed. Emphasis is placed on the correlation of the matrix data with data obtained in gas-phase flash photolysis studies. Conclusions regarding the structure and bonding of these species are compared with the predictions of simple molecular orbital theory. Recent results on the infrared and ultraviolet spectra of the C_2^-, NO_2^-, and $ClHCl^-$ ions isolated in an inert, non-ionic environment are also presented.

12749. Moore-Sitterly, C., **Committee 4: Structure of atomic spectra** (Commission 14, International Astronomical Union Report), *Trans. I.A.U.* **14A,** 133-137 (1970).

12750. Swanson, N., Kuyatt, C. E., Cooper, J. W., Krauss, M., **Alternative decay channels of a CO^- Feshbach resonance,** *Phys. Rev. Lett.* **28,** No. 15, 948-951 (Apr. 10, 1972).

Key words: CO; CO^-; decay channels; energy loss spectra; Feshbach resonance.

By means of on- and off-resonance energy-loss measurements, we have observed the decay of the 10.04-eV resonance in CO to the $A\ ^1\Pi$, $a\ ^3\Pi$, and $a'\ ^3\Sigma^+$ states. The measurements identify the resonance as a $^2\Sigma^+$ state of CO^-.

12751. Pope, C. I., **A simplified method for determining residual thiosulfate in processed microfilm,** *Photogr. Sci. Eng.* **13,** No. 5, 278-279 (Sept.-Oct. 1969).

12752. Schubauer, G. B., **Early developments in hot-wire anemometry at NBS and a look at some elsewhere,** (Proc. Int. Symp. on Hot-Wire Anemometry, University of Maryland, College Park, Md., Mar. 20-21, 1967), Chapter in *Advances in Hot-Wire Anemometry,* W. L. Melnik and J. R. Weske, eds., pp. 13-24 (July 1968).

Key words: Anemometer; hot-wire; measurement of turbulence; turbulence.

The paper reviews the history of hot-wire anemometer development at NBS as applied to the measurement of turbulence. It makes limited mention of work done elsewhere, mainly to place NBS work in proper perspective. The story begins in the middle 1920's with early attempts to measure turbulence, followed by an account of the work of Dryden and Kuethe, which suddenly advanced the hot-wire anemometer as a useful and productive instrument for turbulence measurement. Work at the Technische Hoogeschool at Delft along similar lines, but coming a little later, is described. This is followed by an account of subsequent development of hot-wire equipment at NBS. Finally, departing from NBS work entirely but furthering the theme, "How it Began," an account is given of the birth of the constant-temperature method.

12753. Smith, M. W., Wiese, W. L., **Graphical presentations of systematic trends of atomic oscillator strengths along isoelectronic sequences and new oscillator strengths derived by interpolation,** *Astrophys. J. Supplement Series* **23,** Supplement No. 196, 103-196 (June 1971).

Key words: Atomic oscillator strengths; interpolated data; systematic trends.

Recently detected systematic trends of atomic oscillator strengths along isoelectronic sequences are utilized for the determination of new numerical data and for the evaluation of the reliability of existing material. All well-established systematic trends, which number about 100, are presented graphically. New oscillator strengths are interpolated from the graphs, mainly for the higher ions with wavelengths located principally in the vacuum ultraviolet, and are tabulated with their estimated uncertainties. The graphs are ordered according to isoelectronic sequences and are given with full grids to allow the addition of future data.

12754. Simmons, J. H., Macedo, P. B., **Shear and volume structural relaxation in immiscible oxide melts,** (Proc. Conf. Physics of Non-Crystalline Solids, Sheffield, England, Sept. 1970), Chapter 7 in *Amorphous Materials,* R. W. Douglas and B. Ellis, eds., pp. 69-78 (John Wiley and Sons, London, 1972).

Key words: Critical-point effect; immiscible glasses; longitudinal ultrasonics; phase separation; shear ultrasonics; structural relaxation.

The influence of composition fluctuations on the structural relaxation mechanism above the critical point of a series of immiscible oxide glasses is investigated by shear and longitudinal ultrasonic spectroscopy. The results are analyzed to determine the nature of the interaction between the fluctuations in composition and the viscous flow processes.

12755. Rosasco, G. J., Benoit, C., Weber, A., **Light scattering study of the attenuation and dispersion of hypersound in ammonium bromide,** (Proc. 2d Int. Conf. on Light Scattering in Solids, Paris, France, July 19-23, 1971), Chapter in *Light Scattering in Solids,* M. Balkanski, ed., pp. 483-488 (Flammarion Sciences Publ., Paris, France, 1971).

Key words: Acoustic phonons; ammonium bromide; Brillouin scattering; elastic constants; light scattering; relaxation phenomena.

By means of Brillouin scattering, the attenuation and velocity dispersion of hypersonic acoustic waves have been measured in the disordered, cubic phase of NH_4Br. Shear waves determined by the elastic constant C_{44} show no dispersion. Longitudinal waves propagating in the ⟨ 100 ⟩ plane show velocity dispersion and associated attenuation. The L-mode data are adequately fit by a single relaxation model for the dispersion and attenuation as a function of frequency at 24 °C. The strength of the relaxation, $[C(\infty) - C(0)]/C(0)$ for the elastic constant C_{11} is 2.5%; for C_{12}, 8.8%; and for $(C_{11} - C_{12})/2$, 0.6%. The relaxation time measured in this experiment is 1.16×10^{-11} sec. Data which shows that the dispersion increases as the temperature is lowered toward the order-disorder λ-type transition at 234.5 K is also presented. A model is introduced which qualitatively explains the features of this dispersion.

12756. Berger, M. J., Seltzer, S. M., Eisen, H. A., Silverman, J., **Absorption of electron energy in multi-layer targets,** *Trans. Amer. Nucl. Soc.* **14,** No. 1, 887-888 (June 1971).

12757. Sher, A. H., Keery, W. J., Dyson, H. E., **Improved infrared response measurements in semiconductor nuclear radiation detectors,** *IEEE Trans. Nucl. Sci.* **NS-19,** No. 1, 341-344 (Feb. 1972).

Key words: Defect level; germanium; impurity levels; infrared response; lithium-drifted diodes; semiconductors.

An infrared response technique has been developed which has been shown to yield more detailed spectra than previous techniques and which can be used to identify more specifically energy levels arising from unwanted impurities and defects in semiconductor diodes used as nuclear radiation detectors. The presence of known impurities in germanium detectors, both lithium-compensated and high purity (uncompensated), has been confirmed using this technique. Such impurities include copper, gold, and iron. Features in the spectra associated with crystalline defects have also been identified.

12758. Sher, A. H., Keery, W. J., **Improved infrared-response technique for determining impurity and defect levels in semiconductors,** *Appl. Phys. Lett.* **20,** No. 3, 120-122 (Feb. 1, 1972).

Key words: Defect level; germanium; impurity levels; infrared response; lithium-drifted diodes; semiconductors; silicon.

The response of reverse-biased germanium diodes to monochromatic infrared radiation has been studied. Specimens included those fabricated from crystals doped with either copper or gold, or subjected to heat treatment. Preliminary results are reported that show the technique to be useful for identifying such impurities or defects in both lithium-compensated and high-purity germanium specimens.

12759. Stephenson, N. C., Roth, R. S., **Structural systematics in the binary system Ta_2O_5-WO_3. V. The structure of the low-temperature form of tantalum oxide L-Ta_2O_5,** *Acta Cryst.* **B27,** 1037-1044 (1971).

Key words: Crystal structure; low temperature form of Ta_2O_5; system Ta_2O_5-WO_3.

The orthogonal unit cell of the compound L-Ta_2O_5 has dimensions $a = 6.198$, $b = 40.29$, $c = 3.888$ Å and contains 11 formula units. The structure was solved in projection from the Patterson function and refined to a conventional R value of 0.088 using full-matrix least-squares methods. The metal atoms are arranged in sheets and are surrounded by oxygen atoms which form either distorted octahedral or pentagonal bipyramidal coordination polyhedra. The structure contains, on the average, three distortion planes per unit cell. These are statistically distributed over four sites, thereby giving the average unit cell a higher symmetry than the real unit cell. The thermal equilibration of the compound, involving detectable structural changes, is discussed in terms of the migration of distortion planes.

12760. Stephenson, N. C., Roth, R. S., **Structural systematics in the binary system Ta_2O_5-WO_3. IV. The structure of $Ta_{38}WO_{98}$,** *Acta Cryst.* **B27,** 1031-1036 (1971).

12761. Stephenson, N. C., Roth, R. S., **Structural systematics in the binary system Ta_2O_5-WO_3. III. The structure of $45Ta_2O_5 \cdot Al_2O_3 \cdot 4WO_3$,** *Acta Cryst.* **B27,** 1025-1031 (1971).

12762. Stephenson, N. C., Roth, R. S., **Structural systematics in the binary system Ta_2O_5-WO_3. II. The structure of $Ta_{30}W_2O_{81}$,** *Acta Cryst.* **B27,** 1018-1024 (1971).

12763. Stephenson, N. C., Roth, R. S., **Structural systematics in the binary system Ta_2O_5-WO_3. I. The structure of $Ta_{22}W_4O_{67}$,** *Acta Cryst.* **B27,** 1010-1017 (1971).

12764. Eisenhauer, C., Chilton, A. B., **Angular distribution of scattered gamma rays from a fan source,** *Trans. Amer. Nucl. Soc.* **14,** No. 1, 402-403 (June 1971).

12765. Sher, A. H., Liu, Y. M., Keery, W. J., **Infrared response measurements on radiation-damaged Si(Li) detectors,** *IEEE Trans. Nucl. Sci.* **NS-19,** No. 3, 312-317 (1972).

Key words: Defect levels; impurity levels; infrared response; lithium-drifted radiation detectors; semiconductors; silicon.

The improved infrared response (IRR) technique has been used to qualitatively compare radiation effects on Si(Li) detectors with energy levels reported for silicon in the literature. Measurements have been made on five commercial silicon detectors and one fabricated in-house, both before and after irradiation with fast neutrons, 1.9-MeV protons, and 1.6-MeV electrons. Effects dependent upon the extent of radiation damage have been observed.

It seems likely that the photo-EMF, or photovoltage effect, is the basic mechanism for the observation of IRR in *p-i-n* diodes with a wide *i*-region. Experimental characteristics of the IRR measurement are in agreement with those of the photovoltage effect.

12766. Meinke, W. W., **Some comments on activation analysis,** *Proc. 2d Inter-American Conference on Radiochemistry, Mexico City, Mexico, Apr. 22-25, 1968,* pp. 54-60. (Published by Secretaría General de la Organización de Estados Americanos, Washington, D.C., 1971).

Key words: Activation analysis; neutron activation; trace analysis; trace characterization.

An overview of the current status of Activation Analysis is given with special note made of the use of neutrons other than reactor-produced neutrons and to the use of separation procedures including group separations. The relation of activation analysis to other methods of analysis is discussed with particular emphasis on the adeptness of the method to handle large numbers of samples for certain elements which are amenable to this method. Activation analysis is inherently an accurate method and its use for trace analysis should join forces with other trace analysis competences to permit a much broader perspective to be applied to the trace analysis problems. The nuclear reactor center with its capability for activation analysis as one facet of general trace competence is a logical focal point for the development of characterization centers to meet the needs in a diverse number of scientific endeavours.

12767. Smith, C. N., **Limit of error calculations used in Integrated Safeguards Experiment,** *Proc. 12th Annual Meeting of the Institute of Nuclear Materials Management, Palm Beach Shores, Fla., June 28-July 1, 1971,* **1,** 193-207 (June 1971).

Key words: Integrated Safeguards Experiment; limit of error calculations; nondestructive assay techniques; safeguards.

The Integrated Safeguards Experiment sponsored by the Atomic Energy Commission relied heavily on nondestructive assay techniques to attain a measured material balance on the mixed oxide fabrication process. This paper describes the calculations involved in determining the limit of error values for material measurements using calorimetry and neutron coincidence counting as well as conventional chemical assay methods.

12768. Geist, J., Kendall, J. M., Sr., **Circumsolar radiation and the international pyrheliometric scale,** *Appl. Opt.* **11,** No. 6, 1437-1439 (June 1972).

Key words: Circumsolar radiation; Eppley Angstrom pyrheliometer; international pyrheliometric scale; Primary Absolute Cavity Radiometer.

The responsivity as a function of angle is calculated for Primary Absolute Cavity Radiometers (PACRAD) with 2.45 and 3.32° angular field of view limiting apertures, and for a simplified model of the Eppley Angstrom (E-A) pyrheliometer. From this data, the response of the three instruments to various mathematical models of circumsolar radiation is calculated, and compared with experimental data obtained during simultaneous measurements of solar irradiance with the three radiometers. The conclusion is that the difference between the values of solar irradiance measured with the 2.45° PACRAD and with the E-A pyrheliometer is not due to circumsolar radiation.

12769. Rasberry, S. D., **Application of computers in electron probe and x-ray fluorescence analysis,** (Proc. 20th Annual Conf. on Applications of X-Ray Analysis, Denver, Colo., Aug. 11-13, 1971), Chapter in *Advances in X-Ray Analysis,* K. F. J. Heinrich, ed., **15,** 56-59 (Plenum Press, Inc., New York, N.Y., 1972).

Key words: Automatic data acquisition; computer automation of laboratory equipment; computer controlled electron probe; computer controlled x-ray analyzers; electron probe automation.

This paper is a review of automation of electron microprobe and x-ray fluorescence instrumentation. Such a review seems timely because of the great increase in the application of computer systems in this field over the past decade. Some of these applications have been conceived to meet true technological needs while in other cases they have been undertaken to "keep up with the Joneses." I would like to show not only what automated systems are now feasible but also when and how they should be employed. The "when" and "how" of automation are largely dependent upon the application being considered; in this study, x-ray applications have been divided into the following classes: (1) on-stream process-control, (2) off-line quality assurance, (3) routine service laboratory, (4) general-purpose analytical laboratory. Several phases are present in these classes, including: specimen preparation and loading, measurement, data acquisition and transfer, data processing and display, and finally, archival data storage. Various workers have undertaken the automation of all these operations in one or the other of the classes of applications; from a review of their work and by examining details of each operation within the framework of a given application, we can now draw conclusions on the extent of desirable automation.

12770. Sugar, J., Kaufman, V., **Fourth spectrum of lutetium,** *J. Opt. Soc. Amer.* **62,** No. 4, 562-570 (Apr. 1972).

Key words: Lutetium; spectra; theory.

Spectra of lutetium obtained with a sliding spark were photographed in the wavelength range 400-3200 Å. Wavelengths of 246 lines, comprising all lines identified as Lu IV appearing in the spark at 50-A peak current, are given. Fifty-seven energy levels were deduced from these lines, including nearly all levels of the $4f^{13}(5d, 6s, 6p, 6d,$ and $7s)$ configurations and their connection to the $4f^{14}\ {}^1S_0$ ground state. An ionization energy of $364\,500 \pm 200\ cm^{-1}$ was derived. The energy levels are interpreted by means of a theoretical analysis utilizing fitted radial parameters. With these results, trends of Slater and spin-orbit parameters and configuration energy differences for fourth spectra of the rare earths are found. The fundamental energy differences between lowest levels of the $4f^N$ and $4f^{N-1}5d$ configurations for the fourth and fifth spectra are deduced.

12771. Schaffer, R., **Documentation interest of the National Bureau of Standards and collaborating groups for communication of laboratory results in clinical analysis,** (Proc. Conf. Clinically Oriented Documentation of Laboratory Data, Buffalo, N.Y., May 10-12, 1971), Chapter in *Clinically Oriented Docu-*

mentation of Laboratory Data, E. R. Gabrieli, ed., pp. 419-424 (Academic Press, Inc., New York and London, 1972).

Key words: Clinical analysis; referee methods for clinical analysis; standard reference materials.

The National Bureau of Standards is actively at work to help clinical laboratories obtain analyses at the level of accuracy that they require and to secure inter-laboratory comparability of results. For achieving these objectives, the Bureau's principal effort has been the certification of Standard Reference Materials for the clinical laboratory. Secondly, a joint program has begun between clinical chemists and NBS for developing referee methods for clinical analysis (methods whose accuracy are known).

12772. Schaffer, R., **Isotopic methods (of carbohydrate analysis),** Paper in *The Carbohydrates, Chemistry and Biochemistry, Second Edition*, W. Pigman and D. Horton, eds., **11B,** 765-776 (Academic Press, Inc., New York and London, 1970).

Key words: Isotope-dilution analysis; isotopic distribution; kinetic isotope effects; labeled carbohydrates.

Isotopically labeled carbohydrates are considered for use as quantitative analytical reagents and for tracing the course of the isotopic portion of a labeled carbohydrate through complex reactions.

12773. Shafer, M. R., **Discussion of ASME paper 64-WA/FM-1, density effect and Reynolds number effect on gas turbine flowmeters by W. F. Z. Lee and H. J. Evans,** *J. Basic Eng. Trans. ASME, Series D.* **87,** No. 4, 1052-1053 (Dec. 1965).

12774. Forman, R. A., Piermarini, G. J., Barnett, J. D., Block, S., **Pressure measurement made by the utilization of ruby sharp-line luminescence,** *Science* **176,** 284-285 (Apr. 21, 1972).

Key words: Calibration; diamond cell; high-pressure; luminescence.

A rapid, convenient technique for precision pressure measurement in the diamond-anvil high-pressure cell, which makes use of the sharp-line (R-line) luminescence of ruby, has been developed. The observed shift is -0.77 ± 0.03 reciprocal centimeters per kilobar for R_1 and -0.84 ± 0.03 reciprocal centimeters per kilobar for R_2 to lower energy and is approximately linear in the range studied (to 22 kilobars). Line-broadening has been observed in some instances and has been tentatively identified with nonhydrostatic conditions surrounding the ruby sample.

12775. Linsky, J. L., **A proof of the relation between reflectivity and emissivity in an isothermal scattering and absorptive atmosphere,** *J. Quant. Spectrosc. Radiat. Trans.* **12,** No. 5, 777-781 (May 1972).

12776. Roberts, J. R., Voigt, P. A., Nagy, J. J., **Continuous emission from hydrogen plasmas. I. The theoretical hydrogen emission coefficients,** *Proc. 9th Int. Conf. Phenomena in Ionized Gases, Bucharest, Romania, Sept. 1-6, 1969*, p. 595 (Editura Academiei Republicii Socialiste Romania, Bucharest, Romania, 1969).

Key words: Continuum; emission coefficients; emission intensity; hydrogen.

Extensive calculations of the continuous hydrogen emission coefficient for a temperature range from 7,000 to 16,000 K and a wavelength range from 1,500 to 15,000 Å have been carried out. The four major reasons for this new calculation are: (a) some of the most recent calculations differ by at least 25 percent in certain spectral regions from these new calculations; (b) a high intensity wall-stabilized hydrogen arc is now available which would allow spectral radiance calibration by means of the accurately calculable hydrogen emission coefficient into the vacuum ultraviolet region and portions of the visible and infrared spectral regions; (c) the contribution of the far wings of Stark broadened hydrogen lines as an addition to this continuum is usually neglected, but will be considered here in detail; and (d) newly available absorption coefficients for H^- and H_2^+.

12777. Coxon, B., **Conformational analysis via nuclear magnetic resonance spectroscopy,** Article 93 in *Methods in Carbohydrate Chemistry*, R. L. Whistler and J. N. BeMiller, eds., **VI,** 513-539 (Academic Press, Inc., New York, N.Y., 1972).

Key words: Conformational analysis; iterative analysis; long-range coupling constants; n.m.r. spectroscopy; nuclear Overhauser effects; spin-spin coupling constants; variable temperature studies.

Instrumentation for conformational analysis of carbohydrates by n.m.r. spectroscopy is described, together with the preparation of suitable solutions. Spectral assignments may be confirmed by (a) solvent shifts, (b) exchange processes, (c) isotopic substitution, (d) effects of temperature, and (e) double-resonance techniques. Iterative analysis of spectra and interpretation of spin-spin coupling constants over two to five bonds are discussed. The study of conformational equilibria by means of variable-temperature techniques and nuclear Overhauser effects is described. An indication of the potential value of the magnetic resonance of nuclei other than protons is given.

12778. Perls, T. A., Stern, J., **Motion,** Chapter 3 in *ISA Transducer Compendium, Second Edition*, Part II, 105-111 (IFI/Plenum, New York, N.Y., June 1970).

12779. Yokel, F. Y., Somes, N. F., **Performance criteria for tall buildings,** (Proc. 5th CIB Congress, Paris-Versailles, France, June 1971), Chapter in *Research Into Practice, The Challenge of Application* **1,** 587-592 (June 1971).

12780. Stiehler, R. D., **Letter to the Editor,** *Modern Plastics* **49,** No. 5, 8 (May 1972).

12781. Smith, C. N., **X-ray standards for law enforcement,** *The Police Chief*, p. 46 (International Association of Chiefs of Police, Gaithersburg, Md., May 1972).

12782. Liu, Y. M., Coleman, J. A., **Radiation damage effects by electrons, protons, and neutrons in Si(Li) detectors,** *IEEE Trans. Nucl. Sci.* **NS-19,** No. 3, 346-352 (1972).

12783. Radebaugh, R., Siegwarth, J. D., **Numerical analysis of continuous and discrete heat exchangers for dilution refrigerators,** (Proc. Comm. I, Conf. on Cryophysics and Cryoengineering, Tokyo, Japan, Sept. 11-12, 1970), *Bull. Inst. Int. Froid, Annexe 1970-2*, pp. 249-254 (Int. Inst. of Refrigeration, Paris, France, 1970).

12784. Clark, A. F., Kropschot, R. H., **Low temperature specific heat and thermal expansion of alloys,** (Proc. Comm. I, Conf. on Cryophysics and Cryoengineering, Tokyo, Japan, Sept. 11-12, 1970), *Bull. Inst. Int. Froid, Annexe 1970-2*, pp. 249-254 (Int. Inst. of Refrigeration, Paris, France, 1970).

Key words: Aluminum alloys; copper-nickel alloys; cryogenics; specific heat; stainless steel; thermal expansion; titanium alloys.

Grüneisen was the first to show that statistical thermodynamics could be used to relate thermal expansion and specific heat. Using these relations we have calculated the specific heats of several alloy systems of importance in cryogenic design. Specific heats of copper-nickel alloys, austenitic stainless steels, aluminum alloys and titanium alloys have been calculated in the temperature range 4-300 K and comparisons made with the limited amount of experimental data. Results indicate that, to engineering accuracy, the specific heat of an alloy system can be readily predicted over a large temperature range from the experimentally determined thermal expansion.

12785. Andrews, J. R., **A frequency calibrator for UHF using an avalanche transistor,** *QST* **LVI,** No. 5, 16-18 (May 1972).

12786. Oser, H. J., **Translator and Editor of the book: Bounda-**

ry layers of flow and temperature, by A. Walz, 297 pages (MIT Press, Cambridge, Mass., 1969).

Key words: Airfoil theory; boundary layer; drag; heat transfer; laminar; lift; skin friction; subsonic; supersonic; transition; turbulent.

A translation of the monograph: Strömungs-und Temperaturgrenzschichten by Alfred Walz. The book describes theory and computation of laminar and turbulent boundary layers without and with heat transfer.

12787. Milligan, D. E., Jacox, M. E., **Infrared and ultraviolet spectroscopic studies of molecular ions trapped in inert solid matrices,** *Proc. 19th Annual Conf. on Mass Spectrometry and Allied Topics, Atlanta, Ga., May 2-7, 1971*, pp. 100-104 (American Society for Mass Spectrometry, ASTM Committee E-14 and Naval Research Laboratory, Washington, D.C., 1971).

12788. Horton, W. S., Carson, C. C., **Gas analysis: Determination of gases in metals,** Chapter 103 in *Treatise on Analytical Chemistry*, I. M. Kolthoff and P. J. Elving, eds., **10,** Part 1, Section E, 6017-6144 (John Wiley & Sons, Inc., New York, N.Y., 1972).

Key words: Gases in metals; hot extraction; hydrogen; Kjeldahl; nitrogen; oxygen; vacuum-fusion analysis.

Methods for the determination of oxygen, hydrogen and nitrogen in metals are discussed. General historical and technical information is given as well as procedural details and assessment of accuracy for some methods are given. Methods include vacuum-fusion, inert gas fusion, hot extraction, Kjeldahl, spectrographic and isotopic as well as others. This is an invited contribution to form a chapter of Kolthoff and Elving's Treatise on Analytical Chemistry.

12789. Meyerson, M. R., **Ultrahigh-strength materials,** Chapter 19 in *Materials Science and Technology for Design Engineers*, pp. 366-389 (Hayden Book Company, Inc., New York, N.Y., 1972).

Key words: Alloy steels; ausformed steels; cold-drawn steels; dispersion hardened alloys; fiber and whisker reinforced materials; maraging steels; refractory alloys; stainless steels; strengthening mechanisms; superalloys; titanium alloys; tool steels; ultrahigh strength.

This state-of-the-art survey is to be a chapter in a book entitled "Materials Science and Technology for Design Engineers." Written for non-metallurgists, it offers a review of the known strengthening mechanisms and describes the characteristics and mechanical properties of current commercial alloys which attain ultrastrength levels at room and elevated temperatures. Included are alloy steels, tool steels, ausformed steels, cold-drawn steels, hardenable stainless steels, precipitation-hardened stainless steels, maraging steels, titanium alloys, superalloys, refractory alloys, dispersion-hardened alloys, and fiber and whisker reinforced materials.

12790. Hougen, J. T., **An interesting example of Hund's coupling case (c) in $HgAr^+$,** *J. Mol. Spectrosc.* **42,** 381-384 (1972).

Key words: $HgAr^+$; Hund's case (c); Ω-type doubling; rotational levels.

The rotational energy levels of a diatomic molecule in a Hund's case (c) $\Omega = 1/2$ state arising from $^2D_{5/2} + {}^1S_0$ separated atoms are shown to be given by an expression of the form $B[(J+1/2)^2 + 8] \mp 1/2p(J+1/2) - D[(J+1/2)^2 + 8 \mp 1/2\,(p/B)\,(J+1/2)]^2$, where the upper and lower sign choices correspond to rotational levels of parity $(-1)^{J-1/2}$ and $(-1)^{J+1/2}$, respectively, and where $p \cong +6B$.

12791. King, D. A., Madey, T. E., Yates, J. T., Jr., **Interaction of oxygen with polycrystalline tungsten, Part 3—Electron stimulated desorption,** *J. Chem. Soc. Faraday Trans. I*, **68,** 1347-1359 (1972).

Key words: Adsorption; chemisorption; desorption; electron stimulated desorption; oxidation; oxygen; tungsten.

This paper is a sequel to a detailed study of the kinetics of adsorption and desorption in the interaction of O_2 with polycrystalline tungsten, in which a number of oxide and O atom states were identified by thermal desorption. In electron stimulated desorption (ESD) studies two states of adsorbed oxygen were distinguished, β_1 and β_2; the former has a high ESD cross section and the latter a low cross section. In this paper an attempt is made to correlate the states observed in the thermal desorption study with these β_1 and β_2 states. The ESD properties of the β_1 state are determined, and the sticking probability for readsorption onto an oxygen-saturated surface depleted of β_1 by ESD is determined as a function of the incremental oxygen coverage. The steady state between electronic desorption and readsorption from the gas phase is examined, and isotopic exchange between ^{16}O and ^{18}O in the β_2 and β_1 states is observed and characterized. The appearance of the β_1 state is related in a complex way to the formation of tungsten oxides which can be thermally desorbed in the temperature range 1200-1600 K.

12792. Cox, D. M., Smith, S. J., **Absolute measurement of 2*S* atom production by dissociative excitation of molecular deuterium,** *Phys. Rev. A* **5,** No. 6, 2428-2442 (June 1972).

Key words: Absolute measurement; cross section; deuterium; dissociative excitation; metastable.

We have measured the cross section for production of metastable (2S) atoms by the process of dissociative excitation of molecular deuterium by electron impact. The measurement includes the quantitative evaluation of detection efficiency, density, and geometrical factors necessary to establish an absolute scale on a purely experimental basis. The method depends on the application of an rf field at the Lamb-shift frequency (1059 MHz) to quench the metastables at the point of excitation. The radiation induced by the applied field is isotropic so that the absolute cross section depends on a simple solid angle correction. The cross sections at 23.8 and 39.1 eV are 2.97×10^{-18} and 3.40×10^{-18} cm², respectively, with a probable error estimated to be ± 14%. The energy dependence of the cross section was also measured from threshold to 500 eV.

12793. Opal, C. B., Beaty, E. C., **Measurements of large angle inelastic scattering cross sections for electrons on helium,** *J. Phys. B: At. Mol. Phys.* **5,** No. 2, 627-635 (Mar. 1972).

12794. Hidalgo, M. B., Geltman, S., **A high energy approximation: III. Helium excitation by electrons,** *J. Phys. B: At. Mol. Phys.* **5,** No. 3, 617-626 (Mar. 1972).

12795. Albers, J., Mountain, R. D., **Asymptotic form of the pair-correlation function in liquids,** *Phys. Rev. A* **5,** No. 6, 2629-2632 (June 1972).

12796. Maienthal, E. J., **Polarographic analysis at NBS,** *Amer. Lab.* **4,** No. 6, 12-21 (June 1972).

12797. Bay, Z., White, J. A., **Frequency dependence of the speed of light in space,** *Phys. Rev. D* **5,** No. 4, 796-799 (Feb. 15, 1972).

12798. Rathbone, D. Z., Jr., **Cutting the costs of cooling,** *Plant Eng.* **26,** No. 12, 88-90 (June 15, 1972).

12799. Pilling, M. J., Bass, A. M., Braun, W., **A curve of growth determination of the *f*-values for the fourth positive system of CO and the Lyman-Birge-Hopfield system of N_2,** *J. Quant. Spectrosc. Radiat. Trans.* **11,** 1593-1604 (1971).

12800. Hubbell, J. H., **Survey of photon-attenuation-coefficient measurements 10 eV to 100 GeV,** *Atomic Data* **3,** No. 3, 241-297 (Nov. 1971).

12801. Spiegel, V., Jr., **Evaluation of the neutron source ab-**

sorption correction in a manganous sulfate bath, (Proc. Amer. Nucl. Soc. National Topical Meeting on Neutron Sources and Applications, Augusta, Ga., Apr. 18-21, 1971), Chapter in *Neutron Sources and Applications,* **II,** 1-170–1-171 (1971).

12802. Smith, J. M., **Automatic data evaluation, manipulation, display, and plotting with SPEED,** *Comput. Graphics* **4,** No. 2, 41-53 (Fall 1970).

12803. Karp, S. S., Rath, G. J., Wright, G. P., **A simulation model of admission and discharge policies for an intensive care unit,** *Proc. 1970 Summer Computer Simulation Conference, Denver, Colo., June 10-12, 1970,* pp. 1108-1114 (June 1970).

12804. Slattery, W. J., **Standards: Information and sources,** *Proc. 2d Annual Plant Engineering and Western Maintenance Conf., Anaheim, Calif., Sept. 23-25, 1969,* pp. 49-57 (American Institute of Plant Engineers, Region 6, Cincinnati, Ohio, 1969).

12805. Paffenbarger, G. C., **Dental cements, direct filling resins. Composite and adhesive restorative materials: A resume,** (Proc. Engineering Foundation Research Conferences, Engineering in Medicine-Bioceramics, New England College, Henniker, New Hampshire, August 3-7, 1970), *J. Biomed. Mater. Res. Symp.* No. 2, Part 2, 363-393 (John Wiley & Sons, Inc., New York, N.Y., Jan. 1972).

12806. Guevara, F. A., McInteer, B. B., Ottesen, D., Hanley, J. M., **A critique of the high-temperature viscosity measurements of Trautz and Zink, Los Alamos Scientific Laboratory, University of California, Los Alamos, New Mexico, Report No. LA-4643-MS,** pp. 1-10 (June 1971).

12807. Klebanoff, P. S., Tidstrom, K. D., **Mechanism by which a two-dimensional roughness element induces boundary-layer transition,** *Phys. Fluids* **15,** No. 7, 1173-1188 (July 1972).

Key words: Boundary layer; roughness; stability; transition; two-dimensional.

An experimental investigation of the effect of two-dimensional roughness elements on boundary-layer transition is described. Primary emphasis is given to the nature of disturbances within the recovery zone, i.e., that region in the immediate downstream of the roughness where the mean flow has been distorted by the presence of the roughness. Detailed measurements of mean velocity distributions, of disturbance spectra, and intensity, growth, and decay of disturbances at discrete frequencies were made for a range of unit Reynolds numbers. The measurements demonstrate that the behavior can best be understood by considering wave-type disturbances, and that the basic mechanism by which a two-dimensional roughness element induces earlier transition to turbulent flow is by the destabilizing influence of the flow within the recovery zone. Comparison with the behavior expected from stability theory supports this conclusion.

12808. Greer, W. L., Rubin, R. J., **Quantum theory of heat transport in an isotopically substituted, one-dimensional, harmonic crystal,** *J. Math. Phys.* **13,** No. 3, 379-385 (Mar. 1972).

12809. Jacox, M. E., Milligan, D. E., **Spectrum and structure of the HO_2 free radical,** *J. Mol. Spectry.* **42,** No. 3, 495-513 (June 1972).

Key words: ClOO; H-atom reaction; HO_2; H_2O_2; infrared spectrum; matrix isolation; normal coordinate analysis; O_3; ultraviolet spectrum; vacuum-ultraviolet photolysis.

In studies of the vacuum-ultraviolet photolysis of $Ar:O_2:HCl$ and $Ar:O_2:H_2O$ samples at 14 K the free radical HO_2 has been stabilized in considerably greater concentrations than in earlier experiments, in which the mercury-arc photolysis of HBr or of HI had been used to provide a source of H atoms. Appreciable concentrations of H_2O_2 and O_3 and, in the experiments using HCl as an H-atom source, of HOCl and ClOO were also stabilized. The infrared spectra of the mixed oxygen-isotopic species of DO_2 have been reported for the first time. The data for the four oxygen-isotopic species of HO_2 have been subjected to a normal coordinate analysis, using a four-constant valence-force field, and the calculated DO_2 frequencies have been compared with the observed values. The previous assignment of the 1389-cm^{-1} absorption as the OH deformation fundamental and of the 1101-cm^{-1} absorption as the oxygen–oxygen stretching fundamental has been definitively established. A satisfactory fit to the observed absorption pattern for the oxygen-isotopic species of DO_2 has been obtained for a valence angle of $105 \pm 5°$. The magnitudes of the two stretching force constants of HO_2 suggest that the electronic structure of HO_2 may approach that of O_2^-, lending some support to the previous identification of an electronic transition of HO_2 near that of O_2^-.

12810. Levine, J., Hall, J. L., **Design and operation of a methane absorption stabilized laser strainmeter,** *J. Geophys. Res.* **77,** No. 14, 2595-2609 (May 10, 1972).

Key words: Interferometer; methane absorption stabilized; strainmeter.

A unique 30-meter laser strainmeter is described. The system uses a Fabry-Perot geometry and dynamically adjusts the frequency of the illuminating laser to follow a single fringe. The reference length for the system is provided by a second laser whose wavelength is stabilized by a vibration-rotation absorption line in methane. The system shows excellent sensitivity, wide bandwidth, and essentially no drift. A sample of the earth-tide record obtained with the laser strainmeter and the initial motion observed for the nuclear explosion Boxcar are shown. The instrument should also be useful for observations of free oscillations of the earth.

12811. Winogradoff, N. M., Haller, W. K., Hockey, B. J., **Cross-sectional energy distributions in gigawatt laser pulses: Implications and determination,** *Opto-Electron. Lett.* **3,** 145-148 (1971).

Key words: Beam uniformity; glass damage; laser induced sputtering; neodymium glass laser.

Cross-sectional beam uniformity is essential for quantitative work on non-linear optical phenomena and in the measurement of the threshold for laser induced damage in glass. A technique of obtaining detailed information on the beam uniformity by using laser induced sputtering on suitable glass surfaces in described.

12812. Spencer, L. V., Woolf, S., **A "forced reflection"-type of collimator design,** Paper in Chapter on Shielding and Dosimetry, *Trans. Amer. Nucl. Soc.* **14,** No. 1, 887 (June 1971).

12813. Jednačak, J., Hudomalj, M., Pravdić, V., Haller, W., **Electrokinetics of glass surfaces. I. Charge densities at the solid/gas and the solid/liquid interfaces of porous glasses,** *Croat. Chem. Acta* **44,** 149-156 (1972).

12814. Kuyatt, C. E., Plummer, E. W., **Field emission deflection energy analyzer,** *Rev. Sci. Instr.* **43,** No. 1, 109-111 (Jan. 1972).

12815. Liebman, J. F., **Comment on the paper "Oxygen monofluoride (OF, $^2\Pi$): Hartree-Fock wavefunction, binding energy, ionization potential, electron affinity, dipole and quadrupole moments, and spectroscopic constants. A comparison of theoretical and experimental results" by** P. A. G. O'Hare and A. C. Wahl, *J. Chem. Phys.* **56,** No. 8, 4242-4243 (Apr. 15, 1972).

12816. Brinckman, F. E., Johannesen, R. B., Handy, L. B., **Pi-bonding effects in organoxytungsten (VI) fluorides,** *J. Fluorine Chem. Short Commun.* **1,** 493-497 (1971/72).

12817. Becker, D. A., LaFleur, P. D., **Determination of trace quantities of uranium in biological materials by neutron activation analysis using a rapid radiochemical separation,** *Anal. Chem.* **44,** No. 8, 1508-1511 (July 1972).

Key words: Biological materials; neutron activation analysis; rapid radiochemical separation; solvent extraction; trace analysis; uranium.

Neutron activation analysis has been applied to the determination of trace quantities of uranium in biological materials, using the short-lived radioisotope ^{239}U ($T_{1/2}$= 23.5m). A solvent extraction technique was developed for the extraction of uranium by the reagent hydrogen bis(2-ethylhexyl) phosphate (HDEHP). The technique developed was found to be applicable also to the analysis of uranium in other materials such as aluminum, copper oxide and zirconium. Extraction efficiencies for uranium using HDEHP are presented for nitric, perchloric, hydrochloric and hydrofluoric acids. The analysis for uranium at levels of 10^{-6}g to 10^{-9}g was made in practical samples, and good agreement obtained with other analytical techniques.

12818. Leung, P. S., Rush, J. J., Taylor, T. I., **Study of hindered rotation in crystals by neutron transmission measurements: Comparison of calculated and measured scattering cross sections,** *J. Chem. Phys.* **57,** No. 1, 175-182 (July 1, 1972).

Key words: Ammonium salts; cross section; crystals; hindered rotation; methylbenzenes; neutron scattering; torsional vibrations.

Total neutron cross sections have been measured as a function of neutron wavelength (λ_n= 5 – 11 Å) and sample temperature for $(NH_4)_2SiF_6$, $(NH_4)_2S_2O_8$, durene and hexamethylbenzene. The experimental results are compared to previous cross-section data for other ammonium salts and methyl-substituted compounds and are correlated with the rotational freedom of the NH_4^+ ions and methyl groups. A relatively simple theoretical procedure is described for calculating total scattering cross sections of hydrogenous crystals using torsional and translational lattice-mode frequencies obtained from neutron or optical spectra. Cross-section variations vs wavelength ($\Delta\sigma_s/\Delta\lambda$) and temperature ($\Delta\sigma_s/\Delta T$) are calculated for a large group of ammonium salts and methyl-substituted organics (including those for which experimental cross sections are presented here) and are directly compared with measured cross-section results. In every case the experimental and theoretical results agree within about 10% or less. Thus the previously observed empirical relationship between $\Delta\sigma_s/\Delta\lambda$ and $\Delta\sigma_s/\Delta T$ and the rotational and vibrational behavior of ions and molecules in solids is placed on a more quantitative basis. These comparisons reinforce the usefulness of the neutron cross-section method as a supplement to spectroscopic techniques.

12819. Prince, E., **Configuration of the water molecule in cupric fluoride dihydrate at 298 K,** *J. Chem. Phys.* **56,** No. 9, 4352-4355 (May 1, 1972).

**Publications with prices and SD Catalog numbers indicated may be purchased directly from the Superintendent of Documents, U.S. Government Printing Office, Washington, D.C. 20402 (foreign: one-fourth additional). NBS nonperiodical series are also available from the National Technical Information Service (NTIS), Springfield, Va., 22151 (formerly the Clearinghouse for Federal Scientific and Technical Information). Reprints from outside journals and the NBS Journal of Research may often be obtained directly from the authors by title only.*

JOURNAL OF RESEARCH of the National Bureau of Standards — A. Physics and Chemistry
Vol. 76A, No. 6, November–December 1972

INDEX TO VOLUME 76A

January to December 1972

A

Ab inito Gaussian wave functions ... 661
Absolute fluorometry ... 593
Absolute fluorometry in biochemistry ... 593
Absolute quantum efficiencies ... 561
Absolute spectrofluorometry ... 547
Absolute spectroradiometric measurements ... 427
Absolute spectroradiometry ... 427
Absolute standard source of radiation ... 427
Absorbance ... 405
Absorption spectra of krypton and xenon in the wavelength 330–600 Å ... 1
Absorptivity data ... 469
Accurate calculations of properties of the two-tube electrostatic lens. I. Improved digital methods for the precise calculation of electric fields and trajectories ... 27
Accurate measurement of molar absorptivities ... 483
Accurate measurements of and corrections for nonlinearities in radiometers ... 437
Accurate spectrophotometer for measuring the transmittance of solid and liquid materials ... 405
Accuracy ... 437, 469
Actiometers ... 547
$A^2\Sigma$ ... 665
An alternative to accurate pyrometry in distinguishing concurrent vaporization reactions. Postulated results using the vaporization of gold in analyzing the vaporization of beryllium oxide in water vapor ... 511
Analyses of iron, titanium, nickel ... 517
Anatomy and thermal history of laser self-focusing damage tracks in glass ... 337
Antiparallel chain sheet structures ... 351
Apollo 14 lunar samples ... 517
Aqueous solvents in phosphorimetry ... 579
Argon arcs ... 71
Argon transition probabilities ... 71
Ausloos, P., Rebbert, R. E., Pulse radiolysis of neopentane in the gas phase ... 329
—, *Sieck, L. W.*, Photoionization of propylene, cyclopropane, and ethylene, The effect of internal energy on the bimolecular reactions of $C_2H_3^+$ and $C_3H_5^+$ ... 253
—, —, *Lias, S. G., Hellner, L.*, Photoionization of C_4H_8 isomers. Unimolecular and bimolecular reactions of $C_4^+H_8^+$ ions ... 115
Autoionization ... 1
Automation of accurate spectrophotometer ... 405

B

Barnes, J. D., Khoury, F., The formation of curved polymer crystals: poly(4-methylpentene-1) ... 225
Beam geometry ... 455
Beers, Y., Klein, G. P., The Stark splitting of millimeter wave transitions of water ... 521
Beryllia hydrates (gases) ... 511
Brown, J. E., The characterization of linear polyethylene SRM 1475. II. Determination of total methyl content by infrared spectrophotometry ... 141
—, The characterization of linear polyethylene SRM 1475. III. Density determination ... 143
—, *Verdier, P. H.*, The characterization of linear polyethylene SRM 1475. IX. Number average molecular weight of fractions by membrane osmometry ... 161
Brown, R. L., Spin-relaxation effects on the EPR spectrum of gaseous hydrogen atoms ... 103
Bullman, G. W., Wood, L. A., Decker, G. E., Modulus of natural rubber cross-linked by dicumyl peroxide. I. Experimental observations ... 51
Burke, R. W., Deardorff, E. R., Menis, O., Liquid absorbance standards ... 469
Burnett, R. W., Accurate measurement of molar absorptivities ... 483

C

Calculation of electric fields ... 27
Calculation of electron trajectories ... 27
Calibrated photodetector ... 427
Calibration of spectrofluorometers ... 547
Callis, J. B., Crosby, G. A., Demas, J. N., Absolute quantum efficiencies ... 561
Calorimetry ... 13
Calorimetry in quantum yields ... 561
Case, W. E., Rasmussen, A. L., Schmidt, L. B., West, E. D., Reference calorimeter for laser energy measurements ... 13
α- and β-$CaSO_4 \cdot {}^1/_2H_2O$ ... 41
$CaSO_4 \cdot 2H_2O$ ... 41
Caspi, E., Shadmi, Y., Theoretical investigation of the odd configuration of Ni II ... 125
Cavity ... 347
Ce I and Ce II ... 285
Cerium spectra ... 285
C_4H_8 isomers ... 115
Chain-folded ... 225
Characterization of linear polyethylene SRM 1475. I. Introduction ... 137
Characterization of linear polyethylene SRM 1475. II. Determination of total methyl content by infrared spectrophotometry ... 141
Characterization of linear polyethylene SRM 1475. III. Density determination ... 143
Characterization of linear polyethylene SRM 1475. IV. Melt flow rate ... 145
Characterization of linear polyethylene SRM 1475. V. Solution viscosity measurements ... 147
Characterization of linear polyethylene SRM 1475. VI. Preparation of calibrating fractions ... 149
Characterization of linear polyethylene SRM 1475. VII. Differential refractive index of polyethylene solutions ... 151
Characterization of linear polyethylene SRM 1475. VIII. Light scattering studies on polyethylene in 1-chloronaphthalene ... 156
Characterization of linear polyethylene SRM 1475. IX. Number average molecular weight of fractions by membrane osmometry ... 161
Characterization of linear polyethylene SRM 1475. X. Gel permeation chromotography ... 163
Chemistry ... 67
Chen, R. F., Measurements of absolute values in biochemical fluorescence spectroscopy ... 593
1-Chloronaphthalene ... 147, 151
Christensen, R. G., The characterization of linear polyethylene SRM 1475. V. Solution viscosity measurements ... 147
—, The characterization of linear polyethylene SRM 1475. VI.

Page

Preparation of calibrating fractions 149
Cilia 213
Clarke, F. J. J., High accuracy spectrophotometry at the National Physical Laboratory 375
Clausius-Mossotti function 37
Clifton, J. R., Thermal analysis of calcium sulfate dihydrate and supposed α and β forms of calcium sulfate hemihydrate from 25 to 500 °C 41
Clinical spectrophotometry, accuracy, precision 499
Clinical standards 491
Codling, K., Madden, R. P., The absorption spectra of krypton and xenon in the wavelength range 330–600 Å 1
Collisional stabilization 115, 253
Column extraction fractionation 149
Compressed liquid 81
Compressibility 207
Concentration dependence 161
Considerations on organic compounds in solution and inorganic ions in glasses as fluorescent standards reference materials 641
Contaminants 511
Corliss, C. H., Verges, J., Martin, W. C., Infared spectra of cerium (Ce I and Ce II) between 0.8 and 2.4 μm 285
Creep 51
Critical point 207
Crosby, G. A., Demas, J. N., Callis, J. B., Absolute quantum efficiencies 561
Cross-linking 51
Cryogenics 263
Crystal, curved 225
Crystallization 143
Cycloheptane 77
Cyclohexane 77
Cyclopentane 77
Cylindrical cavity 347

D

Demas, J. N., Crosby, G. A., Callis, J. B., Absolute quantum efficiencies 561
Deardorff, E. R., Burke, R. W., Menis, O., Liquid absorbance standards 469
Decalin 147
Decker, G. E., Wood, L. A., Bullman, G. W., Modulus of natural rubber cross-linked by dicumyl peroxide. I. Experimental observations 51
Degree of crystallinity 143
Densities 81
Densities of compressed liquid methane and the equation of state 81
Density 143
Detector nonlinearity 455
Detectors, absolute 547
Determination of iron, titanium, and nickel in Apollo 14 samples by cathode ray polarography 517
Development of a new fluorescent reagent and its application to the automated assay of amino acids and peptides at the picomole level 637
Di Chio, D., Kuyatt, C. E., Natali, S., Accurate calculations of properties of the two-tube electrostatic lens. I. Improved digital methods for the precise calculation of electric fields and trajectories 27
Dicumyl peroxide 51
Dielectric constant 37
Dielectric constant of compressed gaseous and liquid oxygen 37
Differential cathode ray polarography 517
Differential scanning calorimetry 41
Differential solutions 151
Differential thermal analysis 41
Diffusely reflecting 347
Dilute solution theory of polymer crystal growth: fractionation effect 213
DiMarzio, E. A., Sanchez, I. C., Dilute solution theory of polymer crystal growth: fractionation effect 213
dn/dc 151

Page

Dissolution temperature 213
Douglas, T. B., An alternative to accurate pyrometry in distinguishing concurrent vaporization reactions. Postulated results using the vaporization of gold in analyzing the vaporization of beryllium oxide in water vapor 511

E

Effect of acid on a standard cell 321
Electron impact excitation 661
Electron lens 27
Electron scavengers 329
Electron spin resonance 103
Electronic transition probabilities 665
Emf-temperature coefficient of "acid" standard cells of the saturated cadmium sulfate type from 15 to 40 °C 321
Emf-temperature coefficients of standard cells 185, 321
Emfs of standard cells 185
Emission spectra 641
Emissivity 347
End-to-end distance 156
Energy levels 125
Enzymes 607
Equation of state 81, 207
Equilibrium 71
Exchange amplitude 661
Excitation of O_2 $^1\Delta_g$ by electron impact 661
Excitation spectra 641
Experimental procedures 67
Extrusion plastometer 145

F

Fanconi, V., Lattice vibrations of antiparallel chain sheet structures 351
Far ultraviolet 1
Field, B. F., Hamer, W. J., Field, B. F., The emf-temperature coefficient of "acid" standard cells of the saturated cadmium sulfate type from 15 to 40 °C 321
Fluid 207
Fluorescence 641
Fluorescence spectra, corrected 547
Fluorescence standards 613, 641
Fluorometric analysis 607
Fluorometry, amino acids 637
Fluorometry of enzymes 607
Fluorometry of substrates 607
Fluorometry, peptides 637
Formation of curved polymer crystals: poly(4-methylpentene-1) 225
Fractionation 137, 149, 213
Frolen, L., Ross, G., The characterization of linear polyethylene SRM 1475. X. Gel permeation chromatography 163
—, —, Wims, A. M., Verdier, P. H., The characterization of linear polyethylene SRM 1475. VIII. Light scattering studies on polyethylenes in 1-chloronaphthalene 156
Fussell, W. B., Normal emissivity of an isothermal, diffusely reflecting cylindrical cavity (with top) as a function of inside radius 347

G

Garvin, D., Guidelines for the reporting of numerical data and experimental procedures 67
Gas phase 329
Gas-phase kinetics 655
Gel permeation chromatography 163
g-Factors 115
Glass 337
Glass standards 641
Glass standards in fluorescence 613
Glass transition 51
Gold 511
Gold alloy 263
Goodwin, R. D. Prydz, R., Densities of compressed liquid methane and the equation of state 81

Page

Gorden, R., Jr., Sieck, L. W., Ion-molecule reactions in isopropanol: Implications for its radiolysis 655
Guidelines for the reporting of numerical data and experimental procedures 67
Guilbault, G. G., Newer fluorometric methods for the analysis of biologically important compounds 607

H

Haller, W., Simmons, J. H., Anatomy and thermal history of laser self-focusing damage tracks in glass 337
Hamer, W. J., Thermodynamics of standard cells of the saturated cadmium sulfate type 185
—, *Skapars, A., Field, B. F.*, The Emf-temperature coefficient of "acid" standard cells of the saturated cadmium sulfate type from 15 to 40 °C 321
Hartree-Fock 665
Heat capacity changes in standard cells 321
Helium 207
Hellner, L., Sieck, L. W., Lias, S. G., Ausloos, P., Photoionization of C_4H_8 isomers. Unimolecular and bimolecular reactions of the $C_4^+H_8^+$ ions 115
Herron, J. T., Huie, R. E., Rates of reaction of atomic oxygen. III. Spiropentane, cyclopentane, cyclohexane, and cycloheptane 77
High accuracy 405, 455
High accuracy spectrophotometry 375
High accuracy spectrophotometry at the Physical Laboratory 375
Hoeve, C. A. J., Wagner, H. L., Verdier, P. H., The characterization of linear polyethylene SRM 1475. I. Introduction 137
Honeycomb lattice 351
Huie, R. E., Herror, J. T., Rates of reaction of atomic oxygen. III. Spiropentane, cyclopentane, cyclohexane, cycloheptane 77
Hydrocarbons 253
Hydrogen atoms 103

I

Improved state equation in the vicinity of the critical point 207
Indentation measurements 51
Infrared 141
Infrared spectra 285
Infrared spectra of cerium (Ce I and Ce II) between 0.8 and 2.4 μm 285
Interference 455
Instrumentation 405
Ion-molecule reactions 253, 329, 655
Inorganic ions 613
Inorganic ions in glasses and polycrystalline pellets as fluorescence standard reference materials 613, 655
Ion-molecule reactions in isopropanol: Implications for the radiolysis 655
Isomerization 115

J

Julienne, P. S., Krauss, M., Excitation of $O_2\ ^1\Delta_g$ by electron impact 661
—, *Marchetti, M., Krauss, M.*, Vibrational and electronic oscillator strengths of LiO 665

K

Khoury, F., Barnes, J. D., The formation of curved polymer crystals: poly(4-methylpentene-1) 225
Klein, G. P., Beers, Y., The Stark splitting of millimeter wave transitions of water 521
Krauss, M., Julienne, P. S., Excitation of $O_2\ ^1\Delta_g$ by electron impact 661
—, *Marchetti, M., Julienne, P. S.*, Vibrational and electronic oscillator strengths of LiO 665
Krypton 1
Kuyatt, C. E., Natali, S., Di Chio, D., Accurate calculations of properties of the two-tube electrostatic lens. I. Improved digital methods for the precise calculation of electric fields and trajectories 27

L

Page

Lamellar 225
Laser 13
Laser calorimetry 13
Laser damage 337
Laser energy measurement 13
Laser power measurement 13
Laser, use in quantum yields 561
Lattice vibrations 351
Lattice vibrations of antiparallel chain sheet structures 351
Lias, S. G., Sieck, L. W., Hellner, L., Ausloos, P., Photoionization of C_4H_8 isomers. Unimolecular and bimolecular reaction of the $C_4^+H_8^+$ ions 115
Light scattering 156
Limiting viscosity number 147
Linear polyethylene 137, 141, 143, 147, 149, 156, 161, 163
LiO 665
Liquid absorbance standards 469
Liquid helium 263
Liquid hydrogen 263
Liquid nitrogen 263
Load 145
Low temperature 207
Low temperature thermocouples: KP, "normal" silver, and copper versus Au-0.02 at % Fe and Au-0.07 at % Fe 263
LTE 71

M

Madden, R. P., Codling, K., The absorption spectra of krypton and xenon in the wavelength range 330–600 Å 1
Maienthal, J. E., The determination of iron, titanium, and nickel in Apollo 14 samples by cathode ray polarography 517
Marchetti, M., Julienne, P. S., Krauss, M., Vibrational and electronic oscillator strengths of LiO 665
Martin, W. C., Verges, J., Corliss, C. H., Infrared spectra of cerium (Ce I and Ce II) between 0.8 and 2.4 μm 285
Mass spectrometry 655
Maurey, J. R., The characterization of linear polyethylene SRM 1475. IV. Melt flow rate 145
Mavrodineanu, R., An accurate spectrophotometer for measuring the transmittance of solid and liquid materials 405
Measurements of absolute values in biochemical fluorescence spectroscopy 593
Melhuish, W. H., Absolute spectrofluorometry 547
Melt flow rate 145
Membrane 161
Menis, O., Burke, R. W., Deardorff, E. R., Liquid absorbance standards 469
Methane 81, 207
Methyl 141
Methylene 141
Micron microscopy 225
Mielenz, K. D., Physical parameters in high-accuracy spectrophotometry 455
Millimeter waves 521
Molar absorptivity in clinical chemistry 483
Modulus of natural rubber cross-linked by dicumyl peroxide. I. Experimental observations 51
Modulus: rubber, natural 51
Molecular weight 137
Molecular weight distribution 137
Molecular weight distribution (MWD) 163
Mw 156

N

Natali, S., Di Chio, D., Kuyatt, E. E., Accurate calculations of properties of the two-tube electrostatic lens. I. Improved digital methods for the precise calculation of electric fields and trajectors 27
National Bureau of Standards 137
Neopentane 329
Neutralization 329
Newer fluorometric methods for the analysis of biologically

Page

important compounds ... 607
Nickel ... 125
Nine-point relaxation formulas ... 27
Nonlinearity ... 437
Normal emissivity ... 347
Normal emissivity of an isothermal diffusely reflecting cylindrical cavity (with top) as a function of inside radius ... 347
Number average ... 163
Number average molecular weight ... 141, 161
Numerical data ... 67

O

Ochkur-Rudge approximation ... 661
Optical cuvettes ... 499
Optical microscopy ... 225
Orifice ... 145
Orifice die ... 145
Orthobaric densities ... 81
Osmometer ... 161
Osmotic pressure ... 161
$O_2\ ^1\Delta_g$ state ... 661
Oxygen ... 37, 77

P

Parameters ... 125
Pellet variability ... 137
Penton, J. R., Widdowson, G. M., Williams, G. Z., Problems associated with the need for standardization in clinical spectrophotometric and fluorometric measurements ... 491
Phosphorimetry ... 579
Photocell linearity ... 437
Photodetectors in quantum yields ... 561
Photoelectronic linearity ... 375
Photoionization ... 1, 115, 253, 655
Photoionization of C_4H_8 isomers. Unimolecular and bimolecular reactions of the $C_4^+H_8^+$ ions ... 115
Photoionization of propylene, cylopropane, and ethylene. The effect of internal energy on the bimolecular reactions of $C_2H_4^+$ and $C_3H_6^+$ ... 253
Photometric accuracy ... 437, 509
Physical parameters in high-accuracy spectrophotometry ... 455
Physics ... 67
Picomole fluorometry ... 637
Polarization ... 455
Polyethylene fractions ... 156
Polymer ... 143, 225
Poly(4-methylpentene-1) ... 225
Popenoe, C. H., Shumaker, J. B., A study of equilibrium in argon arcs ... 71
Powell, R. L., Sparks, L. L., Low temperature thermocouples: KP, "normal" and copper versus Au-0.02 at% and Au 0.07 at% Fe ... 263
Predictor-corrector method ... 27
Preliminary extrudate ... 145
Problems associated with the need for standardization in clinical spectrophotometric and fluorometric measurements ... 491
Proton affinity ... 655
Prydz, R., Goodwin, R. D., Densities of compressed liquid methane and the equation of state ... 81
Pulse radiolysis ... 329
Pulse radiolysis of neopentane in the gas phase ... 329
Pyrometry ... 511

Q

Quantum counters ... 547
Quantum efficiencies ... 561
Quinine derivatives ... 641

R

Radiation ... 347
Radiation addition method ... 437
Radiolysis ... 655
Rand, R. N., Role of spectrophotometric standards in the clinical chemistry laboratory ... 499
Random errors in molar absorptivity ... 483
Rare earth ... 641
Rare-earth-doped glasses ... 613
Rasmussen, A. L., Schmidt, L. B., West, E. D., Case, W. E., Reference calorimeter for laser energy measurements ... 13
Rate constant ... 213
Rate constants ... 115, 253
Rate of constants ... 77
Rates of reaction of atomic oxygen. III. Spiropentane, cyclopentane, cyclohexane, and cycloheptane ... 77
Rebbert, R. E., Ausloos, P., Pulse radiolysis of neopentane in the gas phase ... 329
Recrystallation ... 143
Reference calorimeter for laser energy measurements ... 13
Reference vaporization ... 511
Reflectance ... 347, 375
Refractive index ... 151
Refractometer ... 151
Reisfield, R., Inorganic ions in glasses and polycrystalline pellets as fluorescence standard reference materials ... 613
Relative quantum efficiencies ... 641
Resonances ... 1
Role of spectrophotometric standards in the clinical chemistry laboratory ... 499
Rotating capillary cell ... 579
Ross, G. S., Frolen, L., The characterization of linear polyethylene SRM 1475. X. Gel permeation chromatography ... 163
—, —, *Wims, A. M., Verdier, P. H.*, The characterization of linear polyethylene SRM 1475. VIII. Light scattering studies on polyethylenes in 1-chloronaphthlene ... 156
Rutgers, G. A. W., Absolute spectroradiometric measurements ... 427

S

Sanders, C. L., Accurate measurements of and corrections for nonlinearities in radiometers ... 437
Scaling law ... 207
Sanchez, I. C., DiMarzio, E. A., Dilute solution theory of polymer crystal growth: fractionation effect ... 213
Schmidt, L. B., West, E. D., Case, W. E., Rasmussen, A. L., Reference calorimeter for laser energy measurements ... 13
Second virial coefficient ... 156
Self-focusing ... 337
Shadmi, Y., Caspi, E., Theoretical investigation of the odd configuration of Ni II ... 125
Shumaker, J. B., Popenoe, C. H., A study of equilibrium in argon arcs ... 71
Sieck, L. W., Ausloos, P., Photoionization of propylene, cyclopropane, and ethylene. The effect of internal energy on the bimolecular reactions of $C_2H_4^+$ and $C_3H_6^+$ ... 253
—, *Gordean, R., Jr.*, Ion-molecular reactions in isopropanol: Implications for the radiolysis ... 655
—, *Lias, S. G., Hellner, L., Ausloos, P.*, Photoionization of C_4H_8 isomers. Unimolecular and bimolecular reactions of the $C_4^+H_8^+$ ions ... 115
Silicone pad ... 607
Simmons, J. H., Haller, W., Anatomy and thermal history of laser self-focusing damage tracks in glass ... 337
Skapers, A., Hamer, W. J., Field, B. F. The emf-temperature coefficient of "acid" standard cells of the saturated cadmium sulfate type from 15 to 40 °C ... 321
Solid surface fluorometry ... 607
Solution grown ... 25
Solution standards ... 641
Solution viscosity ... 147
Solutions properties ... 156
Solvents for phosphorimetry ... 579
Sparks, L. L., Powell, R. L., Low temperature thermocouples: KP, "normal silver," and copper versus Au-0.02 at % Fe and Au-0.07 at % Fe ... 263
Specific heat ... 207
Spectra ... 141, 285

Page

Spectrofluorometers, design 547
Spectrofluorometry, absolute 547
Spectrophotometric 405, 491
Spectrophotometric standards 509
Spectrophotometric standards, clinical 499
Spectrophotometry 141, 405, 455
Spin exchange 103
Spin relaxation 103
Spin relaxation effects on the EPR spectrum of gaseous hydrogen atoms 103
Spiropentane 77
Standard cells 321
Standard lamps 547
Standard potential of standard cells 185
Standard reference material 137
Standard reference material in spectrophotometry 405
Standard reference materials 469, 491
Standard reference materials in fluorometry 593
Standardization 491
Standardization, spectrophotometric 491
Standards, fluorescence 547
Standards, spectrophotometric 509
Stark effect 521
Stark splitting of millimeter wave transitions of water 521
Structures of ions 253
Study of equilibrium in argon arcs 71
Systematic errors in molar absorptivity 483

T

Temperature consistency 511
Test extrudate 145
Thermodynamic parameters (estimated) 511
Thermocouples 263
Thermodynamics of standard cells 185
Thermodynamics of standard cells of the saturated cadmium sulfate type 185
Thermopiles 547
Theoretical investigation of the odd configuration of Ni II 125
Theory 125
Thermal analysis of calcium sulfate and supposed α and β forms of calcium hemihydrates from 25 to 500 °C 41
Thermogravimetry 41
Transmittance 375, 405, 455
1,2,4-Trichlorobenzene 147, 151
Two-tube electrostatic lens 27

U

Udenfriend, S., Development of a new fluorescent reagent and its application to the automated assay of amino acids and peptides at the picomole level 637
Undercooling 213

V

Vapor phase 115
Velapoldi, R. A., Considerations on organic compounds in solution and inorganic ions in glasses as fluorescent standard reference materials 641
Venable, W. H., Jr., Spectrophotometric standards 509
Verbeke, O. B., An improved state equation in the vicinity of the critical point 207
Verdier, P. H., Brown, J. E., The characterization of linear polyethylene SRM 1475. IX. Number average molecular weight of fractions by membrane osmometry 161
—, *Frolen, L. J., Ross, G. S., Wims, A. M.*, The characterization of linear polyethylene SRM 1475. VIII. Light scattering studies on polyethylenes 156
—, *Hoeve, C. A. J., Wagner, H. L.*, The characterization of linear polyethylene SRM 1475, I. Introduction 137
Verges, J., Corliss, C. H., Martin, W. C., Infrared spectra of cerium (Ce I and Ce II) between 0.8 and 2.4 μm 285
Vibrational and electronic oscillator strengths of LiO 665
Vibrational transition probabilities 661
Virial coefficients 161
Viscometer 147

W

Wagner, H. L., The characterization of linear polyethylene SRM 1475. VII. Differential refractive index of polyethylene solutions 151
—, *Hoeve, C. A. J., Verdier, P. H.*, The characterization of linear polyethylene SRM 1475. I. Introduction 137
Water 521
Wavelengths 285
Weight average 163
West, E. D., Case, W. E., Rasmussen, A. L. Schmidt, L. B., Reference calorimeter for laser energy measurements 13
Widdowson, G. M., Penton, J. R., Williams, G. Z., Problems associated with the need for standardization in clinical spectrophotometric and fluorometric measurements 491
Williams, G. Z., Penton, J. R., Widdowson, G. M., Problems associated with the need for standardization in clinical spectrophotometric and fluorometric measurements 491
Wims, A. M., Frolen, L. J., Ross, G. S., Verdier, P. H., The characterization of linear polyethylene SRM 1475. VIII. Light scattering studies on polyethylenes in 1-chloronaphthalene 156
Winefordner, J. D., Phosphorimetry 579
Wood, L. A., Bullman, G. W., Decker, C. E., Modulus of natural rubber cross-linked by dicumyl peroxide. I. Experimental orbervations 51

X

Xenon 1, 207
$X^2\Pi$ 665

Y

Younglove, B. A., Dielectric constant of compressed gaseous and liquid oxygen 37

G

POSTAGE AND FEES PAID
U.S. GOVERNMENT PRINTING OFFICE
375

PENALTY FOR PRIVATE USE, $300

JOURNAL OF RESEARCH of the National Bureau of Standards
A. Physics and Chemistry

Vol. 76A, No. 6 November–December 1972

Contents

Page

Accuracy in Spectrophotometry and Luminescence Measurements

Proceedings of the Conference held at the National Bureau of Standards
Gaithersburg, Maryland, March 22–24, 1972

Part 2. Luminescence Measurements—Lectures and Panel Papers

Absolute spectrofluorometry. W. H. Melhuish. 547

Absolute quantum efficiencies. G. A. Crosby, J. N. Demas, and J. B. Callis. 561

Phosphorimetry. J. D. Winefordner. 579

Measurements of absolute values in biochemical fluorescence spectroscopy. Raymond F. Chen. 593

Newer fluorometric methods for the analysis of biologically important compounds. G. G. Guilbault. 607

Inorganic ions in glasses and polycrystalline pellets as fluorescence standard reference materials. R. Reisfeld. 613

Development of a new fluorescent reagent and its application to the automated assay of amino acids and peptides at the picomolelevel. Sidney Udenfriend. 637

Considerations on organic compounds in solution and inorganic ions in glasses as fluorescent standard reference materials. R. A. Velapoldi. 641

Other NBS Papers

Ion-molecule reactions in isopropanol: Implications for its radiolysis. R. Gorden, Jr., and L. W. Sieck. 655

Excitation of $O_2^1\Delta_g$ by electron impact. P. S. Julienne and M. Krauss. 661

Vibrational and electronic oscillator strengths of LiO. M. Marchetti, P. S. Julienne, and M. Krauss. 665

Publications of the National Bureau of Standards. 669

Index to Volume 76A, January to December 1972 689

Library of Congress Catalog Card Number: 62–37059

For sale by the Superintendent of Documents, U.S. Government Printing Office, Washington, D.C. 20402. (Order by SD Catalog No. C 13.22/sec.A:76/6). Single copy price varies. This issue $2.25. Subscription price $17.00 a year; $4.25 additional for foreign mailing.

UNITED STATES GOVERNMENT PRINTING OFFICE, WASHINGTON : 1972